UNIVERSITÀ DEGLI STUDI DI MESSINA

Dipartimento di Scienze Chimiche, Biologiche, Farmaceutiche e Ambientali

DOTTORATO DI RICERCA IN SCIENZE CHIMICHE
XXXII CICLO

Thermodynamic investigation on As(III) and As(V) in aqueous solution and extraction from natural water samples by Polymer Inclusion Membranes (PIMs)

Donatella Chillé

Supervisor
Prof. Claudia Foti

Coordinator
Prof. Paola Dugo

Academic Year 2018 – 2019

"Tenta l'incompiuto, lo straordinario
Vivi in eccesso, cominciando adesso
Goditi il trionfo, crea il tuo miracolo
Cerca il vero amore dietro ad ogni
ostacolo!"

(Il mestiere della vita – Tiziano Ferro)

Acknowledgements

Three years could appear like an infinitely long period of time but now that I am going to write my doctoral thesis, I realize that they have passed really quickly. During this period, I had the pleasure to meet so many people who have enriched me from a professional but mainly human point and to them I address my thanks. However, there are people who deserve to be mentioned as they were pillars for me during this experience. In particular, my supervisor Prof. Claudia Foti, a very important person who, every day, guided my research activity always providing me with valuable advices. Also every single member of the analytical research group and especially Anna, Rosalia and Antonio with whome, having to share the office, I also shared "joys and sorrows". Thank you very much for EVERYTHING.

I spent part of the second year of my PhD at the University of Girona (Spain), guest of the Prof. Clàudia Fontàs. A kind person, always available both at work and out, who allowed me to know, appreciate and even "export" a research line very far from mine. Receiving compliments, especially in the context of an international congress, was a great satisfaction for me! Many thanks also to Laura, Gemma and Ruben. You were really important figures for me because you made me feel like home from the first day I have been there, alleviating the lack of all the affections I had left in my beloved Sicily (or Chichilia), where you will always be welcome. Thanks also to Soetkin, Ibrahim, Marta and Mayra, who accompanied my days in the laboratory between a PIM and a laugh! Of course, I cannot fail to mention Enriqueta, always friendly and present for any suggestion, and Eva who patiently explained to me the principles of EDXRF, helping to carry out part of my research work. All of you will always have a special place in my heart!

Among the special thanks, I cannot fail to include Fausta, my so-called left arm (since she is left-handed). We shared high school, graduation years and part of the PhD period, thus we can say that we have been supporting each other for more than half of our lives! Thanks for all the tips, relative to work and life, and to always being there even when we have been located in different countries.

A deserved thanks goes to my FAMILY. My parents and my sister know that I am not a person of many words, but on this occasion I want to say that a good part of my success is due to them, to their advices, to their continuous encouraging me to overcome the limits that I have often imposed myself unjustifiably.

Thank you so much!

Index

Aim of the work

Arsenic is considered a powerfull poison, used from ancient times for committing suicides and murders. Its toxicity is well known and it represents an important hazard for human health. It must be remembered that the toxicity, as well as the mobility and bioavailability of an element are related to the chemical form in which the element itself is present and for this reason it is important to distinguish among the different forms of arsenic in order to have awareness of the risk connected to its exposure. Despite this, very few studies are reported in literature about the thermodynamic behaviour of arsenic, especially when it combines with molecules of biological importance. Accordingly, this research work stems from the desire to enrich the literature database regarding the arsenic speciation in aqueous solution. The speciation studies play an important role in the present-day analytical research, especially in the environmental field where the increase of pollution due, for example, to heavy metals reflects in a world problem for human health and ecosystem. The total determination of an element is not sufficient to explain the possible produced effect and thus the identification of the individual chemical and physical forms, called speciation analysis, is needed. This kind of study also reveals very useful in medical field when chelating therapy is necessary for removing metals from human body. In this case, the knowledge of the exact chemical form of the metal, for example the oxidation state, is crucial since the chelating agent could act differently depending on it.

In the present thesis, arsenic was treated considering two different oxidation states, in particular +5 and +3, using arsenate and arsenite respectively as starting molecules. The introduction describes the history of arsenic, its chemical and physical properties as well as the distribution in the environment (air, soil, water), the effects on human health and the application fields.

After a first section in which all the chemicals, analytical techniques, mathematical and computational approaches are described, the second one (Section II) is focused on the metallic behavior of arsenic in the trivalent oxidation state. The first investigation, regarding the acid-base properties of arsenite, was performed in aqueous solution but also by exploiting *ab initio* molecular dynamic simulations. Its interaction with different types of ligands was analysed at T = 298.15 K and different ionic strength values, by employing NaCl as background salt. In this section, a wide space was reserved for thiol ligands, given the high affinity of As(III),

often cited in literature [1-3], for the -SH groups of proteins. In addition to the classic thermodynamic approach, conducted through different analytical techniques including potentiometry, spectrophotometry and calorimetry, which allowed to determine the best speciation models together with the thermodynamic parameters of the obtained species, also *ab initio* molecular dynamic studies were performed in order to better understand the coordination mode of the metalloid with the functional groups present in the molecules. In order to complete the study relative to the interaction of As(III) with ligands of biological interest, also carboxylic acids, as well as amino acids and nucleotides were taken into account, performing an investigation less extensive, since the formation of weakly complexes was registered. In order to evaluate the possible use of phosphonic ligands for removing As(III) from environmental matrices, the binding ability of phosphonic acids derived from nitrilotriacetic acid by replacing the carboxyl groups with phosphonic ones were investigated in a wide range of ionic strength ($0.1 < I$/mol L^{-1} <1) by means of potentiometry and calorimetry and the sequestering ability was examined in conditions simulating sea water ($I = 0.7$ mol L^{-1} e pH = 8.1) and a fresh water ($I = 0.001$ mol L^{-1} e pH = 7). For these systems, also mass spectrometry experiments (LD MS/MS) were carried out in order to gain information about the structures of the complexes.

For the metal-ligand systems considered more interesting from the thermodynamic point of view, also the dependence of the stability constants on the ionic strength was taken into consideration by using the Debye-Hückel type equation. It is a mathematical model that allows to determine the stability constants at ionic strength values different from the experimental ones, by knowing the infinite dilution constant (log $^T\beta$) and C, an empirical parameter linked to the charges involved in the formation reaction. This approach is particularly important for predictive purposes in real matrices which are characterized by very different ionic strength conditions. For all the systems, the sequestering ability of the ligands towards the metalloid was evaluated by using an empirical parameter known as pL$_{0.5}$ that will be well discussed later.

Section III is dedicated to the study of arsenate (As(V)) as ligand molecule, by analyzing its non-metallic behavior with respect to bi- and trivalent cations. Specifically, the acid-base properties were determined in a wide range of ionic strength and T = 298.15 K and, also in this case, the study was completed with the application of molecular dynamic simulations. Successively, considering that in sea water arsenic is mostly present as As(V), speciation studies were performed in presence of the most representative alkaline-earth metals of this fluid, *i.e.* Ca^{2+}, Mg^{2+} and Sr^{2+}. The speciation of arsenate with alkaline-earth metals was

evaluated by means of potentiometry, in order to define the speciation models, and through calorimetry for establishing the thermodynamic parameters for the dependence on temperature. Trivalent cations, specifically Fe^{3+} and Al^{3+}, were chosen as a consequence of the pronounced affinity of arsenate towards these metals, widely discussed in terms of sorption processes onto mineral surfaces, such as metal oxides of Al, Fe and Mn, but poorly investigated as metal-ligand complexes in aqueous solution. Also for this system, the dependence of the stability constants on ionic strength and temperature was dealt with and, to complete the study, the sequestering capability of arsenate towards Fe^{3+} and Al^{3+} was investigated.

Section IV is focused on the research work performed during my PhD abroad at the University of Girona (Spain), under the supervision of Prof. Clàudia Fontàs of the Department of Chemistry. With respect to the previous sections, this one is more applicative and based on the extraction of arsenic, in particular As(III), from natural waters by means of Polymer Inclusion Membranes (PIMs), incorporating the extractant Bis (2,4,4-trimethylpentyl) dithiophosphinic acid, commercially known as Cyanex 301. After preliminary solvent extraction experiments (using a 0.1 mol L^{-1} Cyanex 301 solution in toluene), performed in 0.1 mol L^{-1} HCl solutions containing 10 mg L^{-1} of As(III) or As(V), that demonstrated the complete extraction of As(III) and As(V) after 30 minutes and 24 hours respectively, the extraction was carried out by using Polymer Inclusion Membranes (PIMs). This type of membranes, based on the incorporation of an extractant within a polymeric matrix possess a series of chemical-physical characteristics that will be discussed in the section, are easy to prepare and need a small amount of solvent for the preparation, in contrast with the previous solvent extraction experiments. Membranes with different compositions, in terms of polymer and extractant amount present in the membrane were tested and, finally, the best performance in terms of As(III) extraction was obtained with a PIM containing 50% CTA (Cellulose triacetate) as the polymer and 50% Cyanex 301 (% in mass). It was found that this PIM was not able to extract As(V), and, therefore, can be useful for speciation studies. In order to apply the extraction system to natural waters, some extraction experiments were performed using mineral water, sea water, tap water and spring water samples, all spiked with known concentrations of As(III). Then, the extraction efficiency was evaluated by analyzing the initial and final solutions by emission spectroscopy (ICP-OES). Based on the good efficiency of the PIM as a sorbent to collect As(III), a new analytical methodology was developed by combining the extraction by PIMs followed by detection by Energy Dispersive X-Ray Fluorescence (EDXRF) spectrometry, that allows the direct determination of the arsenic

extracted in the membrane, without any elution step or any other pre-treatment. Also, the detection of As(V) was achieved by applying a previous reducing treatment with sodium thiosulfate and potassium iodide prior its extraction by PIMs and detection by EDXRF. Finally, the developed methodology was successfully used to measure As species in naturally occurring arsenic water samples.

Introduction

Arsenic is a substance well known since ancient time for its poison properties. The name derives from the Persian *zarnikh*, meaning "yellow orpiment". Then it was incorporated into ancient Greek as *arsenikon*, which also means "masculine" or "potent". The term was translated as *arsenicum* in latin and *arsenic* in old French from which the current English word derived [4]. Throughout history, arsenic, thanks to its characteristics of odourless and tasteless, was used to commit several barbaric murders, especially in royal families in order to facilitate rich inheritance. Nero, for example, murdered his stepbrother Britannicus in order to become Emperor of Rome. Because of these events and its potency, arsenic was indicated as "*Poison of Kings and King of Poisons*". Among the prominent families engaged in poisoning, the Borgias were the most notorious. In Italy, a lady which stood out for her poisoning skills was Giulia Toffana. She made "Aqua Toffana" and sold it both as a cosmetic and a devotionary object in vials, basically to women trapped in difficult marriages who wanted to get rid of their husbands. The sale always was accompanied by appropriate instructions in order to avoid accidental poisonings. Giulia and her daughter Girolama were executed in Campo dei Fiori in Rome for the death of hundreds of men.

Moreover, in the 19th century arsenic powder was used by women in order to whiten their faces, their hair and scalp to destroy vermin [5, 6]. The fame of the toxic properties of arsenic was also described in many literary and theatrical works. For example, it was employed by Madame Bovary for her suicide in the novel of the French writer Gustave Flaubert, published in 1856, but also in "*Arsenic and Old Lace*", a play by American playwright Joseph Kesselring, written in 1939. It became best known through the subsequent film adaptation starring by Cary Grant and directed by Frank Capra. In the comedy, the aunts of the leading actor, by renting rooms to lonely old bachelors, put an end to their suffering by serving them a cup of elderberry wine spiked with arsenic, strychnine and "just a pinch of cyanide" while they getting acquainted. Unfortunately, arsenic compounds, such as Lewisite and Adamsite, were also used in the World Wars as chemical weapons. The first one has an odour of geraniums and is a potent respiratory and eye irritant as well as extremely poisonous if absorbed. Adamsite is a vomiting agent. Its effects on health are less dangerous than that produced by Lewisite since they become significant just when the exposure verifies in enclosed space or under adverse weather conditions. In these cases, it may result in more

severe adverse health effects as well as death [7, 8]. Despite its toxicity, arsenic was widely employed in medical fields from ancient times. Hippocrates recommended an arsenic paste for treating ulcers as well as Paracelsus [8, 9]. The use of arsenic as a drug therapy reached the glory in the 18th century when Thomas Fowler, a British physician, prepared the "Fowler solution" made by arsenic trioxide in potassium bicarbonate (1% w/v). This remedy was used empirically for the treatment of several diseases such us chorea, asthma, eczema and psoriasis. The discovery of a decrease in white blood cells counts in subject affected by leukemia when treated with Fowler solution led to the use of this mixture for the treatment of leukemia until the 20th century when it was replaced by radiation therapy [9].

The arsenic decline in medicinal field could be attributed to its toxicity and carcinogenicity, especially skin cancer. The International Agency for Research on Cancer included arsenic and certain arsenic compounds in group 1, namely agents that are carcinogenic to humans [10, 11].

Chemical properties and redox behavior. Arsenic is the 20th most abundant element in the earth's, 14th in the sea and 12th in the human body. It belongs to Group 15 of the Periodic Table with atomic number 33 and atomic mass equal to 74.921. Its more stable isotope is the ^{75}As. Arsenic is part of the metalloids and, for this reason, it exhibits both metallic and non-metallic properties. Elementary arsenic exists in three solid modifications:

- Yellow arsenic is unstable since it is obtained by sudden cooling of arsenic vapours to below 0°C; it is converted in the more stable grey form thanks to heat, light or catalysts such as iodine and bromine.
- Black arsenic is more stable than yellow form but less than Grey and its individuality is not certain.
- Grey arsenic is metallic and represents the ordinary stable form.

Arsenic shows various valences (-3; 0; +3; +5) and it can be present as organic and inorganic forms. It displays -3 oxidation state, for example, in the arsenic trihydride (arsine, AsH_3) compound. It is a colorless gas with a high poisonous power and a disagreeable garlic odor. The +3 oxidation state is shown in arsenic trioxide (As_2O_3), a tasteless and odourless compound used in the past as a lethal poison. Also arsenous acid and arsenites are trivalent compounds. Examples of compounds in which arsenic presents +5 oxidation state are arsenic pentaoxide (As_2O_5), arsenic pentasulfide (As_2S_5) as well as arsenates. Organic compounds

occur as a result of biological activity and some of them, such as 2-chlorovinyldichlorarsine (Lewisite), were used as chemical weapons [12-14].

Depending on the redox potential and pH, arsenic in water mainly exists in trivalent or pentavalent form, since the -3 and 0 valence states rarely occur in nature. Figure i shows the E_h-pH diagram for inorganic species of arsenic in natural environment. Under oxidizing conditions (high E_h values) the As(V) form predominates and the distribution of the oxoanions is related to the pH. In particular, at pHs lower than 2 the principal species is the H_3AsO_4 one; from pH = 7 to pH = 11 the $H_2AsO_4^-$ and $HAsO_4^{2-}$ species prevail and they are progressively substituted by the AsO_4^{3-} for higher pH values. Under reducing conditions (low E_h values) arsenic mainly exists as As(III). Also in this case, the oxoanions distribution is associated to the pH. For pH < 9, the prevalent species is the undissociated one H_3AsO_3 which becomes $H_2AsO_3^-$ once crossed this value. At E_h values below -250 mV, if in presence of sulphur or hydrogen sulphide, arsenic compounds such as As_2S_3 can be found. Arsine and elemental arsenic could be formed but in very strong reducing conditions [2, 15].
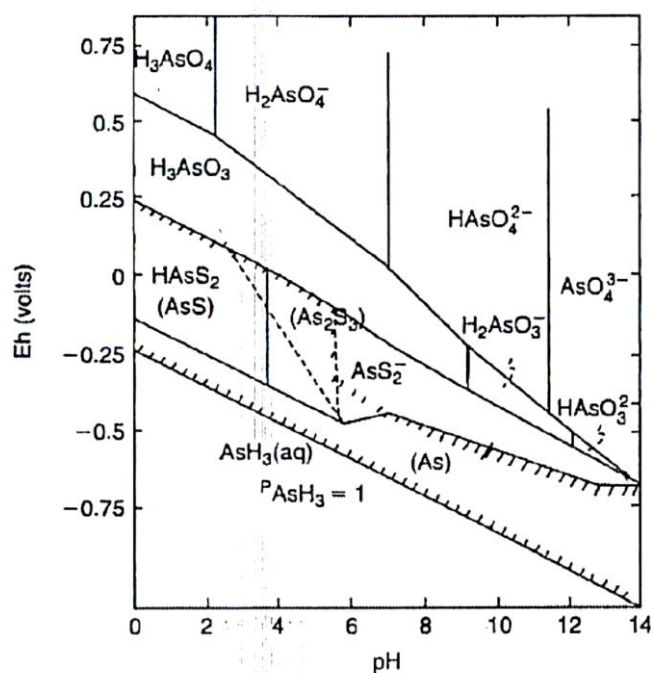
Figure i. E_h-pH diagram for arsenic at T = 298.15 K. Conditions: C_{As} = 0.00001 mol L^{-1} and C_S = 0.001 mol L^{-1} [15].

The redox behavior of arsenic in acidic medium (pH = 1) was well analysed by means of cyclic voltammetry by Yang *et al.* The results showed that the over-potential of As(III) oxidation to As(V) is very high (~ 0.9 V) in the experimental conditions under investigation. This aspect could indicate that on-site peroxidation in acidic wastewater is very difficult [16].

Arsenic in the environment. Arsenic is an ubiquitous element easily found in the environment both for natural and anthropogenic reasons. As mentioned above, it is a component of the earth's crust but it also occurs in minerals and soils and thus, it can reach water and air through wind-blown dust and runoff. Arsenic is naturally present in over 200 different mineral forms but only a few are encountered in relevant amounts, such as realgar (AsS), orpiment (As_2S_3) and arsenopyrite (FeAsS) which represents the most abundant As mineral [17]. The rock erosion together with weathering and volcanic eruptions are events that could contribute to the release of arsenic. In **soil**, arsenic can be found in three main forms: As(III), As(V) and organic arsenic. The As content is affected, basically, by climate, organic and inorganic components of the soils but also by the redox potential. [18, 19]. As an example, during the wet season, the soil conditions become reducing with the consequence of arsenic release from iron hydroxide sites. In the dry season, it remains fixed in the soil texture and therefore the arsenic amount results to be higher [20]. It should be noticed that in oxidizing conditions arsenate is the most stable form and it is easily adsorbed into clay, iron and manganese oxides/hydroxides, avoiding its mobility into the soil [21, 22]. In particular, on amorphous iron hydroxide, As(V) absorption seems to be independent of pH at low As concentrations but it increases when pH decreases (4 < pH < 9) at high As concentrations. Instead, the best adsorption of As(III) verifies at around pH = 7 [23]. In reducing conditions the most mobile arsenite prevails; accordingly, its immobilization could be favored by oxidation. The arsenic mobility is also influenced by the presence of ions defined as competitors with respect to arsenic. Inorganic and organic anions, such as (PO_4^{3-}), silicate (SiO_2^{2-}), sulphate (SO_4^{2-}), nitrate (NO_3^-), bicarbonate (HCO_3^-) and natural organic matter (NOM) can compete with arsenic for adsorption sites [18, 24-26]. Among these ones, the effect due to the presence of the phosphate is the most pronounced, since the arsenate structure is very similar to the phosphate molecule. Moreover, phosphorus is present in considerable amount in the soil, probably because of its use as component in fertilizers in agricultural field. Hence, PO_4^{3-} could be able to substitute the adsorbed AsO_4^{3-} favoring the mobility or, otherwise, prevent its adsorption. Clays and inorganic arsenic compounds can be methylated by microorganisms with the aim to produce, under oxidizing conditions, monomethylarsonic acid (*MMA*), dymethilarsinic acid (*DMA*) and trimethylarsine oxide (*TMAO*). Generally, arsenic levels in untreated and uncontaminated soils are between 1-40 mg kg^{-1}, while larger concentrations are observed in alluvial and organic soils [17]. The recommended value by the European Community is at most 20 μg g^{-1} [27].

In **natural waters** arsenic should be present in low concentrations; the World Health Organization fixed a regulatory value equal to 10 $\mu g\ L^{-1}$ in drinking waters. Normally, the highest concentration is observed in ground waters as a consequence of a strong water-rock interaction and favorable physical and geochemical conditions for the dissolution and mobilization of arsenic [27]. The main forms that can be found in natural waters are the same previously mentioned as regards the soil, namely arsenate and arsenite. Also organic species, such as dimethylarsinate (*DMA*) and monomethylarsonate (*MMA*), have been identified but in very low concentrations and, especially, in surface water as a result of biological activity. [27, 28]. Biomethylation is made by various species of micro-and higher organisms and may affect the mobility of arsenic species. In anoxic conditions, in fact, it causes the reduction of As(V) to soluble As(III) species and mobilizes As from the aquifers into groundwater [20, 29]. The seawater, normally, contains 0.001-0.008 mg L^{-1} of arsenic. The thermodynamically most stable form is arsenate and its pentavalent oxyanions ($H_2AsO_4^-$, $HAsO_4^{2-}$ and AsO_4^{3-}). At lower redox potential and reducing conditions, arsenic in the trivalent oxidation state (H_3AsO_3) prevails [17]. In unpolluted fresh and ground waters, the amount of arsenic ranges from 1-10 $\mu g\ L^{-1}$, reaching values of 5000 $\mu g\ L^{-1}$ in areas of sulfide mineralization and mining [17, 27, 30].

In the **atmosphere**, arsenic is mainly present as a mixture of As(V) and As(III) absorbed on particulate matters. Both natural phenomena (volcanic eruptions, weathering) and anthropogenic activities (pesticides, smelting, fossil fuel combustion, mining activity) promote the arsenic release in the air [27]. Normally, the human exposure to arsenic through air is negligible. The estimated levels in Europe range from 0.2 – 1.5 ng m^{-3} in rural areas, 0.5 – 3 ng m^{-3} in urban areas and 50 ng m^{-3} in industrial areas [14]. The daily respiratory intake of arsenic is approximately 120 ng m^{-3} of which just 30 ng m^{-3} are absorbed [17].

Arsenic toxicology and health effect. Arsenic may reach human organism through many pathways, as explained in the previous paragraphs. However, it seems that the preferential way is represented by the direct consumption of As contaminated drinking water [31]. Groundwater is the most important source of drinking water and it is often employed for the irrigation of vegetables and fruits. Thus, the consumption of agricultural products cultivated by using arsenic contaminated groundwater represents another source of arsenic exposure [32]. Elevated concentrations of arsenic are registered primarily for natural reasons, such as rock erosion, but the use in industrial processes, mining activities, pesticides and fertilizers contributes to the global contamination, basically as a consequence of leaching

processes. In 1963, the World Health Organization fixed a recommended value for arsenic in drinking water equal to 50 µg L^{-1}, but successively it was further reduced to 10 µg L^{-1} in 1992, following the suspicion of carcinogenicity [33]. The FAO/WHO provisional tolerable weekly intake (PTWI) of 15 µg kg^{-1} body weight for a 60-kg man is 2.1 µg kg^{-1}. However, many countries of the world, such as Bangladesh [34, 35], India [35], Argentina [36], Canada [37] and Vietnam [38], present high levels of arsenic in drinking waters; thus, the daily arsenic intake, often, exceed the PTWI [14]. The arsenic poisoning can be differentiated in acute and chronic. The acute toxicity is often related to the accidental ingestion of insecticides or pesticides and rarely as a consequence of a suicide attempt. The prevalent features are nausea, vomiting, diarrhea and excessive salivation. The haematological picture changes and renal and respiratory failure occurs as well as pulmonary edema. Urinary arsenic concentration is the best indicator to detect a recent poisoning.

Chronic toxicity is the most common form and it occurs in people daily exposed to the contaminant for several reasons. Absorbed arsenic is accumulated in liver, heart, kidney and lungs and deposited in the ketarin-rich tissues. The normal amount of arsenic in hair is around 0.08-0.25 µg g^{-1} until 1.0 µg g^{-1} in case of poisoning. In nails the normal concentration is 0.34 µg g^{-1}, while in urine it can vary from 5 to 40 µg per day. A concentration of 100 µg per day is registered in case of acute and subacute poisoning [17]. The effects of the chronic intake of arsenic on human organism are various, ranging from hyperpigmentation, hyperkeratosis, increase of risk of cardiovascular and respiratory disease as well as diabetes mellitus, until malignant change in almost all the organs of the body [39]. A ten-year study, conducted by Choudhury *et al.*, was recently published. In the investigation, a sample of 960 patients coming from different arsenic contaminated districts of Bangladesh and showing cutaneous malignancy (single lesion), was tested from January 2004 to December 2015. The results of the study are very alarming, if we think that only a small portion of the nation was examined. In fact, the 58.65% of the patients (N = 563) was affected by Basal Cell Carcinoma (BCC), Squamous Cell Carcinoma (SCC) was found in 40% (N = 384) of the study population, 1.15% (N =11) resulted to be the melanoma patients and 0.21% (N = 02) of the people showed Merkel Cell Carcinoma (MCC) [40].

In relation to the chemical form in which the element occurs, the exhibited toxicity may be different. As(III) and As(V), in fact, act differently in human organism. For the first one, a high affinity towards sulfhydryl groups of the proteins is documented as well as the resulting toxicity due to the inhibition of important biochemical events [1]. Arsenate presents a very

similar structure to phosphate molecule and this similarity could involve an incorporation of arsenate in some metabolic reactions in which phosphate is normally required [3].

When ingested, inorganic arsenic is readily absorbed in the gastrointestinal tract. It seems that it is badly absorbed through intact human skin but can bind externally to skin and hair. Absorbed arsenic is transported through the blood to the other organs of the body, bound to SH groups of proteins and low-molecular-weight compounds such as *GSH* or cysteine. The major part of arsenic in blood is cleared with a half-time of about 1 hour, while the whole-body half-time of ingested arsenite is about 4 days and the urine is the prevalent excretory pathway [41]. In blood, in fact, the concentration is elevated only for short time after absorption. However, in case of chronic exposure, such as contaminated drinking water intake, arsenic levels can reach a constant state which reflects the degree of exposure [14]. In human organism, alternative steps of reduction of the pentavalent arsenic compounds come in succession with oxidative methylation processes which allow to the formation of differently methylated arsenicals, in particular monomethyl and dymethyl arsenic compounds, generically indicated as *MAs* and *DMAs* when the oxidations state cannot be determined [42, 43]. The Figure ii, taken from Ref. [44], well shows the metabolic conversions of arsenic species. The predominant metabolite of inorganic arsenic, rapidly excreted by most mammals, is represented by the dimethylarsinic acid (DMAs^V) [3].
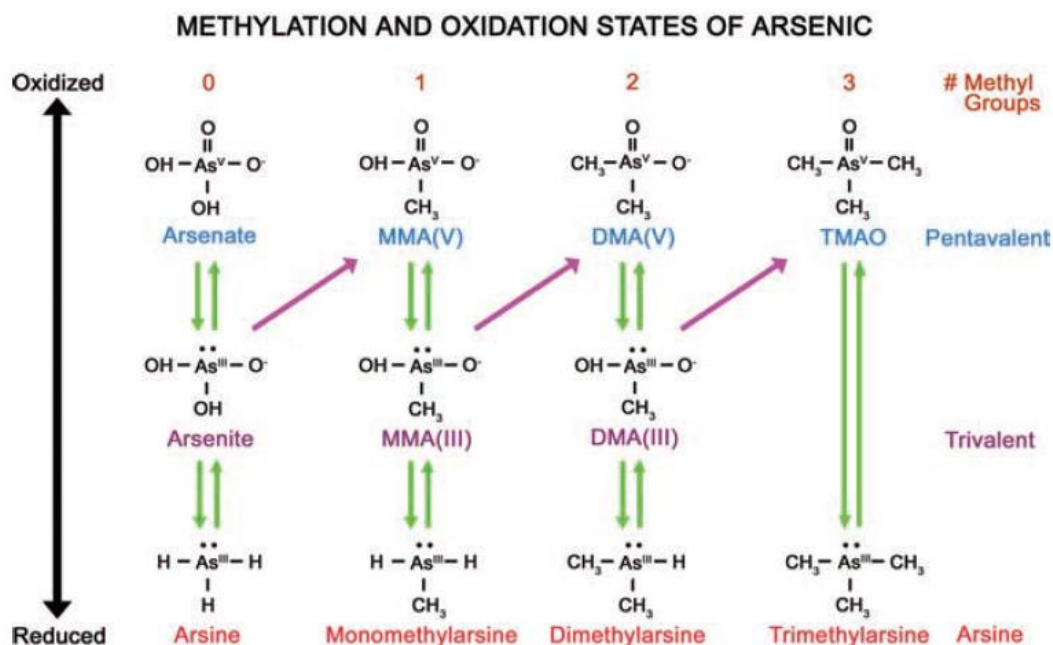
Figure ii. The metabolic conversion of arsenic species [44].

Applications. Probably, the most pronounced use of arsenical compounds is to be attributed to the formulations of pesticides, fungicides and herbicides. Paris Green, a copper acetoarsenite compound, appeared around 1860 and was employed as standard insecticide for about 30 years. Later, it was replaced by lead arsenate, considered less toxic for plants, and it was widely used for many years as pesticide for apple and cherry orchards [8, 45]. Calcium arsenate was used for dusting cotton in order to control boll weevil and the cotton leaf worm [45]. The use of these compounds was limited with the introduction of DDT, dichlorodiphenyltrichloroethane, in 1947, although, ultimately it became infamous for its environmental impacts [2]. Inorganic arsenic compounds, in particular sodium arsenite, were employed since 1890 as weed killers [17]. The application of chromated copper arsenate (CCA) in combination with ammonical copper arsenate (ACA) as wood preservatives dates back to 1940. Nowadays, its employment is approved for nonresidential constructions, such as utility poles or marine facilities [8, 46]. Arsenic is also employed as decolorizing agent in the glass industry, as additive in the production of alloys in order to improve hardness and heat resistance, in textile and tanning industries, in manufacture of fireworks and pigments. Lately, gallium arsenide and indium arsenide play an important role in the fabrication of semiconductors, solar cells, integrated circuits and much more [14, 30].

The importance of arsenic in medical field should be remembered since it was used for more than 2400 years for a several diseases including ulcers, the plague, and malaria [47]. Known medicinal preparations, containing arsenic, include Fowler's solution (potassium arsenite) [48], Donovan's solution (arsenic and mercuric iodides), arsphenamine (Salvarsan), supplanted by neoarsphenamine (Neosalvarsan), easier to prepare than the last one [49] [17]. In the modern era, researchers evidenced that As(III) produces anticancer effects in leukemic [50] and human glioblastoma cells [51] and induces autophagy and apoptosis in human fibrosarcoma [52] and breast cancer cells [53]. Arsenic-containing compounds substituted with organic groups such as modified phenylarsine oxides were examined in order to test their citotoxic abilities on human leukemic cells and breast cancer cells in culture. Among them, p-GSAO (para 4-[*N*-(*S*-glutathionylacetyl)amino]phenylarsenoxide seems to produce a series of effects that lead to apoptosis of angiogenic endothelial cells and inhibition of tumor growth in mice with no apparent toxicity. Arsenic trioxide was approved by FDA in 2000 as chemotherapeutic agent for the treatment of APL (Acute Promyelocytic Leukemia). Employed as single agent, it allowed the 86% complete remission in APL patients showing minimal toxicity equal to any other drug or combined treatment exploited for the same purpose [54].

Section I

Experimental Section

This section is divided in two brief chapters. The first one is dedicated to the description of the chemicals, analytical techniques, computational and mathematical approaches used to perform speciation studies in aqueous solution. The second one deals with the chemicals and analytical techniques employed for arsenic determination in water samples after its extraction by means of PIMs.

1

Chemicals, analytical techniques, mathematical and computational approaches used for thermodynamic studies

1.1 Chemicals

Sodium (meta)arsenite was prepared by weighing the corresponding salt $NaAsO_2$ purchased by Sigma-Aldrich with a purity of 90% and used as it is as well as sodium arsenate dibasic heptahydrate, $Na_2HAsO_4 \bullet 7H_2O$,(Sigma Aldrich, $\geq$ 98%). All the compounds employed for the investigation are summarized in Table 1.1. They were used without any purification and their purity grade was checked by alkalimetric titrations by means of a potentiometer. The employed alkaline-earth metal cations were magnesium chloride hexahydrate, $MgCl_2 \cdot 6H_2O$, (Fluka $\geq$ 99%), calcium choride dehydrate, $CaCl_2 \cdot 2H_2O$, (Fluka $\geq$ 99%) and strontium chloride hexahydrate, $SrCl_2 \cdot 6H_2O$, (Merck $\geq$ 99%). They were prepared by weighing the corresponding solids and their solutions titrated by a standard EDTA (ethylendiaminotetraacetic acid) solution. As regards trivalent metal cations, iron chloride hexahydrate, $FeCl_3 \cdot 6H_2O$, (Sigma Aldrich $\geq$ 99%) and aluminium chloride hexahydrate, $AlCl_3 \cdot 6H_2O$, (Sigma Aldrich $\geq$ 99%) were used. Both were prepared by weighing the respective salts and titrated by a standard EDTA solution for determining their concentrations. In particular, the second one was standardized by a back-titration with EDTA, using a standard $CuSO_4$ solution as titrant. Sodium hydroxide and hydrochloric acid solutions, prepared from concentrated Fluka ampoules, were titrated with potassium hydrogen phthalate and sodium carbonate respectively, previously dried in an oven at 383.15 K for at least one

hour. Moreover, NaOH was stored in dark bottles equipped with soda lime traps, in order to preserve it from CO_2. Also the sodium chloride solution, employed as ionic medium, was prepared by weighing the pure salt (Fluka, puriss.), pre-dried in an oven at 383.15 K. Ultrapure water (conductivity < 0.1 μS cm^{-1}) and grade A glassware were employed for the preparation of each solution.

Table 1.1. List of compounds under investigation and related information.

Ligands	Abbreviation or acronym used	Sellers
Sodium (meta)arsenite	-	Sigma-Aldrich
Sodium arsenate dibasic heptahydrate	*ars*	Sigma-Aldrich
2-mercaptopropanoic acid or thiolactic acid	*tla*	Sigma-Aldrich
2-mercaptosuccinic acid or thiomalic acid	*tma*	Fluka
meso-2,3-Dimercaptosuccinic acid	*dmsa*	Sigma-Aldrich
L-Cysteine	*cys*	Fluka
L-Glutathione reduced	*gsh*	Sigma-Aldrich
1,3-propanedicarboxylic acid or malonic acid	*mal*	Fluka
Propane-1,2,3-tricarboxylic acid or tricarballylic acid	*tca*	Fluka
Butane-1,2,3,4-tetracarboxylic acid	*btc*	Fluka
Benzenehexacarboxylic acid or mellitic acid	*mlt*	Fluka
Glycine	*gly*	Sigma-Aldrich
L-Aspartic Acid	*asp*	Fluka
L-Lysine	*lys*	Fluka
n-(Phosphonomethyl)iminodiacetic acid hydrate	*NTAP*	Sigma-Aldrich
n,n-bis(phosphonometyl)glycine	*NTA2P*	Sigma-Aldrich
Nitrilotri(methylphosphonic acid)	*NTA3P*	Sigma-Aldrich
Adenosine 5′-monophosphate sodium salt	*AMP*	Sigma-Aldrich
Adenosine 5′-diphosphate sodium salt	*ADP*	Sigma-Aldrich
Adenosine 5′-triphosphate sodium salt	*ATP*	Sigma-Aldrich

1.2 Potentiometry [55]

1.2.1 General aspects

Potentiometric methods are based on the measurement of the potential of electrochemical cells when no current passage occurs. The system is composed by:

- A reference electrode, whose potential value is constant over time and independent from the solution composition in which the analyte is dissolved;
- A working electrode, also known as indicator electrode, whose response depends on the activity of the ion of interest.
- An instrument for measuring potential, such as a potentiometer.

In particular, potentiometric titrations allow to measure the potential change when the titrant is added in the cell and they can be applied to redox, acid-base, precipitation and complexation reactions. For this purpose, a typical glass electrode, normally indicated as ISE-H^+, since it is selective towards H^+ ions, was used to study proton exchange in acid-base and complexation equilibria. The operating principle is based on the different ion activity inside and outside the membrane. In fact, the indicator electrode, putted inside a glass tube in which can be also present the reference electrode (combined electrode), is immersed in HCl solution with constant activity, namely 0.1 mol L^{-1}, saturated with AgCl. This internal solution is separated from the solution containing the analyte by the selective membrane. The different H^+ activity between the internal and external solutions generates the potential difference that is only function of the H^+ activity of the external solution since the internal H^+ concentration is constant. The dependence of the activity by the potential can be explained by the following Nernst equation:

$$E = E^0 - s\,log\,\frac{a_{H^+}(int)}{a_{H^+}(ext)} \tag{1.1}$$

where E represents the measured potential value, E^0 is the formal potential and s is the nernstian slope, up to pH $\approx$ 11. It corresponds to 2.303RT/nF and at T = 298.15 K it is equal to 59.16 mV and 29.58 mV for monovalent and bivalent ions respectively. The formal potential, in addition to the standard potential, is composed by other contributions, in particular the junction potential and asymmetry potential. The first one is caused by the charge separation due to the diffusion processes of the ions as a consequence of the concentration gradients. The last one is produced by the no perfect homogeneity of internal and external membrane surfaces.

1.2.2 Potentiometric equipment and procedure

Potentiometric measurements were carried out by means of different systems composed by a Metrohm model 809 Titrando potentiometer equipped with an Orion-Ross 8102 combined glass electrode and an automatic dispenser Metrohm Dosino 800. The system were interconnected with a PC provided with a software named TIAMO 2.2 able to control several parameters very useful for a correct acquisition of experimental data. In particular:

- maximum number of reading cycles, in other words the number of readings of the potential value for each experimental point;

- maximum and minimum adding of titrant

- time interval between the successive readings of the potential;

- final value of potential of the titration.

For the potentiometric systems, the estimated error is $\pm$ 0.15mV for e.m.f., while for titrant volume readings is $\pm$ 0.002mL. All the measurements were performed in thermostated glass jacket cells, generally at T = 298.15 and rarely at T = 288.15, T = 310.15 and T = 318.15 $\pm$ 0.1K. In the reaction cell was bubbled nitrogen in order to eliminate the interference due to CO_2 and O_2 and the solution was kept under magnetic stirring, in order to ensure the homogeneity after each titrant adding. In this thesis, first of all, the acid-base properties of arsenate (As(V)) and arsenite (As(III)) were studied. In particular, 25 mL of solution containing arsenate or arsenite, NaCl as ionic medium and hydrochloric acid (in order to investigate a large pH range) were added in the cell and titrated with NaOH. When the interactions of arsenate with metals or the speciation behaviour of As(III) with ligands were investigated, the potentiometric measurements were carried out as previously described but by adding in cell a specific amount of metals or ligands in order to have a prefixed concentration. Indipendent titrations of HCl with NaOH were carried out in order to establish the formal potential, E^0, and pK_w values at the same experimental conditions of ionic strength and temperature. The details referred to the experimental conditions are reported in Table 1.2.

Table 1.2. Experimental conditions for the acid-base properties of arsenate and arsenite in NaCl and T = 298.15 K.

$C_{Arsenate}$ [a]	$C_{Arsenite}$ [a]	C_{H^+} [b]	*I* range [c]	pH range	N [d]
1-3	- - - -	5-10	0.1-1	2-11	15
- - - -	1-6	5-10	0.1-1	2-11	12

[a] mmol L^{-1}; [b] mmol L^{-1}; [c] mol L^{-1} [d] number of titrations.

Arsenate was studied only as ligand molecule and its interaction with several metal cations was evaluated a T = 298.15 K, in NaCl as background salt, considering a large range of ionic strength (0.1 < I/mol L^{-1} < 1) and different metal-ligand ratios. All the experimental conditions are included in the Table 1.3.

Table 1.3. Experimental conditions for the M^{n+} -arsenate (*ars*) systems in NaCl and T = 298.15 K.

System	c_M [a]	c_L [a]	C_M/C_L ratio	Ionic Strength range [b]	pH range	n [c]
Ca^{2+}-*ars*	1-5	1-10	0.5-2	0.1-1	2-10	12
Mg^{2+}-*ars*$^-$	1-5	1-10	0.3-2	0.1-1	2-10	12
Sr^{2+}-*ars*	1-5	1-10	0.5-2	0.1-1	2-10	12
Fe^{3+}-*ars*	0.3-1	0.5-3	0.1-0.2	0.1-0.7	2-4.5	14
Al^{3+}-*ars*	0.5-1	1-4	0.125-0.5	0.1-0.7	2-4.5	12

[a] mmol L^{-1}; [b] mol L^{-1}; [c] number of titrations.

As regards As(III), it was investigated from the metallic point of view and for this aim, different classes of ligands were taken into account in order to perform speciation studies. The list of the ligands under investigation is reported in Table 1.4 together with the employed experimental conditions.

Table 1.4. Experimental conditions for the As(III) − ligands systems in NaCl and T = 298.15 K.

System	$c_M^{a)}$	$c_L^{a)}$	C_M/C_L ratio	Ionic Strength range[b]	pH range	$n^{b)}$
As(III)-*tla*	1-10	1-20	0.3-2	0.15	2-11	12
As(III)-*tma*	1-10	1-15	0.3-2	0.15	2-11	8
As(III)-*dmsa*	1-2	1-3	0.5-2	0.15	2-11	14
As(III)-*mal*	1-5	1.5-10	0.2-2	0.15	2-10	8
As(III)-*tca*	3-8	2-10	0.3-2.5	0.15	2-10	8
As(III)-*btc*	2-8	2-10	0.3-4	0.15	2-10	6
As(III)-*mlt*	2-8	2-8	0.2-4	0.15	2-10	6
As(III)-*cys*	1-3	1-9	0.2-2	0.15-1	2-10	20
As(III)-*gsh*	1-5	2-9	0.2-1	0.15-1	2-10	20
As(III)-*gly*	3-6	2-10	0.5-2	0.15	2-10	6
As(III)-*asp*	3-6	2-10	0.3-2	0.15	2-10	6
As(III)-*lys*	3-6	2-10	0.3-2	0.15	2-10	6
As(III)-*NTAP*	1-5	1-8	0.5-2	0.1-1	2-10	14
As(III)-*NTA2P*	4-5	2-8	0.5-2	0.1-1	2-10	12
As(III)-*NTA3P*	3-5	2-8	0.5-2	0.1-1	2-10	12
As(III)-*AMP*	1-3	1-4	0.5-2	0.15	2-10	5
As(III)-*ADP*	1-2	1-4	0.3-2	0.15	2-10	5
As(III)-*ATP*	1-5	1-5	0.5-2	0.15	2-10	7

[a]mmol L^{-1}; [b]mol L^{-1}; [c] number of titrations.

As concerning the dimercaptosuccinic acid, measurements of metal-ligand systems were preceded from the study of the acid-base properties at the same ionic strength (I = 0.15 mol L^{-1}) and temperatures (T = 288.15 K, T = 298.15 K, 310.15 K and T = 318.15 K) used for mixed systems. Ligand concentrations ranging from 1 to 3 mmol L^{-1} and metal concentration between 1 and 2 mmol L^{-1} were employed and a wide range of pH (2-11) was investigated. For other systems, the determination of the acid-base properties of the ligand was not necessary since they were previously obtained.

1.3 UV-Vis spectrophotometry [55]

1.3.1 General aspects

Spectroscopy methods are based on the absorption or emission, from an atom or a molecule, of electromagnetic radiation. This one can be viewed both as a particle, called photon, and a wave that propagate through oscillating electric and magnetic fields, perpendicular to each other. To the electromagnetic radiation is associated an energy that follows the Plank's law:

$$E = h \bullet \nu \qquad\qquad (1.2)$$

In particular, in absorption spectroscopy of visible light, the energy of the photon is transferred to the analyte, with the consequent relocation of a valence electrone in a higher-energy, or excited, state. This transition is possible only if the radiation has an energy equal to the difference in energy between the two quantized energy states of the analyte. The possible electronic transitions are several, as can be seen in Table 1.5, but the most employed in chemical analysis are the last two, since they involve functional groups very useful for identifying a molecule and also because the interested wavelengths are easily accessible.

Table 1.5. Permissible Electronic Transitions.

Transition	**Wavelength Range (nm)**	*Examples*
σ → σ*	< 200	C-C, C-H
n → σ*	160-260	H_2O, CH_3OH, CH_3Cl
π → π*	200-500	C=C, C=O, C=N, C≡C
n → π*	250-600	C=O, C=N, N=N, N=O

The functional groups and the bonds that allow that a molecule absorb ultraviolet and visible radiation are called chromophores. Also transition metal ions can absorb energy and it is due to valence electrons in *d*-orbitals. Normally, these ones are iso-energetic; however, the interaction with a ligand or solvent perturbs this condition and causes a split in two o more groups with different energy. The absorption, also, can take place as a consequence of a partial electron transfer in an excited state between a donor and an acceptor. In analytical chemistry, the UV-Vis spectroscopy is widely used inasmuch the absorbed radiation allows to obtain qualitative and quantitative information about an analyte. Graphically, the result is a spectrum obtained by representing the intensity of the absorbed radiation as a function of the wavelength. In particular, the qualitative analysis is carried out by comparing the spectra under investigation with literature data, while for the quantitative one is necessary to follow the Lambert-Beer Law that linearly correlates the intensity of the absorbed radiation with the

analyte concentration. In particular, when a sample absorbs energy, a decrease in terms of intensity of the radiation is registered. This aspect can be linked with the concentration of the molecules that absorb (higher is the concentration of the particles higher is the attenuation) and with the optic path of the radiation (longer is it, higher is the absorbed light and greater the attenuation phenomenon). This one can be explained by the term *Transmittance*

$$T = \frac{P_T}{P_0} \tag{1.3}$$

where P_0 is the intensity of the incident radiation and P_T is the transmitted radiation intensity through the solution. An alternative way to express the attenuation of the electromagnetic radiation is the *Absorbance*, defined as:

$$A = -logT = -log\frac{P_T}{P_0} = log\frac{P_0}{P_T} \tag{1.4}$$

As mentioned before, absorbance is directly proportional to the concentration and to the optical path, according to the following relation:

$$A = \varepsilon \bullet b \bullet C \tag{1.5}$$

where:

ε = molar extinction coefficient (L mol^{-1} cm^{-1}). It depends on the wavelength of the absorbed radiation, on the solvent and chemical species that lead to the absorption;

b = thickness of the cell or optical path of the solution (cm), generally equal to 1 cm;

c = concentration of the absorbent species (mol L^{-1})

However, this is a limiting law because its validity ceases at high concentrations, *i.e.* for concentrations ≤ 0.01 mol L^{-1}.

1.3.2 UV-Vis equipment and procedure

Spectrophotometric measurements were performed by using a Varian Cary 50 UV-Vis spectrophotometer equipped with an optical fiber probe with a path length equal to 1 cm. The system is interconnected with a PC provided with a software named Varian Cary WinUV, able to register the spectra in a wavelength interval ranging from ultraviolet region to visible one. The titrant was added in the cell through a 665 Metrohm automatic burette and, at the same time, the pH change was monitored by means of a combined glass electrode (Thermo/Orion Ross type 8102) connected to a Metrohm 713 potentiometer. Accordingly, two sets of data is possible to collect: absorbance values *vs* λ (nm) and pH *vs* titrant volume

(mL). Each experiment was carried out in thermostated glass cell following the same procedure previously described for potentiometric measurements. The metal-ligand systems were investigated on 25 mL of solution containing the appropriate amount of metal, ligand and background salt (for reaching a prefixed ionic strength value) at T = 298.15K. When necessary, independent titrations of metals or ligands solutions were performed in order to calculate the molar absorption coefficients. All the specific experimental conditions are reported in Table 1.6.

Table 1.6. Experimental conditions for the metal-ligands systems investigated by spectrophotometry in NaCl and T = 298.15 K.

System	c_M [a)]	c_L [a)]	C_M/C_L ratio	Ionic strength [b)] range	pH range	Wavelength range [c)]	N [d)]
Fe^{3+}-*ars*	0.02-0.05	0.1-0.2	0.05-0.5	0.1-0.7	2-4	200-500	14
As(III)-*tla*	0.05-0.15	0.3-0.5	0.05-0.5	0.15	2-11	210-300	3
As(III)-*tma*	0.05-0.15	0.3-0.5	0.05-05	0.15	2-11	210-300	3
As(III)-*dmsa*	0.05-0.15	0.05-0.15	0.5-2	0.15	2-11	210-300	4
As(III)-*cys*	0.1-0.3	0.2-0.4	0.5-1	0.15	2-10	220-280	3

[a)] mmol L^{-1}; [b)] mol L^{-1}; [c)] nm; [d)] number of titrations.

1.4 Calorimetry [56]

1.4.1 General aspects

The titration calorimetry or direct calorimetry is a technique in which the heat, developed or absorbed in a chemical reaction, is measured as a function of the titrant volume added during the measurement. Most of the experiments were performed by an isoperibolic calorimeter constituted by a reaction cell quasi-adiabatic, immersed in a thermostated bath. The temperature change in the reaction cell, proportional to the difference between the temperature of the bath and the cell itself, could be caused by a chemical reaction or a physical interaction between the sample and the titrant which lead to the formation of new species in solution. With this technique the resulting data, expressed as heat produced as a consequence of the added titrant, were analysed in order to calculate thermodynamic parameters such as K, ΔH^0 e ΔS^0. Also a nano-isothermal calorimeter was employed and it will be examined in the next subparagraph.

1.4.2 Instrumental equipment and procedure

The instrumental equipments employed in this study were a CSC isoperibolic calorimeter, model 4300, visible in Figure 1.1 and nano-isothermal titration calorimeter Nano-ITC (TA Instruments).

Figure 1.1. CSC isoperibolic calorimeter

For the first instrument, titration was performed continuously since the titrant was added with constant rate. The reaction cell, constituted by a glass vessel covered with a silver layer with a capacity of 25 or 50 mL, is immersed in 25mL thermostated bath, thermically isolated and with a temperature stability of ± 0.0005°C. The titrant adding took place by means of a 2.5 mL Hamilton syringe in glass and Teflon, model 1002TLL. The stirring of the solution in the dewar was guaranteed by a glass stirrer whose rate is easily adjustable, while the temperature was controlled by a thermistor also immersed in the reaction cell and part of the Wheatstone bridge. The thermistor is crossed by a small current. When the temperature in the dewar changes, as a consequence of the titrant adding, the resistence and, consequently, the voltage through the Wheatstone bridge proportionally vary. This voltage is amplified in the electrical circuit and the temperature variations are measured by a multimeter connected with the Wheatstone bridge. A personal computer, managed by a specific software named CALOR8, collected data automatically. This computer program is also able to fix the parameters for the measurement such as:

- the rate of buret delivery in mL/min and the delay of the burette in seconds (both measured previously);
- the initial volume;
- total time and time intervals, expressed in seconds, for the readings of the baselines, the calibrations and the titration;
- the values of HTRI and HTRV (the voltage across the standard resistor and the heating resistance calibration, respectively) and the starting potential of the measurement.

Daily, before starting experiments, it was necessary to check the voltage across the Wheatstone bridge and set it to zero. Moreover, the determination of the dilution heats for each solution, by titrating pure solvent with the same titrant employed for the subsequent measures, was required in order to subtract this amount of heat to the total determined in the measurements.

Once put the solution in the dewar, this one was allocated in the thermostated bath and the solution was heated up by means of a heater in order to make equal the temperatures of the solution and bath. The good operation of the heating resistance was periodically checked by a chemical calibration which consists in titrating a THAM [tris-(hydroxymethyl)amino-methane] buffer with HCl. The accuracy of the apparatus for the measured heat is $Q \pm 0.008$ J and for the volume $v \pm 0.001$ mL. After inserting all the input data previously described, the measure started. For the acid-base properties of As(III) and As(V), 25 ml of solution

containing arsenate or arsenite sodium salts and NaCl as ionic medium were titrated with HCl solution. Details are reported in Table 1.7. The study of As(III)-ligand complexes were performed by adding the ligand under investigation as sodium salt to 25 mL of a solution containing the metal, the ionic medium and sometimes HCl. Details are listed in Table 1.8. Regarding arsenate-metals invetigations, 25 mL of solution featured by the metal cation under study and the necessary amount of ionic medium, in order to obtain a prefixed ionic strength, were titrated by the arsenate salt solution having a pH equal to 11.6. The details of the experimental conditions are shown in Table 1.9.

As regards the second equipment, it was constituted by an active cell volume of 0.988 mL and equipped with a 250 μL injection syringe. The reaction mixture in the sample cell was stirred at 250 rpm during the titrations. The reference cell was always filled with ultrapure water. All solutions were gently degassed under vacuum for about 15 min before each run. Measurements were run in the overfilled mode which does not require any correction for liquid evaporation and for the presence of the vapor phase [57]. The power curve was integrated by NanoAnalyze (TA Instruments) to obtain the gross heat evolved/absorbed in the reaction. The calorimeter was calibrated chemically by a test HCl/TRIS reaction according to the procedure previously described [58]. The instrument was also checked through electrical calibrations.

ITC measurements were carried out by titrating a $12 \div 15$ mmol L^{-1} aqueous solution of As(III) (containing HCl) into an aqueous solution of either *NTAP* ($1.8 \div 2.1$ mmol L^{-1}) or *NTA2P* ($2 \div 2.5$ mmol L^{-1}); both the solutions of the titrant (syringe) and the titrate (cell) were adjusted to $I = 0.1$ mol L^{-1} by adding proper amounts of NaCl. Different pH windows, in the range $3.0 \leq pH \leq 10.8$ were monitored; typically, three titrations were carried out per each pH window. Heats of dilution were determined in separate "blank" experiments by titrating the solution of As(III) (containing suitable amount of HCl and ionic medium) into a solution containing the ionic medium (0.1 mol L^{-1}) only.

The net heats of reaction, obtained by subtracting the heat evolved/absorbed in the blank experiments, were analyzed by HypCal [59]. This software, specifically designed for the determination of equilibrium constants and formation enthalpies of complexes in solution, makes use of a non-linear least-squares minimization of the function:

$$U = \Sigma \, (Q_{obs.} - Q_{calc.})^2 \tag{1.6}$$

where $Q_{obs.}$ is the observed heat for a given reaction step, corrected for the dilution (blank) effects, while $Q_{calc.}$ is given by the equation:

$$Q_{calc.} = - \Sigma \left(\delta n \Delta H \right) \tag{1.7}$$

where δn is the change in the number of moles of a reaction product and ΔH is the molar formation enthalpy of the reaction product. The summation is carried out over all the reaction steps of the specific chemical system. The squared residuals $(Q_{obs.} - Q_{calc.})^2$ are summed over all the titration points. The parameters were determined by simultaneously analyzing calorimetric data from different titrations carried out at different pH ranges.

Table 1.7. Experimental conditions for the acid-base properties of arsenite and arsenate in NaCl and T = 298.15 K.

System	$C_{As(III)/As(V)}$[a]	C_H[b]	Ionic Strength range[b]	pH range
As(III)	20	1	0.1-1	3.2-10.5
As(V)	10	0.5	0.1 and 0.7	2.2-11.3

[a]mmol L^{-1}; [b]mol L^{-1}.

Table 1.8. Experimental conditions for the As(III)–ligands systems in NaCl and T = 298.15 K.

System	c_M[a]	c_L[a]	C_H[a]	Ionic Strength range[b]	pH range
As(III)-*tla*	4	400	4	0.15	2.4-9.8
As(III)-*tma*	4	400	4	0.15	2.4-9.8
As(III)-*cys*	5	500	1	0.15	3-10.3
As(III)-*gsh*	5	500	5	0.15	2.5-9.5
As(III)-*NTAP*	12-15	1.8-2.1		0.1	3-10.8
As(III)-*NTA2P*	12-15	2-2.5		0.1	3-10.8

[a]mmol L^{-1}; [b]mol L^{-1}.

Table 1.9. Experimental conditions for the M^{n+} -arsenate systems in NaCl and T = 298.15 K

System	c_M[a]	c_L[b]	C_H[a]	Ionic Strength range[b]	pH range
Mg^{2+}-*ars*	5-7.5	0.1	-	0.7	2.3-9.1
Ca^{2+}-*ars*	5-7.5	0.1	-	0.7	2.3-7.1
Sr^{2+}-*ars*	5-7.5	0.1	-	0.7	2.3-7.1
Fe^{3+}-*ars*	1	0.03	2	0.1-0.7	2.5-2.7
Al^{3+}-*ars*	2	0.05	0.5	0.1-0.7	3.5-4.5

[a]mmol L^{-1}; [b]mol L^{-1}.

1.5 Raman Spectroscopy [55]

1.5.1 General aspects

Raman spectroscopy is a technique widely used in the study of materials, both in the solid and liquid state or in the gas phase. It is classifies as non-destructive method, which allows to obtain information in short times, which does not require particular conditions for the execution of the measurements and can be performed directly on the sample without any preparation. In a Raman scattering experiment, the sample is irradiate with a monochromatic electromagnetic radiation coming from a laser source. The electromagnetic radiation interacting with the electrons of the molecules causing an oscillating electric dipole responsible for the process of diffusion of the incident radiation. By analyzing the diffuse radiation it is possible to distinguish components with different energies. The Rayleigh component comes from an elastic diffusion process that does not involve energy exchange with the system and has the same energy of the incident radiation. Both the Stokes (lower energy with respect to the incident radiation) and the anti-Stokes (higher energy with respect to the incident radiation) components derived from inelastic diffusion processes and produce the so-called *Raman effect*. Generally, the Stokes lines are more intense than the anti-Stokes ones, because, at room temperature, the ground state is more populated than a possible excited state. The main requirement of the source is the production of a monochromatic and intense beam in order to generate a Raman diffusion with a sufficient intensity to be measured with an appropriate signal/noise ratio. For these reasons, laser sources are often employed, especially Nd:YAG laser thanks to its ability to eliminate fluorescence phenomena. In a Raman spectrum, the intensity of the light emission is expressed as a function of absolute frequency (υ), reported as cm^{-1}, or most commonly as Raman shift ($\Delta\upsilon$), namely the difference in wave numbers between the observed radiation and the incident one.

1.5.2 Instrumental equipment

A Jobin Yvon HR 800 micro-Raman spectrometer with a 632.8 nm He−Ne laser line as the excitation source and coupled with a Peltier-cooled charge-coupled device (CCD) sensor was used to acquire Raman spectra. The spectra were collected in the 400−3000 cm^{-1} range using an Olympus BX-41 microscope with a long working-distance ×50 microscope objective. Integration times ranged from 10 to 20 s. In presence of fluorescence phenomena, interferring with the Raman signal at 632.8 nm laser line, spectra were compared to those acquired with a BRAVO Handheld Raman Spectrometer by Duo LASER. This instrument works with two

excitation lasers with wavelengths located in the range 700−1100 nm, which allow to mitigate the fluorescence phenomena.

1.6 Mass Spectrometry [60]

1.6.1 General aspects

Mass Spectrometry is an analytical technique used both for the identification on unknown substances and for the analysis of substances in traces. Often, it is employed in combination with separative techniques, such as Gas Chromatography (GC), High Performance Liquid Chromatography (HPLC) and, recently, Inductive Plasma. Mass spectrometry is able to separate a mixture of ions as a function of its mass/charge ratio, by using static or oscillating magnetic fields. The mixture is obtained by ionizing the molecules of the sample by means of a beam of electrons with known energy. The ionized molecules are unstable and tend to fragment into lighter ions according to the typical fragmentation scheme of their chemical structure. The diagram showing the abundance of each ion as a function of the mass/charge ratio is the so-called mass spectrum, typical of each compound as it is directly related to its chemical structure and to the ionization conditions to which it is subjected. In the spectrum, the *molecular ion* is aradical derived from the loss of an electron from the original molecule. The molecular ion is subject to other fragmentations which led to the formation of molecules and / or neutral radicals (not detectable by the instrument), or cations and / or radical cations, named *fragment ions*, which are discriminated on the basis of their mass/charge ratio and revealed by a detector.

The analyte can be ionized with different techniques that can be divided into hard and soft, according to the produced fragmentations. Electron Ionization (EI) is a method in which energetic electrons impact with solid or gas pahse atoms or molecules to produce ions. It is a hard ionization because it produces a high fragmentation of the molecule that can be very useful for structure determination of unknown compounds. On the other hand, Chemical Ionization (CI) represents a soft ionization technique in which the molecules of a reagent gas are ionized by electron ionization. Subsequently, the produced ions react with analyte molecules in the gas phase in order to achieve ionization. Another soft ionization is represented by Laser Desorption (LD). In this technique, the sample is ionized by means of a laser beam, such as CO_2 (emitting in the far infrared) or Nd/YAG (neodymium / yttrium-aluminum-garnet), which acts in the UV region. If the sample is absorbed on a matrix, the technique is called MALDI (Matrix-Assisted Laser Desorption/Ionization). The matrix is

often made by organic compounds among which the most commonly used are the sinapinic acid, the α-Cyano-4-hydroxycinnamic (α-CHA) acid and the 2,5-dihydroxybenzoic acid (DHB) [61]. It must possess some chemical-physical characteristics:

- – it must be evaporable, but the evaporation not should be significant during the preparation of the sample or before the measurements are performed;
- – it must be a source of protons in order to encourage the sample ionization;
- – it must possess polar groups and it must be water-soluble.

Thanks to the desorption phenomenon, the sample is released in a "clustered" form, namely complexed with the matrix. The matrix damps the effects of the laser beam ensuring adequate protection for the analyte, which is ionized and vaporized by the excess energy transferred secondarily by the matrix itself. Often the MALDI technique is combined with spectrometers equipped with a flight time analyzer.

1.6.2 Instrumental equipment

LD MS and MS/MS analyses were performed using a 5800 MALDI TOF–TOF Analyzer (AB SCIEX) equipped with a neodymium–yttrium–aluminum–garnet laser (laser wavelength 349 nm), in reflection positive-ion mode with a mass accuracy of 5 ppm. At least 4000 laser shots were typically accumulated with a laser pulse rate of 400 Hz in the MS mode, whereas in the MS/MS mode spectra up to 5000 laser shots were acquired and averaged with a pulse rate of 1000 Hz. MS/MS experiments were performed at a collision energy of 1-2 kV, and ambient air was used as the collision gas with a medium pressure of 10^{-6} Torr. After acquisition, spectra were handled using Data Explorer version 4.0.

1.7 Computational methods

1.7.1 Ab initio molecular dynamics

Molecular dynamics (MD) is a computer simulation method used for investigating the temporal evolution of atoms and molecules. By interacting to each other, the constituents of matter lead to the dynamical evolution of the system. *Ab initio* MD methods are computational approaches which, relying upon the quantum mechanics' laws, are able to accurately determine the forces between atoms and molecules. The term *ab initio* means "from first principles" and indicates that no massive parametrizations are present in the typical inputs of an *ab initio* calculation, with a very few exceptions. These methods try to solve the electronic Schrödinger equation by taking into account the positions of the nuclei and the number of electrons. This way, they typically produce information relative to electron densities, energies and other properties of the system. When the Born-Oppenheimer approximation is employed, the dynamics of the nuclei and that of the electrons are decoupled. Since nuclei are significantly heavier than electrons, they can be usefully treated as classical particles, while the electronic subsystem is handled through quantum mechanics (*i.e.*, Density Functional Theory). One of the major advantages in employing *ab initio* methods is represented by their capability to reliably simulate and investigate chemical reactions.

1.7.2 Ab initio molecular dynamics simulations of acid-base properties of As(III) and As(V)

In order to perform *ab initio* molecular dynamics simulations at different pH conditions, five numerical samples containing As(III) species were placed in cubic super-cells. In particular, in one simulation box, As(III) was surrounded by 128 water molecules, while in another one the As(III) species was solvated by 126 water molecules and 2 hydroxide anions. The three remaining boxes were filled with different amounts of water/hydroxide anions, specifically 124 H_2O/4 OH^-, 122 H_2O/6 OH^-, 120 H_2O/8 OH^-. These particular alkaline conditions were chosen in order to reproduce the experimental potentiometric measurements. The same procedure was followed for the As(V) species. Trajectories of 20 ps were accumulated for all the investigated numerical samples, with exception of that having As(III) in presence of 128 water molecules, the latter being simulated for a longer time (*i.e.*, 100 ps). This way, we have been able to appreciate the third hydrolysis step within the timescales typically affordable by *ab initio* molecular dynamics simulations.

All the simulations have been executed by means of the software package CP2K [62],based on the Born-Oppenheimer approach. Electronic wave-functions were expanded on double zeta valence plus polarization (DZVP) basis sets. The gradient-corrected Becke–Lee–Yang–Parr (BLYP) [63, 64] functional in conjunction with D3(BJ) Grimme's dispersion corrections [65, 66] was adopted for exchange and correlation (XC) effects, while Goedecker–Teter–Hutter [67] pseudopotentials were selected to mimic the core electronic interaction. A cutoff energy for the wave function representation of 40 Rydberg (Ry) and a cutoff of 400 Ry for the charge density were employed whereas a timestep of 0.5 fs, typical for Born–Oppenheimer MD, was chosen. All the simulations were performed at the average temperature of 300 K kept constant thanks to the canonical sampling through velocity rescaling method [68].

1.7.3 Ab initio molecular dynamics simulation of As(III)- tla, tma and dmsa systems

With the aim of studying As(III)-*tla* and *tma* interactions from the *ab initio* molecular dynamics standpoint, a numerical sample composed by one thiolactic acid molecule, one arsenic atom and 70 water molecules was placed in a cubic simulation box with edge equal to 13.39 Å under periodic boundary conditions. Such a configuration was equilibrated by using DFT-based Born-Oppenheimer molecular dynamics (BOMD) including empirical dispersion corrections for 5 ps followed by an accumulation run of 50 ps. Different distances between the As atom and the *tla* molecule were tested in order to evaluate the effects on chelation. The same procedure was adopted in the case of *tma,* employing an edge size of the cubic box equal to 13.51 Å. For *dmsa*, 100 water molecules were selected to ensure an appropriate solvation of the molecule whilst a cubic side of 14.88 Å was chosen so as to reproduce the typical water density under ambient conditions. Moreover, in order to avoid spurious divergences caused by the infinite replica of the charged simulation boxes, since As(III) presents a +3 charge, a compensating *jellium* background was added. In order to investigate the chelation process in presence of an increasing number of ligand molecules, numerical samples composed by 3 *tla* molecules, one arsenic atom and 90 water molecules were simulated by BOMD. Similarly, a bigger sample was simulated for the *tma* case as well. To carry out all the simulations, the characteristics described in the previous paragraph were adopted.

1.8 Calculations

1.8.1 Computer programs

For the elaboration of the experimental data, several computer programs were employed in order to determine all the thermodynamic parameters depending on ionic strength and temperature. They are well explained below:

- STACO and BSTAC [69] were used for the elaboration of potentiometric data. Both, by employing the nonlinear minimal least squares method, allow the refinement of the analytical parameters derived from potentiometric measurements at different ionic strength (also taking into account the variation of this one during the titration). These programs are able to calculate the protonation and the stability constant values of the complexes and they also refine the parameters for the dependence on the ionic strength of the constants. In particular, STACO minimize the sum of the quadratic wastes related to the added titrant volumes, while BSTAC performs the same procedure but with respect to the measured potential.

For both calculation programs, a further procedure can be exploited based on two refinement cycles. The first one by employing unit weight, while the second one by using the weight $1/\sigma^2$, where σ derived from the first cycle. This process allows, in the second refinement cycle, to overlook the data affected by high errors in the first cycle.

- ES5CM99 [70] was employed for the elaboration of calorimetric measurements. It allows to determine enthalpy changes in aqueous solution starting from calorimetric data and, moreover, it is able to calculate the concentration of all the species in each point of the titration.

- LIANA [69] is a computer program, written in Pascal code, used for the optimization of experimental data with several peculiarity which make it adapt for the application to analytical chemistry. About this:

  - It may employed for the calculation of the parameters of linear and non-linear equations;
  - Equations can be divided in several partial equations;
  - Different equations may be reported in the same input and the parameters can be present in distinct equations;
  - It is possible to attribute different weights to different variables;
  - Graphs can be displayed for a more rapid evaluation of the results;
  - It allows to solve two or more linear systems simultaneously.

– <u>HYPSPEC</u> [71] is the software used for the determination of equilibrium constants from spectrophotometric data. It is able to process UV/visible, Raman, infrared, luminescence and fluorescence data provided that the spectral intensity of each chemical species is proportional to the concentration of the species in solution. Spectra can be obtained by titration or from a set of individual solutions (batch data).

– <u>HYSS</u> [72] is a software able to perform both titration simulations and calculation of species concentrations. In the first case, a speciation model is specified by means of a set of equilibrium constants and the titration is simulated by reporting a set of titration conditions and calculating the concentrations of each complex species as the titration proceeds. In the second case, a model and a set conditions, such as a pH range, is necessary. The final result is a plot of concentrations suitable for publication.

– <u>HypCal</u> is a windows computer program developed for determining from isothermal titration calorimetry either formation enthalpies using previously determined stability constants or formation enthalpies and stability constants. The program is suitable in the case of complex systems and also competitive ligand systems can be treated. Moreover, it can be used as a simulation program since it is able to designe experiments. Further details are available on Refs. [59, 73].

1.8.2 Equilibrium constants

Protonation constants are expressed as decimal logarithm following the equations reported below:

$$iH^+ + L^{z-} = H_iL^{(z-i)-} \qquad\qquad \beta_i^H \quad (1.8)$$

or

$$iH^+ + H_{i-1}L^{(z-i+1)-} = H_iL^{(z-i)-} \qquad\qquad K_i^H \quad (1.9)$$

where i indicates the protonation step.

The stability constants of the metal-ligand systems refer to the following equilibria:

$$pM^{n+} + qL^{z-} + rH^+ = M_pL_qH_r^{(n-qz+r)} \qquad\qquad \beta_{pqr} \quad (1.10)$$

or

$$pM^{n+} + L_qH_r^{-(qz+r)} = M_pL_qH_r^{(n-qz+r)} \qquad\qquad K_{pqr} \quad (1.11)$$
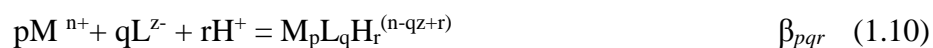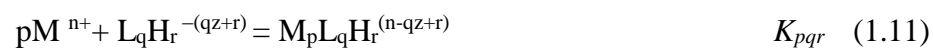
1.8.3 Dependence of the stability constants on the ionic strength

The ionic strength critically influences the protonation constants as well as the hydrolysis of the metal cations and the stability constants of the complex species.

In an ideal solution, the equilibrium constants are calculated considering the concentrations, c, of the species in solution. But a real system, constituted by electrolytes, behaves differently due to the attraction or repulsive forces between ions presents in solutions that prevent to the ions itself to be independent from each other. For this reason, the concentration is replaced by the activity, a, which represents the effective number of particles that take an active part in a given phenomenon. The molar concentration and the activity are correlated by the following relationship:

$$a = \gamma \bullet c$$

where γ is defined as activity coefficient and describes the linearity deviation of the real system from the ideal one and it can be calculated starting from the Debye-Hückel theory. On the basis of that, ions in solutions are considered as point masses whose interactions are only of electrostatic nature and the activity coefficient is associated to the ionic strength, as reported below:

$$\log \gamma_{\pm} = -A \left| z_{+} \cdot z_{-} \right| \sqrt{I_m} \tag{1.12}$$

A is a parameter depending on the solvent and temperature and in water at 298.15 K is equal to 0.5100 $\text{mol}^{-1/2}\,\text{kg}^{1/2}$; z_+ and z_- are the charges of cations and anions respectively and I is the ionic strength. This one represents a limit law as it is valid only at very low concentrations ($I \leq 0.001$ mol L^{-1}). At a later time, considering the idea that ions cannot stay at distance lower than the sum of their radii, Debye and Hückel proposed an extension of the law, suitable until $I \leq 0.01$ mol L^{-1}:

$$\log \gamma_{\pm} = -A \frac{\left| z_{+} \cdot z_{-} \right| \sqrt{I_m}}{1 + 1.5 \sqrt{I_m}} \tag{1.13}$$

Later, another parameter, indicated as *L* or *C,* was added to the equation. It depends on the electrolyte and the ionic strength:

$$\log \gamma_{\pm} = -A \frac{\left| z_{+} \cdot z_{-} \right| \sqrt{I_m}}{1 + 1.5 \sqrt{I_m}} + L(I) \tag{1.14}$$

In our systems, in order to evaluate the dependence of the stability constants on the ionic strength, the employed mathematical model was a Debye-Hückel type equation like that here presented:

$$\log\beta = \log{}^{T}\beta - A\frac{z^{*}\sqrt{I}}{1+1.5\sqrt{I}} + CI \qquad (1.15)$$

where β = protonation or formation constant, ${}^{T}\beta$ = protonation or formation constant at infinite dilution, C is an empirical parameter that dependes on the charges involved in the reaction and $z^{*} = \sum(\text{charges})^{2}{}_{\text{reactants}} - \sum(\text{charges})^{2}{}_{\text{products}}$.

1.8.4 Dependence of the stability constants on the Temperature [74]

The dependence of the formation constants on the temperature can be studied through the Van't Hoff equation, described below:

$$\log^{\mathrm{T}} \beta = \log \beta_{\theta} + \frac{1}{2.303 \mathrm{R}} \Delta H_{\theta}^{0} \left(\frac{1}{\theta} - \frac{1}{T} \right) \tag{1.16}$$

where:

$\log {}^{T}\beta$ = equilibrium constant at a given temperature (expressed in Kelvin);

θ = reference temperature (expressed in Kelvin);

$\log \beta_{\theta}$ = equilibrium constant at $T = 298.15$ K;

R = 8.314472 J K^{-1} mol^{-1}, when ΔH_{θ} is expressed in J mol^{-1}.

This equation allows to calculate the enthalpy changes for a given species by knowing $\log \beta$ values at different temperatures or, in other case, to evaluate the stability constants at a specified temperature, when ΔH_{θ}^{0} is determined by calorimetric titrations. It can be applied both to molar and molal concentration scales. By employing the following relations and the stability constants of the species, $\log \beta_{i}$, the calculation of the Gibbs free energy, ΔG_{i}, and $T\Delta S_{i}$ values may be possible

$$\Delta G_{i} = -RT \ln \beta_{i} \tag{1.17}$$

$$\Delta G_{i} = \Delta H_{i} - T\Delta S_{i} \tag{1.18}$$

The validity of the Van't Hoff equation is verified when the enthalpy changes are approximately constant in a given temperature range.

1.9 Sequestering ability

The evaluation of the capability of a molecule to sequester metal cations is an aspect of great importance especially in environmental and medicinal fields. Chelating agents, namely molecules able to link a specific metal by exerting a chelating effect are often employed to remove heavy metals from natural matrices contaminated for many reasons [75-77]. The same criterion is adopted in the chelation therapy, a medical procedure employed to detoxify the organism from heavy metals. It is the preferred medical treatment for metal poisoning, including mercury, lead, arsenic, uranium and so on [78]. The choice of the sequestering ligand is related to the type of metal to be removed. For example, thiol compounds, such as the dimercaptosuccinic acid (*dmsa*), show high affinity towards soft metals, namely mercury, arsenic and lead [79, 80]. However, the estimation of the sequestering ability of a ligand towards a specific metal is influenced by many factors, in particular the experimental conditions (pH, ionic strength, temperature, ionic medium), the acid-base properties of the ligand as well as the hydrolysis behavior of the metal. Moreover, also the possible interactions with other metals or ligands simultaneously present in natural systems could affect. In order to take into account all these phenomena, the research group proposed in 2006 a semiempirical parameter, initially used without a specific name [81-83], later called pL_{50} [84, 85] and nowadays known as $pL_{0.5}$. It represents the total ligand concentration required to sequester the 50% of a metal present in traces in a given condition, even when other components are simoultaneously present. In can be easily calculated by using the common speciation programs and following the steps reported by Crea *et al.* [86]. The so called sequestration diagram is obtained by plotting the sum of the mole fraction (χ) of the complex species towards pL (pL = -log C_L; C_L = total ligand concentration). It is a sort of sigmoidal, dose-responde curve represented by the Boltzman type equation with asymptote 1 for pL $\rightarrow$ $-\infty$ and asymptote 0 for pL $\rightarrow$ $+\infty$:

$$\chi = \frac{1}{1 + 10^{(pL - pL_{0.5})}} \tag{1.19}$$

The interpretation of this parameter is quite intuitive, since the higher $pL_{0.5}$ the higher the efficiency of the ligand to sequester the metal cation. Moreover, among the advantages there is the possibility to consider all the components and species that could be present in a given system until the capacity of the computer program used for building the speciation/sequestration diagrams for the system under investigation is reached [87, 88].

2

Analytical techniques for arsenic determination in water samples

The fourth section of this research work, as already mentioned, is dedicated to the study carried out at the University of Girona (Spain) and based on the detection of arsenic in natural waters. Therefore, this section could be viewed as the applicative part of the thermodynamic study conducted previously at the University of Messina. The investigation concerned the extraction of arsenic from natural waters by means of PIMs incorporating Cyanex 301 as extractant and the consequent determination of the metalloid. Two techniques were followed to evaluate the extraction efficiency:

– the analysis of the aqueous samples by means of Inductive Coupled Plasma - Optical Emission Spectrometry (ICP-OES), in order to determine the arsenic left in solution and, thus, not extracted by the membranes;

– the direct analysis of the PIMs, containing the extracted arsenic, by means of Energy Dispersive X-Ray Fluorescence (EDXRF) Spectrometry.

Below, a description of both analytical techniques is given.

2.1 Chemicals

As(III)/As(V) stock solutions (150 mg L^{-1}) were prepared by weighing the corresponding salts $NaAsO_2$ (Fluka)/ $Na_2HAsO_4 \cdot 7H_2O$ (Merck) and the working solutions were obtained by diluting the stock solutions in appropriate media, such us 0.1 mol L^{-1} hydrochloric acid, 0.1 mol L^{-1} sodium chloride and 0.1 mol L^{-1} nitric acid (Panreac) solutions. Sodium thiosulfate and potassium iodide (Panreac) were used for the preparation of 1% (w/v) and 0.5% (w/v) solutions respectively, employed for the As(V) reduction. The polymers used for preparing

membranes were polyvinylchloride (PVC) and cellulose triacetate (CTA) purchased from Fluka and Across Organics respectively and the solvents employed for dissolving the polymers were tetrahydrofuran for PVC and chloroform for CTA. Bis(2,4,4-trimethylpentyl)dithiophosphinic acid, Cyanex 301, (Cytec) was employed as extractant and used as received. Calibration standards of As were prepared using a standard As solution (1000 mg L^{-1}) for ICP purchased from Sigma Aldrich.

2.2 Inductive Coupled Plasma - Optical Emission Spectroscopy (ICP-OES) [55]

2.2.1 General aspects

The atomic emission spectrometry inductively coupled with plasma and optic detector (ICP-OES) is a technique widely used for the determination of inorganic elements present in different matrices and it is one of the analytical methodologies more frequently employed for the determination of heavy metals in low concentrations. The instrument is featured by a torch, where the nebulised sample is introduced after the generation of the plasma, and by an optic part which collects and quantifies the light intensity emitted by the analysed elements. To start the ICP discharge, a spark or a voltaic arc is applied to the argon. This discharge absorbs energy from the magnetic field and transforms the argon into a stable plasma whose temperature is between 7000 and 10000 °K, condition in which all the elements in the nebulised sample reach an energy level higher than the fundamental state. The electrons in the excited state return to the ground state either directly or through intermediate states. In these steps, the emission of light energy quanta occurs which generates an emission spectrum at different wavelengths (lines). Each line of the spectrum originates from a particular electronic transition between two different energy levels, and since each atomic species is characterized by a series of possible states or energy levels, the atoms produce their own characteristic emission spectrum. To carry out the analytical determination, the sample is taken automatically and transported to the pneumatic nebulizer by a peristaltic pump. The aerosol produced by the pneumatic or ultrasonic reaches the plasma; here, following phenomena of thermal excitation, the production of the light emission spectrum is made up of the characteristic lines of the elements present. The quantitative determination of the analytes present in the sample can be performed by comparing the intensities of the signals obtained on the sample, with respect to multi-element reference solutions of known concentration.

2.2.2 Instrumental equipment and procedure

For the analysis of the arsenic in aqueous solutions, an Agilent ICP-OES 5100 Synchronous Vertical Dual View (SVDV) spectrometer was used and the determination was performed at $\lambda = 193.696$ nm. Samples were introduced into the plasma with a peristaltic pump.

2.3 Energy Dispersive X-Ray Fluorescence (EDXRF) Spectrometry [89]

2.3.1 General aspects

This analytical technique is widely used for the elemental analysis or chemical characterization of a sample. It is based on the principle of the X-Ray fluorescence spectrometry: the use of an excitation radiation produces an ionization in the inner shells of the atoms present in the sample as a consequence of a photoelectric absorption. When the photon, having an energy larger than the binding energy of an electron of the inner orbital, impacts on the atom, part of the energy is absorbed (photoelectric absorption) and the electron is ejected from its position. This event produces a vacancy that brings the atom into an unstable state (ionized atom). In this case, two processed could occur:

– the emission of other photoelectrons (Auger effect) due to a rearrangement;

– the transfer of an electron from one of the outer orbitals to fill the vacancy. The difference in energy between the initial and the final states gives origin to the X-Rays emission.

Of course, not all the transitions are allowed, in accordance with the quantum mechanics postulates, and this aspect makes this technique able to uniquely identify the atoms present in the sample. The transitions are, generally, indicated with the name of the element under investigation, followed by the name of the shell in which the initial hole occurred plus a Greek letter (α, β, γ) indicating the intensity of the line, *e.g.* As Kα. When the incident X-Ray photon interacts with the sample, a part of the radiation could also be transmitted through the sample or scattered back from it. The last event occurs when the photon impacts on the electrons of the target element and, in this case, it can be a *coherent* scatter (Rayleigh scatter), when no change in energy is registered, or *incoherent* scatter (Compton), when part of the energy of the photon is transferred during the collision. Therefore, in the spectrum, peaks related to Rayleigh and Compton scatter of the incident beam could be observed.

In the energy dispersive analysis, on the other hand, the fluorescence radiation emitted by the sample is detected, as a function of energy, by a solid-state detector that allows to identify all the detectable elements present in the sample in a single measurement. This allows, among other things, to shorten the measurement times drastically with respect to dispersive wave analysis.

2.3.2 Instrumental equipment and procedure

For the arsenic analysis contained in PIMs, a touch-control S2 RANGER EDXRF system (Bruker AXS, GmbH, Germany) with a Pd X-ray tube (max. power of 50 W) and a XFLASH™ Silicon Drift Detector (SDD) with a resolution of 129 eV at Mn-K$_\alpha$ was used. The X-ray tube was set at 40 kV and the intensity was adjusted to 250 µA to obtain a maximum count rate of 100.000 counts/s. In order to get the best signal to noise ratio and the best analytical response for As measurement, an Al foil of 500 µm thickness was employed as primary filter. Measurement time was set at 200s as a trade-off between an acceptable repeatability of measurements and total analysis time. The software employed to control the equipment and to perform data elaboration was Spectra EDX (Bruker AXS, GmbH, Germany). PIMs were arranged between two 4.0 µm thick prolene X-ray foils (purchased from Chemplex Industries, Inc., Palm City, US) placed in Teflon cups of 3.4 cm which incorporates a snap-on ring at the end of the cell for attachments of thin-film supports. On the top of the cell, a boric acid pellet (1.5 cm height) was placed as a back stopper. Then, samples were introduced in the sample holder of the equipment for EDXRF analysis.

Section II

Arsenic(III): acid-base properties and interaction with different classes of ligands in aqueous solution

As already mentioned, arsenic is a metalloid, which means it can behave like metal or non-metal. In the trivalent forms, (As(III)), it behaves like cadmium, with a preference for thiol ligands [90]. In this section, the metallic behavior of As(III) was investigated by studying its interaction with several ligand classes. First of all, the acid-base properties of arsenite were determined, considering the effect of ionic strength and temperature, and the hydrolysis mechanism was elucidated by means of molecular dynamics simulations. Later, since most of As(III) effects are attributed to its marked affinity towards the sulfhydryl groups of the proteins [1, 3, 4, 44] the research work saw as protagonists the thiol compounds. In particular, thiolactic acid (*tla*), thiomalic acid (*tma*), dimercaptosuccinic acid (*dmsa*), cysteine (*cys*) and glutathione (*gsh*) were in depth studied and then, in order to complete the study with ligands of biological interest, carboxylic acids, amino acids and nucleotides were also investigated. Finally, for their chelating properties, phosphonic acids derived from nitrilotriacetic acid were also analyzed in order to evaluate their sequestering ability towards As(III) and, therefore, their possible use as chelating ligands in the removal techniques. The best speciation models were selected on the basis of several criteria, in particular the best fit between experimental and calculated curves, probability, formation percentages of the species and simplicity [91, 92] and the stability constants (log β) of all the determined metal-ligand species were defined. Also the sequestering ability, well discussed in 1.9 paragraph of the Section I, was evaluated for all the systems in different experimental conditions.

1

As(III) acid-base properties: results and discussion

The common oxidation states of arsenic in natural waters are +3 and +5. As regards the first one, it occurs in aqueous solution as H_3AsO_3 and it seems that it has not been isolated as pure material. It is featured by three hydroxyl groups linked to the central arsenic atom and, in presence of alkali metal cations, it is converted in arsenite ions $[AsO(OH)_2]^-$, $[AsO_2(OH)]^{2-}$, and $[AsO_3]^{3-}$. The peculiarity of this compound is that, at the pH of most natural waters, it exists in indissociated form that make more difficult its removal with respect to arsenate which can be easily removed thanks to the presence of anionic charges [93, 94]. In this chapter, the typical thermodynamic parameters of arsenite were determined through potentiometric and calorimetric titrations in an ionic strength range between 0.1 and 1 mol L^{-1} and at T = 298.15 K. The possibility to model the ionic strength dependence with the help of the Debye Hückel type equation, allowed to define the protonation constants at ionic strength values different from those under study and, thus, to simulate the species distribution in conditions of natural and biological fluids. The classical experimental investigations were accompanied by computational studies which, by employing *ab initio* molecular dynamics techniques, atomistically traced the hydrolysis steps of As(III) in an aqueous environment.

1.1 Computational results

For arsenous acid, three hydrolysis steps are expected. The first one (Figure 1.1a, taken from Ref. [95]) involves a water dissociation induced by arsenic, in which a water molecule binds to As atom and releases a H^+ proton to another water molecule by following the known Grotthuss mechanism. This process occurs in 65 fs (τ_1), a timescale hard to explore experimentally which differs from that reported by Canaval *et al.* [96] equal to 144 fs but it is in agreement with the value (60 fs) ascribed by Coskuner *et al.* [97]. The second step (Figure 1.1 b), along the line of the previous one, occurs in 270 fs (τ_2), similar to that obtained by a QM/MM scheme [96] and at Hartree–Fock level of theory in a QMCF-MD simulation [62]. It is important to highlight that the solvation shells play a key role for the transfer of the proton during the hydrolysis phases and this aspect takes on greater importance in the third step which allows to the formation of arsenous acid (H_3AsO_3). In this case, longer times are registered equal to 28 ps (τ_3) and the formation of an hydroxide anion (OH^-) in one of the solvation shell of the $[As(OH_2)]^+$ complex is required in order to promote the proton transfer between two water molecules and the OH^- species. This one results very slow because of the electrostatic stabilization due to alternating charged layers (Figure 1.1 c). In order to check the As(III) behavior in alkaline conditions, two pairs of OH^- were put in the simulation cells. The addition of hydroxide anions decreases the timescale of one order of magnitude (28 ps vs. 1.5 ps). This value further drops (130 fs) when two more and other two more OH^- species are added, indicating an ultrafast protonic re-organization. Therefore, after ~ 1.4 ps the transient arsenous acid evolves to di-hydrogen arsenite species ($H_2AsO_3^-$) that represents the more stable species under such a condition.
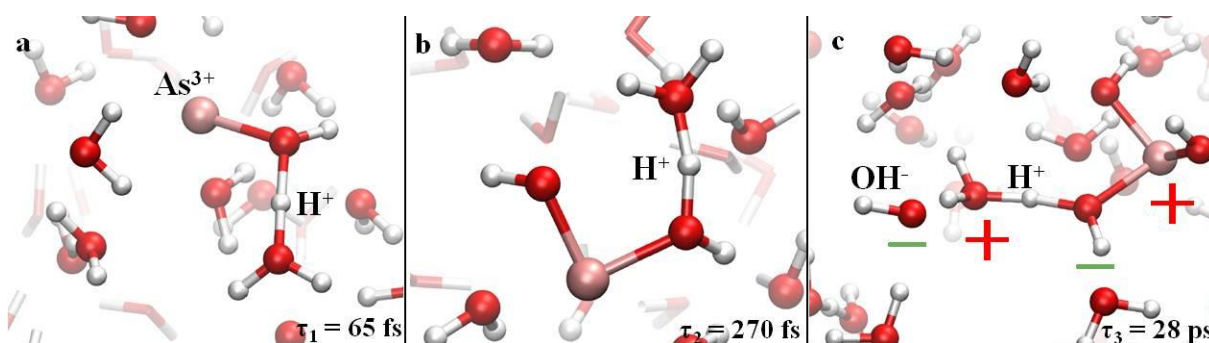
Figure 1.1. Hydrolysis steps of As(III) until the formation of arsenous acid (H_3AsO_3). Red, white, and pink spheres represent oxygen, hydrogen and arsenic atoms, respectively. In (c) the signs indicate the local charge established after the proton transfer which stabilizes the adjacent water counter-ions [95].

1.2 Experimental results

1.2.1 Protonation constants determination

The acid-base properties of As(III) were studied by employing different arsenite concentrations, at ionic strength ranging from 0.1 to 1 mol L^{-1} and at T = 298.15 K. From literature data [98], we know that As(III) in aqueous solution is mainly present as arsenous acid (H_3AsO_3) and the main protonation equilibrium, for a large pH range, turns out to be the following:

$$H^+ + H_2AsO_3^- = H_3AsO_3^0 \tag{2.1}$$

Arsenous acid, as anticipated in the previous paragraph, presents other two protonation equilibria, specifically:

$$H^+ + HAsO_3^{2-} = H_2AsO_3^- \tag{2.2}$$

$$H^+ + AsO_3^{3-} = HAsO_3^{2-} \tag{2.3}$$

However, these protonation constants have values equal to 12.13 and 13.4 respectively [98, 99], that are not easily detectable and moreover the investigation of this pH range is not of interest for natural waters. For these reasons, the potentiometric titrations were performed in 2-11 pH range and only one protonation step was evaluated. The protonation constant, obtained by processing potentiometric measurements by means of BSTAC program, is reported in Table 1.1 at different values of ionic strength. As can be noticed, the protonation values decrease by increasing the ionic strength. For example, log K changes from 9.124 at I ~ 0.1 mol L^{-1} to 9.021 at I ~ 1 mol L^{-1}.

Table 1.1. Experimental protonation constant of As(III) in NaCl at $0.1 < I/$ mol L$^{-1} < 1$ and at T = 298.15 K

I/mol L^{-1}	log K[a]
0.111	9.124 ± 0.003[b]
0.247	9.059 ± 0.002
0.494	9.028 ± 0.002
0.971	9.021 ± 0.002

[a] K refers to the equilibrium (1.9); [b] ± standard deviation.

1.2.2 Dependence on ionic strength

The dependence of the protonation constant on the ionic strength was studied by taking into account the values reported in Table 1.1, elaborated by means of the Debye-Hückel type equation (eq. 1.15), which allowed to obtain the following $\log^T K$ value together with the empirical parameter C, at T = 298.15 K:

$$\log {}^T K = 9.331 \pm 0.006$$

$$C = 0.097 \pm 0.009$$

As already mentioned, the knowledge of these parameters is of great importance since it gives the possibility to evaluate the protonation constants in conditions that differ from the experimental ones. The influence of the ionic strength is also visible on the species distribution, as can be observed in Figure 1.2.
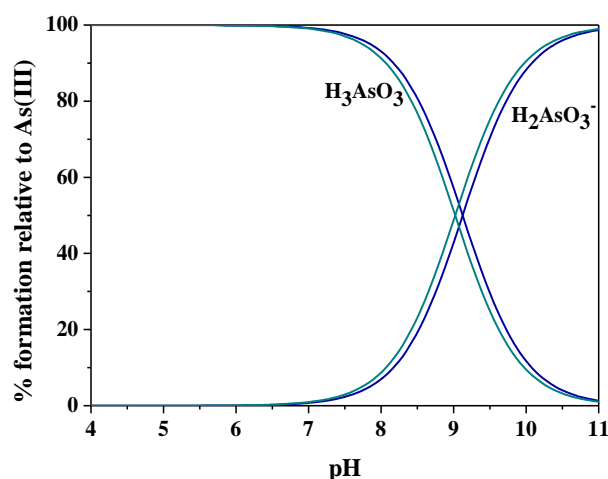
Figure 1.2. Distribution diagram for As(III) species in NaCl at $I = 0.1$ mol L^{-1} (blue lines), $I = 1$ mol L^{-1} (cyan lines) and T = 298.15 K. $C_{As(III)} = 1$ mmol L^{-1}.

The increase of the ionic strength from 0.1 mol L^{-1} to 1 mol L^{-1} causes a shift of the curves towards lower pHs and, as already indicated, the predominant species up to pH ~ 7 is the indissociated one. Above this value, the deprotonation process takes place and at pH close to 9 there is the coexistence of $H_3AsO_3/H_2AsO_3^-$ species. In the pH range under investigation no further protonation steps were identified, as also confirmed by the *ab initio* MD simulations under alkaline conditions.

1.2.3 Dependence on temperature

In order to complete the thermodynamic picture and to evaluate the dependence of the protonation constant on the temperature, the formation enthalpy was determined by means of

calorimetric titrations at T = 298.15 K, and in NaCl at different ionic strength values, in particular 0.1, 0.5 and 1 mol L^{-1}. ΔH values together with ΔG and TΔS results are summarized in Table 1.2. Specifically, ΔG and TΔS values were calculated from eqs. 1.17 and 1.18 respectively.

Table 1.2. Thermodynamic formation parameters for arsenous acid in NaCl at different ionic strengths and T = 298.15 K

I/mol L^{-1}	ΔH[a),b)]	$-\Delta G$[a),b)]	TΔS[a),b)]
0.1	-26.5 ± 0.3[c)]	52.04 ± 0.02[c)]	25.5 ± 0.3[c)]
0.5	-30.1 ± 0.3	51.51 ± 0.01	21.4 ± 0.3
1	-23.2 ± 0.4	51.45 ± 0.01	28.2 ± 0.4

[a)] Parameters refer to equilibrium (1.9); [b)] In kJ mol^{-1}; [c)] $\pm$ standard deviation.

As can be observed, the enthalpy values are negative for all the ionic strengths and, in absolute value, they are similar to TΔS. Thus, the main contribution to the free energy cannot be due to the entropic one, probably because of the presence of the hydroxyl groups linked to As(III) atom that could cause some loss of rotational freedom.

The Van't Hoff equation (eq. 1.16) allows to calculate, by using the ΔH values determined at T = 298.15 K, the protonation constants at different temperatures. An example of the species distribution by varying the temperature is given in Figure. 1.3 at I = 0.1 mol L^{-1}, T = 298.15 K and T = 310.15 K.
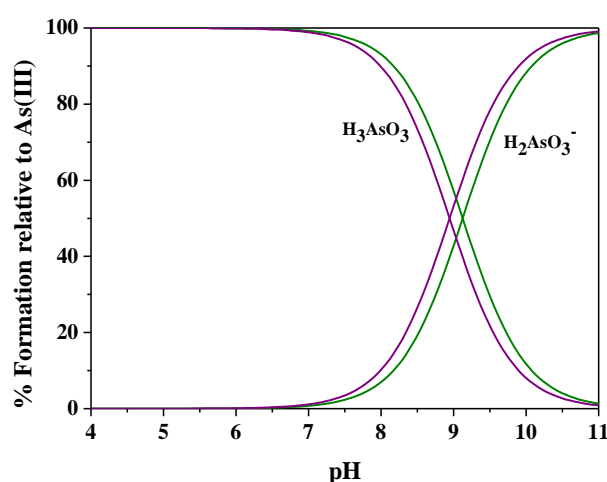
Figure 1.3. Distribution diagram for As(III) species in NaCl at I = 0.1 mol L^{-1} and T = 298.15 K (green lines) and T = 310.15 K (purple lines); C$_{As(III)}$ = 1 mmol L^{-1}.

The diagram shows a displacement of the curve towards lower pHs when temperature increases as a consequence of the decreasing of the protonation constants.

The possibility to calculate the protonation constants at ionic strengths and temperatures different from those under investigation allowed to simulate the distribution in some natural fluids. Specifically fresh water ($I = 0.001$ mol L^{-1}, T = 298.15 K, pH = 5), sea water ($I = 0.7$ mol L^{-1}, T = 298.15 K, pH = 8.1) and blood ($I = 0.15$ mol L^{-1}, T = 310.15 K, pH = 7.4), reported in Figure 1.4.
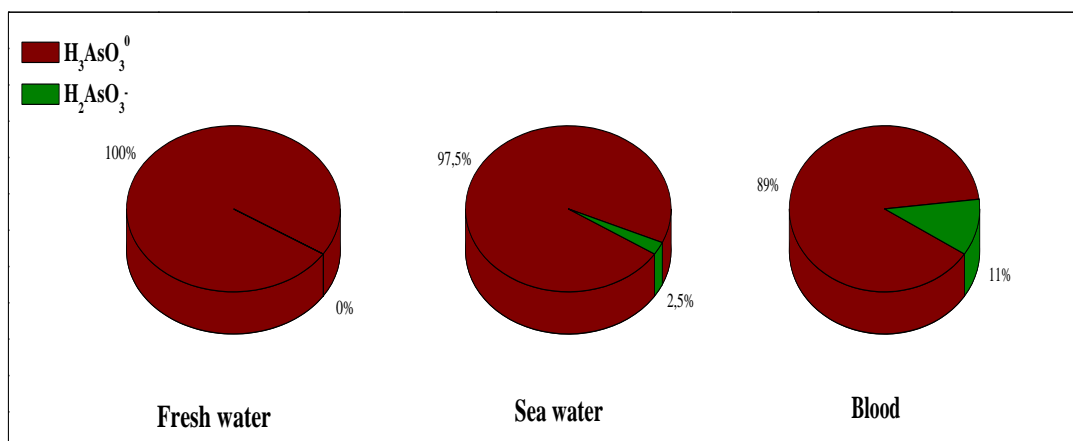
Figure. 1.4 As(III) distribution in some natural and biological fluids

As can be noticed, the distribution of arsenic species is widely affected by the considered conditions. In fresh water, arsenic is totally present in indissociated form, namely as arsenous acid. Also at the conditions of sea water, H_3AsO_3 is the predominant species, with a formation percentages equal to 97.5%. Only the 2.5% is in the anionic form ($H_2AsO_3^-$). Slightly different is the situation at physiological conditions, in which the anionic species reaches a significant formation percentage (18%), although it is lower than the other one which results equal to 89%.

1.3 Final remarks

The synergical utilization of computational methods together with experimetal one allowed to explore the hydrolytic behavior of As(III). In particular:

- the time (τ_3) that leads to the formation of the stable arsenous acid (H_3AsO_3) statistically occurs at 28 ps. This result is not in agreement with that one reported by Canaval *et al.* which evidenced a under-estimated equal to 12 ps when hybrid QM/MM simulations were used [96].

- By adding hydroxide ions (OH^-), τ_3 decreases of more than one order of magnitude leading to the formation of the $H_2AsO_3^-$ anionic species, which becomes the predominant under the explored experimental conditions.

- No further species are observed both by MD simulations and experimental procedures.

- Calorimetric titrations provided the formation enthalpy of the only equilibrium (2.1) and the values of ΔG together with the TΔS were calculated by means of eqs. (1.17) and (1.18).

2

As(III)-thiols interactions: results and discussion

The main cause of the nefarious effects caused by As(III) is linked to its affinity towards sulfhydryl groups, especially present in cellular proteins. The bond with a specific protein, in fact, could alter the conformation and inhibit the biochemical functions. It was verified that it interferes with the activity of abot 200 enzymes, among which glutathione reductase [100], thioredoxin reducatse [101] and pyruvate dehydrogenase. In this case, for example, arsenic forms a very stable complex with the lipoic acid by binding with the thiol groups present in the molecule. This strong interaction blocks the reaction catalyzed by the pyruvate dehydrogenase complex, which consists in oxidizing the pyruvate to acetyl-CoA, main substrate of the Krebs cycle [1]. The high toxicity of Lewisite (β-chlorovinyldichloroarsine), a chemical warfare agent rediscovered by Captain W. Lee Lewis during the latter part of World War I, is related precisely to the inhibition of the oxidation of the piruvic acid [102]. On the other hand, *what kills can cure* and thus arsenic, since ancient times, was exploited to treat several desease. Thomas Fawler, for example, developed a solution of arsenic trioxide in potassium bicarbonate (1% w/v) which became a standard remedy to nurse anemia, Hodgkin's disease, and leukemia [9]. Indeed, As_2O_3 was successfully employed as chemotherapeutic agent for treating some types of cancer. Specifically, the direct binding of arsenic to cysteine residues in zinc fingers located in the promyolocytic leukemia fusion protein (PML-RARα) could be one of the possible modes of action leading to APL remission [103]. Despite this, very few studies are reported in literature describing the As(III)-thiols interaction from the thermodynamic point of view. Considering that this aspect is of relevance to understand the mechanism of action of As(III), most of this thesis work is focused on the interaction of

As(III) with thiol ligands. Thiols are organosulfur compounds that contain a sulfur-hydrogen bond, analogous to the hydroxyl group (-OH) of alcohol, named thiol or sulfhydryl group. These compounds, especially molecules with low molecular weight, are characterized by a strong odor similar to that of garlic or rotten eggs. For this reason, they are used as odorants in order to detect possible gas leaks since natural gas in pure form is odorless. Thus, the characteristic "smell of gas" is due to the smell of the thiol used as odorant. Thiols represent the major portion of antioxidants in the body and they play an important role in defense against reactive oxygen species. Moreover, the role played in detoxification, signal transduction, apoptosis and various other functions at molecular level is not to be underestimated. In fact, decreased levels of thiols were registered in various medical disorders including chronic renal failure and others related to kidney, cardiovascular disorders, diabetes mellitus, alcoholic cirrhosis and many others [104]. Many thiols are often employed as chelating agents in chelation therapy with the aim to remove toxic metal ion from sensitive tissue sites in the critical organs. This can be possible if the affinity of the metal towards the complexing agents is higher than for the sensitive biological molecules [105].

In this thesis, to describe the As(III)-thiols interactions, thiolactic acid (*tla*), thiomalic acid (*tma*) and dimercaptosuccinin acid (*dmsa*) were initially chosen as model molecules. Thiolactic acid *(tla)* is a metabolite of *Tiopronin*, a thiol drug used to control the rate of cystine precipitation and excretion in the cystinuria disease [106]. Thiopronin has activity comparable to that of gold salts and penicillamine in rheumatoid arthritis. This activity would seem to be due to the antioxidant action of the drug [107, 108]. Thiomalic acid *(tma)* is biologically important and it is employed as antidote against cadmium, mercury and arsenic poisoning. A study of Patil *et al.* demonstrated that *tma* coordinates with zinc, cadmium, mercury and lead through sulphur and one of the oxygen atoms of the carboxylate group [109]. Dimercaptosuccinic acid *(dmsa)* is the US standard of care for the treatment of lead, arsenic, and mercury poisoning and it is approved for the removal of lead by the Food and Drug Administration. It was first synthesized by V. Nirenburg in the Urals Polytechnic Institute, following a commission by one of the electrical enterprises of Sverdlovsk which was looking for a medicine to prevent poisoning of the personnel which used tons of mercury. Its distribution is, basically, extracellular type and it is primarily excreted by urine [110]. All the systems were investigated by means of potentiometry and spectrophotometry in NaCl at $I =$ 0.15 mol L^{-1} and T = 298.15 K. *Ab initio* molecular dynamics simulations were also performed in order to have more information regarding the coordination of the metalloid to

the functional groups in the molecules. Raman spectroscopy was employed as confirmation technique about the coordination sites preferred by As(III).

Once defined the interactions with model molecules, gluthatione (*gsh*) and cysteine (*cys*) were studied given the biological importance of these molecules in human organism. Cysteine *(cys)* is a nonessential aminoacid whose thiol side chain often participates in enzymatic reactions, as a nucleophile. It is synthesized by the human body in presence of sufficient amount of methionine under physiological conditions. Due to the presence of the thiol group, cysteine can undergo redox processes. In particular, the oxidation can produce a disulfide bond, also called disulfide bridge, in which two sulfur atoms of two thiol compounds are linked by a single covalent bond. A typical molecule in which this type of bond is observable is the cystine, derived from the fusion, through sulfhydryl groups, of two cysteine molecules. This reaction is reversible, since the reduction of this disulphide bond regenerates two cysteine molecules. This amino acid is significantly present in human hair and the presence of the disulfide bridges lends the typical wavy shape. About its applications, cysteine is widely employed in the food, pharmaceutical and personal-care industries. For example, cysteine is used as odour precursor in the flavour and fragrance industries [111, 112]. The thiol residue of cysteine is involved in many reactions with metal cofactors in enzymes. Examples include zinc in zinc fingers and alcohol dehydrogenase, copper in the blue copper proteins and many others [113, 114]. The sulfhydryl group also shows high affinity for metals such as mercury, lead, and cadmium and, thus, proteins containing cysteine, such as metallothionein, could bind these metals [115]. Recently the use of *tla* has been proposed in the skin desfoliant treatments (peeling) [116]. Glutathione *(gsh)* is the tripeptide γ-L-glutamyl-L-cysteinylglycine and it represents the intracellular thiol present in major concentration. It performs various functions, such as protecting cells from the toxic effects of reactive oxygen compounds (ROS), it takes part in reactions which involve the synthesis of proteins and nucleic acids and in all the reactions that detoxify free radicals and peroxides. Moreover, it serves as storage and transport form of cysteine moieties [117, 118]. The investigation was mainly carried out through potentiometry. Spectrophotometry was only employed for As(III)-*cys* system because in the case of glutathione, at the best experimental conditions (low concentrations in order to have a maximum value of absorbance equal to 1), the formation percentages of the complex species were too low to be determined. For both systems, the study was conducted in a wide range of ionic strength ($0.15 < I/$mol L$^{-1} < 1$) and at T = 298.15 K. For spectrophotometric measurements only $I = 0.15$ mol L^{-1} was taken into account. Calorimetry technique was used in order to determine the formation enthalpies of the complex species at $I = 0.15$ mol L^{-1} in

NaCl and T = 298.15 K as well as for As(III)-*tla*, *tma* and *dmsa* systems. For the determination of the stability constants of the complex species, As(III) hydrolysis constant, obtained and discussed in the previous chapter, and ligands protonation constants were taken into account. All the ligands are shown in Figure 2.1.

2-mercaptopropanoic acid or thiolactic acid (*tla*)   2-mercaptosuccinic acid or thiomalic acid (*tma*)   *Meso*-2,3-dimercaptosuccinic acid (*dmsa*)

Glutathione (*gsh*)   Cysteine (*cys*)
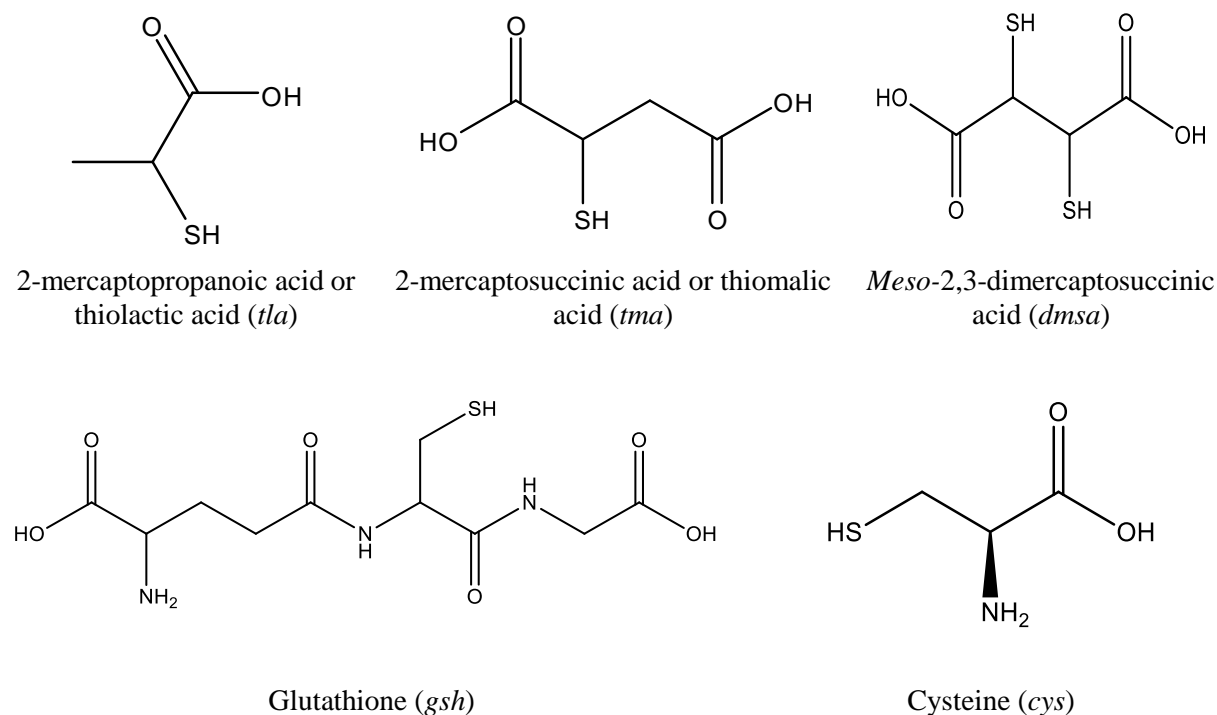
Figure 2.1. Ligands under investigation

2.1 Ligand protonation constants

Before investigating the interaction of As(III) with thiol compounds, the knowledge of the acid-base properties of the metal and of the ligands is mandatory. In this paragraph the protonation constants of all the studied ligands are listed in Table 2.1. For *tla*, *tma*, *cys* and *gsh* molecules, data were available inasmuch they have already been determined by the research group in NaCl at different ionic strengths and T = 298.15 K. The reported values, when necessary, were recalculated at the ionic strength of interest. For *dmsa* ligand, the acid-base properties were studied during this research work and they were determined at $I = 0.15$ mol L^{-1} and at various temperatures, in particular T = 288.15 K, T = 298.15 K, T = 310.15 K and T = 318.15 K. They are presented in Table 2.2. As can be noticed, all the values increase by increasing the temperature. As an example, the protonation constant of the monoprotonated species (LH) is 10.96 at T = 288.15 K while it shows a value equal to 11.32 at T = 318.15 K, that is almost an order of magnitude higher.

Table 2.1. Protonation constants of *tla, tma, dmsa, cys* and *gsh* at different ionic strength in NaCl at T = 298.15 K

Ligand	Species [a]	$I = 0.15$ [b]	$I = 0.5$ [b]	$I = 0.75$ [b]	$I = 1$ [b]	Ref.
		$\log\beta^H$				
tla	**LH**	10.02	-	-	-	[119]
	LH₂	13.52	-	-	-	
tma	**LH**	10.227	-	-	-	[119]
	LH₂	14.997	-	-	-	
	LH₃	18.507	-	-	-	
dmsa	**LH**	11.01 ± 0.04[c]	-	-	-	This thesis
	LH₂	20.32 ± 0.03	-	-	-	
	LH₃	23.87 ± 0.02	-	-	-	
	LH₄	26.39 ± 0.03	-	-	-	
cys	**LH**	10.46	10.28	10.27	10.26	[79]
	LH₂	18.78	18.54	18.55	18.56	
	LH₃	21.04	20.68	20.61	20.54	
gsh	**LH**	9.447	9.298	9.284	9.302	[120]
	LH₂	18.08	17.851	17.848	17.884	
	LH₃	21.567	21.312	21.31	21.375	
	LH₄	23.686	23.485	23.50	23.616	

[a] According to the reaction (1.8), charges omitted for simplicity; [b] in mol L^{-1}; [c] $\pm$ standard deviation.

Table 2.2. Protonation constants of *dmsa* at $I = 0.15$ mol L^{-1} in NaCl and at different temperatures

Species [a]			**$\log\beta^H$**		
	T/K	288.15	310.15	318.15	Ref.
LH		10.96 ± 0.02[b]	11.27 ± 0.02	11.32 ± 0.03	This thesis
LH₂		20.15 ± 0.03	20.64 ± 0.02	20.82 ± 0.03	
LH₃		23.51 ± 0.05	24.35 ± 0.02	24.61 ± 0.02	
LH₄		26.14 ± 0.04	26.85 ± 0.02	27.09 ± 0.02	

[a] According to the reaction (1.8), charges omitted for simplicity; [b] $\pm$ standard deviation.

2.2 As(III)-*tla*, -*tma* and -*dmsa* complexes

2.2.1 Thermodynamic results

For the investigation of the As(III) interaction with thiolactic, thiomalic and dimercaptosuccinic acids, potentiometric and spectrophotometric titrations were performed by using different metal-ligand ratios, reported in Table 1.4 and Table 1.6 respectively of the Section I, and at $I = 0.15$ mol L^{-1} and T = 298.15 K.

After several trials, the elaboration of the data allowed to define the best speciation models on the basis of the criteria exposed in the introductory part of the Section II, as well as the stability constants of the complex species, listed in Table 2.3. For As(III) –*tla* and –*tma* systems, the speciation models are featured by monocoordinated species (differently protonated) as well as tricoordinated ones. Specifically, for *tla* the mono-coordinated species are the ML with log β = 3.33 and the mono-protonated MLH whose log β is equal to 12.11. These results were well confirmed by spectrophotometric titrations, carried out in the range $210 < \lambda < 300$ nm. The values of the stability constants (log β = 12.99 and 3.94 for MLH and ML respectively), in fact, are in agreement with those determined by potentiometry, as can be seen in Table 2.3.

Table 2.3. Formation constants of As(III)- *tla, tma* and *dmsa* complex species at $I = 0.15$ mol L^{-1} in NaCl and T = 298.15 K

		log β[a]	
Ligand	**Species**	**Potentiometry**	**Spectrophotometry**
tla	**MLH**	12.11 ± 0.05[b]	12.99 ± 0.04[b]
	ML	3.33 ± 0.06	3.94 ± 0.02
	M(LH)₃	36.28 ± 0.05	-
tma	**MLH₂**	17.98 ± 0.01	18.00 [c]
	MLH	13.48 ± 0.01	13.74 ± 0.02
	ML	4.41 ± 0.02	3.82 ± 0.05
	M(LH₂)₃	52.13 ± 0.05	-
	M(LH)₃	37.70 ± 0.06	-
dmsa	**MLH₃**	29.97 ± 0.08[c]	30.27 ± 0.04[c]
	MLH₂	25.87 ± 0.09	26.32 ± 0.03
	MLH	16.59 ± 0.09	17.16 ± 0.02

[a] Refers to the reaction (1.10), charges omitted for simplicity; [b] ± standard deviation; [c] value kept constant.

In light of the data reported in literature in which As(III) often coordinates three molecules of thiol ligand [121, 122], also tri-coordinated species were insert in the calculation. However, only the M(LH)$_3$ was defined but in presence of higher ligand concentrations. For As(III)-*tma* system, a similar speciation model was found, but since thiomalic acid presents three binding sites, also di-protonated species, such as MLH$_2$ and M(LH$_2$)$_3$, were determined. Also in this case the spectrophotometry played a key role for the definition of the model, since no data are reported in literature for an adequate comparison. Although in the elaboration of the spectrophotometric data it was necessary to keep constant the value of the stability constant of the MLH$_2$ species, the other two, relative to the simple metal-ligand species (ML) and the mono-protonated one (MLH), were determined in the same range of wavelengths used for As(III)-*tla* system, showing a good correspondence with the potentiometric results (Table 2.3). It is important to highlight that the concentrations usable in spectrophotometry are quite low thus, in these experimental conditions, is not possible to define species with a stoichiometry that requires ligand concentrations two or three order of magnitude higher than the metal cation. First of all, preliminary experiments, for both systems, were performed on the solutions containing only the ligand together with HCl and NaCl in order to determine the molar absorption coefficients of the ligand species. Later, the same experiments were carried out on solutions containing different metal-ligand ratios, the background salt and hydrochloric acid with the aim to investigate a wide pH range (2 < pH < 11). As an example, the absorption coefficients of the As(III)-*tma* complexes together with those of the ligand species are showed in Figure 2.2.

Figure 2.2. Molar absorption coefficients of As(III)-*tma* complexes together with those of the ligand species.

By observing the formation constants of the ML species can be noticed that the stability increases from *tla* to *tma*, namely with the increase of the carboxylic groups. This aspect could suggest a possible involvement of these functional groups on the coordination.

Once the stability constants are known, the distribution of the complex species, on the basis of the pH variation, can be evaluated. Examples are given in Figure 2.3 considering two different experimental conditions, in particular:

- Low ligand concentrations ($C_M = 1$ mmol L^{-1} and $C_L = 5$ mmol L^{-1})
- High ligand concentrations ($C_M = 1$ mmol L^{-1} and $C_L = 20$ mmol L^{-1})
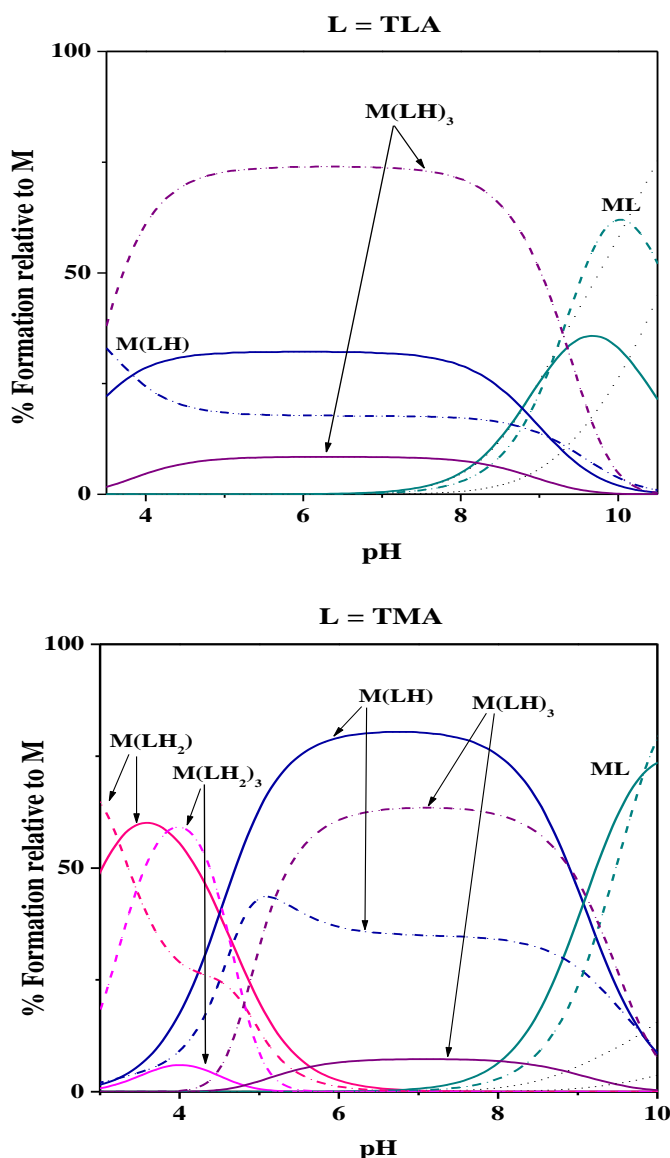
Figure 2.3. Distribution diagrams of As(III)-*tla* and –*tma* systems at $I = 0.15$ mol L^{-1} in NaCl, T = 298.15 K. Low concentration of ligand (solid lines), high concentrations of ligand (dotted lines).

It is easily observable that the tri-coordinated complexes prevail when high concentrations of ligand are taken into account. Otherwise, their formation percentages are not significant, since at physiological pH, $M(LH)_3$ species for both systems reach ~10% unlike the monocordinate complex (MLH) which presents a formation percentage close to 80% in the case of *tma* and ~30% in the case of *tla*. The greater stability of the As(III)-*tma* complexes with respect to As(III)-*tla* species is also detectable in the distribution diagram which shows formation percentages certainly higher than *tla* for both MLH and ML species.

As regards the As(III)-*dmsa* system, only mono-coordinated species were determined and their stability constants are listed in Table 2.3. By considering the partial formation constants (log K_{111} = 5.58, log K_{112} = 5.55, log K_{113} = 6.10) can be noticed that the stability of the complexes considerably increases with respect to *tla* and *tma* ligands which present log K_{111} = 2.09 and 3.25 respectively. Potentiometric measurements were also performed at the same temperatures indicated for the determination of the protonation constants, namely T = 288.15 K, 310.15 K and 318.15 K. Values are listed in Table 2.4.

Table 2.4. Experimental formation constant values of As(III)-*dmsa* species in NaCl at *I* = 0.15 mol L^{-1}

Species	logβ[a]			
	288.15[b]	**298.15**[b]	**310.15**[b]	**318.15**[b]
MLH$_3$	30.02 ± 0.05[c]	29.97 ± 0.08[c]	29.85 ± 0.07[c]	29.76 ± 0.07[c]
MLH$_2$	26.10 ± 0.06	25.87 ± 0.09	25.66 ± 0.08	25.45 ± 0.07
MLH	16.85 ± 0.05	16.59 ± 0.09	16.32 ± 0.08	16.07 ± 0.08

[a] Refers to the reaction (1.10), charges omitted for simplicity; [b] in K; [c] ± standard deviation.

It is easy to notice that the stability of all the species slightly decreases by increasing the temperature value. As an example, log β_{113} = 30.02 and 29.76 at T = 288.15 and 318.15 K respectively. By means of spectrophotometry, the speciation model was verified by performing titrations on the ligand, together with specific amounts of NaCl and HCl, in order to establish the molar absorption coefficients of the LH, LH$_2$, LH$_3$ and LH$_4$ species and later on the mixture metal-ligand in the same experimental conditions. The obtained stability constants are in agreement with the potentiometric ones, showing a minimum deviation equal to 0.3 and a maximum equal to 0.6. In Figure 2.4 an example of spectrophotometric titration relative to As(III)-*dmsa* system is given, while Figure 2.5 shows the molar absorption coefficients of As(III)-*dmsa* complexes together with those of the ligand species.
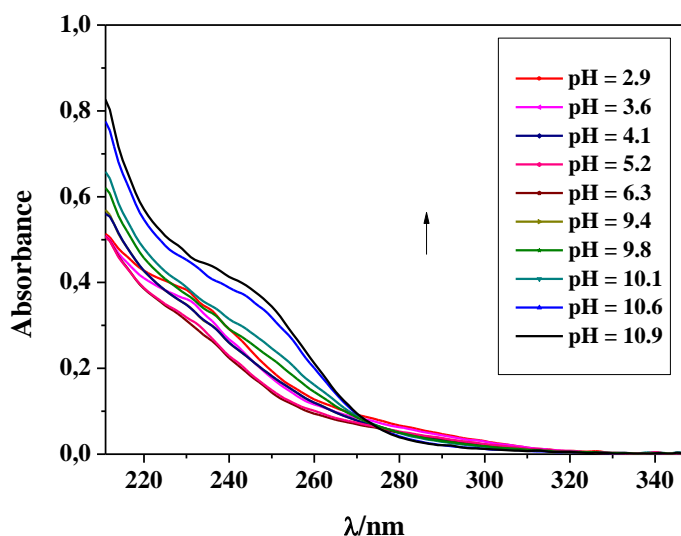
Figure 2.4. Example of spectrophotometric titration relative to As(III)-*dmsa* system. Conditions: $C_M = 0.05$ mmol L^{-1}, $C_L = 0.1$ mmol L^{-1}, $I = 0.15$ mol L^{-1} in NaCl and T = 298.15 K.
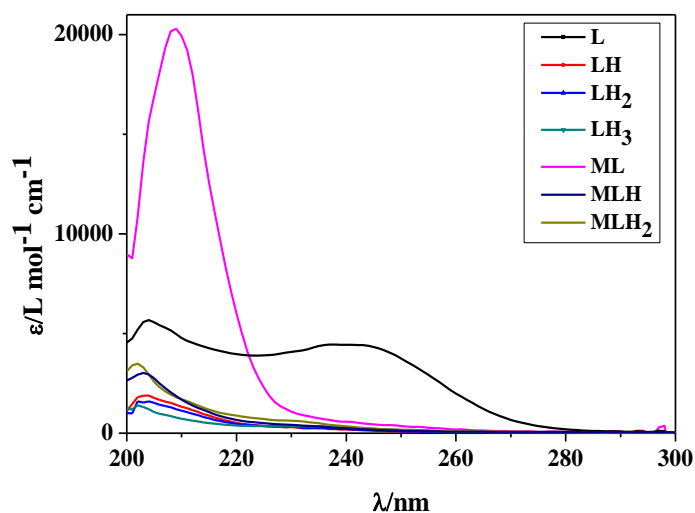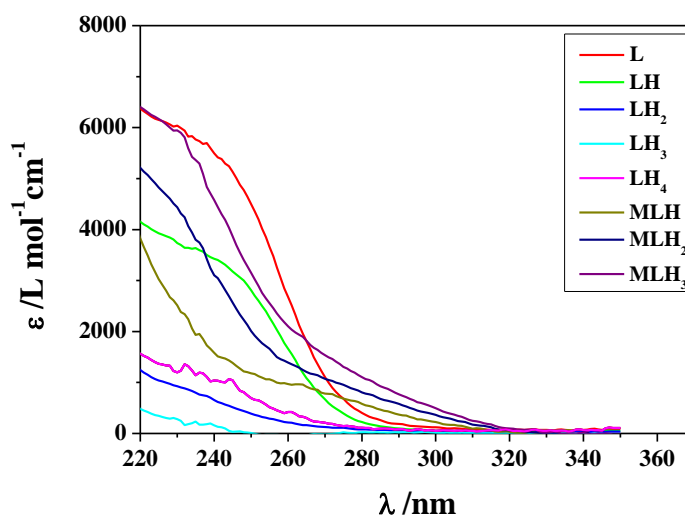

Figure 2.5. Molar absorption coefficients of As(III)-*dmsa* complexes together with those of the ligand species.

The distribution diagram of the As(III)-*dmsa* species (Figure 2.6) further points out the stability of the complexes, since the formation percentages of all the species, at the same experimental conditions used for *tla* and *tma*, reach values close to 100% and the di-protonated species (MLH$_2$) results to be the prevalent in all the investigated pH range.

Certainly, the involvement of the second thiol group, as already reported in literature [123], is responsible for the greater stability that increases by increasing the number of carboxylic groups (one in *tla* and two in *tma* and *dmsa*) and especially by increasing the number of thiolic groups (one in *tla* and *tma* and two in *dmsa*).
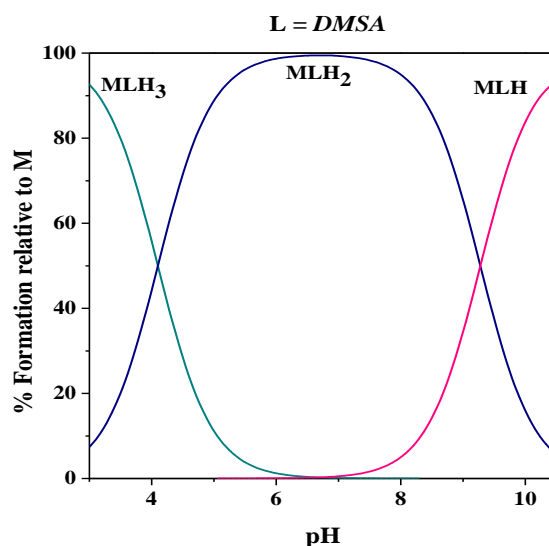
Figure 2.6. Species distribution relative to As(III)-*dmsa* system. Conditions: $C_M = 1$ mmol L^{-1} and $C_L = 5$ mmol L^{-1}, $I = 0.15$ mol L^{-1} in NaCl and T = 298.15 K.

2.2.2 Dependence on temperature

The use of the calorimetry technique allowed to determine the formation enthalpies of the complex species at the same experimental conditions of ionic strength and temperature used for potentiometric and spectrophotometric measurements. In Table 2.5 enthalpy change values of the protonation ligands at $T = 298.15$ K and at $I = 0.15$ mol L^{-1} in NaCl are reported. The enthalpy values together with the ΔG and TΔS ones are listed in Table 2.6 as partial equilibria.

Table 2.5. Overall protonation thermodynamic parameters of *tla, tma* and *dmsa* at $T = 298.15$ K and at $I = 0.15$ mol L^{-1} in NaCl

Ligand	Species [a]	-ΔG [b]	ΔH [b]	TΔS [b]	Ref.
tla	**LH**	57.2	-23.7	33.5	[119]
	LH$_2$	77.1	-21.8	55.3	
tma	**LH**	58.3	-10	48	[124]
	LH$_2$	85.5	-9	76	
	LH$_3$	105.6	-11	95	
dmsa	**LH**	62.8 ± 0.2 [c]	22 ± 3 [c]	84.8 ± 3 [c]	This thesis
	LH$_2$	115.9 ± 0.2	40 ± 3	155.9 ± 3	
	LH$_3$	136.2 ± 0.1	65 ± 2	201.2 ± 2	
	LH$_4$	150.6 ± 0.2	57 ± 3	207.6 ± 3	

[a] Referred to the reaction (1.8); [b] in kJ mol^{-1}; [c] $\pm$ standard deviation

Table 2.6. Thermodynamic formation parameters for As(III)-*tla*, -*tma* and –*dmsa* species in NaCl at $I = 0.15$ mol L^{-1} and T = 298.15 K

Ligand	Species [a]	- ΔG [b]	ΔH [b]	TΔS [b]
tla	**MLH**	11.9 ± 0.2 [c]	43 ± 1	55 ± 1
	ML	19.0 ± 0.3	-1 ± 1	18 ± 1
tma	**MLH$_2$**	17.0 ± 0.1	3.7 ± 0.5	20.7 ± 0.5
	MLH	18.5 ± 0.1	1.6 ± 0.5	20.1 ± 0.5
	ML	25.2 ± 0.1	-7.6 ± 0.6	17.6 ± 0.6
dmsa	**MLH$_3$**	34.8 ± 0.5	-85 ± 4	-50.2 ± 4
	MLH$_2$	31.7 ± 0.5	-72 ± 5	-40.3 ± 5
	MLH	32.1 ± 0.5	-72 ± 7	-39.9 ± 7

[a] According to reaction (1.11); [b] in kJ mol^{-1}; [c] $\pm$ standard deviation

As regards As(III)-*tla* and –*tma* systems, all the formation processes are endothermic with the exception of the ML species and the major contribution to the free energy is attributable to the entropic one, since TΔS > ΔH. This behavior suggest that the interactions are not pure soft-soft and also the carboxylic group could be involved in the chelation reaction. For As(III)-*dmsa* system, an opposite trend is observed since all the species exhibit negative enthalpies with values higher than TΔS. This aspect highlights the presence of a strong interaction between *dmsa* and As(III), likely due to the two thiolic binding sites. Moreover, negative entropy values could be due to an increase in the order caused by the solvation processes. This

evidence was independently strengthen by the state-of-the-art *ab initio* molecular dynamics simulations reported in the relative section.

2.2.3 Computational results

In order to gain information regarding the coordination mode of arsenic with the functional groups of the ligand molecules, *ab initio* molecular dynamics simulations were performed. Cassone *et al.* [95] clarified that the stable hydrolytic species that As(III) forms in liquid water is arsenous acid (H_3AsO_3). However, to observe the chelation phenomena within reasonable timescales in DFT-based molecular dynamics simulations, the dehydration of arsenic is necessary. Only when arsenic is released from its coordination with three hydroxide anions the chelation event occurs. The starting configuration, when diluted *tla* solution is employed, is reported in Figure 2.7a [125]. After about 1 ps the proton transfer from the thiol group to the water environment is registered (Figure 2.7b) and in few hundreds of femtoseconds the arsenic results to be completely chelated by *tla* (Figure 2.7c). As can be noticed, the preferred sites for the chelation phenomena is located between the sulfur and the oxygen atom of the carboxylic group and the average distance As-S and As-O falls at 2.30 Å and 2.03 Å respectively. It is important to underline that an hydroxide anion, coming from the water environment, binds to arsenic atom and stabilizes the overall complex. For simplicity, it is not showed.

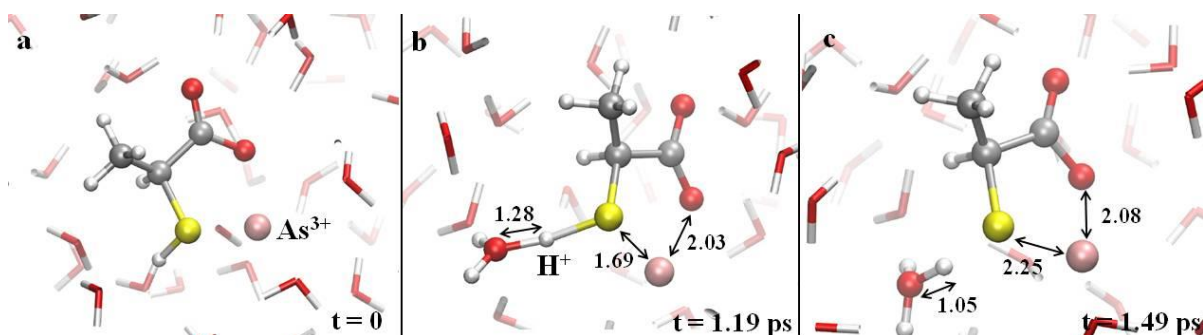**Figure 2.7.** Chelation event of As(III) in presence of *tla*. a) As(III) starts to interact with *tla*; b) this phenomena induces the release of the proton of the thiol group to a water molecule with the final chelation (c) of arsenic by the sulfur of the thiol group and the oxygen of the adjacent carboxyl group. Red, white, pink, and yellow spheres represent oxygen, hydrogen, arsenic, and sulfur atoms, respectively [125].

The same procedure was followed for *tma* but no spontaneous chelation process was observed, indicating that for more complex thioacids, longer times, not investigable with BOMD techniques, are required. However, since the most probable sites for chelation are represented by sulfur and adjacent oxygen, the structure was manually constructed and, as a consequence, a spontaneous proton transfer from the carboxylic group to the water environment was observed. The equilibrium structures of As(III)-*tla* and As(III)-*tma* complexes are showed in Figure 2.8 and for both a key role is played by the thiolic group as well as the carboxylic ones.
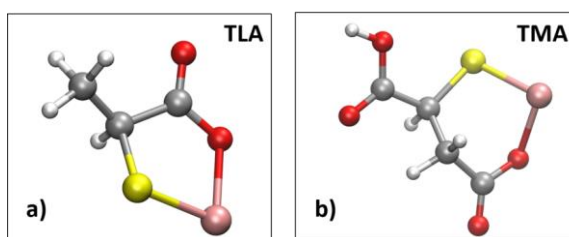
Figure 2.8. Structures of As(III)-*tla* (a) and As(III)-*tma* (b) complexes in dilute solutions [125].

When higher concentrations of ligands are used, the formation of complexes with different stoichiometry is expected. In fact, the presence of tri-coordinated species, such as ML_3, is evidenced in literature [1, 126, 127] and for this reason, BOMD simulations were again exploited. Figure 2.9 reports the chelation phenomenon when three molecules of ligands are taken into account.
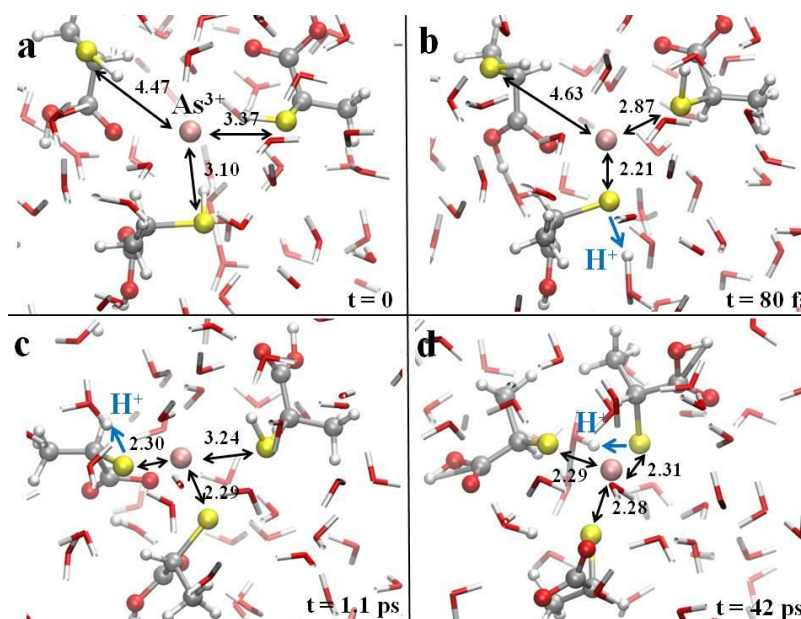
Figure 2.9. Chelation phenomenon of As(III) in presence of three molecules of *tla*. Blu arrows mark the proton transfer and the As(III)-S distances are reported in Å [125].

Starting configuration is represented in Figure 2.9a. The first proton transfer from one of the *tla* molecules to the local water environment occurs in few femtoseconds (Figure 2.9b). The second one, from the second molecule, verifies after 1ps (Figure 2.9c) as well as in the case of ML reported in Figure 2.7b. The third proton migration for forming the ML_3 species occurs in few picoseconds. The limiting step of the reaction is the formation of an OH^- in one of the solvation shells of the complex, which results necessary for promoting a proton transfer from the sulfur atom of the third *tla* molecule to a nearby water molecule in order to achieve the final stable tridentate configuration represented in Figure 2.9d. As regards the As(III)-*tma* systems the same considerations can be made.

Also to clarify the interaction of As(III) with the dimercaprosuccinic acid, *ab initio* molecular dynamics simulations proved to be of fundamental importance. In contrast to *tla* and *tma* ligands, the carboxylic group does not interact directly with As(III) which results chelated by both sulfur atoms of the thiol groups, as displayed in Figure 2.10. This structure seems to be the most plausible under idealized neutral conditions reproduced in such simulations. However, one of the carboxylic groups takes part in the stabilization process of the complex. In fact, once arsenic is chelated by the sulfur atoms, the carboxylic group deprotonates in favor of the solvent. Thus, when an hydroxide group bonds to As atom, as in the previous cases, the deprotonated carboxylic group strongly interacts with the OH^- moiety, as visible in Figure 2.10.
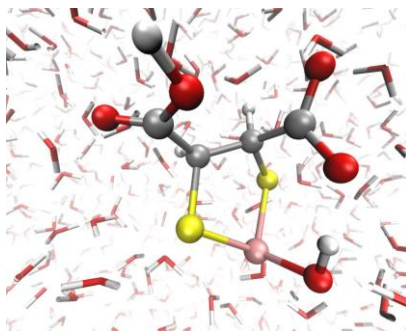
Figure 2.10. As(III)-*dmsa* complex obtained through *ab initio* molecular dynamics simulations. Red, white, pink, and yellow spheres are oxygen, hydrogen, arsenic, and sulfur atoms, respectively.

This molecular configuration was hold up to the end of the simulations, suggesting that a greater stability of the complex was achieved under such a circumstance. The computational results allowed to better explain the trend of the thermodynamic parameters previously discussed and the increase of the stability of the species by moving from the mono to the di-thiol ligands (*tla* and *tma vs. dmsa*), but also from the mono to the di-carboxylic ones (*tla vs.*

tma and *dmsa*). Moreover, they are able to explain another aspect emerged from the elaboration of the experimental calorimetric measurements which showed negative entropies for As(III)-*dmsa* complexes. As represented in Figure 2.11, the sulphur-water oxygen radial distribution function $g_{S-Ow}(r)$ clearly evidences a more ordered local water environment around *dmsa* when it chelates As(III). In fact, not only the position of all the peaks and of all the dips of $g_{S-Ow}(r)$ shifts to smaller distances, but also more pronounced saddle points characterize its profile. This finding further strengthens the observations made by analyzing data emerged from the previously presented calorimetric experiments.
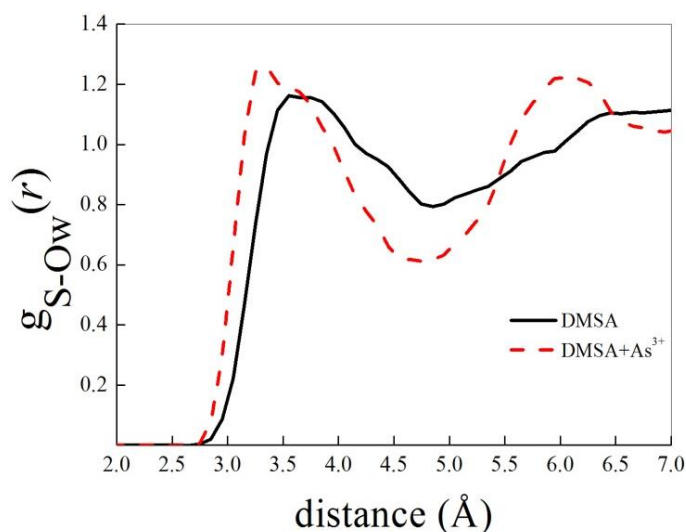
Figure 2.11. Atomistic (*i.e.*, sulphur-water oxygen) radial distribution functions of pure *dmsa* in aqueous solution (black curve) and of an As(III)-*dmsa* complex (see Figure 2.10) in water (red dashed curve).

2.2.4 Raman spectroscopy

Raman spectroscopy was employed in order to obtain information about the coordination mechanism of As(III) towards ligands. Measurements were only performed on *tla* and *tma* because *dmsa* is poorly soluble and, with this technique, higher concentrations ($C_L = 300$ mmol L^{-1} and $C_M = 150$ mmol L^{-1}) are required to have significant signals. The analysis of the spectra, displayed in Figure 2.12a for *tla* and As(III)-*tla* system together with *tma* and As(III)-*tma* system in Figure 2.12b, reveals a modification of the vibrational modes of the S-H bond when the chelation process occurs. In fact, by observing the *tla* spectrum the S-H stretching line is visible at 2567 cm^{-1}. This one disappears as a consequence of the interaction of arsenic with the sulfur atom and a modification of the region between 300 and 600 cm^{-1}, with the formation of a new band at about 460 cm^{-1} is detectable. Since this new band was reported for

arsenic-sulfur crystals [128] and for thioarsenite [129] species in aqueous solution, indicating the As-S bond, it was associated to the formation of the As-S bond. A similar discussion can be made for As(III)-*tma* system though, in this case, only the disappearance of the S-H stretching line is distinctly evident while a poor modification of the region between 300 and 600 cm^{-1} is reported. For this reason, the formation of the complex is less clear with respect to the previous ligand. However, the S-H breaking bond further highlights the involvement of the sulfur atom in the chelation process as already supposed by the experimental measurements and computational calculations.

Figure 2.12. Experimental Raman spectra of *tla* and As(III)-*tla* system (a); Experimental Raman spectra of *tma* and As(III)-*tma* system (b)
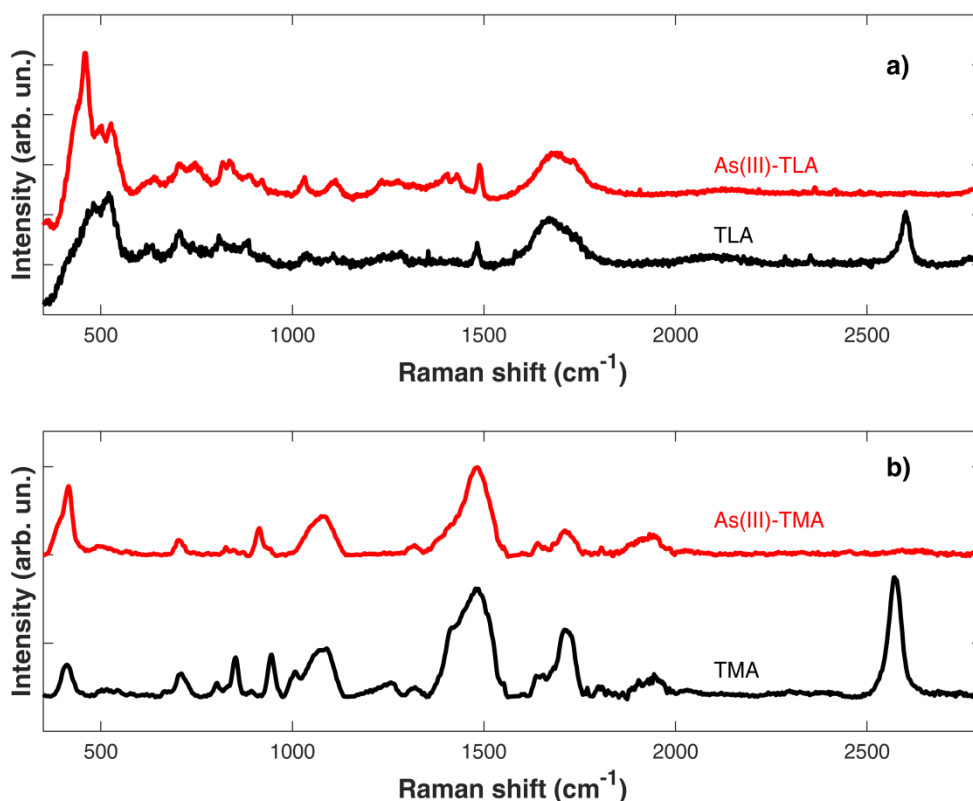
.

2.3 As(III)-*cys* and -*gsh* complexes

2.3.1 *Thermodynamic results*

Once the analysis of the model molecules evidenced and confirmed the interaction of As(III) with the sulfur atom of the thiol groups present on them, the study was expanded on molecules, such as glutathione and cysteine, having a considerable importance for many biological functions.

The investigation was mainly carried out by means of potentiometry at T = 298.15 K, by employing different metal-ligand concentrations in NaCl as background salt, and in a wide range of ionic strength ($0.15 < I/\text{mol L}^{-1} < 1$), in order to also evaluate the dependence of the stability constants on the ionic strength. The elaboration of the potentiometric data by means of BSTAC and STACO computer programs allowed to define the best speciation model for both systems. As regards As(III)-*cys* system, six simple metal-ligand complexes, differently protonated, were determined at $I = 0.15$ mol L^{-1}. In particular, three of them are mono-coordinated species, namely ML, MLH and MLH$_2$ while for the other ones As(III) is coordinated by three ligand molecules, by forming ML$_3$, M(LH)$_3$ and M(LH$_2$)$_3$ species. The speciation model together with the relative formation constants are listed in Table 2.7.

Table 2.7. Experimental formation constants obtained by potentiometry at T = 298.15 K and at different ionic strength values.

		log β[a]			
Ligand	**Species**	$I = 0.15$[b]	$I = 0.5$[b]	$I = 0.75$[b]	$I = 1$[b]
cys	**MLH$_2$**	21.17 ± 0.02[c]	21.31 ± 0.02[c]	20.90 ± 0.05[c]	19.8 ± 0.6[c]
	MLH	13.76 ± 0.02	13.45 ± 0.02	13.30 ± 0.03	12.74 ± 0.08
	ML	4.67 ± 0.02	4.41 ± 0.02	4.32 ± 0.03	3.77 ± 0.09
	ML$_3$	10.95 ± 0.04	9.86 ± 0.05	10.21 ± 0.04	10.6 ± 0.1
	M(LH)$_3$	39.24 ± 0.07	-	-	-
	M(LH$_2$)$_3$	63.98 ± 0.01	62.39 ± 0.06	62.21 ± 0.05	61.7 ± 0.1
gsh	**MLH$_3$**	23.69 ± 0.03	23.29 ± 0.03	23.46 ± 0.04	23.80 ± 0.03
	MLH$_2$	20.30 ± 0.02	20.04 ± 0.01	20.19 ± 0.02	20.39 ± 0.02
	MLH	11.33 ± 0.03	10.82 ± 0.07	11.14 ± 0.05	11.27 ± 0.04

[a] β refer to the reaction (1.10), charges omitted for simplicity; [b] in mol L^{-1}; [c] ± standard deviation.

The stability of the obtained complexes is comparable with that reported for the systems examined in the previous paragraph. For example, the ML species shows a log β equal to 4.67 similar to that displayed by the same species in the case of As(III)-*tma* system that was equal to 4.41. This speciation model was verified for all the range of ionic strength and it was confirmed with the exception of the M(LH)$_3$ tri-coordinated species which could not be determined at $I > 0.15$ mol L^{-1}. As can be noticed, all the stability constants decrease by increasing the ionic strength value except the formation constant of the ML$_3$ complex which decreases by going from $I = 0.15$ mol L^{-1} to $I = 0.5$ mol L^{-1} and then increases again. It should be highlight that the formation of the tri-coordinated complexes is sizable only when concentrations of ligand higher than 4 mmol L^{-1} are used. The distribution diagram (Figure 2.13) better explains this concept. When C$_L$ = 2 mmol L^{-1} (dashed line), the predominant species are the mono-coordinated ones which reach formation percentages close to 25%, 45% and 50% for MLH$_2$, MLH and ML respectively, while the tri-coordinated species reach a maximum of 20%. The situation changes when C$_L$ = 5 mmol L^{-1} since the tri-chalated complexes, especially M(LH$_2$)$_3$ and ML$_3$, show formation percentages higher than 50%.
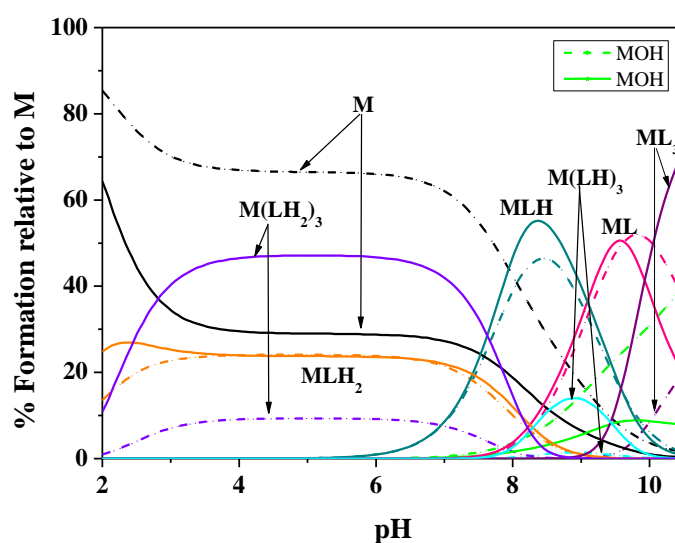
Figure 2.13. Distribution of the As(III)-*cys* species at $I = 0.15$ mol L^{-1} in NaCl and T = 298.15 K. Conditions: C$_M$ = 1 mmol L^{-1} and C$_L$ = 2 mmol L^{-1} (dashed line); C$_M$ = 1 mmol L^{-1} and C$_L$ = 5 mmol L^{-1} (solid line).

For all these reasons, their determination by means of spectrophotometry was not been possible. They were kept constant in the calculation process and only the mono-coordinated species were refined. Measurements were carried out at $I = 0.15$ mol L^{-1} in NaCl, T = 298.15

K by varying metal-ligand concentration ratios. Several spectra were collected and some of them are showed in Figure 2.14, in which the absorbance increases by increasing the pH.
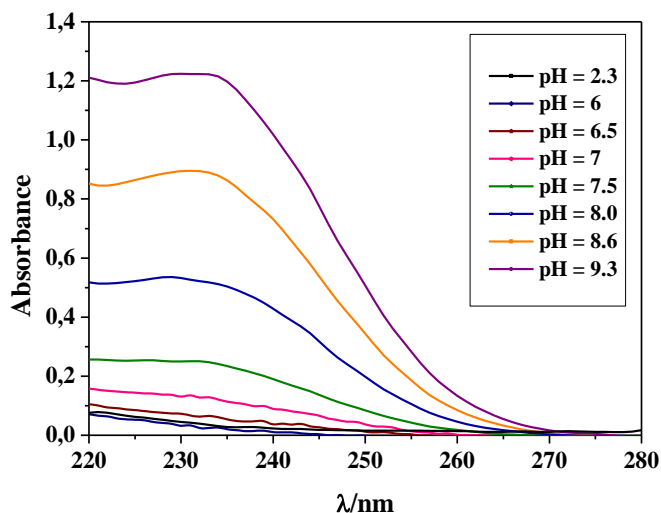
Figure 2.14. Experimental absorbance spectra of As(III)-*cys* solutions at $I = 0.15$ mol L^{-1} in NaCl and T = 298.15 K. Conditions: $C_M = 0.2$ mmol L^{-1}; $C_L = 0.4$ mmol L^{-1}.

The stability constants determined by means of Hyspec software program, reported in Table 2.8, are in good agreement with the potentiometric ones, showing a minimum deviation equal to 0.04 and a maximum equal to 0.5.

Table 2.8. Comparison between the experimental formation constants obtained both by potentiometry and spectrophotometry at T = 298.15 K and $I = 0.15$ mol L^{-1} for As(III)-c*ys* system.

	log β[a]	
	Potentiometry	**Spectrophotometry**
Species	$I = 0.15$[b]	
MLH$_2$	21.17 ± 0.02[c]	21.72 ± 0.04[c]
MLH	13.76 ± 0.02	13.75 ± 0.01
ML	4.67 ± 0.02	4.98 ± 0.01
ML$_3$	10.95 ± 0.04	10.95[d]
M(LH)$_3$	39.24 ± 0.07	39.24
M(LH$_2$)$_3$	63.98 ± 0.01	63.98

[a]β refer to the reaction (1.10), charges omitted for simplicity; [b] in mol L^{-1}; [c] $\pm$ standard deviation; [d] values kept constants.

As(III)-*gsh* system was investigated only through potentiometric technique because, no suitable experimental conditions were found in order to also exploit the spectrophotometry.

Potentiometric titrations were perfomed in a wide range of pH (2 < pH < 10.5) as well as ionic strength (0.15 < I/mol L^{-1} < 1), by using NaCl as ionic medium and T = 298.15 K. A simpler speciation model, with respect to As(III)-*cys*, was found, featured by simple metal-ligand mono-coordinated species with different protonation degrees. The complex species together with the overall formation constant values are listed in Table 2.7. All the stability constants decrease by going from I = 0.15 mol L^{-1} to I = 0.5 mol L^{-1} and then they increase again. This trend can be also observed in the distribution diagram (Figure 2.15), drawn at two different ionic strengths, specifically I = 0.15 mol L^{-1} (dashed line) and I = 1 mol L^{-1} (solid line). The formation percentages, in fact, tend to increase by about 20% by going from the lowest ionic strength to the highest one, with the only exception of the MLH species whose formation percentage remains the same at both values.
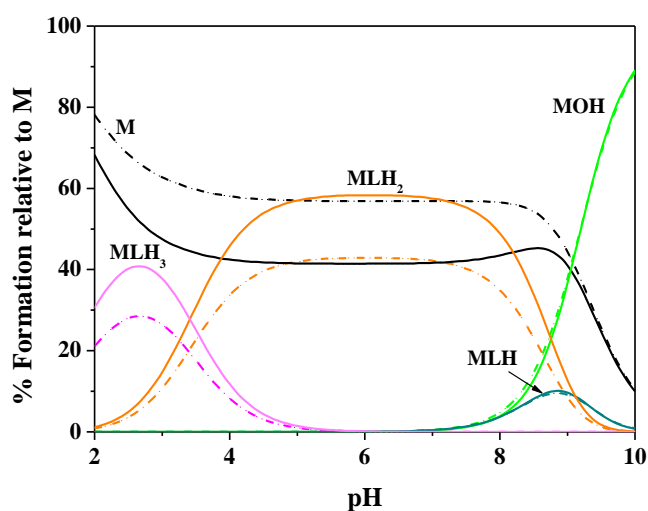
Figure 2.15. Distribution of the As(III)-*gsh* species at I = 0.15 mol L^{-1} (dashed line) and I = 1 mol L^{-1} (solid line) in NaCl and T = 298.15 K. Conditions: C_M = 1 mmol L^{-1} and C_L = 5 mmol L^{-1}.

Since for this system the ML complex was not determined, in order to have an idea on the stability of the species, the partial formation constants can be taken into account. For example, for the reaction M + HL = MLH, log K = 1.88 at I = 0.15 mol L^{-1} was obtained, value similar to that of the same species for As(III)-*tla* system (log K_{111} = 2.09), which proves that the interaction is not particularly strong unlike MLH of the As(III)-*dmsa* system whose log K_{111}, as already reported, is equal to 5.58.

2.3.2 Dependence on ionic strength

The dependence of the stability constants on the ionic strength for As(III)-*cys* and As(III)-*gsh* system was evaluated by means of the Debye-Hückel type equation (eq. 1.15) in the range between 0.15 mol L^{-1} and 1 mol L^{-1}, at T = 298.15 K and by taking into account the formation constants of all the species reported in Table 2.7. For As(III)-*cys* system, the M(LH)$_3$ species, not being determinable at ionic strengths different from I = 0.15 mol L^{-1}, was not considered in the calculation. The values relative to log $^{T}\beta$ and the empirical C parameter are listed in Table 2.9. The knowledge of these parameters allows the determination of the stability constants at I different from those under study, giving the possibility to simulate conditions not experimentally explorable.

Table 2.9. Equilibrium constants for As(III)-*cys* and −*gsh* species at infinite dilution together with C parameter for the ionic strength dependence at T = 298.15 K

Ligand	Species[a]	log $^{T}\beta$	C
cys	MLH$_2$	22.4 ± 0.2[b]	-0.9 ± 0.4 [b]
	MLH	15.1 ± 0.1	-0.2 ± 0.2
	ML	6.3 ± 0.1	0.2 ± 0.2
	ML$_3$	12.0 ± 0.2	0.7 ± 0.3
	M(LH$_2$)$_3$	66.3 ± 0.1	-1.1 ± 0.2
gsh	MLH$_3$	24.8 ± 0.1	1.3 ± 0.2
	MLH$_2$	22.01 ± 0.04	1.7 ± 0.06
	MLH	13.3 ± 0.1	1.7 ± 0.1

[a] According to reaction (1.10), charges omitted for simplicity; [b] ± standard deviation.

2.3.3 Dependence on temperature

In order to complete the thermodynamic study, it is important to determine the enthalpy change values that accompany the formation reactions of the complex species. It is possible by means of calorimetric titrations, carried out at I = 0.15 mol L^{-1} in NaCl and T = 298.15 K. The elaboration of the data was conducted by using Es5CM99 computer program which takes into account the enthalpy changes of the protonated species of the ligands (Table 2.10) as well as the enthalpy change of the hydrolysis reaction of As(III), listed in Table 1.2 of the Chapter 1 of the present section. In that case, the reaction under study was a protonation equilibrium. In the latter, being the opposite reaction, the used enthalpy value is the same but with positive sign. In Table 2.11 the overall thermodynamic formation parameters for As(III)-*cys* and −*gsh* are reported. For As(III)-*cys* system, all the values are weakly endothermic except for the

MLH species whose enthalpy change is slightly exothermic with a value equal to -9 kJ mol^{-1}. As can be also noticed, the major contribution to the free energy is due to the entropic one, underlining the electrostatic character of the interactions. For As(III)-*gsh* system, the opposite trend can be observed and all the values are exothermic with the exception of the MLH species which presents $\Delta H = 23$ kJ mol^{-1}, namely weakly endothermic. Also in this case, TΔS > ΔH and the metal-ligand interactions can be considered of electrostatic type.

Table 2.10. Protonation thermodynamic parameters of *cys* and *gsh* at $T = 298.15$ K and at $I = 0.15$ mol L^{-1} in NaCl

Ligand	Species [a]	-ΔG [b]	ΔH [b]	TΔS [b]	Ref.
cys	**LH**	57.9	-42	15.9	[130]
	LH$_2$	104.4	-77	27.4	
	LH$_3$	115.9	-81	34.9	
Gsh	**LH**	53.9	-36.3	17.6	[131]
	LH$_2$	103.2	-67.7	35.5	
	LH$_3$	123.1	-71.5	51.6	
	LH$_4$	135.2	-66.5	68.7	

[a] Referred to the reaction (1.8); [b] in kJ mol^{-1}; [c] ± standard deviation

Table 2.11. Overall thermodynamic formation parameters for As(III)-*cys* a–d -*gsh* species in NaCl at $I = 0.15$ mol L^{-1} and T = 298.15 K

Ligand	Species [a]	-ΔG [b]	ΔH [b]	TΔS [b]
cys	**MLH$_2$**	120.8 ± 0.1	30 ± 5[c]	150.8 ± 5
	MLH	78.5 ± 0.1	-9 ± 1	69.5 ± 1
	ML	26.6 ± 0.1	5 ± 1	31.6 ± 1
	ML$_3$	62.5 ± 0.2	10 ± 1	75.5 ± 1
gsh	**MLH$_3$**	135.2 ± 0.2	-26 ± 3	109.2 ± 3
	MLH$_2$	115.8 ± 0.1	-65 ± 2	50.8 ± 2
	MLH	64.6 ± 0.2	23 ± 3	87.6 ± 3

[a] According to reaction (1.10); [b] in kJ mol^{-1}; [c] ± standard deviation

In literature, very few data are reported for an appropriate comparison. Spuches *et al.* [122], by means of isothermal titration calorimetry, were able to determine the formation enthalpy of three species for As(III)-*gsh* system, in particular ML, ML$_2$ and ML$_3$, by showing ΔH values equal to -2.5, -3.1 and -33.1 kcal mol^{-1} respectively. Therefore, although a real comparison between values not can be made, it can be noticed as the exothermic behavior is kept.

2.4 Sequestering ability

In order to complete the investigation relative to As(III) interaction with thiol ligands, the ability of these molecules to sequester the metal was evaluated by using the $pL_{0.5}$, an empirical parameter well explained in 1.9 paragraph of the Section I. For these compounds, the study was carried out at physiological conditions, namely $I = 0.15$ mol L^{-1}, T $= 310.15$ K and pH $= 7.4$. The obtained $pL_{0.5}$ are reported in Table 2.12.

Table 2.12. $pL_{0.5}$ values for As(III)-*tla*, -*tma*, -*dmsa*, -*cys* and −*gsh* systems at $I = 0.15$ mol L^{-1} in NaCl, T $= 310.15$ K and pH $= 7.4$

Ligand	$pL_{0.5}$
tla	2.62
tma	3.50
dmsa	5.25
cys	3.90
gsh	2.48

By analyzing the sequestration diagram in Figure 2.16, the best performance is achieved by *dmsa*, presenting a value of $pL_{0.5}$ equal to 5.25.
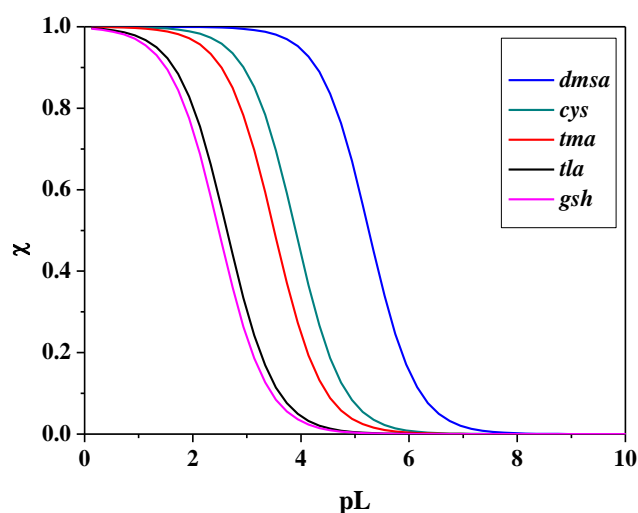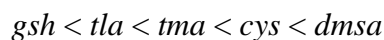

Figure 2.16. Sequestration diagram of As(III)-*tla*, -*tma*, -*dmsa*, -*cys* and −*gsh* species at $I =$ 0.15 mol L^{-1} in NaCl, T $= 310.15$ K and pH $= 7.4$.

This result was expected since the greater affinity of As(III) towards di-thiol molecules than mono-thiols was already proved [123]. In particular, $pL_{0.5}$ increases by following the trend reported below:

$$gsh < tla < tma < cys < dmsa$$

Similar binding ability was found for *tla* and *gsh* molecules, having $pL_{0.5}$ values equal to 2.62 and 2.48 respectively. The presence of a second carboxylic group in the structure of *tma* that participates to the interaction with As(III), stabilizing the complex species, improves the sequestering ability of one order of magnitude ($pL_{0.5} = 3.50$) and a comparable behavior can be observed for cysteine, which shows a $pL_{0.5}$ equal to 3.90.

2.5 Literature comparison

In literature no many thermodynamic data are reported about the interaction of As(III) with thiol compounds in aqueous solutions. In general, it is common opinion that As(III) coordinates the thiol ligands in order to form tri-coordinated species, generally named as ML_3. [1, 123]. Just some examples can be mentioned. Scott *et al.* [127] through a NMR study involving As(III) in presence of glutathione demonstrated the formation of tri-coordinated species, but no information about the thermodynamic behavior (stability constants or thermodynamic parameters depending on temperature) are given. This investigation, moreover, was carried out by considering high concentrations of metal (0.6 mol L^{-1}) and ligand (2 mol L^{-1}), conditions that deviate from the real systems in which the concentration of arsenic is micromolar and that of glutathione around 10 mmol L^{-1}. On the other hand, Spuches *et al.* [122] performed a thermodynamic study on As(III) interaction with several thiols among which *gsh* and *dmsa* ligands. In this investigation, also 1:1 and 1:2 species were determined. However, the limit of this paper is that the authors worked at fixed pH values and the exact stoichiometry of the species is not well defined. To conclude, Rey *et al.* [121] evaluated the interaction of As(III) with *cys* and *gsh*, observing a similar behavior for both systems, in which the formation of $As(LH)_3$ and $As(L)(OH)_2$ species are registered.

2.6 Final remarks

The combined use of potentiometric, spectrophotometric, calorimetric titrations as well as raman spectroscopy and molecular dynamics simulations allowed to examine the interaction of As(III) with *tla*, *tma*, *dmsa, cys* and *gsh* ligands from the thermodynamic point of view. In particular:

- Potentiometry allowed to define the best speciation model for all the systems together with the stability constant values. These one were confirmed by means of spectrophotometry technique with the exception of As(III)-*gsh* system and the enthalpy changes for all the systems were determined through titration calorimetry.

- For As(III)-*cys* and As(III)-*gsh* the dependence on ionic strength was evaluated and the $\log {}^{T}\beta$ together the empirical *C* parameter were determined in order to predict the speciation in systems featured by variable composition.

- Molecular dynamics simulations proved that the preferred sites for the chelation phenomenon are located between the sulfur atom and the adjacent oxygen atom for *tla* and *tma* while, for *dmsa* both thiolic groups are involved in the chelation process. For this reason, As(III)-*dmsa* complexes show greater stability with respect to the previous ones.

- Finally, for all the systems under study, the sequestering ability at physiological conditions (pH = 7.4, $I = 0.15$ mol L^{-1} and T = 310.15 K) was calculated by means of pL$_{0.5}$ which was able to further demonstrate that the interaction of As(III) with di-thiol compounds is stronger than the mono ones as well as the involvement of the carboxylic group play a role in the stabilization of the complexes.

3

As(III)-carboxylic acids, -amino acids and -nucleotides interactions: results and discussion

In light of the results obtained for As(III)-thiol compounds in which the involvement of the carboxylic group in the coordination mode was highlighted for both *tla* and *tma* systems by means of *ab initio* molecular dynamics simulations, the study regarding the interaction of As(III) in aqueous solution was extended to carboxylic ligands. Carboxylic groups are of biological interest and may be present in macromolecules easily found in the environment, as well as arsenic, and, for this reason, a critically speciation analysis should be made. Therefore, carboxylic acids having an increasing number of carboxylic groups were chosen, in particular malonic, tricarballylic, butan tetracarboxylic and mellitic acids. In order to complete the investigation relative to As(III) interaction with molecules that perform important biological functions in human organism, also amino acids and nucleotides were included. As regards the amino acids, three molecules representative of the class were selected, having in the structure one amino group (glycine), two carboxylic and one amino groups (aspartic acid) and two amino and one carboxylic groups (lysine). As concerns the nucleotides, the attention was focused on three important nucleotides, such as adenosine-5'-tri-, di- and monophosphate. All the systems are discussed in the following paragraphs.

3.1 As(III)-carboxylate complexes

3.1.1 General aspects

Carboxylic acids are widely distributed in nature and they are often involved as intermediates in degradation pathways of fats, amino acids and carbohydrates. Moreover, they are employed in many applications in medicine, agriculture, food field and other industries. In food industry, for example, they are used to lend specific organoleptic properties or stability to the food. On the other hand, they can be naturally present, such as the citric acid in citrus fruits. Their use is also extended for the preparation of several cosmetics for different purposes, such as the improvement of the skin texture as well as for the acne treatment. In this thesis, four carboxylic acids with increasing numbers of carboxylic groups were employed. In particular, malonic acid (*mal*), tricarballylic acid (*tca*), Butane-1,2,3,4-tetracarboxylic acid (*btc*) and mellitic acid (*mlt*), reported in Figure 3.1

1,3-propanedicarboxylic acid or malonic acid (*mal*)

Propane-1,2,3-tricarboxylic acid or tricarballylic acid (*tca*)

Butane-1,2,3,4-tetracarboxylic acid (*btc*)

Benzene-1,2,3,4,5,6-hexacarboxylic acid or mellitic acid (*mlt*)
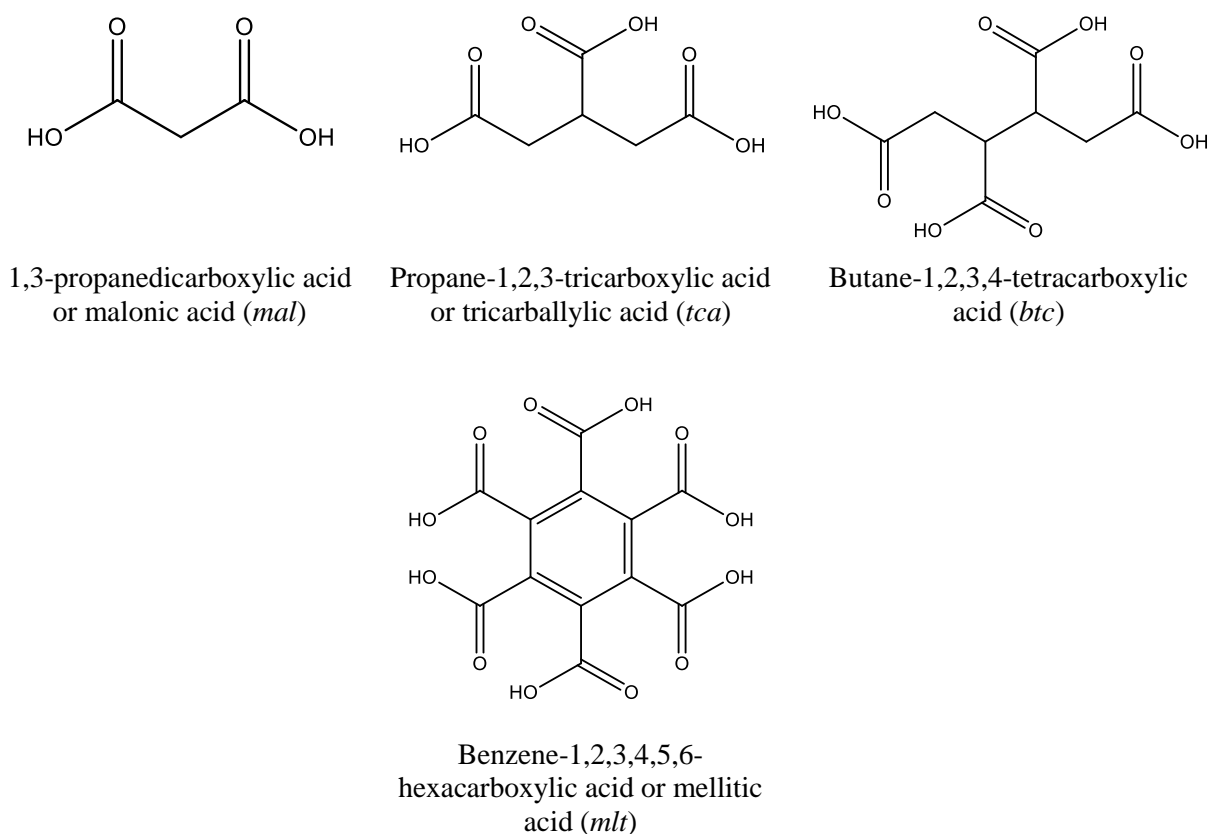
Figure 3.1. Carboxylic acids under investigation

Malonic acid (*mal*) is the second-smallest aliphatic dicarboxylic acid after the oxalic one. It can be naturally found in some fruits and it seems to accumulate in peel tissues and in juice of oranges during maturation and storage on shelf. Therefore, it could be used as a reliable

indicator of orange fruit senescence [132]. Malonic acid has many others applications. For example, it is employed in the manufacture of barbiturates, closed-chain ureic compounds whose nucleus is malonylurea, namely a combination of urea and malonic acid [133]. Moreover, *mal* is used in electronic industry [134], in food in order to control acidity or as excipient in pharmaceutical formulations, but also as natural preservative additive for foods [135]. From the biochemistry point of view, malonic acid acts against succinate dehydrogenase (complex II) in the respiratory electron transport chain [136].

Tricarballylic acid (*tca*) is a tricarboxylic acid that inhibits the enzyme aconitase which is responsible for catalyzing the stereo-specific isomerization of citrate to isocitrate via cis-aconitate in the tricarboxylic acid cycle. Thus, its possible inhibition could interfere with the Krebs cycle [137].

Butane-1,2,3,4-tetracarboxylic acid (*btc*) is a tetracarboxylic acid which finds application in durable press (DP) or easy care finishing. It is widely used as substituent of urea-formaldehyde and melamine-formaldehyde resins which were shelved because of the environmental concerns due to formaldehyde [138].

Mellitic acid (*mlt*) also known as graphitic acid or benzenehexacarboxylic acid was discovered in 1799 by Martin Heinrich Klaproth which found it in the mineral *mellite* which represents the aluminium salt of the acid. This molecule takes on great importance in the speciation of natural fluids, since it represents one of the simplest constituents of the larger molecules present in natural fluids, such as humic and fulvic acids. Moreover it can be found in the environment as a degradation product of natural organic matter and its high charge makes it an ideal model molecules for speciation studies of natural organic matter with heavy metals [139].

3.1.2 Ligand protonation constants

For studying the interaction of As(III) with carboxylic acids, the acid-base properties of the ligands must be taken into account. For all the carboxylic acids under investigation, they were determined by the research group in the past years and they are summarized in Table 3.1 at I = 0.15 mol L^{-1} in NaCl and T = 298.15 K

Table 3.1. Protonation constants of *mal, tca, btc* and *mlt* at I = 0.15 mol L^{-1} in NaCl and T = 298.15 K

Ligand	Species [a]	$\log\beta^H$ I = 0.15 [b]	Ref.
mal	LH	5.22	[140]
	LH$_2$	7.99	
tca	LH	5.819	[140]
	LH$_2$	10.331	
	LH$_3$	13.729	
btc	LH	6.21	[140]
	LH$_2$	11.31	
	LH$_3$	15.39	
	LH$_4$	18.55	
mlt	LH	6.39	[141]
	LH$_2$	11.623	
	LH$_3$	15.743	
	LH$_4$	18.500	
	LH$_5$	20.176	
	LH$_6$	20.898	

[a] According to the reaction (1.8), charges omitted for simplicity; [b] in mol L^{-1};

3.1.3 Thermodynamic results

The study relative to As(III)-carboxylate systems was only performed at I = 0.15 mol L^{-1} in NaCl and T = 298.15 K by means of potentiometric titrations, by using diverse metal-ligand ratios as reported in the 1.2.2 paragraph of the section I. The use of different metal-ligand concentrations allowed to evaluate various stoichiometry for the complex species in order to define the final speciation model as well as the formation constants, reported in Table 3.2.

Table 3.2. Overall stability constants for As(III)-*mal, -tca, -btc* and *-mlt* systems at $I = 0.15$ mol L^{-1} in NaCl and T = 298.15 K

	logβ	
Ligand	**Species** [a]	**$I = 0.15$** [b]
mal	ML	1.63 ± 0.02 [c]
	MLH	7.331 ± 0.009
tca	ML	1.10 ± 0.04
	MLH	7.22 ± 0.02
	MLH$_2$	11.78 ± 0.02
btc	MLH	7.52 ± 0.04
	MLH$_2$	12.76 ± 0.02
	MLH$_3$	17.07 ± 0.02
mlt	ML	3.37 ± 0.01
	MLH	8.87 ± 0.01
	MLH$_2$	13.72 ± 0.04
	MLH$_3$	17.17 ± 0.04
	MLH$_4$	20.10 ± 0.07

[a] According to the reaction (1.10), charges omitted for simplicity; [b] in mol L^{-1};

[c] $\pm$ standard deviation.

All the speciation models are featured by simple metal-ligand species with different protonation degrees and for As(III)-*mal*, *-tca* and *–mlt* systems a common species, namely ML, can be identified. As can be noticed, the stability of these complexes is very weak. In particular, the value of the formation constant slightly decreases by going from malonic acid to tricarballilic acid and then it increases of around two order of magnitude in the case of mellitic acid. Specifically, log β_{110} = 1.63, 1.10 and 3.37 for *mal*, *tca* and *mlt* respectively. A similar trend is also visible in other systems [142] and it could be due to the fact that malonic acid, being smaller than tricarballilic acid, stronger interacts with As(III). On the other hand, mellitic acid, having six carboxylic groups in its structure, could exert a chelating effect on the metal, showing a stability higher than the other ones. For As(III)-*btc* system, the ML species was not determined. However, a comparison between the partial stability constants of the MLH species for all the systems can be made. Specifically, log K_{111} = 2.11, 1.39, 1.31 and 2.48 for *mal*, *tca*, *btc* and *mlt* respectively. Thus, as previously mentioned, the stability is higher for malonic and mellitic acids than tricarballylic and butantetracarboxylic acids, which present similar values. The poorly stability of these complexes is further highlighted in the

distribution diagrams in Figure 3.2. For As(III)-*tca* and -*btc* systems, the complex species reach low formation percentages, close to 20%, for all the investigated pH range. As regards the other two systems, the situation is slightly different. For example, at physiological pH, namely 7.4, the ML is the predominant species for both systems, showing formation percentages close to 30% and 90% for As(III)-*mal* and As(III)-*mlt* respectively.
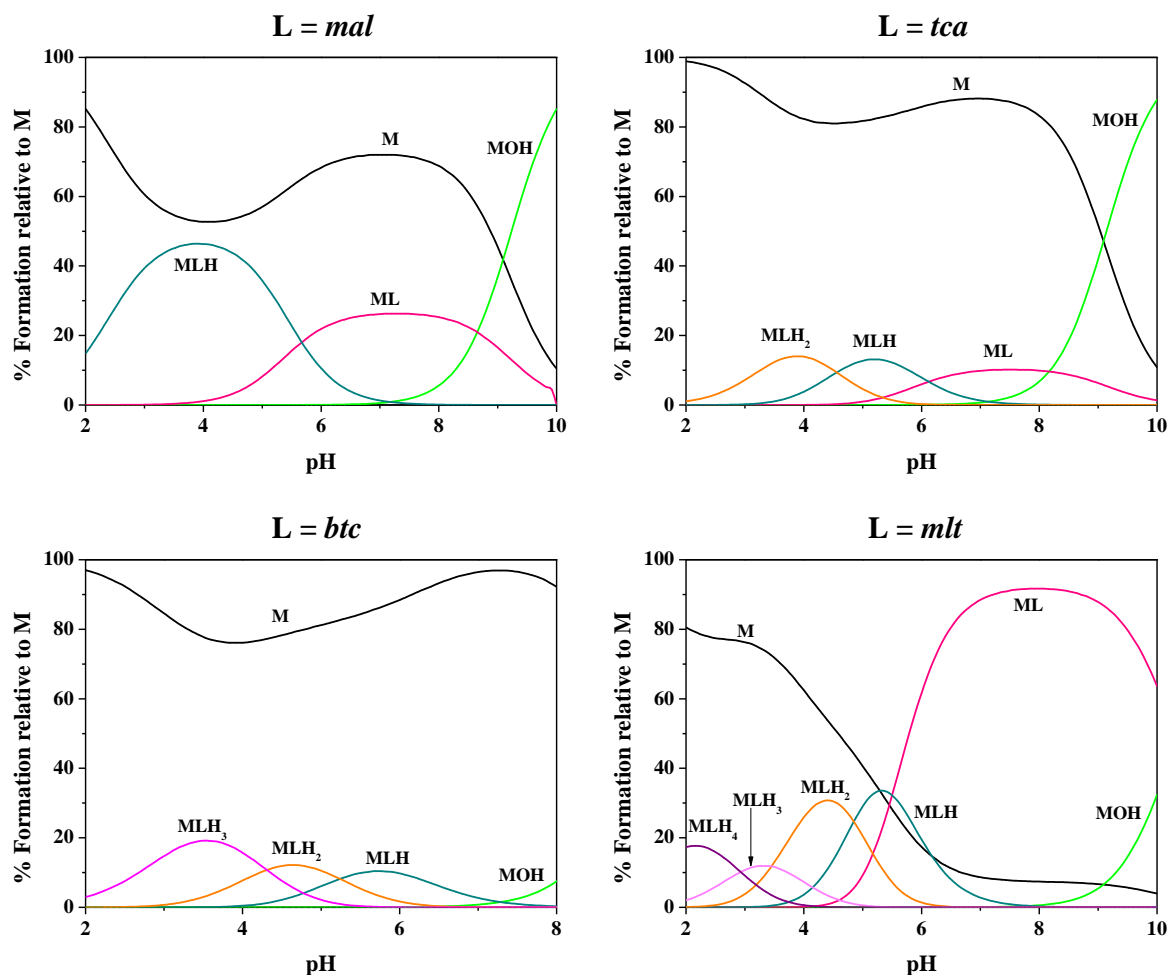

Figure 3.2. Distribution diagrams at $I = 0.15$ mol L^{-1} in NaCl and T = 298.15 K. Conditions: $C_M = 5$ mmol L^{-1} and $C_L = 10$ mmol L^{-1}.

3.2 As(III)-amino acids complexes

3.2.1 General aspects

Amino acids are organic compounds featured by amino ($-NH_2$) and carboxylic (-COOH) groups along with a side chain that can vary from one amino acid to another. In biochemistry, generally, the term *amino acids* refers to L-α-amino acids in which the amino and the carboxylic groups are linked to the same carbon atom, called α carbon with L configuration. Thus, they possess optic activity with the exception of the glycine that is achiral. Since all amino acids contain amino and carboxylic functional groups, they show an amphiprotic behavior. Below pH 2.2, both the carboxylic and amino groups are protonated, with a net positive charge. Above pH 9.4, the carboxylic group is deprotonated as well as the amino groups, with a final negative charge. At a pH between 2.2 and 9.4, the carboxylic group is deprotonated (COO-) but the amino group not yet (NH_3^+); thus, the molecule presents a net zero charge and it is called *zwitterion*.

The amino acids represent the constitutive units of the protein and, in this case, they are defined *proteinogenic*. In nature, 20 proteinogenic amino acids are known; in particular, 8 of them are indicated as *essential amino acids*. They cannot be synthesized from other compounds in the human body and they must be taken through the food.

In this research work, the attention was focused on three amino acids only featured by amino and carboxylic groups, namely glycine (*gly*), aspartic acid (*asp*)and lysine (*lys*), represented in Figure 3.3.

Glycine (*gly*)   Aspartic acid (*asp*)   Lysine (*lys*)
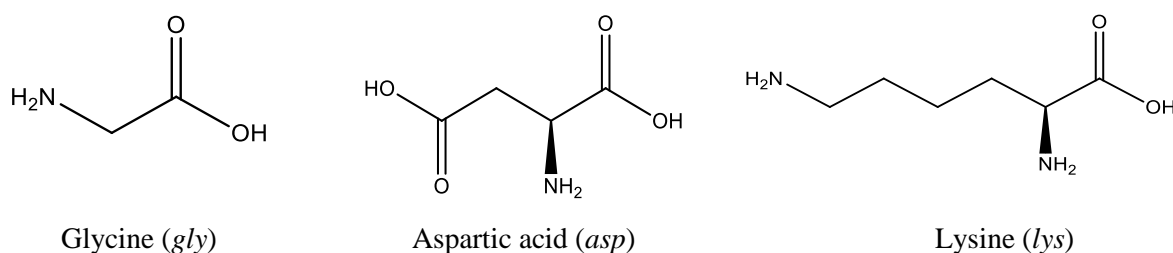
Figure 3.3. Amino acids under study

The aim of the study was to evaluate the interaction of As(III) with the mentioned amino acids by starting from the simplest compound, *i.e.* glycine, and continuing with molecules in which an increase of carboxylic groups or amino ones was alternately reported, in order to investigate the influence of these ones on the complexation phenomenon.

Glycine is the simplest amino acid whose said chain is featured by an hydrogen atom which makes it an achiral compound. It is considered as a precursor to proteins which, generally,

incorporate only small quantities of glycine, with the exception of collagen, which is constituted by about 35% of this amino acid which seems to play an important role in the cartilage regeneration by enhancing collagen synthesis [143]. Glycine is the main inhibitory neurostransmitter of the spinal cord. Possible interferences with its release within the spinal cord could cause spastic paralysis as a consequence of uninhibited muscle contraction. Moreover, glycine takes part in detoxification processes in the human body, since it can conjugate, in liver and kidney, with some toxic substances, such as benzoic acid, in order to form non-toxic compounds easily removed by urine (*e.g.* hippuric acid) [144].

Aspartic acid is an amino acid *no essential* whose side chain is polar. It has an α-amino group as well as an α-carboxylic one and, at physiological conditions, the first one is protonated while the second one is deprotonated. The side chain at physiological conditions is negatively charged and this aspect allows to interact with other amino acids, enzymes, and proteins. In the brain, it acts as excitatory neurotransmitter which excites the NMDA receptors although not in the same way of glutamate [145]. Aspartic acid can be mainly found in food rich in proteins, such as meat, fish, eggs, milk, beetroot, mushrooms. This amino acid plays an important role in the Krebs Cycle, within which several amino acids and biochemicals are produced and it is also involved in the Urea Cycle which converts highly toxic ammonia to urea for excretion. It is used as supplement in order to increase the fatigue resistance and decrease the weariness; in fact, in combination with magnesium and potassium, it can be employed to prevent cramps. Aspartic acid is also present in the sweetener called aspartame, a dipeptide obtained synthetically through the reaction between aspartic acid and the methyl ester of the amino acid known as phenylalanine.

Lysine is a polar amino acid whose side chain has an amino group which confers a basic behavior to the molecule. It is indicated as *essential* amino acid since the human organism cannot synthesized it and it must be obtained from the diet. Lysine play key roles in human body, in particular in proteinogenesis, but also in the crosslinking of collagen polypeptides [146, 147], uptake of essential mineral nutrients and the production of carnitine, very important in fatty acid metaolism [148]. Lysine is mainly present in meat, cheese, milk, eggs, in some fishes (cod and sardines) and legumes. A low intake of this amino acid in the diet can cause various disorders. For example, a lack of lysine and, especially, of hydroxylysine could be the cause of a disease state of the connective tissue [149]. Moreover, it seems that lysine is involved in the uptake of iron and in the concentration of ferritin in blood plasma. Thus, a deficiency of this amino acid could produce anemia [150]. On the other hand, an accumulation of the amino acid in blood can cause hyperlysinemia, a metabolic disorder in

which the protein responsible of the the breakdown of lysine is non functional because of a genetic mutation [151].

3.2.2 Ligand protonation constants

The protonation constants of the amino acids used in this research work are taken from literature data and they are listed in Table 3.3. These data, when necessary, were recalculated at the same experimental conditions employed for metal-ligand investigations, namely $I = 0.15$ mol L^{-1} in NaCl and T = 298.15 K.

Table 3.3. Protonation constants of *gly, asp* and *lys* at $I = 0.15$ mol L^{-1} in NaCl and T = 298.15 K

		$\log\beta^H$	
Ligand	Species [a]	$I = 0.15$ [b]	Ref.
gly	LH	9.571	[152]
	LH$_2$	11.933	
asp	LH	9.63	[153]
	LH$_2$	13.09	
	LH$_3$	15.039	
lys	LH	11.06	[154]
	LH$_2$	20.26	
	LH$_3$	22.21	
	LH$_4$	18.55	

[a] According to the reaction (1.8), charges omitted for simplicity; [b] in mol L^{-1};

3.2.3 Thermodynamic results

Also the study relative to the interactions of As(III) with some amino acids were carried out by exploiting the potentiometric technique. Measurements were conducted a $I = 0.15$ mol L^{-1} in NaCl, T = 298.15 K and by using different metal-ligand concentrations. The elaboration of the data by means of BSTAC and STACO computer programs allowed to establish the best speciation models which are listed in Table 3.4 together with the relative formation constants. Also in this case, simple metal-ligand species (differently protonated) characterize the speciation model and the ML complex represents the common species for all the systems. The overall stability is slightly higher than the As(III)-carboxylate systems previously discussed,

since the minimum and maximum log β_{110} were equal to 1.10 and 3.37 for As(III)-*tca* and As(III)-*mlt* *vs.* log $\beta_{110} = 2.65$ and 3.73 for As(III)-a*sp* and −*gly* respectively.

Table 3.4. Overall stability constants for As(III)-*gly, -asp* and *-lys* systems at $I = 0.15$ mol L^{-1} in NaCl and T = 298.15 K

		logβ
Ligand	**Species** [a]	**$I = 0.15$** [b]
asp	ML	2.65 ± 0.03[c]
	MLH	10.79 ± 0.09
	MLH$_2$	15.39 ± 0.01
lys	ML	3.3 ± 0.1
	MLH	13.24 ± 0.06
	MLH$_2$	21.85 ± 0.06
gly	ML	3.73 ± 0.02
	MLH	10.87 ± 0.05

[a] According to the reaction (1.10), charges omitted for simplicity; [b] in mol L^{-1}; [c] $\pm$ standard deviation.

In Figure 3.4 the distribution of the complex species for all the systems is reported. Although the diagrams were drawn by considering moderately high ligand concentrations, if we refer to biological systems, the formation percentages of the species are quite low. For As(III)-*asp* system, the MLH species is present in all the investigated pH range and at pH = 7.4 it shows the maximum formation percentage close to 10% (at the limit of significance). The other two complex species, namely MLH$_2$ and ML, present the maximum percentage ($\sim$ 50% for MLH$_2$ and 30% for ML) at pH $\sim$ 3 and pH $\sim$ 9.5 respectively. As concerning As(III)-*lys* system, the prevalent species in the pH under study is the MLH$_2$ one, which maintains a constant formation percentage close to 20% between pH = 2 and pH = 8. At pH $\sim$ 9, MLH species shows the maximum value in term of formation percentage (close to 20%) and the ML one, partly covered by the previous one, can be considered not particularly important. Different is the situation for As(III)-*gly* system. In this case, the mono-protonated species reaches percentages not particularly significative ($\sim$ 20%), but the simple metal-ligand species, ML, which starts to form from pH = 6, reaches a formation percentage

close to 80% at pH = 9, underlining the importance of this species in terms of stability with respect to the other ones for the previous systems.
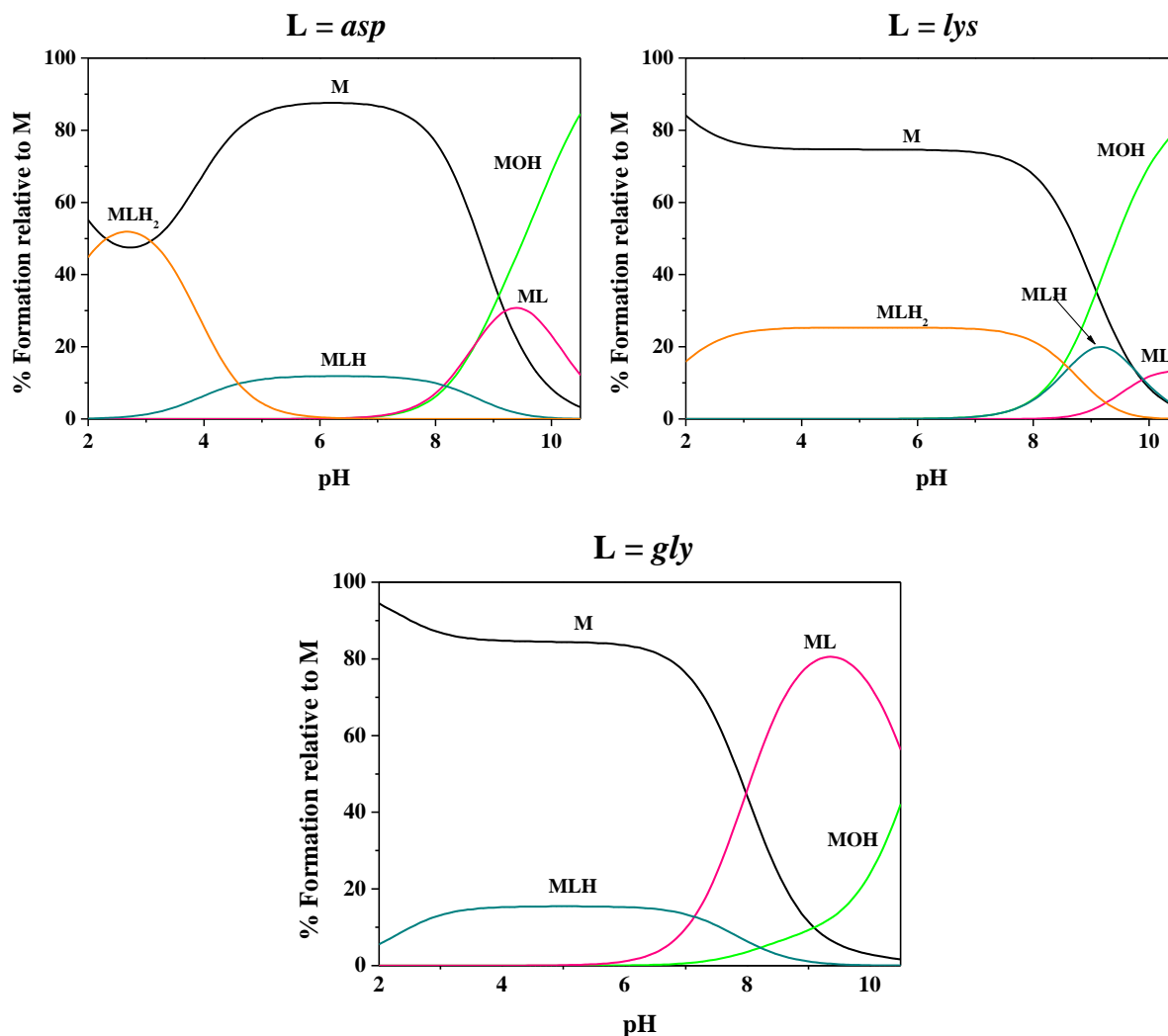

Figure 3.4. Species distributions for As(III)-*asp*, -*lys* and –*gly* at $I = 0.15$ mol L^{-1} in NaCl and T = 298.15 K. Conditions: $C_M = 5$ mmol L^{-1} and $C_L = 10$ mmol L^{-1}.

3.3 As(III)-nucleotide complexes

3.3.1 General aspects

Nucleotides are organic compounds constitutive of the nucleic acids (DNA and RNA), macromolecules able to save the genetic information. They are featured by three units:

- − a nitrogenous base (purine or pyrimidine);
- − a five-carbon sugar (ribose or deoxyribose);
- − at least one phosphate group.

The presence of the phosphoric residue confers strongly acid character to the nucleotides. They participate to numerous metabolic processes in the cells. In particular, triphosphate nucleotides play a fundamental role in the energetic metabolism of the cell. The adenosine triphosphate, for example, represents the instrument through which the cell performs processes which need energy. In general, all the triphosphate nucleotides can be viewed as an energetic storage, readily destinable to any vital process. In this thesis, adenosine 5' monophosphate (*AMP*), adenosine 5' diphosphate (*ADP*) and adenosine 5' triphosphate (*ATP*) were employed and their structures are showed in Figure 3.5.

Adenosine triphosphate (*ATP*) is a nucleotide in which the ribose sugar is linked to three phospahate groups and to the nitrogenous base called adenine. The breakage of the bond related to the terminal phosphate group, by means of an hydrolysis reaction, produces energy, generally contained in the bonds between the phosphates. Usually only the outer phosphate is removed from *ATP* to yield energy and, when this event occurs, *ATP* is converted into *ADP* (adenosine diphosphate) which has only two phosphate groups. Although *ATP* is frequently converted into *ADP*, it is constantly synthesized from *ADP* and phosphate through the process called cellular respiration. Adenosine monophosphate (*AMP*) can be viewed as the ester of the phosphoric acid and the nucleoside adenosine. It plays an important role in several cellular metabolic processes since it is interconverted into *ADP* and/or *ATP*. In can be formed as a consequence of many processes, such as the hydrolysis of *ADP* or the hydrolysis of *ATP* in order to form *ADP* and pyrophosphate. *AMP* can exist in a cyclic structure named cyclic *AMP*. In some cells the adenylate cyclase enzyme can produce, starting from *ATP*, *cAMP* which is of fundamental importance in cellular metabolism. This reaction is regulated by hormones such as adrenaline or glucagon.
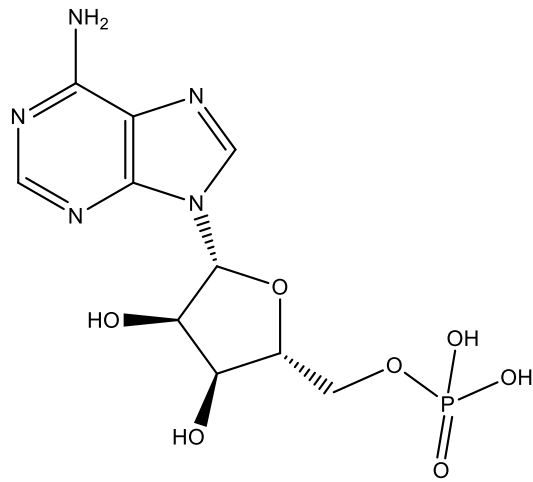
Adenosine 5' monophosphate (*AMP*)
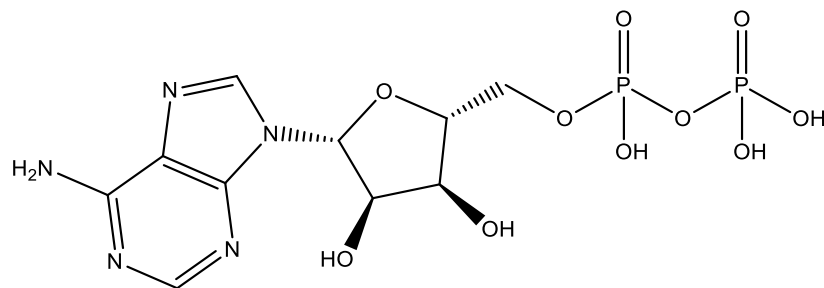
Adenosine 5' diphosphate (*ADP*)
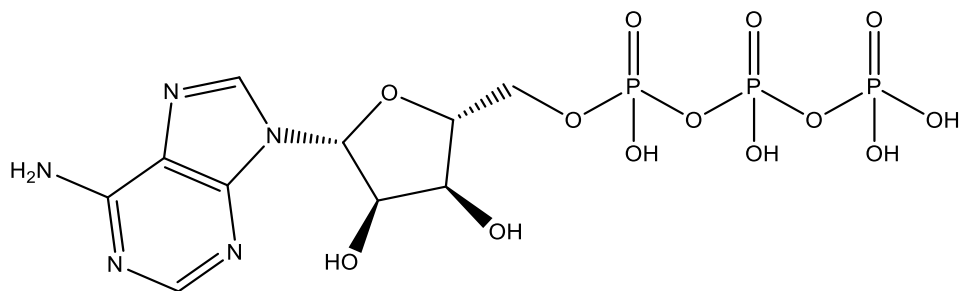
Adenosine 5' triphosphate (*ATP*)

Figure 3.5. Structure of nucleotides under study

3.3.2 Ligand protonation constants

The protonation constants of the nucleotides studied in this research work were taken from literature data recently published by the research group. They were reported at the same ionic strength and temperature (I = 0.15 mol L^{-1} in NaCl and T = 298.15 K) used for the determination of the metal-ligand complexes. Values are listed in Table 3.5.

Table 3.5. Protonation constants of *AMP, ADP* and *ATP* at I = 0.15 mol L^{-1} in NaCl and T = 298.15 K

Ligand	Species [a]	I = 0.15 [b]	Ref.
		$\log\beta^H$	
AMP	**LH**	6.117	[155]
	LH$_2$	9.903	
ADP	**LH**	6.219	[155]
	LH$_2$	10.022	
ATP	**LH**	6.45	[155]
	LH$_2$	10.47	

[a] According to the reaction (1.8), charges omitted for simplicity; [b] in mol L^{-1};

3.3.3 Thermodynamic results

Thermodynamic analysis was carried out with the help of potentiometric measurements performed at I = 0.15 mol L^{-1} in NaCl and T = 298.15 K. A wide range of metal-ligand concentrations, defined in 1.2.2 paragraph of the Section I, was examined in order to better identify the stoichiometry of the species whose formation was evaluated in a large range of pH (2 < pH < 10). For all the systems, the same speciation model was found, featured by di-coordinated simple metal-ligand species differently protonated. In particular, the formation of ML$_2$, ML$_2$H, ML$_2$H$_2$ and ML$_2$H$_3$ species was observed and the respective stability constants are reported in Table 3.6. A critical analysis of the results denotes that the stability of the ML$_2$ species is fairly comparable for As(III)-*AMP* and -*ADP* systems, having log β equal to 5.99 and 6.54 respectively, while for As(III)-*ATP* the value decreases by about 2 orders of magnitude, resulting equal to 4.81. Probably, this opposite trend could be caused by the steric hindrance of the two triophosphate nucleotides which cannot adequately interact with the metal.

Table 3.6. Overall stability constants for As(III)-*AMP, -ADP* and -*ATP* complexes at I = 0.15 mol L^{-1} in NaCl and T = 298.15 K

		logβ
Ligand	**Species** [a]	I **= 0.15** [b]
AMP	**ML$_2$**	5.99 ± 0.02[c]
	ML$_2$H	12.97 ± 0.02
	ML$_2$H$_2$	18.49 ± 0.02
	ML$_2$H$_3$	22.37 ± 0.02
ADP	**ML$_2$**	6.54 ±0.02
	ML$_2$H	13.86 ±0.02
	ML$_2$H$_2$	19.50 ± 0.02
	ML$_2$H$_3$	23.40 ± 0.02
ATP	**ML$_2$**	4.81 ± 0.02
	ML$_2$H	12.06 ± 0.02
	ML$_2$H$_2$	17.91 ± 0.02
	ML$_2$H$_3$	22.04 ± 0.03

[a] According to the reaction (1.10), charges omitted for simplicity; [b] in mol L^{-1};
[c] ± standard deviation.

The speciation profiles are traced in Figure 3.6, by considering I = 0.15 mol L^{-1} in NaCl, T = 298.15 K, C_M = 1 mmol L^{-1} and C_L = 4 mmol L^{-1}. For As(III)-*AMP* system, all the species reach high formation percentages. More in detail, in the pH range between 2 and 5 the predominant species are ML$_2$H$_3$ and ML$_2$H$_2$ with formation percentage close to 60% and 70% respectively. At physiological pH, namely 7.4, the coexistence of ML$_2$H and ML$_2$ is registered and the latter shows the maximum percentage (~ 80%) at pH ~ 8.5. For As(III)-*ADP*, a similar speciation is revealed with greater formation percentages close to 85% for all the complex species. Also in this case, ML$_2$ species is the prevalent one from pH ~ 7.5 until the end of the titration. Instead, as expected after analyzing the formation constants, the As(III)-*ATP* system shows formation percentages of the complex species lower than the other two systems previously studied. For example, the maximum formation percentage reached by the ML$_2$H$_3$ species is ~ 20% at pH ~ 4. Slightly higher are the percentages for ML$_2$H$_2$, ML$_2$H and ML$_2$ which are close to 40% for the first two species and around 35% for the last one.
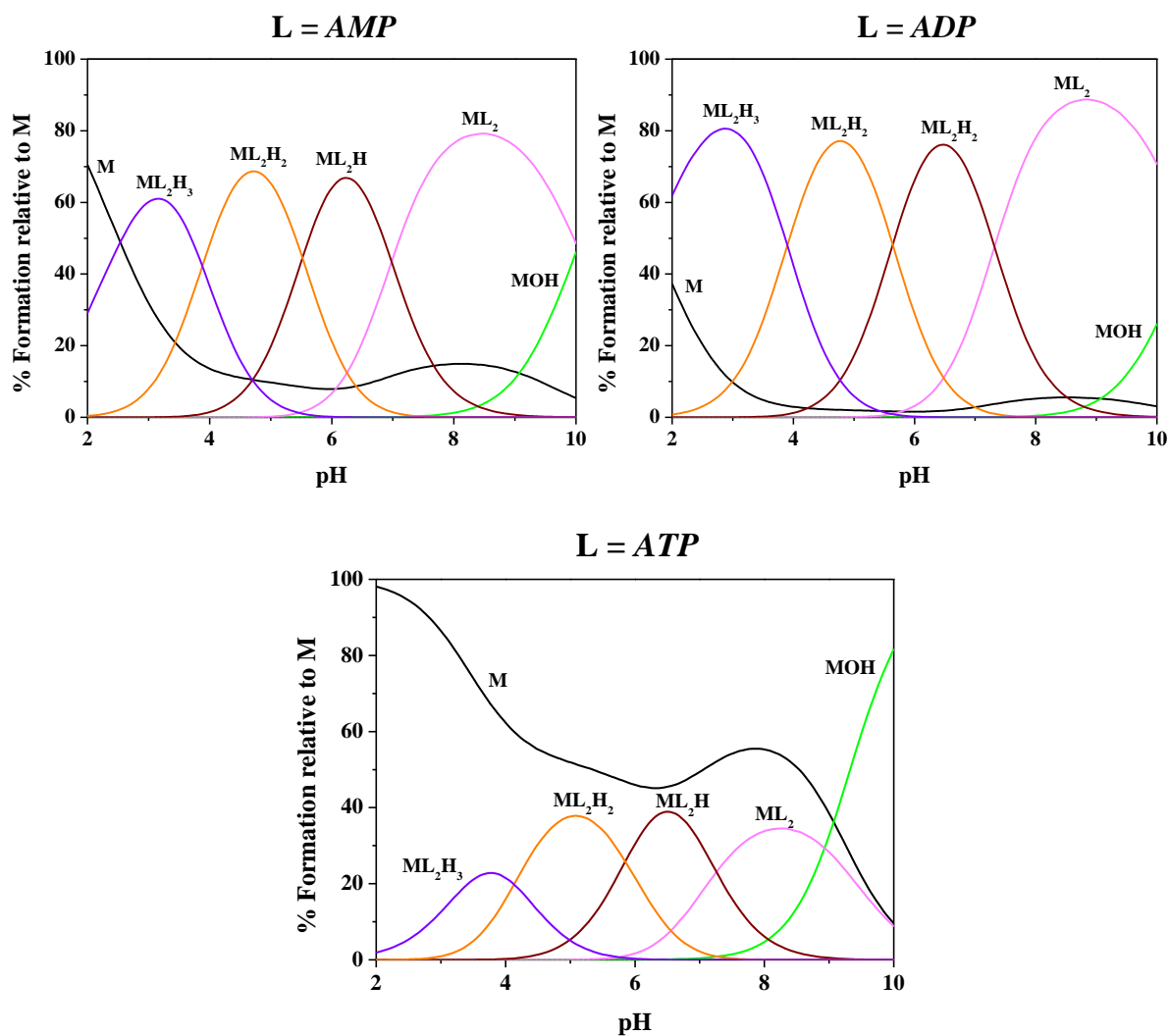
Figure 3.6. Distribution diagrams for As(III)-*AMP*, -*ADP* and -*ATP* species at T = 298.15 K and I = 0.15 mol L^{-1} in NaCl. Conditions: C_M = 1 mmol L^{-1} and C_L = 4 mmol L^{-1}.

3.4 Sequestering ability

3.4.1 As(III)-carboxylate complexes

For As(III)-carboxylate systems, the sequestering ability was calculated at $I = 0.15$ mol L^{-1} and T $= 298.15$ K. For the evaluation of this parameter, two different pH values were taken into account, especially pH $= 5$ and pH $= 7.4$. All the obtained values are reported in Table 3.7. As can be seen, *mal*, *tca* and *btc* show the best sequestering ability at acidic pH, having pL$_{0.5}$ equal to 2.83, 1.64 and 1.66. In particular, the same capability is observed for *tca* and *btc* acids. This aspect is better highlighted in the diagram depicted in Figure 3.7a in which only one curve is visible for both ligands. Mellitic acid, with a pL$_{0.5} = 2.57$, shows a sequestering ability comparable to malonic acid. At physiological pH, the capability to sequester As(III) is reduced, especially for *btc* whose pL$_{0.5}$ results less than 1 and this trend is evident in the diagram in Figure 3.7b. More in detail, the sequestering ability at pH $= 7.4$ increases by following the trend below:

$$btc < tca < mal < mlt$$

In these conditions, mellitic acid shows a good sequestering ability, one order of magnitude higher than that at pH $= 5$. In both cases, malonic and mellitic acids exhibit the best performance. The first one, probably, as a consequence of the two neighboring carboxylic groups which allows to act as bidentate ligand. The second one, presumably, is able to produce a chelating effect on As(III) that makes more stable the complex species.

Table 3.7. pL$_{0.5}$ values for As(III)-*mal*, -*tca*, -*btc*, and -*mlt* systems at $I = 0.15$ mol L^{-1} in NaCl, T $= 298.15$ K and pH $= 5$ or pH $= 7.4$

Ligand	pH	pL$_{0.5}$
mal	5	2.83
	7.4	1.88
tca	5	1.64
	7.4	1.35
btc	5	1.66
	7.4	<1
mlt	5	2.57
	7.4	3.56
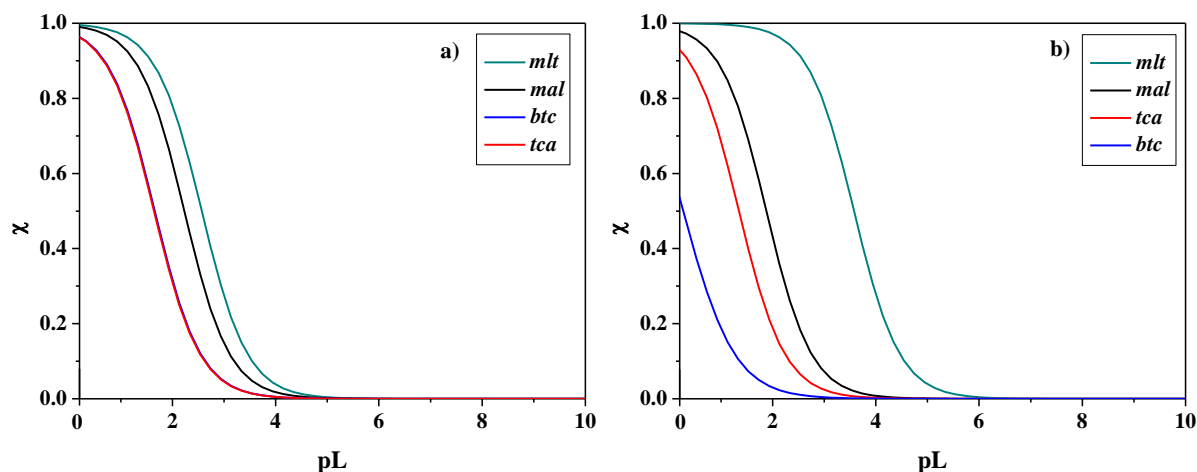
Figure 3.7. Sequestration diagrams for As(III)-*mal*, *-tca*, *-btc* and *-mlt* species at I = 0.15 mol L^{-1} in NaCl and T = 298.15 K. Conditions: a) pH = 5 and b) 7.4.

3.4.2 As(III)-amino acid complexes

For the As(III)-amino acid systems, the sequestering ability was studied at the same experimental conditions of ionic strength and temperature of the previous systems. Also in this case the determination was performed at two different pHs, namely 5 and 7.4. However, as can be observed in Table 3.8, no substantial differences exist between the two pH values.

Table 3.8. pL$_{0.5}$ values for As(III)-*gly*, *-asp* and *-lys* systems at I = 0.15 mol L^{-1} in NaCl, T = 298.15 K and pH = 5 or pH = 7.4

Ligand	pH	pL$_{0.5}$
gly	5	1.55
	7.4	1.99
asp	5	1.55
	7.4	1.47
lys	5	1.82
	7.4	1.85

In general, at pH = 5, the binding ability increases as following:

$$asp = gly < lys$$

Aspartic acid and glycine exhibit the same pL$_{0.5}$ equal to 1.55. Slightly higher is the value for *lys*, whose pL$_{0.5}$ = 1.82. At physiological pH, *asp* and l*ys* display values similar to those indicated for pH = 5, being 1.47 and 1.85 respectively. On the other hand, glycine shows a greater sequestering ability with a value of pL$_{0.5}$ equal to 1.99 but certainly comparable to that

of lysine. Therefore, it seems that the binding capability is influenced by the increase in the number of the amino groups, since *asp* and *gly* have one amino group in the structure while *lys* has one more. Since $pL_{0.5}$ values are very similar for the two pH values under examination, only the sequestration diagram at physiological pH is showed in Figure 3.8.

Figure 3.8. Sequestration diagrams for As(III)-g*ly*, -*asp* and -*lys* species at $I = 0.15$ mol L^{-1} in NaCl, T = 298.15 K and pH = 7.4.

3.4.3 As(III)-nucleotide complexes

To conclude the study relative to the binding capability of ligands of biological interest towards As(III), also nucleotides were examined like the others, thus at $I = 0.15$ mol L^{-1}, T = 298.15 K and two pH values, namely 5 and 7.4. The $pL_{0.5}$ values are reported in Table 3.9.

Table 3.9. $pL_{0.5}$ values for As(III)-*AMP*, -*ADP* and -*ATP* systems at $I = 0.15$ mol L^{-1} in NaCl, T = 298.15 K and pH = 5 or pH = 7.4

Ligand	pH	$pL_{0.5}$
AMP	5	3.37
	7.4	3.25
ADP	5	3.83
	7.4	3.64
ATP	5	2.79
	7.4	2.76

It is easy to notice that the sequestering ability does not change by moving from pH = 5 to pH = 7.4, since the values are very similar and they increase by following the trend below:

$$ATP < AMP < ADP$$

Although in some system [155], recently investigated, the binding capability increases by increasing the number in phosphate groups, namely by going from *AMP* to *ATP*, in this case the trend is unusual. In fact, at pH = 5, as an example, $pL_{0.5}$ values increase from *AMP* ($pL_{0.5}$ = 3.37) to *ADP* ($pL_{0.5}$ = 3.83), as expected, but then they decrease for *ATP*, which shows the lowest $pL_{0.5}$, namely 2.79 at pH = 5. The tendency is exactly the same at pH = 7.4 and it is better observable in the sequestration diagram in Figure 3.9. Probably, since the speciation model is featured by di-coordinated metal-ligand species, the presence of six phosphate groups (ML_2H_x) in the case of *ATP* slightly prevents the interaction of As(III) with the two molecules of ligand.

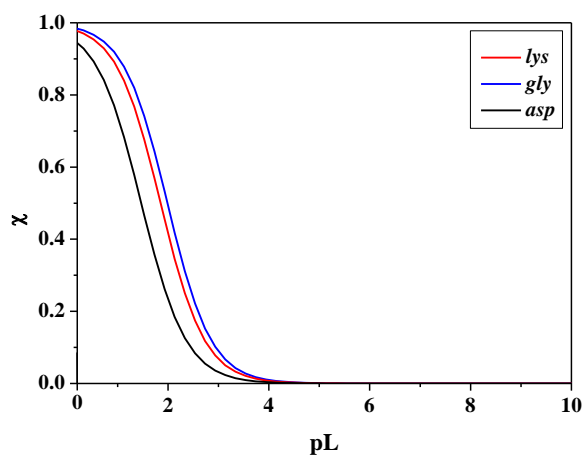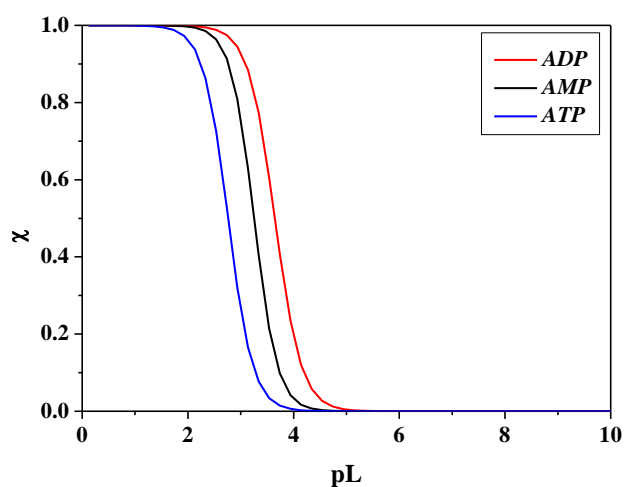**Figure 3.9.** Sequestration diagrams for As(III)-*AMP*, -*ADP*, and -*ATP* species at I = 0.15 mol L^{-1} in NaCl, T = 298.15 K and pH = 7.4.

3.5 Final remarks

A thermodynamic study regarding the interaction of As(III) with molecules of biological interest such as carboxylic acids, amino acids and nucleotides were performed.

The analysis of the obtained results showed that the systems are characterized by a stability not particularly high, having formation constant values for the ML species no more high than 3.7. In particular:

- As(III)-carboxylate systems showed the lowest stability. Among the four carboxylic acids under study, only malonic acid and mellitic acid exhibited higher stability, probably related to their structure which allows to stronger interact with the metal.

- As(III)-amino acids species, probably thanks to the involvement of the amino group, showed a stability slightly higher, which follows the trend: *asp < lys < gly.*

- Regarding to the As(III)-nucleotides interactions, di-coordinated species were identified, showing a stability that increases from *AMP* to *ADP* and then decreases by going from *ADP* to *ATP.*

- Finally, the sequestering ability of all the systems was calculated at $I = 0.15$ mol L^{-1}, T = 298.15 K and two pH values, namely pH = 5 and pH = 7. The obtained $pL_{0.5}$ values demonstrated that, in general, it increases following the tendency reported below:

<p align="center">Amino acids < carboxylic acids < nucleotides</p>

4

As(III)-phosphonic acids interactions: results and discussion

In recent years, the attention of the scientists was paid on the increasingly use of phosphonates in industrial field and on its binding ability.

This ligand class is featured by a stable, covalent carbon-phosphorous bond and the most commonly used compunds are structural similar to the well-known aminopolycarboxylates such as ethylenediaminetetra acetate (*EDTA*) and nitrilotriacetate (*NTA*) [156]. They are mainly used in cooling waters and desalination systems [157] but also in water softening because they are able to block the formation of calcium carbonate [158]. As reported in Ref. [159], Europe is the continent with the highest consumption of phosphonates and it seems that approximately 85% of them in WWTPs (Wastewater Treatment Plants) can be attributed to domestic use. However, the concentration detectable in waste waters effluents, normally, is very low, under the detection limit of the HPLC method discussed by Nowack [160-162] and no genotoxic, mutagenic, carcinogenic nor teratogenic effects were observed related to phosphonates [159]. Moreover, phosphonates, in particular bisphosphonates, are also used in medicine to treat various bone and calcium metabolism diseases and the etidronic acid (*HEDPA*) represents the progenitor [163, 164]. Their high sequestering ability towards heavy metals [165, 166], lantanides [167] and alkaline earth metals [168, 169] was widely documented in many papers reported in literature. In this thesis, three α-aminophosphonates were investigated, namely n-phosphonomethyl iminodiacetic acid, n,n-bis(phosphonomethyl)glycine and nitrilotri(methylphosphonic acid). They are abbreviated as *NTAP*, *NTA2P* and *NTA3P* respectively and the structures are depicted in Figure 4.1. *NTAP*, also indicated as *PMIDA*, is an intermediate in the synthesis of glyphosate, a systemic herbicide and crop desiccant. It is employed to kill weeds, especially annual broadleaf weeds

and grasses that compete with crops. Glyphosate is absorbed through foliage, minimally through roots, and transported to growing points. It inhibits a plant enzyme involved in the synthesis of three aromatic amino acids: tyrosine, tryptophan, and phenylalanine [170]. *NTA2P*, better known as glyphosine, increases sucrose levels in sugarcane and causes chlorosis in maize and other plants [171]. *NTA3P*, also named *ATMP*, performs various functions; it is employed as clining agent, for water treatments, for scaling inhibition and as chelating agent given its excellent chelating ability.

The aim of this chapter is to investigate the interaction between a pollutant, such as As(III), and this class of ligands which, as mentioned above, can be easily found in the environment and they are featured by excellent chelating properties. The study was performed in a wide range of ionic strength by means of potentiometry, in order to know the speciation models and the stability constants of the complex species, togheter with calorimetric experiments (only at $I = 0.1$ mol L^{-1}) in order to determine the formation enthalpy changes related to complex species. Moreover, in order to gain information about the structures of the obtained complexes, mass spectromerty measurements were conducted. Finally, the sequestering ability of *NTAP*, *NTA2P* and *NTA3P* towards As(III) was calculated in conditions that simulate a fresh water and sea water, in particular at pH = 7 and $I = 0.001$ mol L^{-1} in the first case and pH = 8.1 and $I = 0.7$ mol L^{-1} in the last one.
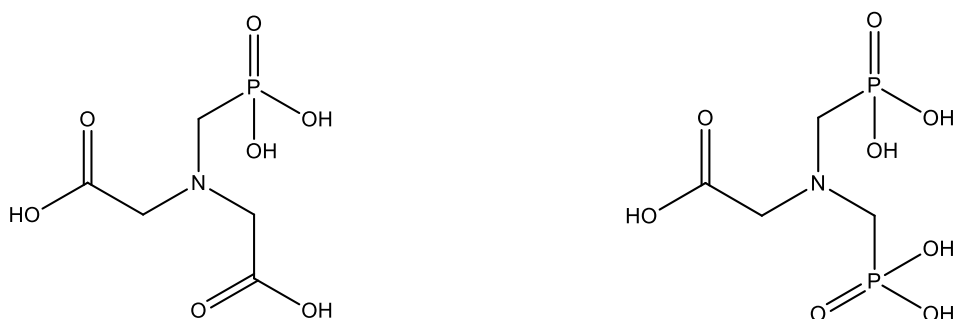
N-(phosphonomethyl)iminodiacetic acid (*NTAP*)   N,N-Bis(phosphonomethyl)glycine (*NTA2P*)
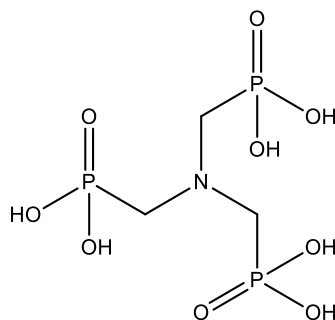
Nitrilotri(methyl phosphonic acid) (*NTA3P*)

Figure 4.1. Phosphonic acids under study

4.1 Ligand protonation constants

With the aim to study the interaction of As(III) with phosphonic acids, the protonation constants of the ligands were previously determined by the research group [166, 168]. They were recalculated at the experimental conditions of ionic strength and temperature used for this investigation and they are reported in Table 4.1.

Table 4.1. Protonation constants of *NTAP, NTA2P* and *NTA3P* at different ionic strength values in NaCl and T = 298.15 K

Ligand	Species [a]	$I = 0.1$ [b]	$I = 0.25$ [b]	$I = 0.5$ [b]	$I = 1$ [b]	Ref.
		logβ^H				
NTAP	**LH**	10.52	10.23	10.09	9.81	[166]
	LH$_2$	16.07	15.67	15.44	15.03	
	LH$_3$	18.05	17.86	17.51	17.34	
	LH$_4$	20.05	19.43	19.33	19.11	
NTA2P	**LH**	11.28	11.08	10.88	10.67	[166]
	LH$_2$	17.64	17.24	16.89	16.50	
	LH$_3$	22.60	22.03	21.60	21.08	
	LH$_4$	24.68	23.93	23.48	22.90	
NTA3P	**LH**	11.984	11.590	11.410	11.390	[168]
	LH$_2$	19.126	18.440	17.990	17.770	
	LH$_3$	24.966	24.020	23.390	23.030	
	LH$_4$	29.529	28.390	27.630	27.180	

[a] According to the reaction (1.8), charges omitted for simplicity; [b] in mol L^{-1};

4.2 As(III)-*NTAP*, *-NTA2P* and *-NTA3P* complexes

4.2.1 Thermodynamic results

The elaboration of the potentiometric data performed by means of BSTAC and STACO computer programs allowed to determine the best speciation model for all the ligand under investigation as well as the stability constants of the species featuring the model. As usual, in the calculation process the hydrolysis constant of the metal and the protonation constants of the ligands were taken into account. Potentiometric titrations were carried out at various ionic strength values, ranging from 0.1 to 1 mol L^{-1}, at T = 298.15 K and in a wide range of pH (2-11). A similar speciation scheme was defined for all the ligands and it is reported in Table 4.2.

Table 4.2. Stability constant values of As(III)-*NTAP, -NTA2P* and *-NTA3P* at different ionic strength values in NaCl and T = 298.15 K

		logβ			
Ligand	**Species**[a]	**$I = 0.1$**[b]	**$I = 0.25$**[b]	**$I = 0.5$**[b]	**$I = 1$**[b]
NTAP	**ML**	4.141 ± 0.004[c]	3.953 ± 0.004[c]	3.39 ± 0.02[c]	3.701 ± 0.007[c]
	MLH	13.229 ± 0.004	12.944 ± 0.005	12.36 ± 0.02	12.718 ± 0.005
	MLH$_2$	18.64 ± 0.01	18.25 ± 0.01	17.64 ± 0.03	17.870 ± 0.008
	MLH$_3$	20.91 ± 0.02	20.63 ± 0.02	19.94 ± 0.05	20.07 ± 0.01
	MLOH	-5.967 ± 0.005	-5.967 ± 0.004	-6.35 ± 0.01	-6.072 ± 0.004
NTA2P	**ML**	4.87 ± 0.04	4.80 ± 0.02	4.30 ± 0.04	3.66 ± 0.03
	MLH	14.01 ± 0.03	13.66 ± 0.02	13.18 ± 0.04	12.52 ± 0.02
	MLH$_2$	20.16 ± 0.04	19.46 ± 0.02	18.90 ± 0.05	18.10 ± 0.02
	MLH$_3$	24.78 ± 0.05	23.68 ± 0.06	23.25 ± 0.05	22.05 ± 0.09
	MLOH	-5.85 ± 0.04	-5.90 ± 0.04	-6.39 ± 0.04	-6.96 ± 0.04
NTA3P	**ML**	5.98 ± 0.03	5.64 ± 0.02	5.295 ± 0.008	5.53 ± 0.02
	MLH	15.10 ± 0.02	14.53 ± 0.02	14.124 ± 0.006	14.38 ± 0.01
	MLH$_2$	22.17 ± 0.01	21.23 ± 0.01	20.541 ± 0.005	20.67 ± 0.01
	MLH$_3$	27.95 ± 0.01	26.803 ± 0.008	25.901 ± 0.005	25.94 ± 0.01
	MLH$_4$	32.516 ± 0.008	31.212 ± 0.004	30.054 ± 0.008	30.01 ± 0.01

[a] According to the reaction (1.10), charges omitted for simplicity; [b] in mol L^{-1}; [c] ± standard deviation.

More in detail, for As(III)-*NTAP* simple metal-ligand species, with diverse protonation degree, were identified, namely ML, MLH, MLH$_2$ and MLH$_3$. Moreover, also an hydrolytic one was included in the model. As can be noticed, the formation constant values decrease from $I = 0.1$ mol L^{-1} to $I = 0.5$ mol L^{-1}. As an example, for the ML species, log β$_{110}$ = 4.141

and 3.39 at $I = 0.1$ mol L^{-1} and $I = 0.5$ mol L^{-1} respectively. Exceeded this value of ionic strength, the stability constants increase again and at $I = 1$ mol L^{-1} log β_{110} results equal to 3.701. As regards As(III)-*NTA2P*, the same speciation model was selected and by observing the ML species, the stability is higher with respect to the previous system; in fact, it shows a log β_{110} equal to 4.87 at $I = 0.1$ mol L^{-1}. In this case, the stability gradually decreases by going from $I = 0.1$ mol L^{-1} to $I = 1$ mol L^{-1}, in the latter showing a log $\beta_{110} = 3.66$. As(III)-*NTA3P* system is characterized by the same trend of that described for As(III)-*NTAP* system, since the formation constants are featured by a decrease until $I = 0.5$ mol L^{-1} and then they increase again. With respect to the other two systems, the stability of the ML species is greater, presenting a value equal to 5.98 at $I = 0.1$ mol L^{-1}, namely one and almost two orders of magnitude higher than As(III)-*NTA2P* and As(III)-*NTA3P* systems at the same ionic strength conditions. Therefore, it seems that the stability of the species is related to the number of phosphonic groups; in particular, the increase in the number of functional groups promotes the interaction with the metal, improving the stability of the complexes. The same tendency was also observed in other systems, studied by the research group, in which phosphonic acids interacted with Al^{3+} [165] This aspect could suggest that phosphonic groups play a key role in the complexation mechanism and the stability order of the complexes could be summarized as follows:

$$NTA3P > NTA2P > NTAP$$

All the systems were investigated in a wide range of pH, as can be seen in the distribution diagrams in Figure 4.2, depicted at T = 298.15 K and at two ionic strength values, namely $I = 0.1$ mol L^{-1} (solid line) and $I = 1$ mol L^{-1} (dashed line). The species distribution of the As(III)-*NTAP* system at $I = 0.1$ mol L^{-1} shows that the predominant species in the pH range between 2 and 9 are MLH$_2$ and MLH which reach formation percentages close to 50% and 60% respectively. The simple metal-ligand species reaches the maximum formation percentage at pH ~ 9.5 followed by the mixed hydrolytic one whose existence is significant at basic pH values. The same speciation model was determined for the As(III)-*NTA2P* system but the diagram displays a different distribution of the species at $I = 0.1$ mol L^{-1}. In this case, MLH$_3$ is dominant in the 2-4.5 pH range, reaching a formation percentage close to 20% at pH ~ 3.5, while the di-protonated and mono-protonated species are the most prevalent from pH ~ 4.5 until pH ~ 9. MLH and ML show formation percentages similar to those of the previous system, while the other ones are about 10% lower in the same experimental conditions. Regarding to As(III)-*NTA3P* system, at $I = 0.1$ mol L^{-1}, from pH = 2 to pH = 4.5 the main

species is the MLH$_4$ with the maximum percentage value equal to 70 at pH = 3. In the pH range between 4.5 until 9.5 the other protonated species are showed with formation percentages close to 50% for MLH$_3$ and MLH$_2$ and 60% for MLH. The ML species is prevalent at basic pH values with a maximum formation (70%) at pH = 10.5.
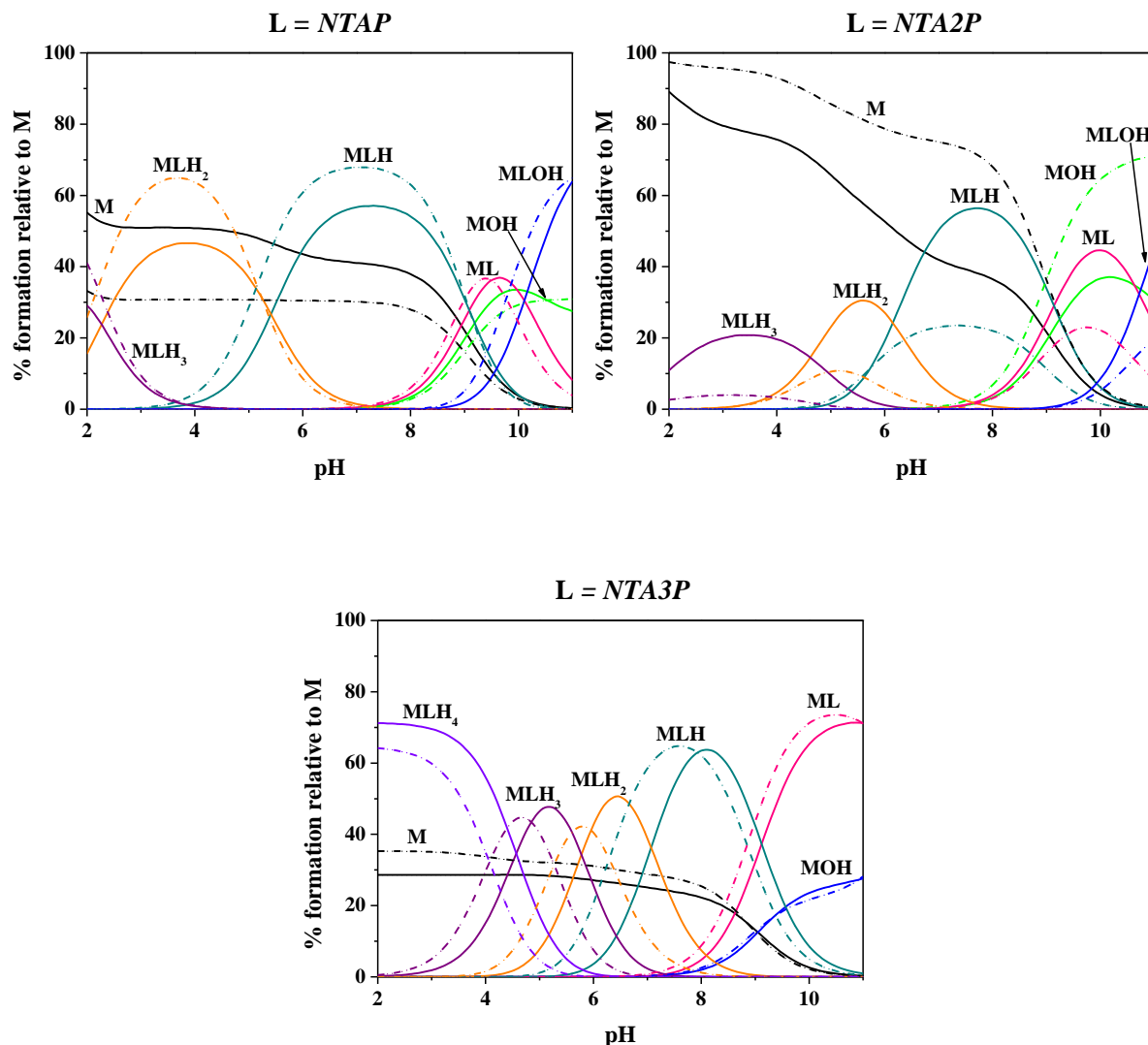

Figure 4.2. Speciation diagrams relative to the As(III)-*NTAXP* system. Conditions: C_M = 2 mmol L^{-1}, C_L = 4 mmol L^{-1}, I = 0.1 mol L^{-1} (solid line) and I = 1 mol L^{-1} (dashed line) in NaCl, T = 298.15 K.

4.2.2 Dependence on ionic strength

Equilibria in solution are strictly related to the ionic strength, which influences the stability constants of the species. As observed in Table 4.2, the formation constants of all the systems are affected by a decrease by going from $I = 0.1$ mol L^{-1} to $I = 0.5$ mol L^{-1}. This trend is also confirmed at $I = 1$ mol L^{-1} for As(III)-*NTA2P* system, while for the other two systems a slight increase is registered at this value of ionic strength. The effect produced by the change of the ionic strength can be better understood by analyzing the distribution diagrams represented in Figures 4.2. For the As(III)-*NTAP* system, the formation percentages of the MLH$_2$ and MLH species, at $I = 1$ mol L^{-1}, increase of about 20% and the curves are subject to a shift towards lower pH values. Also the curves relative to the simple metal-ligand species and the mixed hydrolytic one slightly move to lower pH but they are not affected by changes in the formation percentages. As regards As(III)-*NTA2P* system, the increase of the ionic strength causes a significant decrease of the formation percentages of all the complex species which reach maximum values of 20%. Relative to the As(III)-*NTA3P* system, a negligible decrease relative to the MLH$_4$, MLH$_3$ and MLH$_2$ species is observed, while the opposite trend is noticed for the ML one.

In light of this, when a fluid, be it natural or biological, is under investigation, the knowledge of the formation constants of the species involved in the equilibria at the ionic strength of interest is mandatory. However, these data are not always available and thus the use of mathematical models, such as equation (1.15) is required for the calculation.

By using the Debye-Hückel type equation, the formation constants of Table 4.2 and LIANA program, the log$^T\beta$ values and the C parameter were determined for each complex species. Data are reported in Table 4.3 and they can be used to calculate the formation constants at any ionic strength. As an example, in Table 4.4 the stability constants calculated at the ionic strengths of a fresh water, sea water and at physiological conditions are listed.

Table 4.3. Stability constant values at infinite dilution together with C empirical parameter for As(III)-NTAXP systems at T = 298.15 K

Ligand	Species [a]	log $^T\beta$	C
NTAP	**ML**	6.6 ± 0.1 [b]	2.0 ± 0.2 [b]
	MLH	15.9 ± 0.1	2.2 ± 0.2
	MLH$_2$	21.3 ± 0.1	1.9 ± 0.2
	MLH$_3$	23.5 ± 0.1	1.6 ± 0.2
	MLOH	-3.8 ± 0.1	1.9 ± 0.2
NTA2P	**ML**	8.6 ± 0.2	1.2 ± 0.3
	MLH	18.1 ± 0.2	1.4 ± 0.3
	MLH$_2$	24.4 ± 0.2	1.1 ± 0.3
	MLH$_3$	28.9 ± 0.1	0.5 ± 0.2
	MLOH	-2.8 ± 0.2	0.8 ± 0.2
NTA3P	**ML**	10.0 ± 0.1	3.0 ± 0.2
	MLH	19.7 ± 0.1	3.4 ± 0.2
	MLH$_2$	27.19 ± 0.05	2.9 ± 0.1
	MLH$_3$	33.15 ± 0.08	2.6 ± 0.2
	MLH$_4$	37.7 ± 0.1	2.0 ± 0.2

[a] According to the reaction (1.10), charges omitted for simplicity; [b] $\pm$ standard deviation.

Table 4.4. Calculated stability constants of the As(III)-*NTAXP* systems at different ionic strength values in NaCl and T = 298.15 K.

Species [a]	Ligand	log β [a]		
		$I = 0.001$ [b]	$I = 0.15$ [b]	$I = 0.7$ [b]
ML	*NTAP*	6.3 ± 0.1 [c]	3.9 ± 0.1 [c]	3.54 ± 0.04 [c]
MLH		15.5 ± 0.1	13.00 ± 0.01	12.54 ± 0.05
MLH$_2$		20.9 ± 0.1	18.4 ± 0.1	17.75 ± 0.06
MLH$_3$		23.1 ± 0.1	20.7 ± 0.1	20.00 ± 0.05
MLOH		-4.1 ± 0.1	-6.0 ± 0.1	-6.24 ± 0.06
ML	*NTA2P*	8.2 ± 0.2	5.1 ± 0.1	3.8 ± 0.1
MLH		17.6 ± 0.2	14.1 ± 0.1	12.69 ± 0.09
MLH$_2$		23.9 ± 0.2	20.1 ± 0.1	18.4 ± 0.1
MLH$_3$		28.33 ± 0.09	24.46 ± 0.08	22.41 ± 0.02
MLOH		-3.2 ± 0.2	-5.7 ± 0.1	-6.78 ± 0.09
ML	*NTA3P*	9.5 ± 0.1	5.9 ± 0.1	5.32 ± 0.06
MLH		19.10 ± 0.09	14.99 ± 0.08	14.15 ± 0.05
MLH$_2$		26.49 ± 0.05	21.88 ± 0.04	20.54 ± 0.05
MLH$_3$		32.42 ± 0.08	27.54 ± 0.06	25.88 ± 0.08
MLH$_4$		36.9 ± 0.1	32.01 ± 0.07	30.0 ± 0.1

[a] According to the reaction (1.10), charges omitted for simplicity; [b] in mol L^{-1}; [c] $\pm$ standard deviation.

4.2.3 Dependence on Temperature

The driving forces for the complexation processes occurring in solution include factors and features that have different and often opposing enthalpic and entropic contributions and thus splitting the standard Gibbs energy term into the $\Delta H°$ and T$\Delta S°$ components may help understanding relevant details of the complexation equilibria that are not expressed in the $\Delta G°$ term alone. Isothermal calorimetric (ITC) titrations were carried out with the aim of directly collecting the heat of formation of the complex species formed by As(III), thus providing a complete thermodynamic characterization of the systems investigated. In Table 4.5 the thermodynamic protination parameters of *NTAP* and *NTA2P* ligands are reported at $I = 0.1$ mol L^{-1} in NaCl and T = 298.15 K, while Table 4.6 reports the ΔH values together with the ΔG and TΔS contributions of the metal-ligand species. As(III)-*NTA3P* system is currently under investigation and, for this reason, results are not reported in this thesis.

Table 4.5. Protonation thermodynamic parameters of *NTAP* and *NTA2P* at $T = 298.15$ K and at $I = 0.1$ mol L^{-1} in NaCl

Ligand	Species [a]	-ΔG [b]	ΔH [b]	TΔS [b]	Ref.
NTAP	**LH**	60.0	-11.7	48.3	[166]
	LH₂	91.7	-8.7	83.0	
	LH₃	102.9	-5.5	97.4	
NTA2P	**LH**	64.4	-16.0	48.4	[166]
	LH₂	100.6	-12.2	88.4	
	LH₃	128.9	-7.8	121.1	
	LH₄	140.8	-6.9	133.9	

[a] Referred to the reaction (1.8); [b] in kJ mol^{-1}.

Table 4.6. Thermodynamic formation parameters for As(III)-*NTAP* and –*NTA2P* species at $T = 298.15$ K and at $I = 0.1$ mol L^{-1} in NaCl

Ligand	Species [a]	-ΔG [b]	ΔH [b]	TΔS [b]
NTAP	**MLH₃**	119.4	-14 ± 3 [c]	105
	MLH₂	106.4	-6.4 ± 0.2	100.0
	MLH	75.5	-7.5 ± 0.6	68.0
	ML	23.6	31.7 ± 0.8	55.3
	MLOH	-34.1	65 ± 2	31
NTA2P	**MLH₃**	141.4	-7.9 ± 0.4	133.5
	MLH₂	115.1	-9.9 ± 0.6	105.2
	MLH	80.0	-12.2 ± 0.4	67.8
	ML	27.8	55.4 ± 0.8	83.2
	MLOH	-33.4	85 ± 2	52

[a] Referred to the reaction (1.10); [b] in kJ mol^{-1}, [c] $\pm$ standard deviation

Typical ITC titration curves, obtained for the As(III) - *NTAP* and As(III) - *NTA2P* systems at suitably selected pH ranges, are shown in Figure 4.3-4.5 and 4.6-4.8, respectively. For each system, calorimetric data collected at different pH windows were analyzed together using a proper software (HypCal) which allows for the simultaneous refinement of multiple titrations. The formation of all the complex species of As(III) with both *NTAP* and *NTA2P* is entropy favored and driven and is mainly due to metal and ligand desolvation (release of hydration water molecules upon complexation). The interactions of As(III) with hard anions (phosphonate and carboxylate groups of the ligands) are mostly electrostatic. This evidence was also observed for the complex species formed by the same ligands with Al^{3+} [165] and Ca^{2+} [172], in which the entropic term was found to be the prevailing contribution to the free Gibbs energy value.
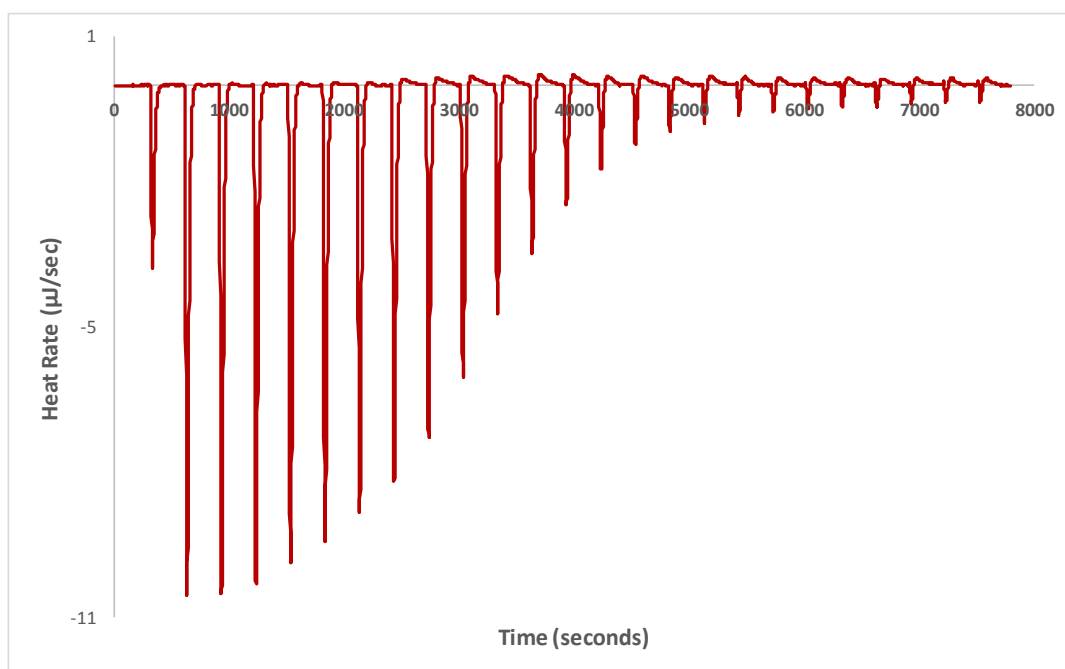

Figure 4.3. Calorimetric titration curve of As(III) (15 mmol L^{-1}) with *NTAP* (2 mmol L^{-1}) at *I* = 0.1 mol L^{-1} (NaCl) and T = 298.15 K. The titration was carried out in the 5.3 ÷ 3.0 pH range.

Figure 4.4. Calorimetric titration curve of As(III) (15 mmol L^{-1}) with *NTAP* (2 mmol L^{-1}) at *I* = 0.1 mol L^{-1} (NaCl) and T = 298.15 K. The titration was carried out in the 7.2 ÷ 3.6 pH range.

Figure 4.5. Calorimetric titration curve of As(III) (12 mmol L^{-1}) with *NTAP* (1.9 mmol L^{-1}) at *I* = 0.1 mol L^{-1} (NaCl) and T = 298.15 K. The titration was carried out in the 10.6 ÷ 9.1 pH range.

Figure 4.6. Calorimetric titration curve of As(III) (15 mmol L^{-1}) with *NTA2P* (2.4 mmol L^{-1}) at $I = 0.1$ mol L^{-1} (NaCl) and T = 298.15 K. The titration was carried out in the 5.7 ÷ 3.5 pH range.
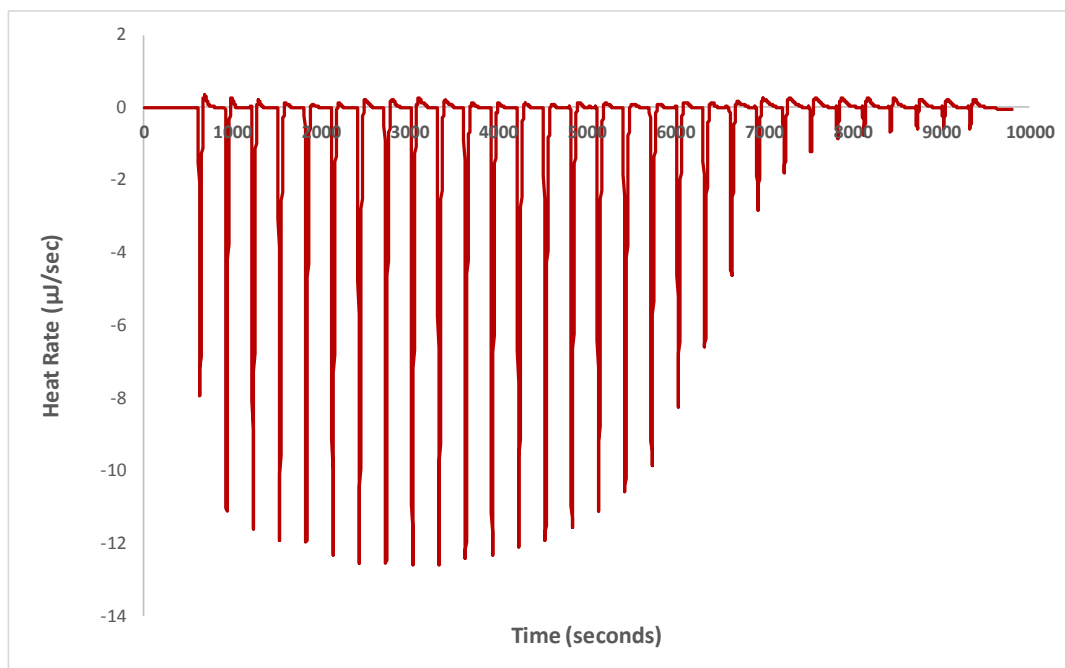

Figure 4.7. Calorimetric titration curve of As(III) (14 mmol L^{-1}) with NTA2P (2.5 mmol L^{-1}) at $I = 0.1$ mol L^{-1} (NaCl) and T = 298.15 K. The titration was carried out in the 9.8 ÷ 7.7 pH range.
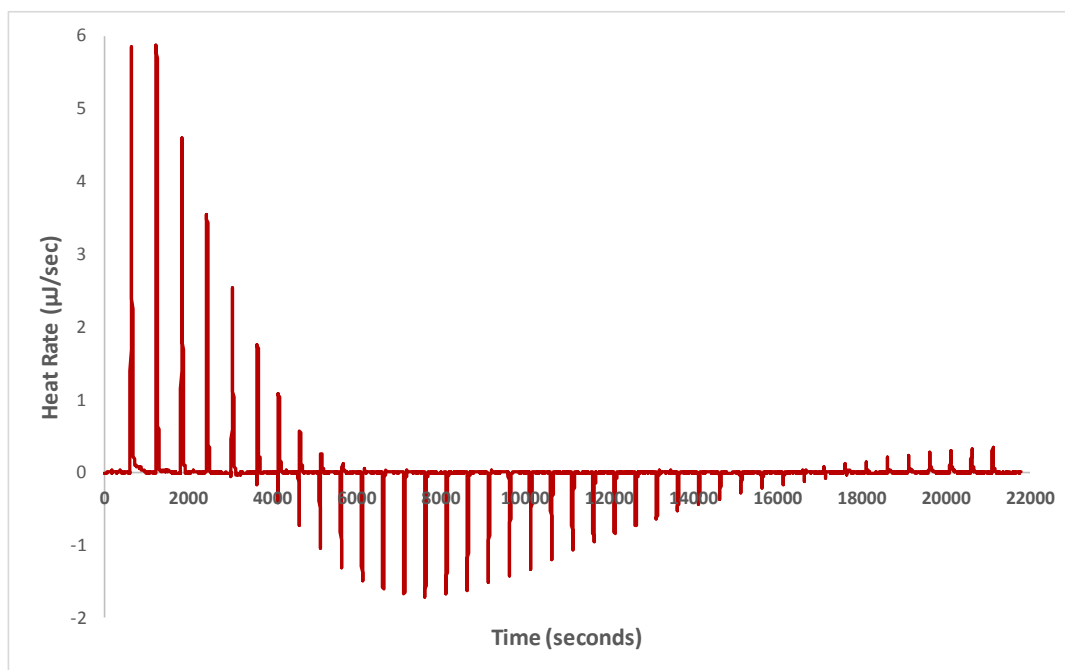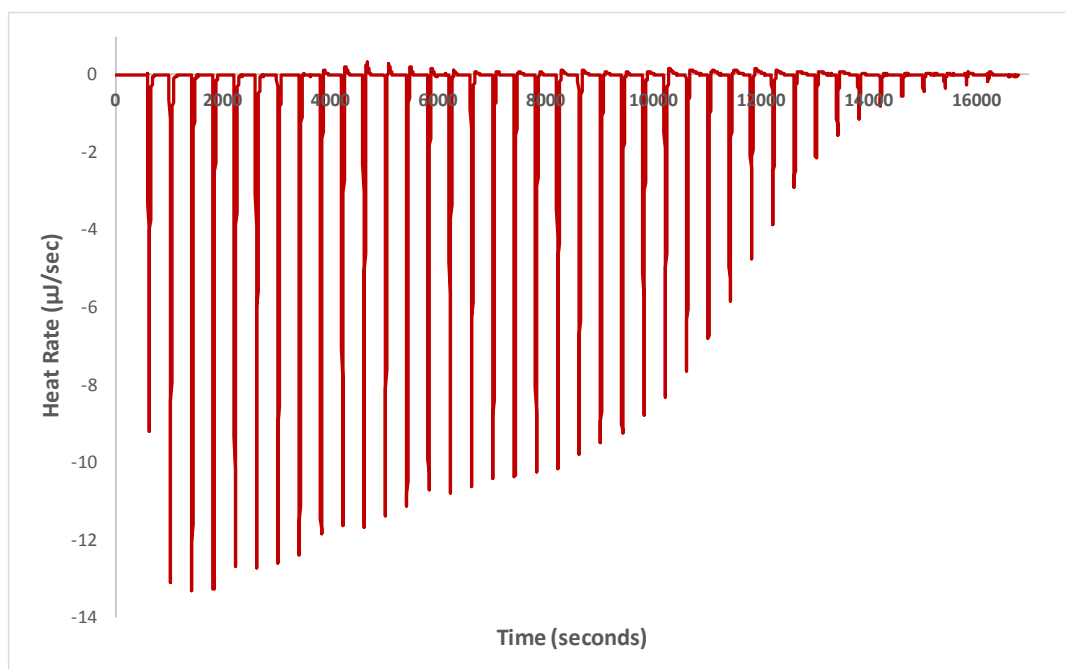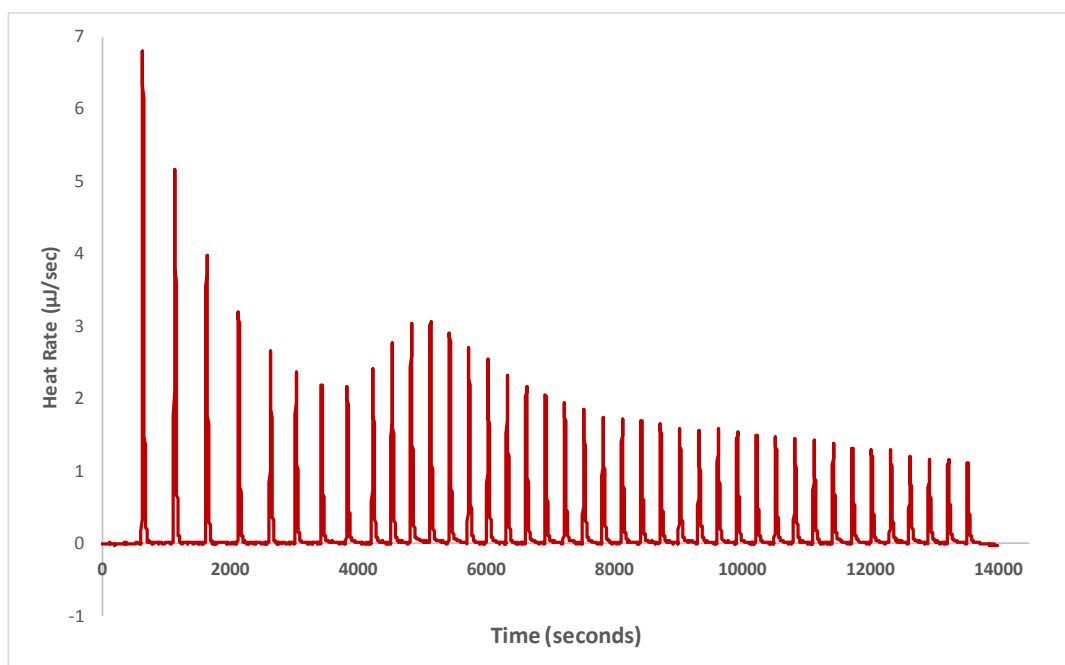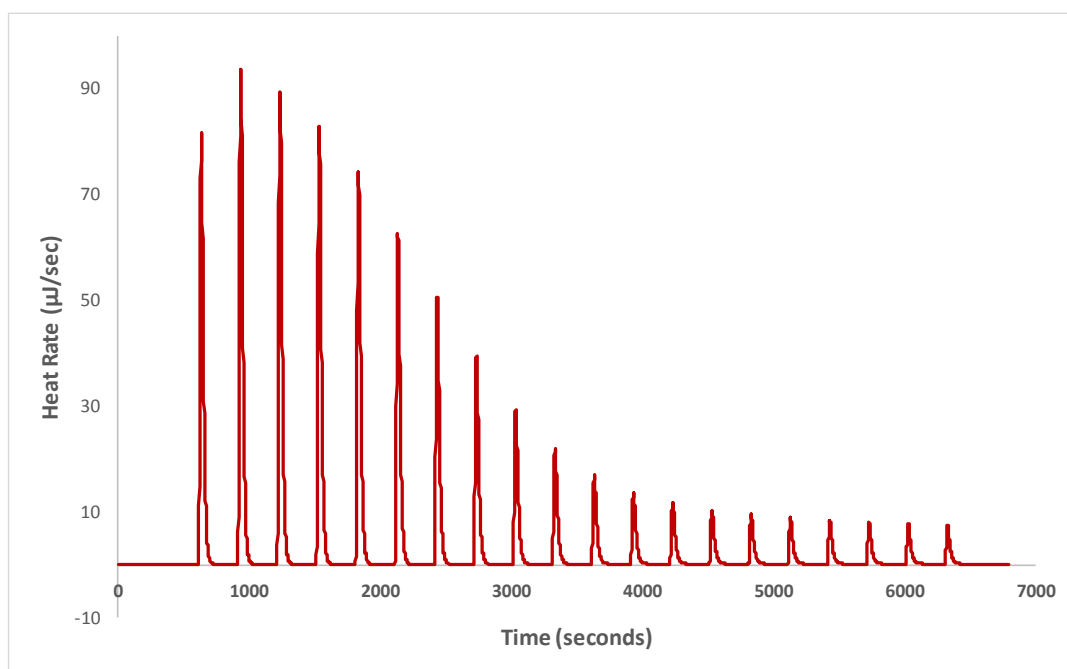
Figure 4.8. Calorimetric titration curve of As(III) (14 mmol L^{-1}) with NTA2P (2.4 mmol L^{-1}) at I = 0.1 mol L^{-1} (NaCl) and T = 298.15 K. The titration was carried out in the 10.8 ÷ 9.3 pH range.

4.2.4 Mass spectrometry results

Electrospray mass spectrometry (ESI-MS) is appropriate for direct analysis of solutions containing preformed ions [173, 174] including metal-ligand systems [80, 175, 176]. Matrix assisted laser desorption mass spectrometry (MALDI-TOF/TOF-MS) is generally employed for studing large biomolecules [177, 178], but the analysis of low molecular weight analytes is also possible through tandem mass spectrometry which is able to provide the required sensitivity and molecular specificity. MALDI MS in this research work was exploited to investigate the complexes between the amino phosphonates *NTAP, NTA2P* and *NTA3P* and ions of As(III). The first step of the study was the optimization of the experimental conditions for the detection and characterization of ligands (*NTAP, NTA2P* and *NTA3P*). An aliquot of a 1mM solution of the ligands was analyzed by MS experiments in negative and positive ionization mode by using traditional matrices (α−CHCA, DHB). Since low abundant molecular ions were detected for all ligands in negative MS experiments, the complete characterization of the complexes (ligands + As(III)) was performed in positive ionization mode using α−CHCA as matrix. The phosphonic acids (*NTAP, NTA2P and NTA3P*) derived from nitrilotriacetic acid (*NTA*) are featured by the presence of variable number of both phosphonic and carboxylic groups. The phosphorus atom shows +5 oxidation state and, being tetra-coordinate, it can support the coordination of multiple metal ion *via* oxygen atoms. The pKa_1 values of organophosphonic acids are similar to the corresponding carboxylic acids $RC(O)OH$ [179, 180]. The amino phosphonic acids can be doubly deprotonated in two defined successive steps and the first proton is a couple orders of magnitude more acidic than the second one [181]. Therefore, the nitrogen atom represents the more basic center in ligands and most probable protonation site (Figure 4.9). Thus, the ligands (*NTAP, NTA2P* and *NTA3P*) are well explained in term of zwitter-ions. Fragmentation of $[L+H]^+$ (*NTAP, NTA2P* and *NTA3P*) follows two pathways (Figure 4.3). First, the cleavage of *C-P* bond that probably occurs via intramolecular H^+ migration from the amino group to the phosphoryl group through a five-membered-ring intermediate (β -cleavage; Figure I **A**, **NTAP** and **NTA2P**: $[C_4H_9NO_5P]^+$, m/z 182.02; **NTA3P**: $[C_3H_{10}NO_6P2]^+$; m/z 217,99779). Analogously, *N-C* bond of amino phosphonates (*NTAP, NTA2P and NTA3P*) is cleaved via intramolecular H• methylene transfer to the phosphoryl group through a six-membered-ring intermediate (Figure II **C**, **NTAP** and **NTA2P**: $[C_3H_9NO_5P]^+$; m/z 170.02; **NTA3P:** $[C_2H_8NO_6P_2]^+$; m/z 203.97).
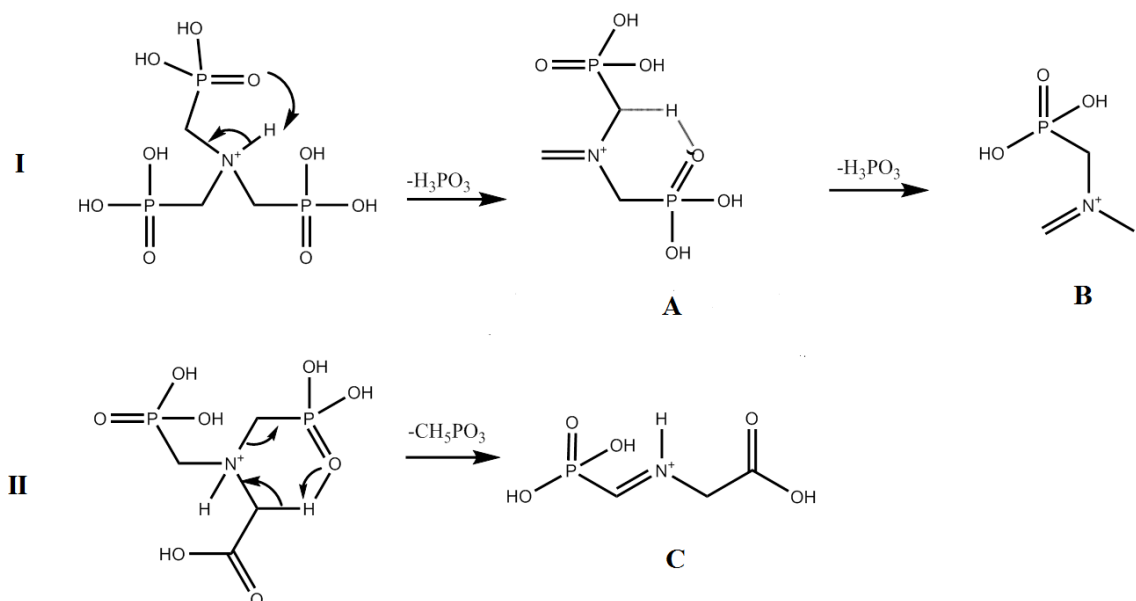
Figure 4.9. Fragmentation pathways of [L-H] $^+$ ions. For **B, NTAP and NTA2P**: n.d; **NTA3P:** $[C_3H_8NO_3P]^{\cdot+}$; m/z 137.03.

The information about ML species were gained in the full-scan MS by deposition of a few μl of the aqueous reaction mixtures. MS information combined with data collected by MS/MS at 1 KeV of collision energy were used to assign the most probable structures of the complexes ML. All the MS analysis indicated the formation of an equimolar complex ($[MLH]^+$) and accurate mass measurements clearly highlighted that in any case the doubly-deprotonated ligands (*NTAP, NTA2P* and *NTA3P*) are involved in the formation of the complex ($[As-LH]^+$). The MALDI-MS spectrum obtained for the complexation of As(III) with *NTA3P* showed the formation of ion of m/z 389.89 ($[C_3H_{12}AsNO_{10}P_3]^+$, Δppm = 5). Fragmentation of this ion by MS/MS is consistent with that observed for free ligand. All observed fragments derived from breakage of *C-P* and *N-C* bonds of the amino phosphonate (Figure 4.10, Table 4.7). The cleavages of *C-P* led to the consecutive neutral loss of 82 Da (H_3PO_3) suggesting that only one phosphonate group to be involved in the coordination of As(III). Therefore, MS/MS data indicated that *NTA3P* acts as a bidentate ligand *via* the phosphonate oxygens and binds As(III) forming a 4-membered chelate ring with the P–O group. The mechanism of the formation of 4-membered chelate ring (O-As-O-P) appears to be rather obvious upon the treatment with As(III), based on the preliminary generation of zwitterionic ligand due to the fact that the central nitrogen is protonated. The hypotesized structure for [As(III)- *NTA3P* H]$^+$ is in agreement with that reported previously for solid state M(II)- *NTA3P* complexes [182-186].

Table 4.7. MALDI MS/MS fragments of [As(III)- *NTA3P* H]$^+$

			m/z	Δppm
[3-AsH]+	[MLH]+	[C$_3$H$_{12}$AsNO$_{10}$P$_3$]+	389.89	5
MS/MS	[ML-H$_2$O]$^+$	[C$_3$H$_{10}$AsNO$_9$P$_3$]$^+$	371.9	12
	[ML-H$_3$PO$_3$]$^+$	[C$_3$H$_9$AsNO$_7$P$_2$]$^+$	307.97	12
	[ML-H$_4$PO$_6$]$^+$	[C$_3$H$_8$AsNO$_4$P]$^+$	227.99	16
		[C$_3$H$_9$NO$_3$P]$^+$	138.08	
		[CH$_5$NO$_3$P]$^+$	110.03	
		[C$_3$H$_{12}$NO$_8$P$_3$]$^{•+}$	283.05	
		[C$_2$H$_7$NO$_3$P]$^+$	124.06	
		[CH$_2$AsO$_4$P]$^{•+}$	183.92	
		[C$_3$H$_8$AsNO$_4$P]$^+$	227.99	
		[C$_2$H$_4$AsNO$_4$P]$^+$	211.95	
		[CH$_2$AsO$_3$P]$^{•+}$	167.92	
		[CH$_6$AsNO$_4$P]$^+$	201.96	
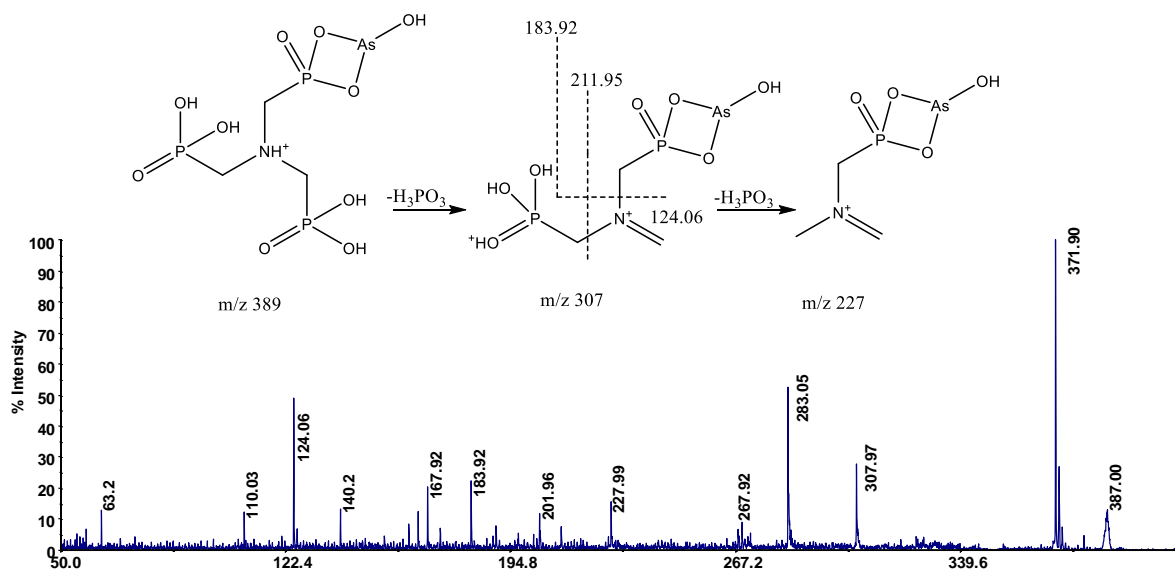
Figure 4.10. MALDI MS/MS spectrum of [As(III)- *NTA3P* H]$^+$.

The presence of a carboxylic group on the coordination of the ligand can be examined by gas-phase fragmentation of the ion m/z 353 ([As(III)- *NTA2P* H]$^+$. Figure 4.11 reports the potential coordination modes of *NTA2P* towards As(III).
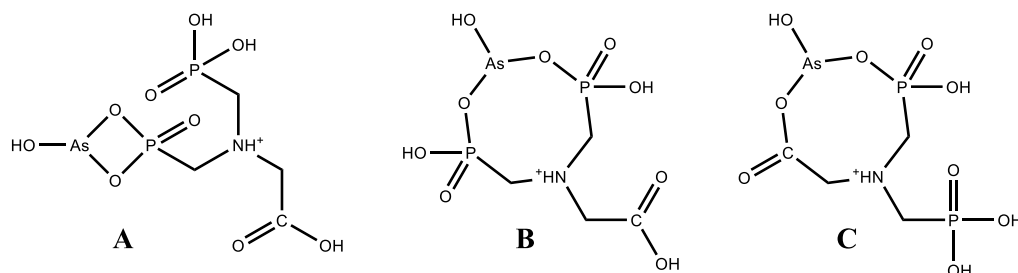
Figure 4.11. Coordination modes of [As(III)- *NTA2P* H]$^+$ complex

The direct and consecutive neutral losses of molecules with low molecular weight, such as H_2O, CO_2 and $C_2H_3O_2$, suggest that a carboxylic group is not involved in the coordination of As(III). The ions deriving from the loss of 82Da (H_3PO_3) or 96 Da (CH_5PO_3) were not detected, and for this the most probable structure of the [As(III)- *NTA2P* H]$^+$ complex is B (Figure 4.11, Figure 4.12).
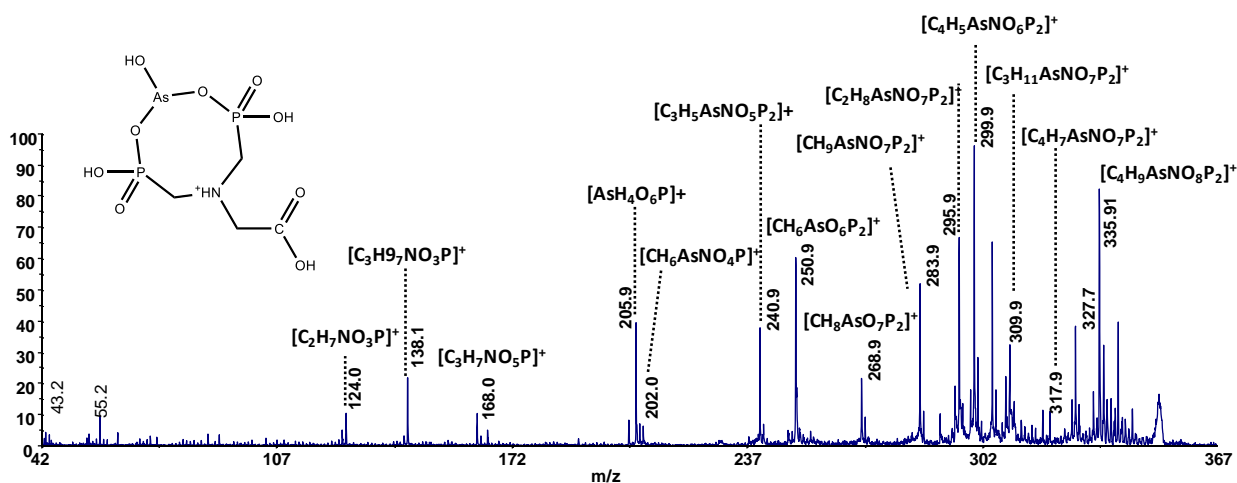
Figure 4.12. MALDI MS/MS spectrum of (B).

The coordination mode of the ligand *NTAP* is different from two mentioned above. MS/MS spectrum of [As(III)- *NTAP* H]+ shows ions arising neutral loss attributable to free carboxylic group. The competitive cleavages of *C-P* and *N-C* bond of amino phosphonates indicate that *NTAP* binds As(III) *via* phosphonate and carboxylic oxygens fashioning 8-membered chelate ring (Figure 4.13).
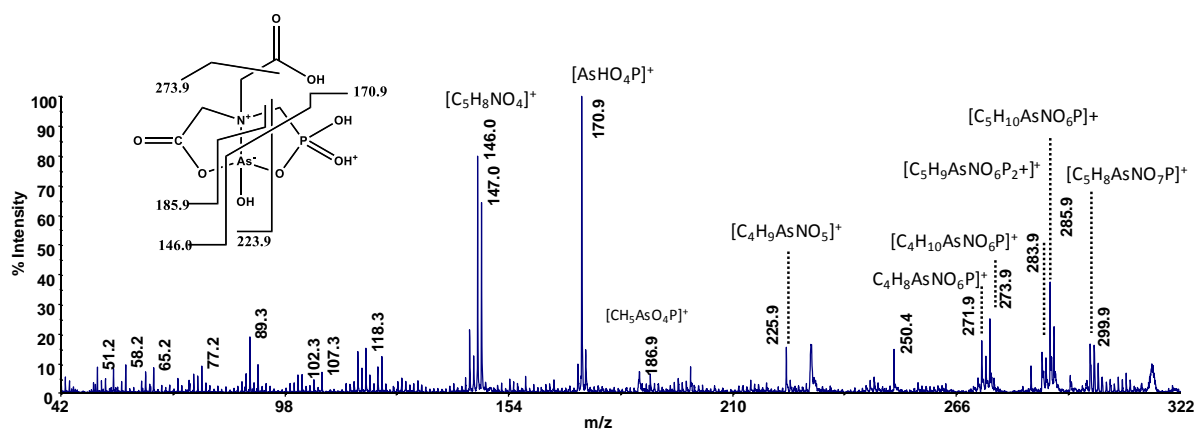
Figure 4.13. MALDI MS/MS spectrum of [As(III)-*NTAP* H$^+$].

The phosphonate moiety of the ligands (*NTAP, NTA2P* and *NTA3P)* always binds to the metal ion. The amino group remains protonated and not coordinated (*NTA2P* and *NTA3P*). Only in the case of *NTAP* the amino group and the carboxylic oxygen participate to coordination of As(III) in the investigated experimental conditions.

4.3 Sequestering ability

The determination of the sequestering ability of *NTAP*, *NTA2P* and *NTA3P* towards As(III) is a fundamental aspect in order to evaluate their possible use in the removal techniques, especially in environmental field. In this work, it was investigated at two experimental conditions, in particular at $I = 0.001$ mol L^{-1} and pH = 7, conditions of a generic fresh water, and at $I = 0.7$ mol L^{-1} and pH = 8.1 for seawater. The pL$_{0.5}$ values are reported in Table 4.8.

Table 4.8. pL$_{0.5}$ values for As(III)-*NTAP*, -*NTA2P* and –*NTA3P* systems at $I = 0.001$ mol L^{-1} and $I = 0.7$ mol L^{-1} in NaCl, pH = 7 and pH = 8.1 respectively and T = 298.15 K.

Ligand	pH	I[a]	pL$_{0.5}$
NTAP	7	0.001	4.43
	8.1	0.7	2.91
NTA2P	7	0.001	5.17
	8.1	0.7	2.33
NTA3P	7	0.001	5.64
	8.1	0.7	3.05

[a] in mol L^{-1}

All the ligands exhibit a good sequestering ability at the conditions of a fresh water, since the pL$_{0.5}$ values are equal to 4.43, 5.17 and 5.64 for *NTAP*, *NTA2P* and *NTA3P* respectively. In the second example, the sequestering ability decreases of almost two order of magnitude, showing pL$_{0.5}$ comparable between the three ligands, since the values are equal to 2.33, 2.91 and 3.05 for *NTA2P*, *NTAP* and *NTA3P* respectively. Thus, in general, the capability of the ligand to complex As(III) increases by increasing the phosphonic groups in the molecule, following the trend *NTA3P* > *NTA2P* > *NTAP*. This tendency is better observable in Figure 4.14a. In the case of seawater, Figure 4.14b, the sequestering ability of *NTA2P* is slightly lower than *NTAP*. Probably, this reversal trend could be attributed to the decrease of the stability of the main species, namely MLH, at pH = 8.1 and $I = 0.7$ mol L^{-1}. In fact, the log K$_{111}$, in the case of *NTA2P*, is equal to 2.06, while for As(III)-*NTAP* system the value is slightly higher, namely 2.66.
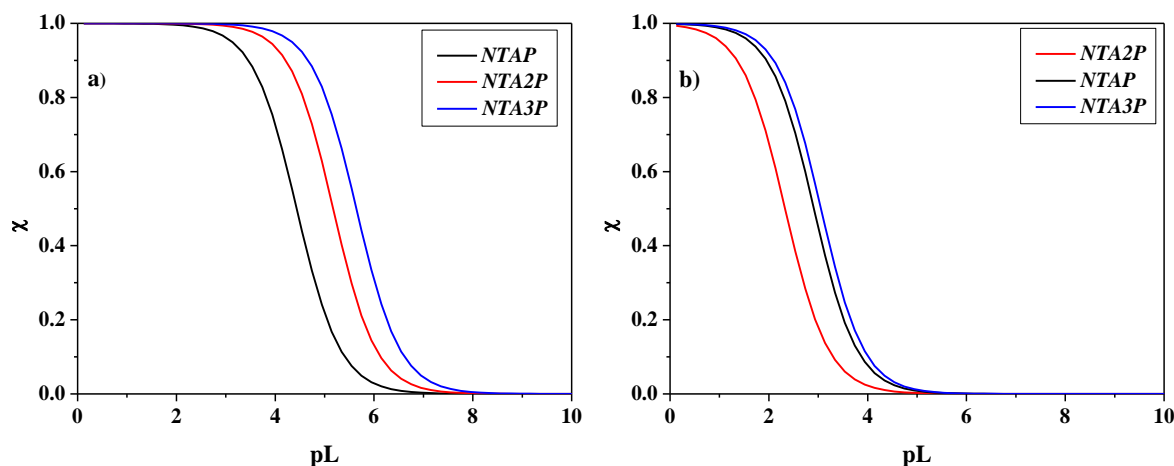
Figure 4.14. Sum of mole fractions of As(III)-*NTAXP* species *vs.* pL at: a) $I = 0.001$ mol L^{-1} and pH = 7.0; b) $I = 0.7$ mol L^{-1} and pH = 8.1 in NaCl at T = 298.15 K.

4.4 Final Remarks

The thermodynamic investigation carried out on As(III)-*NTAXP* systems pointed out the good stability of these complexes. In particular:

- the formation constants of the systems under study increase by increasing the number of the phosphonic groups, being log β_{110} = 4.141, 4.87 and 5.98 for As(III)-*NTAP*, -*NTA2P* and –*NTA3P* respectively.

- The dependence of the stability constants was evaluated and the use of the Debye Hückel type equation allowed to calculate the stability constants at ionic strengths different from those under examination.

- The dependence of the thermodynamic parameters on temperature was studied by means of isothermal calorimetric titrations which evidenced that the main contribution to the free energy is of the entropic type, as observed for other systems in which the same ligands were employed.

- Mass spectrometry experiments clarified how As(III) binds to ligand molecules, pointing out that the phosphonate moiety always interact with the metalloid. Specifically, for *NTAP* both carboxyilic and amino groups coordinates with As(III) while for the other two systems the amino group remains protonated.

- Finally, the sequestering ability of all the ligands was studied in conditions simulating sea water and a fresh water, showing good performances especially in the last case.

5

Empirical relationships

Speciation studies regarding metal-ligand interactions as well as the evaluation of the sequestering ability of a ligand towards a specific metal cation are of great importance, as repeatedly stated in this thesis. However, these investigations are often difficult to achieve in real matrices, such as natural waters, biological fluids, wastewater, since thery are very complex systems, defined multicomponents, that could undergo a series of chemical and physical reactions. For a correct speciation investigation, all the collateral reactions must be taken into account as well as temperature, ionic strength, pH, pressure and so on. For all these reasons, the possibility to reproduce these conditions is almost impossible or at least expensive. Therefore, the experimental approach, clearly favorite, may be supported by modeling studies, such as those already mentioned relative to the dependence of the stability constants on ionic strenght and temperature. A part from this, the formation constants can be modeled by using another approach that considers all the contributions of the functional groups present in the ligands under examination (Additivity Factors Approach) [187-190]. Thus, log K can be reported as:

$$\log K = \sum n_{\text{x-donor}} \tag{2.4}$$

where $n_{\text{x-donor}}$ is representative of –S, -N or –OP donor group. For the calculation, the log K values of the ML species relative to As(III) interaction with thiol ligands, namely *tla*, *tma*, and *cys*, carboxylic acids, namely *mal*, *tca* and *mlt*, and phosphonic acids, namely *NTAP*, *NTA2P* and *NTA3P,* were taken into account at $I = 0.15$ mol L^{-1} in NaCl and T = 298.15 K. The contribution of each functional group is represented by the following equation:

$$\log K = 3.4 n_{\text{S}^-} + 0.58 n_{\text{COO}^-} + 2.1 n_{\text{PO}^-} \tag{2.5}$$

being 3.4 ± 0.4, 0.58 ± 0.09 and 2.1 ± 0.2 the contributions of thiol, carboxylic and phosphoinic groups respectively, with a log K ± 0.7 (95% confidence interval) estimated precision.

This trend confirms the experimental results from which it was observed that the interaction with sulfhydryl groups is greater than phosphonic groups and even higher than carboxylic ones. Figure 5.1 shows the stability constants values, calculated by means of eq. 2.5, plotted as a function of the experimental values and, as can be noticed, a good agreement is registered, being the correlation coefficient, R^2, equal to 0.98 and the slope equal to 0.96 ± 0.04.
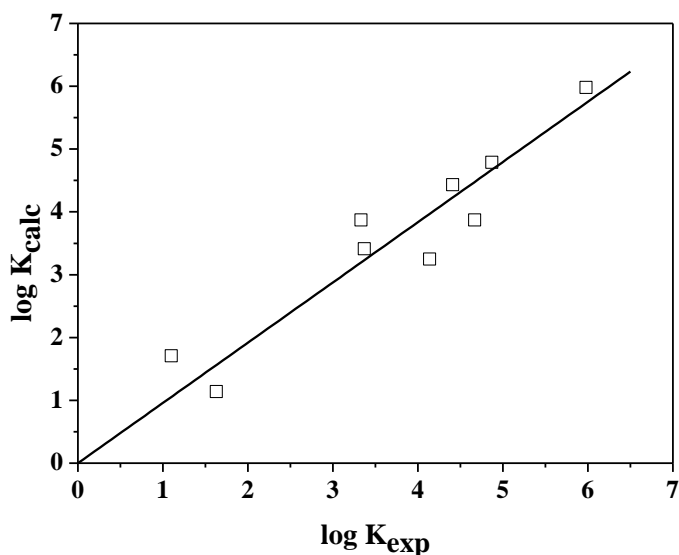
Figure 5.1. Calculated stability constants (eq. 2.5) vs. experimental stability constants of the ML species relative to As(III) interaction with *tla, tma, cys, mal, tca, mlt, NTAP, NTA2P* and *NTA3P* at $I = 0.15$ mol L^{-1} and T = 298.15 K.

As an example, log K of the ML species of *tma* at $I = 0.15$ mol L^{-1} (reported in Table 2.3 of Section II) shows a value equal to 4.41 and the corresponding value, calculated by eq. 2.5, results equal to 4.43.

Section III

Arsenic(V): acid-base properties and interaction with alkaline-earth and trivalent metal cations in aqueous solution

In the +5 oxidation state, arsenic prefers to exist as the arsenate oxyanion [90] and to interact with metal cations. In litearature, several studies are reported on As(V) adsorption onto mineral surfaces, such as clays and metal oxides of Al, Fe and Mn [191-195] but, despite the well-known toxicity of arsenate [3, 8], literature databases are poor in thermodynamic studies performed in aqueous solution. For this reason, in this Section, the acid-base properties of arsenate were analyzed followed by the study relative to arsenate interactions with different metal cations. Specifically, the acid-base properties were studied in a wide range of ionic strength and pH by potentiometry technique, while calorimetric titrations allowed to determine the enthalpy changes. The investigation was completed by the employment of *ab initio* molecular dynamics simulations in order to atomistically trace the hydrolysis steps of arsenate in aqueous environment until alkali conditions. The behavior of arsenate, as ligand molecule, was analyzed towards some bi and trivalent cations of interest for sea water. In particular, as bivalent cations, calcium, magnesium and strontium metal cations were studied, in the range $0.1 < I /\text{mol L}^{-1} < 1$ in NaCl and at T = 298.15 K. Measurements were carried out by exploiting potentiometric titrations in order to define the speciation models and through calorimetry to investigate the dependence on temperature. Also the speciation of arsenate in presence of trivalent metal cation, in particular iron and aluminium, was examined in a wide range of ionic strength and regarding Fe(III)-arsenate system, also spectrophotometry was employed for confirming the speciation model.

1

As(V) acid-base properties: results and discussion

The arsenic atom in arsenate compounds shows a valency equal to +5 and it can be also indicated as pentavalent arsenic or As(V). It is naturally present in a variety of minerals, such as adamite, alarsite, legrandite [196] and its distribution, as already mentioned, is linked to the pH variation. In particular, in highly acidic conditions it mainly exists as arsenic acid, H_3AsO_4; in moderately acidic conditions it is converted in dihydrogen arsenate ion, $H_2AsO_4^-$, followed by hydrogen arsenate ion, $HAsO_4^{2-}$, in moderately basic conditions and finally by the arsenate ion, AsO_3^-, in highly basic conditions. Arsenate is very similar to phosphate anion since arsenic occurs in the same group of phosphorus in the periodic table. It can replace inorganic phosphate in the step of glycolysis that produces 1,3-bisphosphoglycerate from glyceraldehyde 3-phosphate. This one produces 1-arseno-3-phosphoglycerate which is unstable and quickly hydrolyzes, forming the next intermediate in the pathway, 3-phosphoglycerate. Therefore, glycolysis proceeds, but the *ATP* molecule, which should be generated from 1,3-bisphosphoglycerate, is lost. This probably explains the particular toxicity of arsenate for human organism. The acid-base properties of arsenate will be well discussed in this chapter from the experimental and computational point of view, as mentioned at the beginning of the present Section.

1.1 Computational results

For As(V), four hydrolysis steps are expected. Because of its Lewis-acidic character due to a high charge, the times of the hydrolysis steps are limited with respect to those reported for As(III) in Chapter 1 of the Section II. The first step, similar to that of As(III), occurs after 60 fs (τ_1), leading to the formation of As(OH)$^{4+}$ species. The second one, indeed, has a time twice than that registered for As(III), namely 520 fs (τ_2), indicating that other complex interactions, such as water dissociation induced by the transient ion As(OH)$^{4+}$, verify before the formation of As(OH)$_2$$^{3+}$. In the third step, the As(OH)$_3$$^{2+}$ species is formed after several disparate proton transfer attempts, and in less than 2 ps the final product H$_3$AsO$_4$ is reached. The hydrolysis mechanism is depicted in Figure 1.1a-d [95].
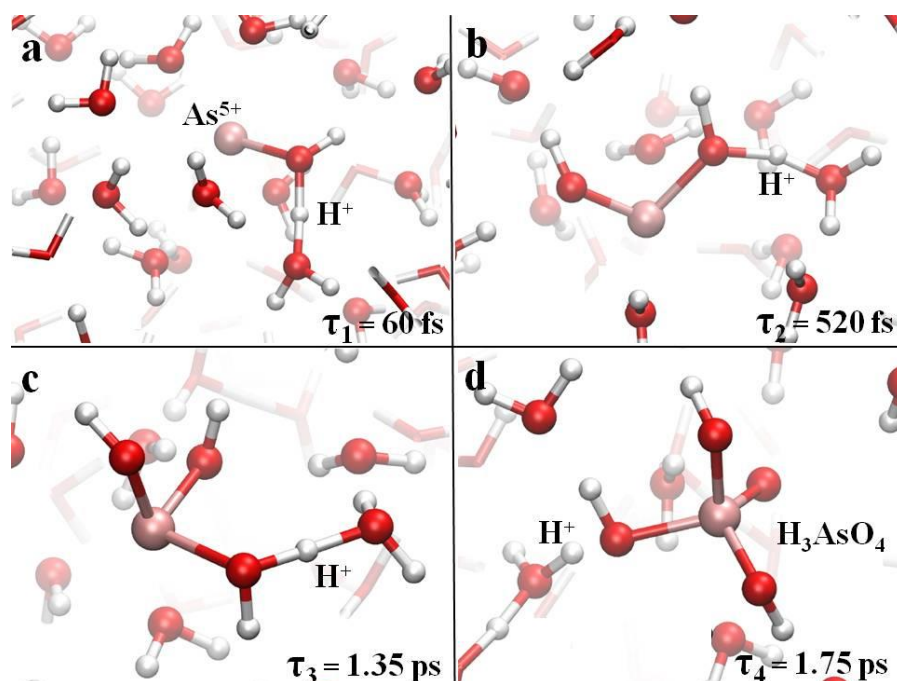
Figure 1.1. Successive hydrolysis steps for As(V) in neutral aqueous solution. Red, white, and pink spheres represent oxygen, hydrogen and arsenic atoms, respectively [95].

In increasing alkaline conditions, the four characteristic times considerably decrease, as visible in Table 1.1, and in conditions defined as "mild" and "high", namely in presence of four and six hydroxide anions respectively, the most stable form is the di-hydrogen arsenate, H$_2$AsO$_4$$^-$, as can be also visible in the distribution diagram in Figure 1.2. By adding other two or four hydroxide anions to the "high" alkaline conditions, thus increasing the pH value, other two species can be identified: hydrogen arsenate (HAsO$_4$$^{2-}$) and the arsenate anion (AsO$_4$$^{3-}$).

Table 1.1. Characteristic time (in fs) for the different hydrolysis steps of As(V) under different conditions of pH. The alkaline conditions marked as "low", "mild", and "high" refer to numerical samples where two, four, and six hydroxide ions are present, respectively.

	Neutr.	Low	Mild	High
τ_1(fs)	60	50	50	50
τ_2(fs)	520	60	50	50
τ_3(fs)	1350	350	150	120
τ_4(fs)	1750	800	400	350

Therefore, the different protonated forms of As(V) can be easily detectable by means of potentiometric titrations in which the pH is changed during the measurements. This aspect will be better discussed in the following paragraphs.

1.2 Experimental results

1.2.1 Protonation constants determination

The stable species H_3AsO_4 is involved in three protonation steps, namely:

$$H^+ + AsO_4^{3-} = HAsO_4^{2-} \tag{3.1}$$

$$H^+ + HAsO_4^{2-} = H_2AsO_4^- \tag{3.2}$$

$$H^+ + H_2AsO_4^{2-} = H_3AsO_4 \tag{3.3}$$

Experimentally, potentiometric measurements were performed in a wide range of pH (2-11), in order to determine all the protonation constants. A vast range of ionic strength (0.1-1 mol L^{-1} in NaCl) was considered and different ligand concentrations, reported in 1.2 paragraph of Section I were employed. All the experiments were performed at T = 298.15 K. The values of the protonation constants obtained from the elaboration of potentiometric data through BSTAC and STACO computer programs are reported in Table 1.2 [197].

Table 1.2. Experimental protonation constants of arsenate in NaCl at different ionic strengths and T = 298.15 K

	$\log\beta^H$			
Species [a]	$I = 0.1$ [b]	$I = 0.25$ [b]	$I = 0.5$ [b]	$I = 1$ [b]
LH	11.08 ± 0.04 [c]	10.79 ± 0.04 [c]	10.62 ± 0.02 [c]	10.51 ± 0.01 [c]
LH$_2$	17.70 ± 0.05	17.29 ± 0.05	17.00 ± 0.02	16.78 ± 0.01
LH$_3$	19.83 ± 0.06	19.56 ± 0.06	19.08 ± 0.03	18.81 ± 0.04

[a] According to equation (1.8); [b] in mol L^{-1}; [c] $\pm$ standard deviation.

As can be noticed, the first protonotation occurs at high alkaline conditions, around pH = 10.5-11; the second one is registered in the pH range 6-7 and the third one in acidic environment, around pH = 2. Moreover, a decrease of the protonation constants is registered when ionic strength increases. As an example, by going from $I = 0.1$ mol L^{-1} to $I = 1$ mol L^{-1}, log β_{011} decreases of almost to order of magnitude, being log $\beta_{011} = 11.08$ and log $\beta_{011} = 10.51$ respectively. Recently, Raposo *et al.* [198] studied the dependence of the protonation constants on the ionic strength in NaCl , KCl and NaClO$_4$ at $I = 0.5$ mol L^{-1} and $I = 1$ mol L^{-1} and reported values are in good agreement with those here determined. As an example, log β = 10.50, 16.73 and 18.71 were indicated for the three protonation steps at $I = 1$ mol L^{-1}. As can be observed in Table 1.2, at the same ionic strength, log β = 10.51, 16.78 and 18.81 respectively. In Figure 1.2 the distribution of the species is represented at two ionic strength values, namely $I = 0.1$ mol L^{-1} (solid line) and $I = 1$ mol L^{-1} (dashed line). The variation of ionic strength does not influence the formation percentages of the species which are close to 100% for LH$_2$ and LH species, the predominant ones for all the investigated pH range. The totally protonated species, LH$_3$, and the deprotonated one, L, are significant at pH < 3 and pH > 10 respectively. However, a shift towards lower pH is highlighted when the ionic strength increases until 1 mol L^{-1}.
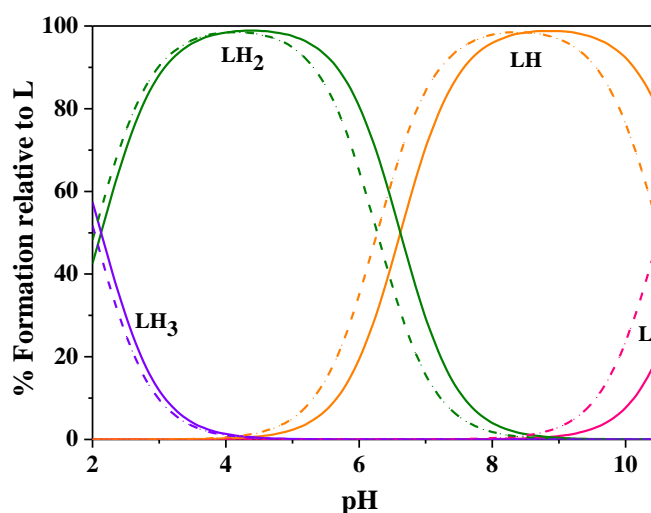

Figure 1.2. Speciation diagram of AsO$_4^{3-}$ (L)-H$^+$ species in NaCl at $I = 0.1$ mol L^{-1} (solid line) and $I = 1$ mol L^{-1} (dashed line). Conditions: C$_L$ = 1 mmol L^{-1}.

1.2.2 Dependence on ionic strength

As already observed, the ionic strength strongly influences the stability of the constants, causing, in this case, a decrease of these one even of one order of magnitude when I is increased and a shift of the speciation curves towards lower pHs. Therefore, for a correct evaluation of the species distribution, the effect produced on the formation constants by the change of the ionic strength needs to be investigated. By fitting the values of the protonation constants reported in Table 1.2 through the Debye-Hückel type equation (eq. 1.15) and LIANA program, the formation constants values extrapolated to $I = 0$ mol L^{-1} and the C empirical parameter can be calculated. Results are listed in Table 1.3. The determination of these two parameters is fundamental for calculating the protonation constants at ionic strengths different from the experimental ones and some examples, at useful ionic strengths, are given in Table 1.4.

Table 1.3. Protonation constant values at infinite dilution together with C empirical parameter for the dependence on ionic strength relative to AsO_4^{3-} (L)-H^+ species.

Species [a]	$\log^T\beta$	C	Ref.
LH	11.68 ± 0.04[b]	0.04 ± 0.06	This thesis [197]
LH₂	18.75 ± 0.04	0.06 ± 0.05	This thesis [197]
LH₃	21.17 ± 0.05	0.09 ± 0.06	This thesis [197]

[a] According to equation (1.8); [b] $\pm$ standard deviation.

Table 1.4. Calculated protonation constants of arsenate in NaCl at different ionic strengths and T = 298.15 K

	$\log\beta^H$				
Species [a]	$I = 0.001$ [b]	$I = 0.1$ [b]	$I = 0.5$[b]	$I = 0.7$[b]	$I = 1$[b]
LH	11.59 ± 0.04[c]	11.03 ± 0.04[c]	10.65 ± 0.02[c]	10.57 ± 0.02[c]	10.50 ± 0.03[c]
LH₂	18.59 ± 0.03	17.66 ± 0.03	17.03 ± 0.02	16.90 ± 0.02	16.77 ± 0.03
LH₃	20.98 ± 0.05	19.86 ± 0.05	19.11 ± 0.03	18.96 ± 0.02	18.81 ± 0.01

[a] According to equation (1.8); [b] in mol L^{-1}; [c] $\pm$ standard deviation.

1.2.3 Dependence on temperature

To complete and, at the same time, to enrich the thermodynamic database regarding the acid-base properties of arsenate, calorimetric titrations were performed at T = 298.15 K and at two ionic strength values, I = 0.1 mol L^{-1} and I = 0.7 mol L^{-1} in order to determine the enthalpy changes. ΔH values, together with ΔG and TΔS values are listed in Table 1.5.

Table 1.5. AsO$_4^{3-}$ thermodynamic parameters[a] in NaCl at I = 0.1 mol L^{-1} and I = 0.7 mol L^{-1} at T = 298.15 K.

Species [b]	-ΔG	ΔH	TΔS	-ΔG	ΔH	TΔS
		I = 0.1[c]			I = 0.7[c]	
LH	63.0	-18.1 ± 0.8[d]	44.9	60.3	-20.3 ± 0.8 [d]	40.0
LH$_2$	100.8	-24.4 ± 0.9	76.4	96.5	-23.2 ± 0.8	73.3
LH$_3$	113.4	-29 ± 1	84	108.2	-21 ± 2	87

[a] in kJ mol^{-1}; [b] according to equation (1.8); [c] in mol L^{-1}; [d] ± standard deviation

In literature few papers report on arsenate thermodynamic protonation parameters [199-202]. Goldberg *et al.* report ΔH_1 = -15.8 kJ mol^{-1} at I = 0 mol L^{-1} and T = 298.15 K while Sellers *et al.* ΔH_1 = -18.2 kJ mol-1 at I = 0.2 mol L^{-1} and T = 298.15 K. Both are in agreement with that determined in this thesis at I = 0.1 mol L^{-1}(-18.1 kJ mol -1), in particular the value indicated by Sellers [202]. The enthalpy values for all the protonation steps show an exothermic trend and no obvious changes are registered from I = 0.1 mol L^{-1} to I = 0.7 mol L^{-1}, since, for example, ΔH_1 = -18.2 kJ mol^{-1} and -20.3 kJ mol^{-1} at I = 0.1 mol L^{-1} and I = 0.7 mol L^{-1} respectively. The knowledge of thermodynamic formation parameters is useful to estimate the effect of temperature on the speciation [79, 80, 203, 204]. An example of species distribution at two different temperatures (T = 298.15 K and T = 310.15 K) and I = 0.1 mol L^{-1} is reported in Figure 1.3, where it can be seen that the variation of temperature, in this case, does not affect the distribution.

Figure 1.3. Species distribution at I = 0.1 mol L^{-1} and T = 298.15 K (pink line) and T = 310.15 K (blue line).

1.3 Final remarks

The acid-base properties of arsenate were determined by means of potentiometry in a wide range of ionic strength. The combined use of experimental procedures and computational methods allowed to conclude that:

- the time (τ_4) that leads to the formation of the stable arsenic acid (H_3AsO_4) statistically occurs at 1.75 ps.

- By adding hydroxide ions (OH^-), namely in conditions defined as "mild" and "high" the most stable species is di-hydrogen arsenate ($H_2AsO_4^-$). The addition of other hydroxide ions to the condition called "high" leads to the formation of $HAsO_4^{2-}$ and AsO_4^{3-}. This is also confirmed by experimental measurements which allowed to determine the first protonation constant in alkaline environment (pH ~ 10), the second one between 6-7 and the third one at acidic pH (pH ~ 2).

- Calorimetric titrations provided the formation enthalpy of all the protonation steps and the effect of temperature on the distribution was evaluated, leading to the conclusion that by going from T = 298.15 K to T = 310.15 K no appreciable changes are observed in the distribution of the species.

2

As(V) interaction with alkaline-earth metals: results and discussion

The aqueous complexes between arsenate and metal cations are rather neglected in the literature since, as previously anticipated, more broad space was given to the study related to the absorption of As (V) on mineral surfaces, clays and metal oxides. However, to better understand the interactions that occur between dissolved arsenic species and mineral surface, the knowledge of arsenic speciation in aqueous phase is required as well as the evaluation of its interaction with inorganic cations normally present in natural waters. The first data concerning the complexes that arsenate forms with the metal cations mostly present in sea water date back to 1956 [199, 201, 205], but the values reported for the stability constants often are in contradiction with each others and these discrepancies, as well as the lack of data, are in some cases highlighted by Nordstrom *et al.* in a recent review [206]. With the aim to contribute to enrich the thermodynamic database relative to As(V), the interactions with the major bivalent cations of natural waters, in particular sea water, will be discussed in the present chapter. In particular, alkaline-earth metal cations such as calcium, magnesium and strontium were investigated. Calcium and magnesium are the most abundant elements of the earth's crust (4.6% and 2.7%, respectively) [207]. Magnesium is the second element for abundance in water and it can be found in some minerals such as magnesite ($MgCO_3$), dolomite ($MgCO_3 \cdot CaCO_3$) and it is also a constituent of many rocks (olivine, talc, amphibole). Calcium is one of the fundamental constituents of the calcareous rocks and it can be found as limestone ($CaCO_3$), gypsum ($CaSO_4 \cdot 2H_2O$) or fluorite (CaF_2).

Calcium, inside the human body, essentially performs plastic functions, going to constitute, as phosphate, the mineral matrix of the bone tissue. One part of the calcium is removable and, by dissolving, keeps calcemia constant. It is essential for the excitation-contraction of the muscle, including the heart; it also activates vitamin K favoring platelet aggregation and blood coagulation. It is essentially taken with the diet: milk derivatives are the richest elements of this mineral and even water can be a good source (the so-called hard waters are rich in calcium). Calcium deficiency can decrease bone and tissue reserve causing osteoporosis.

The 60% of magnesium constitutes the bone tissue as phosphate, the 39% is found in intracellular fluids and the remaining 1% in extracellular fluids as cation. In the organism, it regulates the metabolism since it participates in the activity of many enzymatic systems in the metabolism of glucides, in the biosynthesis of proteins and lipids and it is responsible for the transmission of muscle impulses. As it is an integral part of chlorophyll it is widespread especially in green vegetables [208]. Strontium commonly occurs in nature, being the 15th most abundant element on Earth. Basically, it is present as the sulphate mineral celestine ($SrSO_4$) and the carbonate strontianite ($SrCO_3$). It also exists as ^{90}Sr isotope, a radioactive element and one of the most dangerous components of nuclear fallout, since it is absorbed by the body in a similar way to calcium. In water, most forms of stable and radioactive strontium are dissolved. Stable strontium dissolved in water, basically comes from strontium in rocks and soil that water runs over and through. Only a very small part of the strontium found in water is from dust out of the air. There are no harmful effects of stable strontium in humans at the levels typically found in the environment. In adults, it tends to attach only to the surface of bones, but in children, strontium can replace calcium in the growing bones and thus lead to bone growth problems [209].

The complexes formed by arsenate with alkaline-earth metal cations were analyzed by potentiometry in a wide range of ionic strength and pH with the final purpose to predict the behavior of the complex species in real systems which are featured by variable composition in terms of pH, ionic strength and temperature. In this regard, also calorimetric measurements were performed in order to determine the formation enthalpy of the complexes, useful to calculate, by means of Van't Hoff equation (eq. 1.16), the stability constants at temperature different from 298.15 K.

2.1 Ligand protonation and metal hydrolytic constants

In order to study M^{2+}-arsenate complexes, the protonation constants of the ligand and the hydrolytic constants of the metals must be taken into account for a correct investigation. In particular, the protonation constants of arsenate were reported and discussed in the previous chapter, while the hydrolysis constants of the metals under study are reported in Table 2.1 of the present paragraph. They were calculated from Baes and Mesmer [210] and refer to the reaction:

$$M^{2+} + H_2O = M(OH)^+ + H^+ \qquad (3.4)$$

Table 2.1. Employed metal hydrolysis constant values.

I /mol L^{-1}	$\log\beta^{a)}$		
	$Mg(OH)^+$	$Ca(OH)^+$	$Sr(OH)^+$
0.1	-11.69	-13.06	-13.50
0.25	-11.79	-13.11	-13.55
0.5	-11.88	-13.11	-13.56
1	-11.98	-13.04	-13.49

$^{a)}$According to equation (3.4).

2.2 Ca^{2+}, Ma^{2+} and Sr^{2+} -arsenate complexes

2.2.1 Thermodynamic results

The interaction between arsenate and alkaline earth metal complexes was investigated by potentiometric titrations in a vast range of ionic strength (0.1 < I/mol L^{-1} < 1), in NaCl as background salt, and in a pH range between 2 and 11, except in the case where poorly soluble species were formed, generally around pH ~ 8 [197]. As usual, data were elaborated by means of BSTAC and STACO computer programs, taking into account the hydrolysis constants of the metals and the protonation constants of the ligand. The best speciation model, for each system, was selected on the basis of the criteria exposed in the previously chapters and it is reported in Table 2.2 together with the stability constants for every determined complex species. As can be noticed, the same speciation model was obtained for all the systems under investigation and it is featured by simple metal-ligand species differently protonated, specifically ML, MLH and MLH$_2$. In order to have an idea of the stability of the complexes, the ML can be considered as comparison species between the systems. As can be observed, the log β relative to this species increases by going from Mg^{2+} to Sr^{2+}, showing values equal to 5.21, 5.41 and 6.31 for Mg^{2+}-*ars*, Ca^{2+}-*ars* and Sr^{2+}-*ars* at I = 0.1 mol L^{-1}. Concerning the mono and di-protonated species, the analysis of the partial formation constants, also reported

in in Table 2.2, highlights that these complexes are very weak, since values range from 1.45 to 3.23.

Table 2.2. Experimental stability constants of M^{2+}-arsenate in NaCl at different ionic strengths and T = 298.15 K

	logβ			
Reaction	**$I = 0.1$** [a]	**$I = 0.25$** [b]	**$I = 0.5$** [b]	**$I = 1$** [b]
$Mg^{2+} + AsO_4^{3-}$	5.21 ± 0.02[b]	4.86 ± 0.04	4.66 ± 0.06	4.79 ± 0.09
$Mg^{2+} + AsO_4^{3-} + H^+$	13.15 ± 0.02	12.93 ± 0.06	12.90 ± 0.06	13.74 ± 0.04
$Mg^{2+} + AsO_4^{3-} + 2H^+$	19.15 ± 0.04	18.95 ± 0.04	19.05 ± 0.07	19.92 ± 0.04
$Ca^{2+} + AsO_4^{3-}$	5.41 ± 0.05	5.39 ± 0.02	5.63 ± 0.02	6.57 ± 0.04
$Ca^{2+} + AsO_4^{3-} + H^+$	13.85 ± 0.04	13.37 ± 0.02	13.21 ± 0.03	13.56 ± 0.04
$Ca^{2+} + AsO_4^{3-} + 2H^+$	20.20 ± 0.03	19.73 ± 0.02	19.42 ± 0.02	19.15 ± 0.02
$Sr^{2+} + AsO_4^{3-}$	6.31 ± 0.02	6.10 ± 0.08	6.13 ± 0.03	5.95 ± 0.02
$Sr^{2+} + AsO_4^{3-} + H^+$	13.91 ± 0.03	13.56 ± 0.03	13.48 ± 0.05	13.67 ± 0.02
$Sr^{2+} + AsO_4^{3-} + 2H^+$	20.16 ± 0.04	19.78 ± 0.07	19.46 ± 0.05	19.69 ± 0.02
	logK			
$Mg^{2+} + HAsO_4^{2-}$	2.07	2.14	2.28	3.23
$Mg^{2+} + H_2AsO_4^-$	1.45	1.66	2.05	3.14
$Ca^{2+} + HAsO_4^{2-}$	2.77	2.58	2.59	3.05
$Ca^{2+} + H_2AsO_4^-$	2.5	2.44	2.42	2.37
$Sr^{2+} + HAsO_4^{2-}$	2.83	2.77	2.86	3.16
$Sr^{2+} + H_2AsO_4^-$	2.46	2.49	2.46	2.91

[a] in mol L^{-1}; [b] $\pm$ standard deviation.

Lower stability of the protonated species (MLH and MLH_2) with respect to the ML is further pointed out in the species distribution depicted in Figure 2.1, where until pH = 8, the most arsenate is present as free ligand, variously protonated. For Mg^{2+}-*ars* system, in fact, the formation percentage of the MLH_2 and MLH is below 10%, thus these species can be considered really not significant. Most important is the ML species although its formation is remarkable over pH = 8.5, with a formation percentage around 40% at pH = 9. For Ca^{2+} and Sr^{2+}-*ars* systems, the slightly higher formation percentages are registered, reaching values around 20% for the protonated species while, for ML species, the 50% and 70% are reached for Ca^{2+} and Sr^{2+}-*ars* systems respectively.
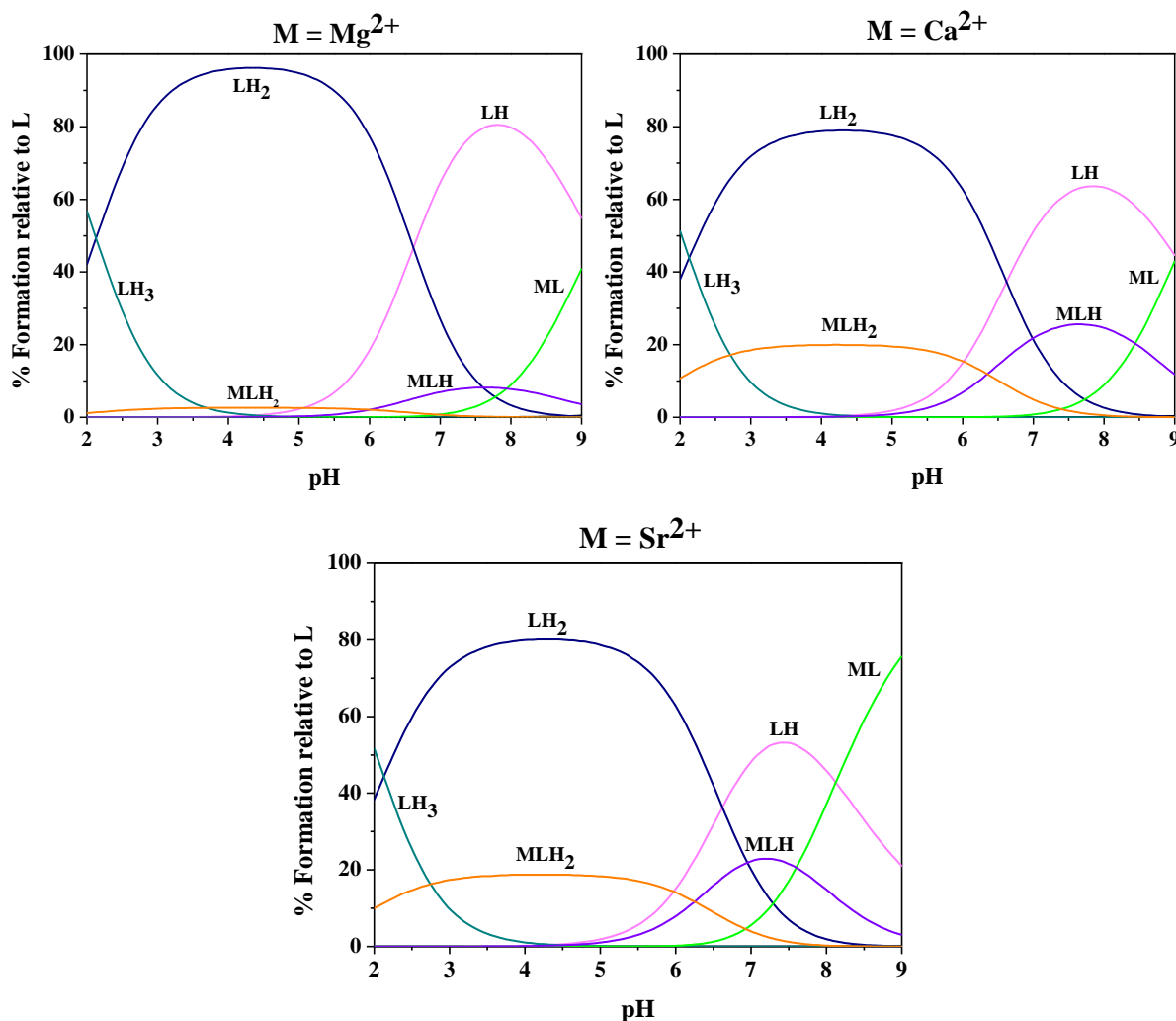
Figure 2.1. Distribution diagram of the M^{2+}-L (L = AsO_4^{3-}) species at $I = 0.1$ mol L^{-1} in NaCl and T = 298.15 K. Conditions: $C_M = C_L = 1$ mmol L^{-1}.

2.2.2 Dependence on ionic strength

The dependence of the stability constants on the ionic strength was evaluated for all the systems, analyzing the formation constant values in a range of ionic strength between 0.1 and 1 mol L^{-1}, by using the Debye-Hückel type equation (1.15) and LIANA computer program. Values of stability constants extrapolated at infinite dilution (log $^T\beta$) and C empirical parameter are listed in Table 2.3. Both are of great importance for calculating the formation constants at any ionic strength in the studied range. Some example of stability constants calculated at different ionic strengths, in particular at typical ionic strengths of fresh water and sea water, are given in Table 2.4.

Table 2.3. Stability constant values at infinite dilution together with C empirical parameter for the dependence on ionic strength relative to M^{2+}-*ars* systems.

Reaction	$\log^T\beta$	C
$Mg^{2+} + AsO_4^{3-}$	6.41 ± 0.02[a]	0.82 ± 0.06
$Mg^{2+} + AsO_4^{3-} + H^+$	14.44 ± 0.05	2.13 ± 0.09
$Mg^{2+} + AsO_4^{3-} + 2H^+$	20.40 ± 0.02	2.36 ± 0.07
$Ca^{2+} + AsO_4^{3-}$	6.47 ± 0.03	2.54 ± 0.04
$Ca^{2+} + AsO_4^{3-} + H^+$	15.14 ± 0.07	1.25 ± 0.10
$Ca^{2+} + AsO_4^{3-} + 2H^+$	21.70 ± 0.01	0.31 ± 0.02
$Sr^{2+} + AsO_4^{3-}$	7.65 ± 0.03	0.79 ± 0.11
$Sr^{2+} + AsO_4^{3-} + H^+$	15.32 ± 0.03	1.21 ± 0.03
$Sr^{2+} + AsO_4^{3-} + 2H^+$	21.58 ± 0.06	0.95 ± 0.10

[a] $\pm$ standard deviation.

Table 2.4. Calculated stability constants of M^{2+}-*ars* systems in NaCl at different ionic strengths and T = 298.15 K

	$\log\beta$				
Reaction	$I = 0.001$ [a]	$I = 0.1$ [a]	$I = 0.5$ [a]	$I = 0.7$ [a]	$I = 1$ [a]
$Mg^{2+} + AsO_4^{3-}$	6.22 ± 0.02[b]	5.17 ± 0.02	4.71 ± 0.02	4.71 ± 0.02	4.78 ± 0.04
$Mg^{2+} + AsO_4^{3-} + H^+$	14.22 ± 0.05	13.12 ± 0.04	13.05 ± 0.03	13.28 ± 0.04	13.71 ± 0.06
$Mg^{2+} + AsO_4^{3-} + 2H^+$	20.19 ± 0.02	19.10 ± 0.01	19.13 ± 0.02	19.40 ± 0.03	19.90 ± 0.05
$Ca^{2+} + AsO_4^{3-}$	6.29 ± 0.02	5.41 ± 0.02	5.64 ± 0.01	5.98 ± 0.01	6.57 ± 0.01
$Ca^{2+} + AsO_4^{3-} + H^+$	14.92 ± 0.06	13.73 ± 0.05	13.31 ± 0.03	13.36 ± 0.04	13.53 ± 0.06
$Ca^{2+} + AsO_4^{3-} + 2H^+$	21.49 ± 0.01	20.20 ± 0.01	19.40 ± 0.01	18.27 ± 0.01	19.15 ± 0.02
$Sr^{2+} + AsO_4^{3-}$	7.46 ± 0.03	6.42 ± 0.02	5.95 ± 0.03	5.93 ± 0.05	5.99 ± 0.08
$Sr^{2+} + AsO_4^{3-} + H^+$	15.10 ± 0.03	13.91 ± 0.02	13.47 ± 0.01	13.51 ± 0.01	13.67 ± 0.01
$Sr^{2+} + AsO_4^{3-} + 2H^+$	21.36 ± 0.06	20.14 ± 0.04	19.60 ± 0.03	19.59 ± 0.05	19.67 ± 0.06

[a] in mol L^{-1}; [b] $\pm$ standard deviation.

2.2.3 Dependence on temperature

In order to complete the thermodynamic investigation relative to the interaction of alkaline earth metal cations, the formation enthalpy values of all the complex species involved in the equilibria were determined at $I = 0.7$ mol L^{-1} and T = 298.15 K. Some trials were also performed at $I = 0.1$ mol L^{-1} but small variations were observed (associated with experimental

errors, in general between 2 and 4 kJ mol^{-1}). For this reason, only results relative to measurements carried out at $I = 0.7$ mol L^{-1} are showed in Table 2.5

Table 2.5. Thermodynamic parameters$^{a)}$ of M^{2+}-*ars* systems in NaCl at $I = 0.7$ mol L^{-1} and T = 298.15 K.

Reaction	-ΔG	ΔH	TΔS
Mg^{2+} + AsO$_4{}^{3-}$	26.9	-2 $\pm$ 2$^{b)}$	25
Mg^{2+} + AsO$_4{}^{3-}$ + H$^+$	75.8	-33 $\pm$ 2	43
Mg^{2+} + AsO$_4{}^{3-}$ + 2H$^+$	110.7	-38 $\pm$ 3	73
Ca^{2+} + AsO$_4{}^{3-}$	34.1	-4 $\pm$ 2	30
Ca^{2+} + AsO$_4{}^{3-}$ + H$^+$	76.2	-13 $\pm$ 2	63
Sr^{2+} + AsO$_4{}^{3-}$ + H$^+$	77.1	-37 $\pm$ 3	40
Sr^{2+} + AsO$_4{}^{3-}$ + 2H$^+$	11.8	-55 $\pm$ 4	57
Mg^{2+} + HAsO$_4{}^{2-}$	15.5	-13	3
Mg^{2+} + H$_2$AsO$_4{}^-$	14.2	-15	0
Ca^{2+} + HAsO$_4{}^{2-}$	15.9	7	23
Sr^{2+} + HAsO$_4{}^{2-}$	16.8	-17	0
Sr^{2+} + H$_2$AsO$_4{}^-$	15.3	-32	-16

$^{a)}$ in kJ mol^{-1};$^{b)}$ $\pm$ standard deviation.

As can be observed by analyzing the values referred to partial equilibria, all the species show enthalpy changes weakly exothermic, except for CaLH species, and the main contribution to the free energy is due to entropic one, especially for Mg^{2+} and Ca^{2+} -*ars* systems. As regards ML species, the determined ΔH values are -2 and -4 kJ mol^{-1} and TΔS = 25 and 30 kJ mol^{-1} for Mg^{2+} and Ca^{2+} respectively. This behavior is typical of hard-hard interactions and it underlines that alkaline earth metal-arsenate interaction is to be considered in greater part of non-covalent type, such as the electrostatic bond. By knowing the enthalpy values at T = 298.15 K it is possible to calculate, by means of Van't Hoff equation (1.16) the stability constants at different T and to examine the distribution of the complex species as the temperature varies. An example is showed in Figure 2.2. As can be observed, an increase of the formation percentages for MgLH$_2$ and MgLH is displayed when temperature decreases from 318.15 K to 278.15 K. For example, at T = 278.15 K the formation percentage of MLH species for Mg^{2+} is close to 70%. The same species at T = 318.15 K shows a formation percentage close to 50%, namely lower than 20%. For CaLH, CaL and MgL the opposite

trend is revealed and, as an example, CaLH presents formation percentages close to 10% and 20% for T = 278.15 K and T = 318.15 K respectively.
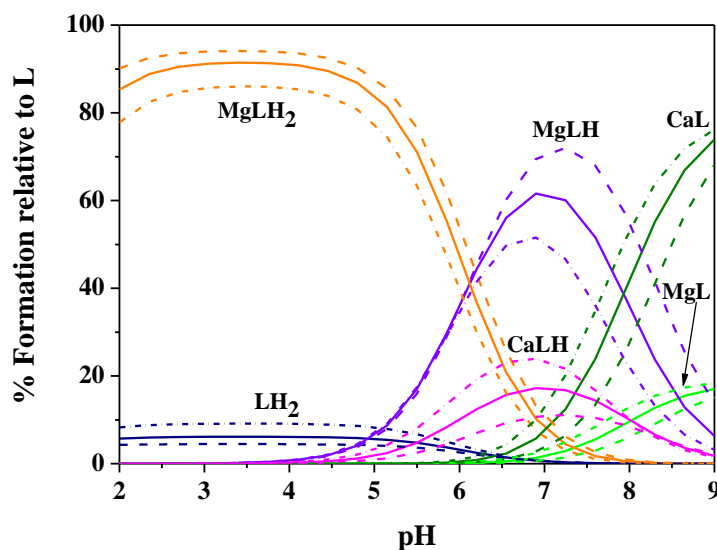

Figure 2.2. Distribution diagram *vs.* pH of M^{2+}-L (L = AsO_4^{3-}) species at I = 0.7 mol L^{-1} in NaCl. Conditions: C_{Ca} = 0.010 mol L^{-1}, C_{Mg} = 0.043 mol L-1, C_{Sr} = 0.000009 mol L^{-1}, C_L = 10^{-12} mol L^{-1}. T = 298.15 K (solid line), T = 278.15 K (dashed line) and T = 318.15 K (short dashed line).

2.2.4 Speciation in natural waters

The investigation of the dependence of the stability constants on the ionic strength and temperature allows to predict the speciation of the systems under different experimental conditions [175, 187, 211-216]. For alkaline earth metal cations-arsenate systems, the speciation in natural waters, namely fresh water and sea water, was discussed by taking into account the stability constant values at I = 0.0016 mol L^{-1}, typical ionic strength for a fresh water, and I = 0.7 mol L^{-1}, that is the mean ionic strength in sea water. The distribution of the species in sea water, by considering the real concentrations of calcium, magnesium and strontium [217], is shown in Figure 2.2. Despite the interactions between alkaline earth metals and arsenate are not strong, the high concentrations of these cations in sea water lead to determine high formation percentages of the complexes, especially for the protonanted species of Mg^{2+}-*ars* system. At the representative pH of sea water (pH = 8.1), the predominant species are CaL (46.8%) and MgLH (31.8%). MgL and CaLH are present in significant percentages, namely 11% and 8.9% respectively, while all the other ones represent a total percentage of 1.5%. In fresh water, where the concentrations of alkaline earth metal

cations is lower, the distribution is very different and it can be seen in Figure 2.3, where the employed metal concentrations were $C_{Ca} = 0.00038$ mol L^{-1}, $C_{Mg} = 0.00017$ mol L^{-1} and $C_{Sr} = 0.00000081$ mol L^{-1}. In these conditions, the protonated forms of the ligands prevail over all pH range. About the metal-ligand complexes, the formation percentages of Ca-LH$_x$ can be considered significant (between 20% and 40%). As regards Mg^{2+}-*ars* system, the only species registered is the MgL but with a low formation percentage close to 10% at pH = 9. At a pH of a generic fresh water (pH = 7), the prevalent species are LH and LH2 (31% each one), while about the complex species CaLH (25.8%) and CaLH$_2$ (9.7%) are recorded.
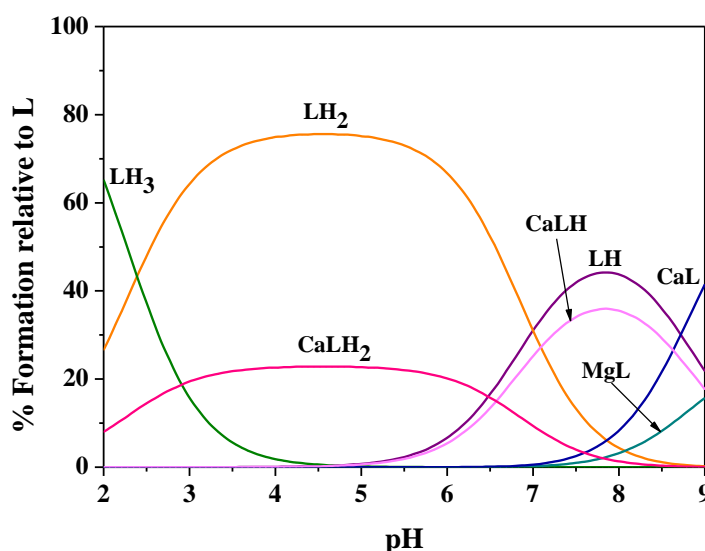

Figure 2.3. Metal-ligand species distribution in NaCl at $I = 0.0016$ mol L^{-1} and T = 298.15 K. Conditions: $C_{Ca} = 0.00038$ mol L^{-1}, $C_{Mg} = 0.00017$ mol L^{-1}, $C_{Sr} = 0.00000081$ mol L^{-1} and $C_L = 10^{-12}$ mol L$^{-1.}$

2.3 Final remarks

The interaction between the main alkaline earth metal cations found in natural waters with arsenate was analyzed. In particular:

- The stability constants of the Mg^{2+}, Ca^{2+} and Sr^{2+} -arsenate species were determined.
- The dependence on the ionic strength was evaluated in a wide range ($0.1 < I$ /mol L^{-1} < 1) and ΔH, ΔG and TΔS were determined at $I = 0.7$ mol L^{-1} and T = 298.15 K, demonstrating the electrostatic nature of the metal-ligand interaction.
- The knowledge of the dependence of the thermodynamic parameters on ionic strength and temperature will be very useful for the application to real systems featured by variable e complex composition.

3

As(V) interaction with Fe³⁺ and Al³⁺: results and discussion

Concernig the study on arsenic contamination of water and soil, one of the most examined processes regards the absorption of arsenic species by mineral surfaces, such as clays or metal oxides of As, Fe and Mn [22, 218-220], at the expense of the investigation of the complexes in aqueous solution [221]. For this reason, with the aim to enrich the thermodynamic database based on As(V), a thermodynamic study focused on arsenate interaction with iron(III) and aluminium(III) was performed in aqueous phase.

Iron is the most abundant metal in the Earth, making up 16% of the mass of our planet, and it is the sixth most abundant element in the entire universe. Its concentration changes in the various layers of the Earth in relation with the depth: it is maximum in the nucleus, probably made by an alloy of iron and nickel, and it decreases until 5% in the earth's crust. Most is found in minerals consisting of various oxides, including hematite (Fe_2O_3), magnetite (Fe_3O_4) and limonite ($FeO(OH)\cdot nH_2O$). It represents the metal most used by mankind, being 95% of the world's metal production. Its low cost and its resistance in the form called steel make it an indispensable building material, especially in the construction of cars, ship hulls and building elements. From the biological point of view, it is essential for human life. It is incorporated in the heme complex, an important component of proteins involved in redox reactions such as breathing. An excessive intake of iron through food is toxic because the excess of iron (II) ions reacts with peroxides in the body forming free radicals [222]. As long as iron remains at normal levels, the body's anti-oxidant mechanisms keep the level of free radicals under control. The distribution of aluminium in the earth's crust is comparable with that of iron (~ 6%). In nature it can be found in mineral combined with other elements, in particular sulphur,

silicon and oxygen. One of the most aluminium-rich mineral (45-60%) is the bauxite, a rock with a red brown or yellow color, which represents the most employed mineral for aluminium production. This element is the most widely used non-ferrous metal and it is almost always alloyed with other elements, such as copper, zinc, magnesium, in order to improve its mechanical properties. From the biological point of view, it is considered a neurotoxin and seems to be correlate with neurodegenerative disorders, such as Alzheimer and Parkinson's diseases although this association is still unclear [223].

In this chapter, the speciation of arsenate in presence of Fe^{3+} and Al^{3+} was analyzed by potentiometry and, as regards Fe^{3+} -*ars* system, also by Uv spectrophotometry. in a wide range of ionic strength between 0.1 and 0.7 mol L^{-1}. Measurements were interrupted around pH = 4 as consequence of precipitation phenomena. Calorimetric titrations were carried out in order to study the dependence of the stability constants on the temperature and finally the sequestering ability of arsenate towards both trivalent metal cations was evaluated in conditions simulating a generic fresh water and sea water.

3.1 Ligand protonation and hydrolysis constants

The protonation constants of the ligand and the hydrolysis constants of the metals were considered for investigating the M^{3+}-arsenate systems. As already explained, the protonation constants of arsenate were reported in the first chapter of this section, while the hydrolysis constants of the Fe^{3+} [224] together with those relative to Al^{3+} [225] are reported in Table 3.1 of the present paragraph.

Table 3.1. Literature values for metal hydrolysis in NaCl at different ionic strengths and T = 298.15 K

Reaction	logβ				Ref.
	$I = 0.1$ [a]	$I = 0.25$ [a]	$I = 0.5$ [a]	$I = 0.7$ [a]	
$Fe^{3+} + H_2O = Fe(OH)^{2+} + H^+$	-2.17	-2.3	-2.43	-2.51	[224]
$Fe^{3+} + 2H_2O = Fe(OH)_2^+ + 2H^+$	-6.3	-6.4	-6.5	-6.5	
$Fe^{3+} + 3H_2O = Fe(OH)_3^0 + 3H^+$	-14.3	-14.4	-14.6	-14.7	
$Fe^{3+} + 4H_2O = Fe(OH)_4^- + 4H^+$	-22.6	-22.7	-22.9	-23.1	
$Al^{3+} + H_2O = Al(OH)^{2+} + H^+$	-5.25	-5.36	-5.43	-5.45	[225]
$Al^{3+} + 2H_2O = Al(OH)_2^+ + 2H^+$	-11.12	-11.30	-11.41	-11.46	
$Al^{3+} + 3H_2O = Al(OH)_3^0 + 3H^+$	-17.77	-17.94	18.04	-18.08	
$Al^{3+} + 4H_2O = Al(OH)_4^- + 4H^+$	-23.25	-23.38	-23.48	-23.53	
$2Al^{3+} + 2H_2O = Al_2(OH)_2^{4+} + 2H^+$	-7.75	-7.74	-7.72	-7.71	
$3Al^{3+} + 4H_2O = Al_3(OH)_4^{5+} + 4H^+$	-13.69	-13.63	-13.58	-13.56	
$13Al^{3+} + 32 H_2O = Al_{13}(OH)_{32}^{+7} + 32H^+$	-103.61	-105.13	-106.54	-107.34	

[a] In mol L^{-1}.

3.2 Fe^{3+} and Al^{3+}-arsenate complexes

3.2.1 Thermodynamic results

In order to study the interactions of Fe^{3+} and Al^{3+} with arsenate, potentiometric titrations were performed by means of an ISE-H^+ electrode at ionic strength ranging from 0.1 mol L^{-1} to 0.7 mol L^{-1} in NaCl as background salt. Different metal-ligand ratios were employed, as reported in 1.2 paragraph of the Section I, with the aim to investigate the presence of species with diverse stoichiometry ratios. The pH range studied (2 < pH < 4) was quite restricted because of poorly soluble species formation in aqueous solution. In these experimental conditions, the best speciation model for Fe^{3+}-*ars* system, reported in Table 3.2, consists of the only simple metal-ligand species (ML), characterized by a high stability since log β = 17.77 at I = 0.1 mol L^{-1} [226].

Table 3.2. Experimental stability constants of Fe^{3+} and Al^{3+} -AsO_4^{3-} species, in NaCl at different ionic strength values and at $T = 298.15$ K

Reaction	logβ			
	ISE-H⁺			
	$I = 0.122$[a]	$I = 0.256$ [a]	$I = 0.486$ [a]	$I = 0.684$ [a]
$Fe^{3+} + AsO_4^{3-} = Fe(AsO_4)^0$	17.77±0.05[b]	17.56±0.06[b]	16.79±0.03[b]	16.50±0.02[b]
	$I = 0.109$	$I = 0.250$	$I = 0.502$	$I = 0.697$
$Al^{3+} + AsO_4^{3-} = Al(AsO_4)^0$	12.68±0.03	12.00±0.06	11.42±0.06	11.39±0.06
$Al^{3+} + AsO_4^{3-}+ H_2O = Al(AsO_4)OH^- + H^+$	8.29±0.05	7.87±0.08	7.44±0.10	7.66±0.08
	Uv/Vis			
	$I = 0.099$	$I = 0.248$	$I = 0.482$	$I = 0.707$
$Fe^{3+} + AsO_4^{3-} = Fe(AsO_4)^0$	17.68±0.02	17.26±0.02	16.68±0.01	16.55±0.07

[a] In mol L^{-1}; [b] ± standard deviation.

Figure 3.1 shows the species distribution, highlighting that the ML species is present in significant amount in all the investigated pH range. The increase of the ionic strength causes a decrease of the formation constant which at $I = 0.7$ mol L^{-1} results equal to 16.50, thus one order of magnitude lower than at $I = 0.1$ mol L^{-1}, and this aspect is also visibile in Figure 3.1, where the distribution at $I = 0.1$ mol L^{-1} is represented as solide line, while at $I = 0.7$ mol L^{-1} as dashed line.
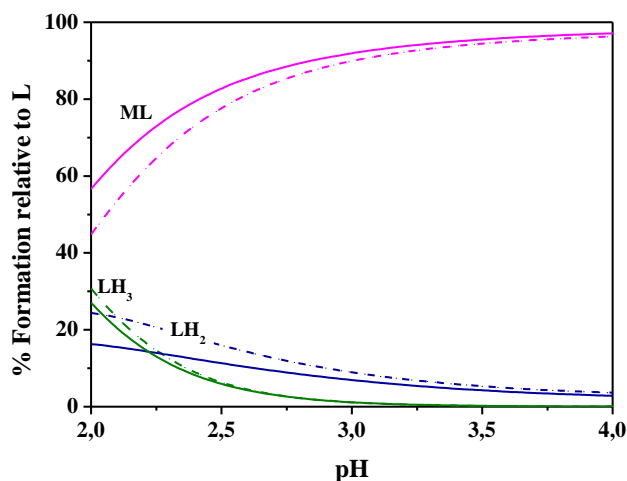

Figure 3.1. Distribution diagram of Fe^{3+}-L (L = AsO_4^{3-}) species at $I = 0.1$ mol L^{-1} (solid line) and $I = 0.7$ mol L^{-1} (dashed line) in NaCl at T = 298.15 K. Conditions: $C_M = C_L = 1$ mmol L^{-1}.

In order to confirm the speciation model obtained by potentiometry, also Uv/Vis spectrophotometry was exploited, carring out measurements in the wavelength range between 200 and 500 nm. Before to study the metal-ligand complexes, spectrophotometric titrations on

the solutions containing only the metal together with NaCl as ionic medium and HCl (to adjust the pH) were performed in order to determine the molar absorption coefficient of the hydrolytic species. They were calculated by means of deconvolution procedures of the experimental data and the molar absorption coefficients of the ML, M, MOH, $M(OH)_2$, $M(OH)_3$ and $M(OH)_4$ species are reported in Figure 3.2 at $I = 0.1$ mol L^{-1} and T = 298.15 K.
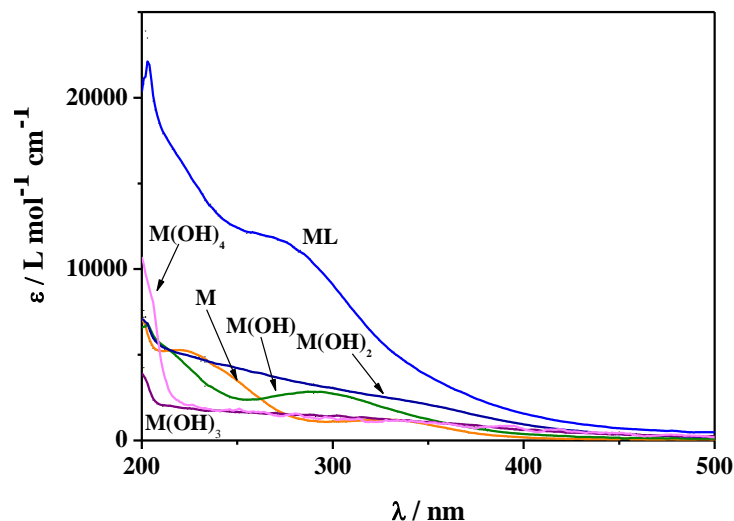

Figure 3.2. Molar absorption coefficients of Fe^{3+}-AsO_4^{3-} species, at $I = 0.1$ mol L^{-1} (NaCl) and T = 298.15 K.

Successively, the metal-ligand complexes were investigated at the same ionic strength and temperature as potentiometric ones, but considering lower concentrations of metal as well as ligand. An example of spectrophotometric titration is depicted in Figure 3.3 which shows an increase of the absorbance from pH = 2.6 to pH = 3.9.
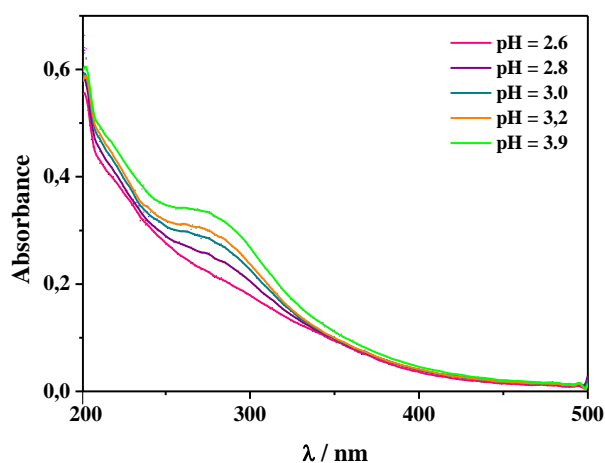

Figure 3.3. Example of spectrophotometric titration for Fe^{3+}-AsO_4^{3-} system. Conditions: C_M = 0.05 mmol L^{-1}, C_L = 0.1 mmol L^{-1}, $I = 0.1$ mol L^{-1} in NaCl, T = 298.15 K.

As can be observed from Table 3.2, the speciation model previously determined by potentiometry is fully confirmed by Uv/Vis spectrophotometry and the stability constants determined with the two techniques are in perfect agreement, showing a minimum and maximum variation equal to 0.05 and 0.3 respectively.

Al^{3+}-*ars* system was studied only through potentiometry in the same range of ionic strength and pH because, also in this case, precipitation phenomena occurred. The speciation model is featured by the simple metal-ligand species, ML, and by the hydrolytic one, MLOH. The formation constants are listed in Table 3.2. As can be noticed, the ML species shows a stability lower with respect to the same species determined for Fe^{3+}-*ars* system, having a log β = 12.68 *vs.*17.77 at I = 0.1 mol L^{-1} and T = 298.15 K. Moreover, as can be seen in Figure 3.4, until pH ~ 4, the protonated LH_2 prevails over complex species whose formation percentages become significant over pH = 4, showing maximum percentages, ~ 40% and ~ 45% at pH = 4.2 and pH = 4.5 for ML and MLOH respectively, at I = 0.1 mol L^{-1} and T = 298.15 K (solid line). The increase of ionic strength to 0.7 mol L^{-1} produces a significant decrease of the ML species percentage (~ 13%) and, on the other hand, an increase of the MLOH formation percentage (~ 72%) (dashed line).

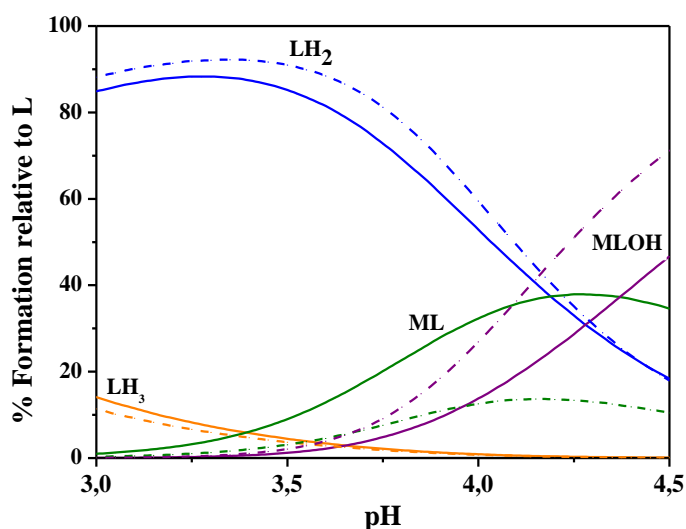**Figure 3.4.** Distribution diagram *vs* pH of Al^{3+}-AsO_4^{3-} (L) species, in NaCl at T = 298.15 K. Conditions: C_M = C_L = 1 mmol L^{-1}, I = 0.1 mol L^{-1} (solid lines) and I = 0.7 mol L^{-1} (dashed lines).

3.2.2 Dependence on ionic strength

The change of ionic strength conditions influences the species distribution, as already observed in the distribution diagrams in Figures 3.1 and 3.4, because it affects the ligand protonation, the hydrolysis of the metal and the stability constants of the complexes [227, 228]. By means of mathematical models, such as the Debye Hückel type equation, the dependence of the species formation constants was studied and the stability constant at infinite dilution and the empirical C parameter were determined for each complex species. They are reported in Table 3.3.

Table 3.3. Formation constant values at infinite dilution with empirical C parameter for the dependence on ionic strength for Fe^{3+} and Al^{3+} -AsO_4^{3-} species at T = 298.15 K

Reaction	log $^T\beta$	C
$Fe^{3+} + AsO_4^{3-} = Fe(AsO_4)^0$	20.0 ± 0.1[a]	-0.2 ± 0.3[a]
$Al^{3+} + AsO_4^{3-} = Al(AsO_4)^0$	14.6 ± 0.1	0.2 ± 0.3
$Al^{3+} + AsO_4^{3-} + H_2O = Al(AsO_4)OH^- + H^+$	9.9 ± 0.1	1.0 ± 0.3

[a] $\pm$ standard deviation

The knowledge of these parameters allowed to calculate the formation constants of the complexes at ionic strength values different from those under investigation, especially at $I = 0.001$ mol L^{-1}, referred to a generic fresh water. Examples of calculated values are listed in Table 3.4 and, as can be noticed, these values are in good agreement with those obtained experimentally and reported in Table 3.2.

Table 3.4. Calculated formation constant values of Fe^{3+} and Al^{3+} -AsO_4^{3-} species in NaCl at different ionic strengths and T = 298.15 K

I/mol L^{-1}	logβ		
	$Fe(AsO_4)$	$Al(AsO_4)$	$Al(AsO_4)OH$
0.001	19.7 ± 0.1[a]	14.3 ± 0.1[a]	9.7 ± 0.1[a]
0.1	17.8 ± 0.1	12.66 ± 0.09	8.3 ± 0.1
0.25	17.32 ± 0.09	12.03 ± 0.07	7.84 ± 0.08
0.5	16.80 ± 0.05	11.55 ± 0.08	7.61 ± 0.09
0.7	16.50 ± 0.06	11.3 ± 0.1	7.6 ± 0.1
1	16.2 ± 0.1	11.1 ± 0.2	7.6 ± 0.2

[a] $\pm$ standard deviation

3.2.3 Dependence on temperature

In order to complete the thermodynamic picture, the formation enthalpies of the complex species for both Fe^{3+} and Al^{3+}-*ars* systems were determined by means of calorimetric titrations performed at T = 298.15 K and I = 0.1 mol L^{-1} and 0.7 mol L^{-1} in NaCl for Fe^{3+}-*ars* system, while for Al^{3+} -*ars* system only I = 0.1 mol L^{-1} was investigated. Fe^{3+} and Al^{3+} are considered hard metal cations as well as O-donor ligands, such as arsenate, are classified as having hard character. These interactions are preferably of electrostatic type and ΔG is essentially due to the entropic contribution, like confirmed by the values listed in Table 3.5. For Fe^{3+}-*ars* system, the enthalpy values are slightly exothermic, being ΔH = -11 kJ mol^{-1} and -15 kJ mol^{-1} at I = 0.1 mol L^{-1} and I = 0.7 mol L^{-1} respectively. For Al^{3+}-*ars* system, both complex species have endothermic enthalpy values, being ΔH = 7 kJ mol^{-1} and ΔH = 62 kJ mol^{-1} at I = 0.1 mol L^{-1} for ML and MLOH respectively. As concerns FeAsO$_4$ complex, the ΔG value, calculated from ΔG^f reported in literature by Welham *et al.* [229], is in agreement with that here indicated, although the ionic strength was not defined in the paper.

Table 3.5. Thermodynamic formation parameters for Fe^{3+} and Al^{3+} -AsO_4^{3-} species at I = 0.1 mol L^{-1} and I = 0.7 mol L^{-1} in NaCl at T = 298.15 K

Reaction	I /mol L^{-1}	ΔH [a]	$-\Delta G$ [a]	$T\Delta S$ [a]
$Fe^{3+} + AsO_4^{3-} = FeAsO_4^0$	0.1	-11 ± 1 [b]	101.4	90
	0.7	-15 ± 3	94.1	79
$Al^{3+} + AsO_4^{3-} = AlAsO_4^0$	0.1	7 ± 2	72.3	79
$Al^{3+} + AsO_4^{3-} + H_2O = AlAsO_4(OH)^-$	0.1	62 ± 3	47.3	109

[a] in kJ mol^{-1}; [b] ± standard deviation

The temperature, like the ionic strength, can significantly influence the stability of the species. The knowledge of the enthalpy values at T = 298.15 K gives the possibility to calculate the stability constants at various temperatures by using the Van't Hoff equation (eq. 1.16) in order to evaluate the influence on the speciation. In this thesis, the stability constants were calculated at T = 288.15 K, T = 310.15 K and T = 318.15 K in NaCl and I = 0.1 and 0.7 mol L^{-1} for Fe^{3+}-*ars* system and I = 0.1 mol L^{-1} for Al^{3+}-*ars* system. They are listed in Table 3.6. As can be notice, for Fe^{3+}-*ars* system, an increase of temperature causes a decrease in the formation constant. As an example, log β changes from 17.77 at T = 298.15 K to 17.38 at 310.15 K for I = 0.1 mol L^{-1}. As regards the ML species of the Al^{3+}-*ars* system shows an opposite trend, since by increasing the temperature an increase in the stability is registered.

For example, at I = 0.1 mol L^{-1}, log β = 12.68 at T = 298.15 K *vs.* log β = 12.98 at T = 310.15 K.

Table 3.6. Calculated formation constant values at different temperatures and ionic strengths for Fe^{3+} and Al^{3+} -AsO_4^{3-} species in NaCl

Species	I /mol L^{-1}	logβ			
		288.15 K	**298.15 K**	**310.15 K**	**318.15 K**
$FeAsO_4^0$	0.1	18.13	17.77	17.38	17.14
	0.7	16.97	16.50	15.95	15.61
$AlAsO_4^0$	0.1	12.43	12.68	12.98	13.16
$AlAsO_4(OH)^-$	0.1	6.29	8.29	10.52	11.91

3.3 Sequestering ability

In natural aquatic environment several reactions could take part, including hydrolysis, complexation, oxidation/reduction, precipitation or dissolution. In order to evaluate the capability of arsenate to sequester the trivalent metal cations under study, all the collateral reaction should be considered and, in particular the acid-base properties of the ligand, the hydrolysis constants of the metals as well as the competition with other ligand or metal simultaneously present in the environment. By using the empirical parameter known as $pL_{0.5}$, well discussed in 1.9 paragraph of the Section I, the sequestering ability of arsenate towards Fe^{3+} and Al^{3+} was investigated in some experimental conditions chosen as examples. Specifically, the conditions of a generic fresh water ($I = 0.001$ mol L^{-1}, pH = 5) and sea water ($I = 0.7$ mol L^{-1} and pH = 8.1) were selected. Results are reported in Table 3.7 and showed in Figure 3.5.

Table 3.7. $pL_{0.5}$ values for Fe^{3+} and Al^{3+} -*ars* systems at different ionic strengths in NaCl, T = 298.15 K and pH = 5 or pH = 8.1.

Metals	pH	$I^{a)}$	$pL_{0.5}$
Fe^{3+}	5	0.001	7.2
	8.1	0.7	4.0
Al^{3+}	5	0.001	5.8
	8.1	0.7	4.4

As can be noticed, arsenate shows a good sequestering ability towards both metal cations, especially at conditions simulating a fresh water, where $pL_{0.5}$ = 7.2 and 5.8 for Fe^{3+} and Al^{3+} respectively. Lower, but not negligible, are the values in sea water conditions, being equal to 4.0 and 4.4 for Fe^{3+} and Al^{3+} respectively. In any cases, the reported values point out the necessity to consider all these interactions in aqueous solution for an exact speciation study.
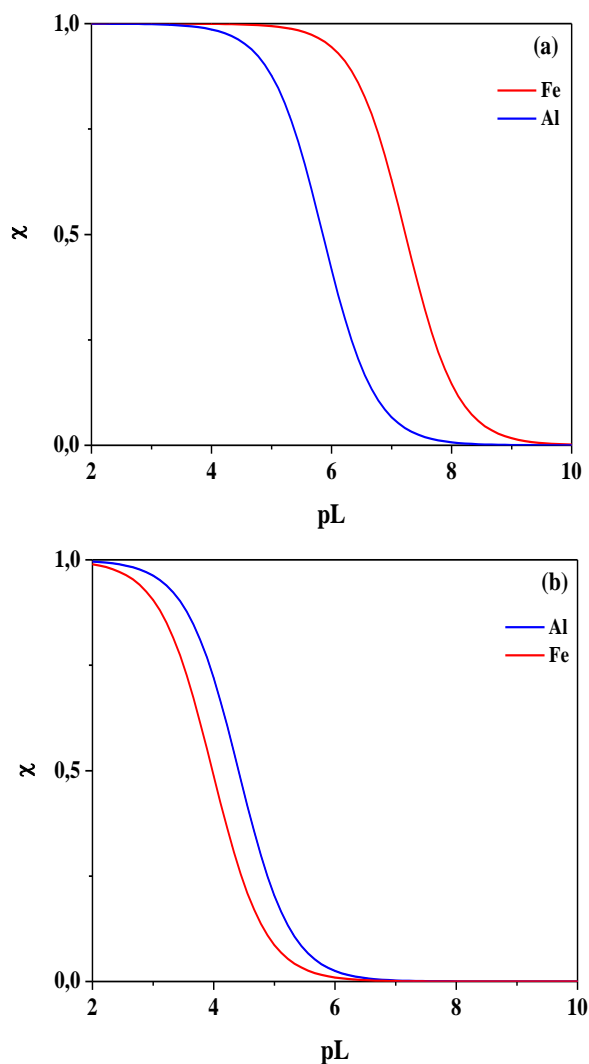
Figure 3.5. Sequestration diagram of Fe^{3+} and Al^{3+} by AsO_4^{3-} at $I = 0.001$ mol L^{-1}, pH = 5, T = 298.15 K (a); $I = 0.7$ mol L^{-1}, pH = 8.1, T = 298.15 K. (b).

3.4 Final remarks

A thermodynamic investigation on Fe^{3+} and Al^{3+}-arsenate systems was performed in NaCl in a wide range of ionic strength ($0.1 < I$/mol L$^{-1} < 0.7$), T = 298.15 K and in a restricted pH range, between 2 and 4, because of precipitation phenomena. In particular:

- As concerning Fe^{3+} -arsenate system, the only determined species was the ML one, showing high formation percentage in all the pH range examined.
- Regarding Al^{3+}-arsenate system, the speciation model was featured by ML and MLOH species, the first one having a stability lower than that reported in the case of Fe^{3+}.
- The dependence of the formation constants on the ionic strength was studied as well as on the temperature and the species distribution was discussed.

- Finally, the sequestering ability of arsenate towards both trivalent metal cations was evaluated in conditions simulating fresh water and sea water, showing that in the first one the sequestering ability of arsenate, especially towards Fe^{3+}, is promoted.

Section IV

Arsenic speciation in natural waters by polymer inclusion membrane preconcentration and X-ray fluorescence detection

Arsenic reaches human organism especially as a consequence of the consumption of water and food contaminated [31]. As already explained in the introduction of this thesis, many areas in the world show high concentrations of arsenic in natural waters, making this phenomenon one of the most important global environmental problems. In light of this, several methodologies are employed in order to detect and remove this pollutant from natural waters. Among them, a simple and novel methodology is represented by the use of polymer inclusion membranes (PIMs) which, easy to prepare, are well suited for the extraction or preconcentration of metals and metalloid from aqueous phases. In this thesis, the versatility of PIMs to extract arsenic from natural waters was combined with Energy Dispersive X-Ray Fluorescence (EDXRF) spectrometry. Even though this technique is not widely used for the detection of pollutants in natural water samples because the low sensitivity of the conventional EDXRF spectrometers, it can be successfully used in combination with a suitable preconcentration procedure. In principle, any preconcentration and separation method developed for any analytical technique could be used in combination with EDXRF. Nevertheless, taking into account that EDXRF operates best on solid samples and gives optimal sensitivity and accuracy for thin and homogeneous targets, preconcentration procedures leading to solid thin targets are ideal for use in combination with this technique. Accordingly, organic functionalized membranes as PIMs are a convenient means of separation for the X-ray fluorescence method because the metal loaded-membrane can be

directly mounted in the spectrometer for its analysis after the separation process. The combination of PIM preconcentration and EDXRF has been applied in the past to detect metallic species such as Hg and Cr [230-233].

The first objective of the study was to investigate the best experimental conditions in terms of PIM composition and pH of the aqueous solution in order to promote the extraction of arsenic from natural waters by using the extractant bis(2,4,4-trimethylpentyl) dithiophosphinic acid, commercially known as Cyanex 301. Once established the best operating conditions, arsenic extracted in the membrane was analyzed by means of EDXRF. The final goal of the study was to apply this combined methodology to arsenic speciation, in order to discriminate between the two main inorganic forms of arsenic found in natural waters, namely As(III) and As(V).

1

Polymer Inclusion Membranes (PIMs)

1.1 General aspects

The polymer–based liquid membrane is a concept that appeared about 50 years ago, but recently the name "polymer inclusion membrane" was attributed to this type of membranes. They are a typology of liquid membrane featured by a liquid phase and a base polymer, often assimilated to the well known liquid–liquid extraction technique. The latter perform the extraction mechanism through the employment of an extractant, dissolved in a large amount of organic solvent, that interacts with the solute (by complexation and/or ion exchange) in an aqueous media at the interface between the organic and aqueous phase. As a result, the solute is transferred to the organic phase. However, this technology possesses several disadvantages, among which the use of large quantities of solvents which are often volatile and toxic and represent a serious hazard for human health. From here, the idea to replace the liquid-liquid extractions with the use of membrane technologies in which the membrane acts as organic phase, by transferring the solute contained in the source aqueous phase into a second aqueous phase, named receiving phase. This technology includes, for example, supported liquid membranes (SLMs) which are featured of an inert microporous membrane in which the extractant is incorporated. The extractant is previously diluted in a small amount of solvent and, as a consequence of the impregnation, it remains into the pores of the membrane through capillarity forces, by creating liquid organic channels into the support of the membrane. After this, the SLM can be used for transporting the solute present in the source phase to the receiving phase where it is back-extracted thanks to the interaction between solute-extractant, forming a hydrophobic ion-pair or a complex that can diffuse through the membrane

(facilitated transport). PIMs operate in a similar way to SLMs but. in order to enhance the stability of the membrane, the extractant is entangled between the chains of a polymer matrix, avoiding any loss to the adjacent solution. The peculiarity of these membranes is the absence of pores and, sometimes, also plasticizers are employed for the fabrication of PIMs in order to facilitate the diffusion process through the membrane and make it more flexible.

PIMs offer a series of advantages among them the improvement in terms of health and environmental safety, thanks to the reduced use of organic solvents, but also the simple preparation and the cheap cost. All these characteristics make them suitable for several analytical applications, ranging from sensing, such as ISEs and optodes, to sample pre-treatment, such as separation or pre-concentration until sampling (passive sampling). [234, 235]. The first use of PIMs in ISEs date back to 1970, when the ion exchangers used for the determination of cations or anions were entrapped in PVC [236]. These membranes, called "polymer membranes", constituted the current "polymer inclusion membranes", although a substantial difference exists between the two typologies. In fact, in ISEs membranes low concentrations of ionophore (1-2% wt) are required to ensure fast ion-exchange to the interface of membrane-sample solution. On the other hand, for PIMs both ion-exchange and transport require high rate and, for ensuring the last requirement, higher concentrations of extractant are necessary ($\geq$ 30% wt) [237]. PIMs were also employed in optical chemical sensors, also known as "optodes", for several applications, ranging from environmental to clinical fields. Many papers are reported in literature and they are well summarized in the following reference [235].

1.2 PIMs composition and preparation

The main components of a PIM are the polymer, which constitutes the skeleton of the membrane, providing mechanical strength to the membrane, and it must be inert to any other chemical species with which could be in contact, and the extractant, also called carrier since it has the function to transport the solute through the membrane. Also plasticizers and chemical modifiers can be employed to improve the separation efficiency and, for this reason, they must be chosen with care. All the constituents will be explained in this paragraph.

Cellulose triacetate (CTA)   **Poly (Vinyl chloride) (PVC)**

Figure 1.1. Polymers employed in this study

The prevalent polymers adopted for the fabrication of PIMs are generally PVC (poly(vinyl chloride)) or CTA (cellulose triacetate), which are preventively dissolved in appropriate solvents before the addition of the extractant. In this work, experiments were carried out testing both polymers.

As concerns the extractant, it can be classified according to the performed extraction mechanism. In particular, basic, acidic and chelating extractants can be mentioned as well as the extractants classified as neutral and belonging to macrocyclic/macromolecular groups.

The basic extractants, generally, include molecules having a basic nitrogen center, such as quaternary ammonium salts. The action mechanism consists in forming an ion-pair between the extractant and the target solute by exchange of the negative counter ion.

Acidic and chelating agents represent a variety of extractants widely used. This category includes phosphoric, phosphonic and phosphinic acids and acts by coordinating with the species of interest.

Neutral or solvating extractants act by "solvating" the solute in order to make it soluble in the liquid phase of the membrane. Among them, phosphorus based, commonly consisting of substituted phosphine oxides or phosphate esters, are included.

Finally, the extractants belonging to macrocyclic/macromolecular groups are based on large crown ether moieties and are very useful for the extraction of oxophilic species.

In this thesis, the chelating extractant called Bis(2,4,4-trimethylpentyl)dithiophosphinic acid, commercially known as Cyanex 301, which is a dithiophosphinic acid derivative, was employed. In Figure 1.2 the structure is depicted.
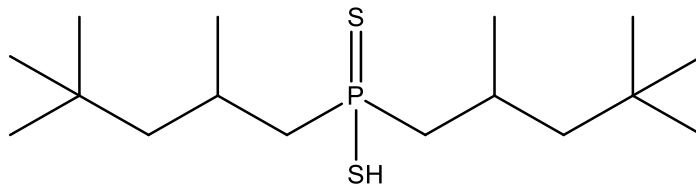

Figure 1.2. Structure of Bis(2,4,4-trimethylpentyl)dithiophosphinic acid

As regards chemical modifiers and plasticizers, they represent the third category of PIMs components. While plasticizers are normally employed to improve the flexibility of the membrane, chemical modifiers are exploited to promote the solubility of the extractant or of the extractant/solute complex in the membrane [234].

The preparation of PIMs is very simple and it is performed by the solvent casting method. In this study, 0.2 g of CTA or 0.4 g of PVC were dissolved in chloroform or tetrahydrofuran for 5 and 2 hours respectively before the addition of the corresponding amount of extractant in order to have a prefixed PIM composition. Then, the resulting solution was poured into a 9.0 cm diameter glass Petri dish, placed horizontally and covered to allow the slow solvent evaporation overnight. Finally, the membranes were peeled off the bottom of the Petri dishes and used for further studies [238]. The resulting PIM is displayed in Figure 1.3a, while Figure 1.3b shows the cross section of a SEM image. As can be observed, a homogeneous structure, transparent and without pores is evident.
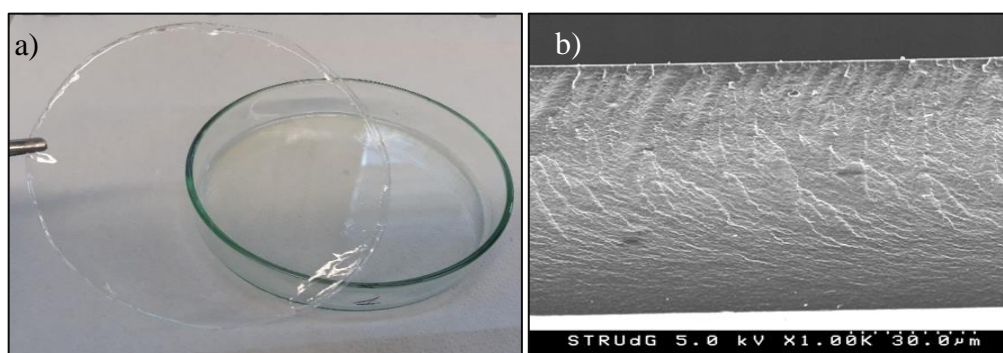

Figure 1.3. a) PIM made by 50% CTA-50% Cyanex 301; b) SEM cross section.

2

Arsenic extraction by PIMs and detection by EDXRF

As already explained, the toxicity of arsenic is related to the speciation, namely to the chemical form in which it is present. In natural waters, arsenic mainly occurs in inorganic species, in particular as arsenate (As(V)) and arsenite (As(III)) in relation to the redox potential and pH. Regarding arsenate (As(V)), in the pH range 6.5–8.5 (pH of many natural waters) it is present as mono and di-protonated species ($HAsO_4^{2-}$ and $H_2AsO_4^{-}$) while, in the same range, trivalent arsenic (As(III)) predominates as arsenous acid (H_3AsO_3) [95]. Taking into account all the risks derived from the arsenic intake, the development of appropriate methodologies able to preconcentrate this pollutant in order to facilitate its detection in natural waters, where it should be found in low concentrations, is required. In the past few years, Guell *et al.* [239] studied As(V) extraction by using a quaternary ammonium salt, commercially known as Aliquat 336. The extraction of arsenic anionic species by this extractant is based on an anion-exchange mechanism which leads to the formation of an ion pair that can be transferred into the organic phase. Guell *et al*., first performed solvent extraction experiments in order to verify the exatraction efficiency of Aliquat 336 and, then, designed a supported liquid membrane (SLM) system with the aim to apply this separation system to various environmental samples. The extraction mechanism based on Aliquat 336 proved to be particularly useful in the case of arsenate since this anionic species can be efficiently exchanged by the chloride anion initially present in the formulation of Aliquat. However, since the predominant species of arsenite are neutral species, as stated above, this extractant was not useful to interact with As(III) at pH < 9. Taking into account the fact that As(III) is the most toxic form of inorganic species found in water, it is of paramount

importance to develop extraction/preconcentration systems for this species. Gupta *et al.* [240] studied the capability of a dithiphosphinic acid derivative, Cyanex 301, to remove arsenic from metallurgical solutions by the solvent extraction technique. Cyanex 301, whose complete name is bis(2,4,4-trimethylpentyl) dithiophosphinic acid, and Cyanex 302 (bis(2,4,4-trimethylpentyl) monothiophosphinic acid) are the dithio and mono analogues, respectively, of Cyanex 272, a dialkyl phosphinic acid reagent which extracts metal cations by a cation exchange mechanism [241]. Literature data confirm that H_3AsO_3 is able to interact with thiol groups by creating an As(III)-thiolate bond with the consequent release of a water molecule, deriving from the deprotonation of the thiol groups and the removal of a hydroxide ligand from the structure of the arsenous acid [122]. It is probable that the interaction between As(III) and Cyanex 301 occurs following exactly this mechanism. In this thesis, Cyanex 301 was entrapped in a polymer inclusion membrane to test its ability to act as sorbents to preconcentrate As and to be afterwards directly analysed by Energy Dispersive X-Ray Fluorescence. This new methodology has been applied to As speciation studies in natural waters. All the aspects concerning this investigation will be discussed in the present chapter.

2.1 Preliminary PIM extraction experiments

Through solvent extraction experiments, Gupta *et al.* [240] demonstrated that both As(III) and As(V), in concentration equal to 0.001 mol L^{-1}, were extracted from 0.01 to 7 mol L^{-1} HCl, HNO_3 and H_2SO_4 media by employing Cyanex 301 dissolved in toluene. Under these experimental conditions, As(V) showed a partial extraction kinetics with respect to As(III), in particular at pH values lower than 2. For our purposes, preliminary PIM extraction experiments were performed in order to evaluate the capability of PIMs, incorporating Cyanex 301, to extract arsenic at lower concentrations and in natural waters. The experiments were carried out at ambient temperature of 22 ± 1 °C by using a membrane (made by PVC or CTA) with an area of 4 cm^2 put in contact with 25 ml of 10 mg L^{-1} As(III)/As(V) diluted in 0.1 mol L^{-1} HCl or NaCl and orbitally stirred for the desired time. The extraction efficiency was calculated as:

$$\text{Extraction Efficiency (\%)} = \frac{[As]_i - [As]_f}{[As]_i} \times 100$$

where $[As]_{in}$ and $[As]_f$ are the initial and final concentration of arsenic in the aqueous phase, respectively before and after the extraction and measured with ICP-OES.

The As(III)/As(V) extraction efficiency was first studied in 0.1 mol L^{-1} HCl by employing different PIM composition. When a PIM made by 70% PVC – 30% Cyanex 301 was used, no extraction occurred neither for As(III) nor for As(V) even after 24 hours. Accordingly, the polymer was changed in order to check if the extraction efficiency could be related to the nature of the polymer. Actually, by using a membrane featured by 50% CTA- 50% Cyanex 301, the extraction process for As(III) was complete after 3 hours at pH=1, as can be seen in Figure 2.1, while As(V) was not extracted.
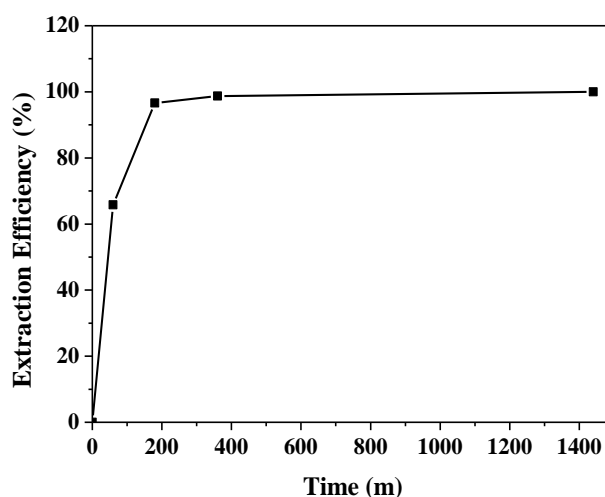

Figure 2.1. As(III) extraction kinetic in 0.1 mol L^{-1} HCl for a PIM made by 50% CTA and 50% Cyanex301. Initial As(III) concentration = 10 mg L^{-1}, pH = 1.

In order to verify if the non-extraction by PVC could be due to a low concentration of extractant, another PIM made by 50% PVC and 50% Cyanex 301 was prepared. With this composition, As(III) was extracted but with a performance lower than in the case of PIM made by CTA. After 3 hours, in fact, the extraction percentage was equal to 21% *versus* the complete extraction occurred with the other polymer. Moreover, the extractant, in this percentage, made the membrane like oily with a not homogeneous structure that causes not reproducible extractions. About As(V), the impossibility to extract it by means of PIMs leads to conclude that Cyanex 301, when entrapped in a polymeric matrix, is selective towards As(III) and thus, it can be useful for speciation studies. Therefore, all the further experiments will be discussed in terms of As(III) extraction.

2.2 As(III) preconcentration in PIMs

In order to achieve a high arsenic enrichment in PIM, circular pieces of only 1 cm diameter were cut from the centre of the PIMs and were used for extraction experiments. For that, a

PIM segment was contacted with either 100 mL or 500 mL water samples with ultra trace amounts of As at pH = 1 (adjusted with nitric acid) and stirred for 24 h, except for different indications. The extraction efficiency was calculated as above and measured by means of ICP-OES at λ = 193.696 nm.

To evaluate the performance of the extraction system parameters such as the pH and the membrane composition were investigated. In Figure 2.2, the effect of PIM composition and pH on As(III) extraction efficiency at two different contact times is displayed. As can be observed, even though at a short times (6h) there is no significant effect on both pH of the solution and amount of carrier in the PIM, at 24h the best results were obtained at pH = 1 and PIMs, made of 50% CTA and 50% Cyanex 301.
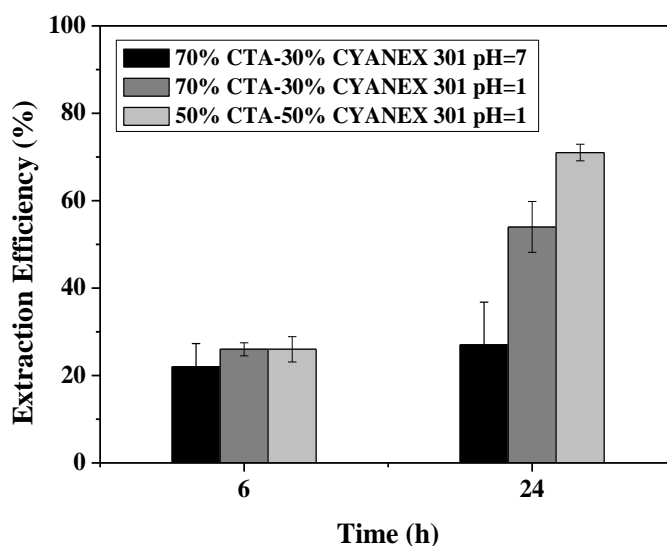
Figure 2.2. Effect of PIM composition and pH on As(III) extraction efficiency at two different contact times. Initial As(III) concentration = 200 μg L^{-1} in ultrapure water; PIM = 0.78 cm^2.

In light of this, all subsequent investigations were performed using PIMs 1 cm in diameter made with PIMs 50%CTA -50% Cyanex 301 and As(III) solutions at pH = 1, adjusted with nitric acid.

2.3 PIMs preconcentration combined with EDXRF for arsenic detection

2.3.1 Testing PIM abilities to perform As determination by EDXRF

Once confirmed the efficiency of PIM containing Cyanex 301 as a sorbent for As(III) extraction in aqueous samples, the possibility to exploit this analytical approach in

combination with EDXRF detection was verified. With this aim, PIMs were put in contact with both 500 mL 0.1 mol L^{-1} nitric acid (blank) and the same volume of a solution of 100 µg L^{-1} of As(III) in 0.1 mol L^{-1} HNO$_3$. After 24 h in agitation, the membranes were analyzed using the measuring conditions described in the second chapter of the experimental section (Section I). EDXRF spectra is displayed in Figure 2.3.

As can be observed, in both spectra, peaks attributable to P and S belonging to the organothiophosphrous extractant Cyanex 301 used are detected. This fact confirms the effective incorporation of this compound within the PIM matrix. In addition, other peaks are detected in the resulting spectra including those deriving from the elastic and inelastic scattering of the primary Pd X-ray source and small peaks of Fe, Cu and Zn, surely resulting from the instrument components itself. Nevertheless, in the region where As-K$_\alpha$ is placed, there are not spectral overlaps and As peak can be properly fitted in the PIM contacted with a solution containing 100 µg L^{-1} of As(III), as visible in Figure 2.3. In fact, the high As analytical response obtained pointed the potential sensitivity of the proposed methodology for the determination of low amounts of As.
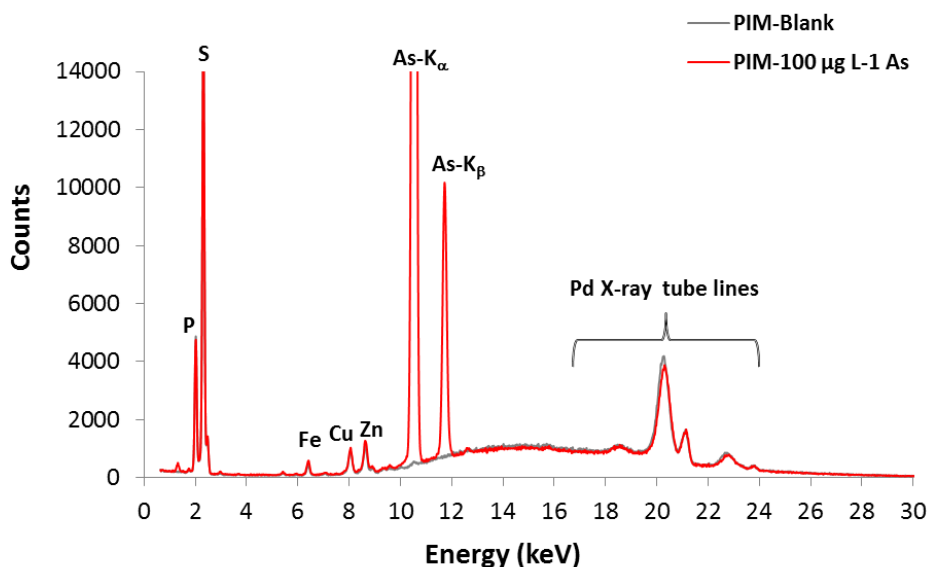
Figure 2.3. EDXRF spectra for the analysis of PIMs contacted with 0.1 mol L^{-1} nitric acid (blank) and with an aqueous solution containing 100 µg L^{-1} of As (III).

In order to better investigate this possibility, the same methodology was used to extract lower concentrations of As (10 and 50 µg L^{-1} arsenite). As it is shown in Figure 2.4, even for the lowest concentration investigated the As peak is distinctly measured. Moreover, the gained results indicate that a linear relationship between the As peak area of each membrane and the

initial As(III) content in the aqueous solution is found and this correlation could be further tested as a calibration approach for quantitative analysis.
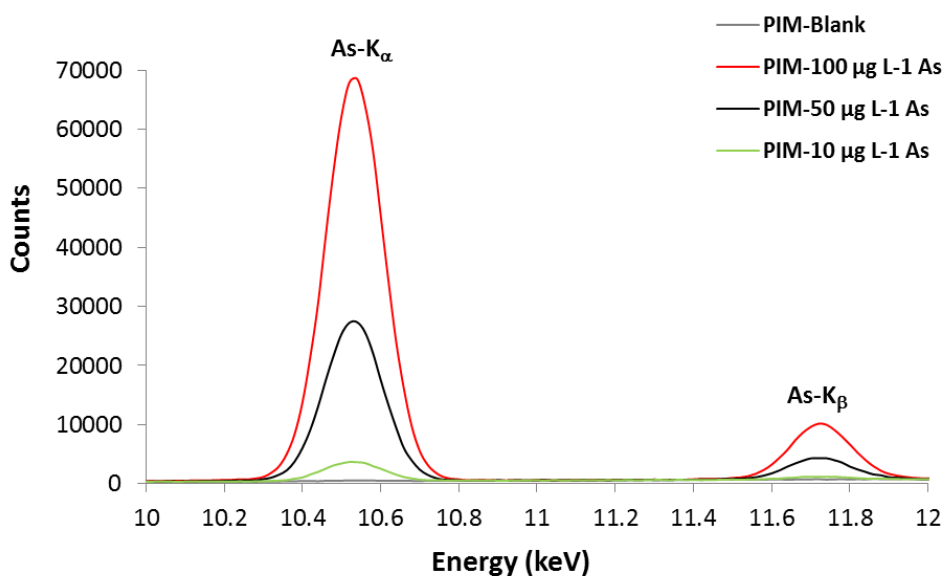
Figure 2.4. EDXRF spectra of PIMs contacted with aqueous solutions containing different As (III) concentration levels.

2.3.2 Analytical figures of merit of the developed method

Once established the best experimental conditions for the extraction and determination of arsenite, analytical figures of merit for developed analytical methodology (PIM-EDXFR) were taken into account and the obtained results are summarized in Table 2.1. For quantification purposes, 500 mL aqueous solutions containing As(III) concentrations in the range 1 - 150 μg L^{-1} at pH = 1, adjusted with nitric acid, were used for performing experiments through the proposed methodology (PIM-EDXRF) and used as calibration standards. As it is shown in Table 2.1 and Figure 2.5, a good linearity was obtained (R^2 > 0.99) over the studied working range without the need of matrix and thickness effect corrections, commonly required in EDXRF analysis of solid samples. In this case, due to the organic nature of the PIM matrix, the attenuation of the incident primary and emergent secondary spectral line radiation is almost negligible, and thus, As intensity is proportional to its concentration.

Figure 2.5. Calibration curve obtained by using aqueous solutions containing As(III) concentrations ranging from 1 to 150 µg L^{-1} at pH = 1 in nitric acid.
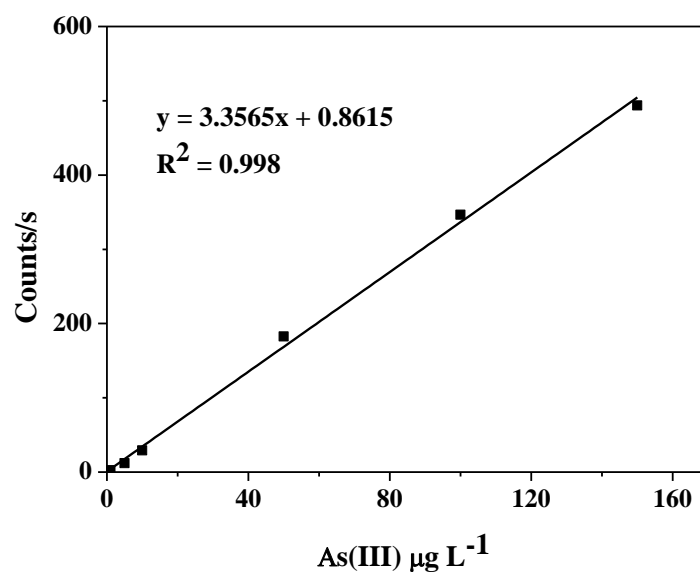
The detection limit of the methodology (LOD) was calculated by analysing a PIM contacted with 200 µg L^{-1} As(III) aqueous solution at acidic pH and using the 3σ criteria. The minimum measurable concentration of arsenic was found to be 0.6 µg L^{-1}, as a further demonstration that this developed methodology is very suitable for detecting arsenic in drinking waters, for which the legal limit is fixed in 10 µg L^{-1}. To investigate the PIM-EDXRF method precision, five independent PIMs previously contacted with 500 mL of 10 µg L^{-1} As(III) aqueous solutions and other five PIMs previously contacted with 500 mL of 100 µg L^{-1} As(III) aqueous solutions, both at pH = 1 in HNO$_3$, were analyzed. Global precision is certainly good, showing RSD values of 5.60% and 5.77% for 10 µg L^{-1} and 100 µg L^{-1} respectively.

Table 2.1. Analytical figures of merit of the developed methodology for As(III) detection.

Parameter	Analytical feature
LOD	0.6 µg L^{-1}
Linear range (ultrapure water)	1 – 150 µg L^{-1}
R^2 (ultrapure water)	0.998
Method precision: n = 5; one measurement (10 µg L^{-1})	RSD: 5.60
n = 5; one measurement (100 µg L^{-1})	RSD: 5.77

2.3.3 Effect of water matrix on As extraction

With the aim to study if the water matrix could affect As(III) extraction, real water sample were spiked with known amounts of As(III). In particular, 10 µg L^{-1} of As(III) were added to

samples of mineral waters, tap water, sea water and ground water and pH was adjusted to 1 with HNO_3. Extraction experiments, in duplicate, were carried out as usual and the membranes were analyzed by EDXRF after 24 h of contact.

The concentration of As(III) extracted in the membrane, calculated by means of the calibration curve previously determined, is reported as histogram (Figure 2.6) for each water samples.
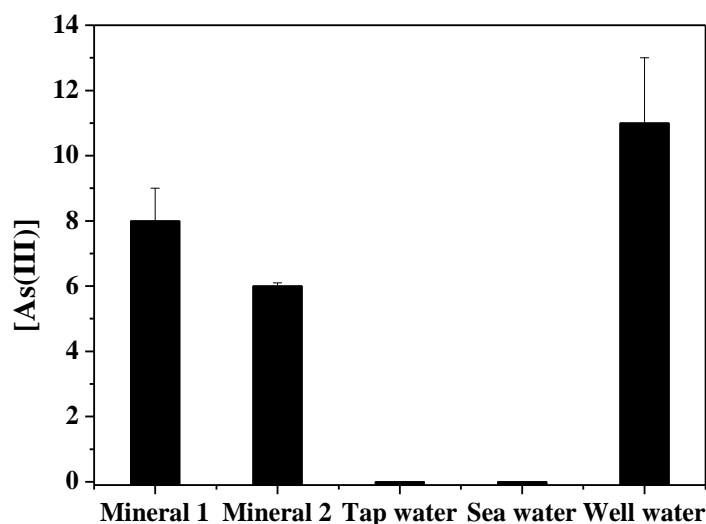
Figure 2.6. Matrix effects on As(III) extraction. Samples spiked with 10 µg L^{-1} of As(III); pH = 1 in HNO_3.

As can be seen, for both mineral waters the extraction process occurs, registering As(III) recovery percentages equal to 98.7 and 72.6 for mineral 1 and mineral 2 respectively, being the highest recovery for As in a ground water sample. To our knowledge, this is the first time that Cyanex 301 entrapped in PIM is used to extract arsenic from natural waters which are considered complex matrices, being constituted by several anions and cations that could interfere in the extraction process. The achieved results point out that the designed system is not affected by the presence of other components and this aspect represents a strength of this method. The situation registered in tap water and seawater, where no extraction was observed, could be explained as a consequence of contemporary extraction by Cyanex 301 of other metals, such as zinc or copper, at the expense of arsenic as reported by Kozlowska *et al.* [242]. In this case, it would be better to operate with a membrane having a greater area in order to improve its extraction capability and to be able to extract all the metals, including arsenic.

3

Arsenic speciation in natural waters

The developed methodology discussed in the previous chapter, allowed to reveal and quantify As(III). Several tests, in fact, demonstrated that arsenate (As(V)) is not extracted by PIMs containing Cyanex 301, independently by the polymer, pH or extractant percentage employed. However, in order to apply the described method to the analysis of real water samples, in which the contained arsenic form is unknown, it is necessary to find a way which permits to detect also As(V). One could be the reduction of As(V) to As(III). In some papers this option was adopted [243, 244] and the reduction process was performed by adding a thiosulfate/iodide mixture to the solution containing As(V). Accordingly, in this research work some tests were carried out in order to verify this possibility. Once the functioning of the method was ascertained, mineral waters were spiked with different As(III)/As(V) amounts and finally the whole methodology was exploited for arsenic determination in spring waters and ground waters, sampled in Catalonia region (northeast of Spain), which naturally contain arsenic as a consequence of rock erosion.

3.1 Reduction of As(V) to As(III) and determination with the developed methodology

Before performing the extraction process, the no-exctraction of As(V) by PIMs was verified again. In a first step, a 1 cm diameter membrane was contacted with 200 µg L^{-1} As(V) aqueous solution at pH = 1 in HNO$_3$ for 24h and, as expected, As(V) was not extracted. Successively, other two solutions containing the same amount of As(V) were prepared and the reduction process was carried out by following two pathways. In particular, in a first solution only the thiosulfate solution (1 mL of 1% solution) was employed as reducing agent while, in the second one, a thiosulfate/iodide mixture (1 ml of 1% solution /1 mL of 0.5% solution respectively) was tested. Then, the extraction process was performed and the membranes were analyzed by EDXRF. In Figure 3.1 the intensities of the Kα lines related to the membranes contacting with the three solutions (As(V), As(V)+thiosulfate solution, As(V)+mixture) are showed and they are compared with the intensity of the As(III) extracted following the same experimental procedure.
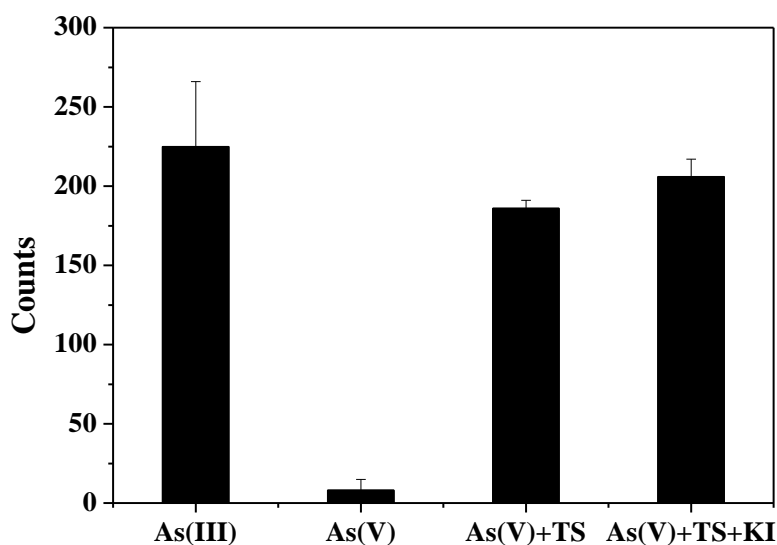
Figure 3.1. Reducing agents' effects on As(V) reduction. Conditions: 200 µg L^{-1} As(V) reduced to As(III) and comparison with the same As(III) concentration in aqueous solutions.

As can be seen, both options lead to the reduction of As(V), as confirmed by the comparison with the intensity registered for As(III) extraction. However, the performance achieved by the thiosulfate/iodide mixture was slightly better and, for this reason, this reducing agent was used for further pre-reductions.

3.2 Speciation studies

Once verified the possibility to reduce the As(V) to As(III), speciation investigations were planned in order to be able to determine also the potentially As(V) present in natural water samples by PIM extraction and EDXRF detection. For this purpose, 1 cm diameter membrane was put in contact with a solution containing both As(III) and As(V) at known concentrations and the mixture was chosen for performing the reduction process. In particular, the experiments were carried out by dividing the sample in two beakers (Method 1), obtaining a volume equal to 500 mL for each beaker. In the first one, only the membrane was added in order to extract only arsenic in the trivalent form. In the second one, the extraction was carried out after the reduction step and it allowed to determine the total arsenic (As(III) + As(V) reduced to As(III)). The amount of the only As(V) was calculated as difference between the total arsenic and the As(III) concentration. The experiment was also conducted in the same beaker (Method 2), by using a first membrane to extract As(III). After 24h the membrane was pulled out, the reducing agent was added and a second membrane was insert in order to perform the second extraction whose analysis led to obtain directly the As(V) concentration by using the calibration curve previously determined. In Figure 3.2 a comparison between the two procedures is given and, as can be observed, no differences exist since the reduction process shows the same results for both methods.

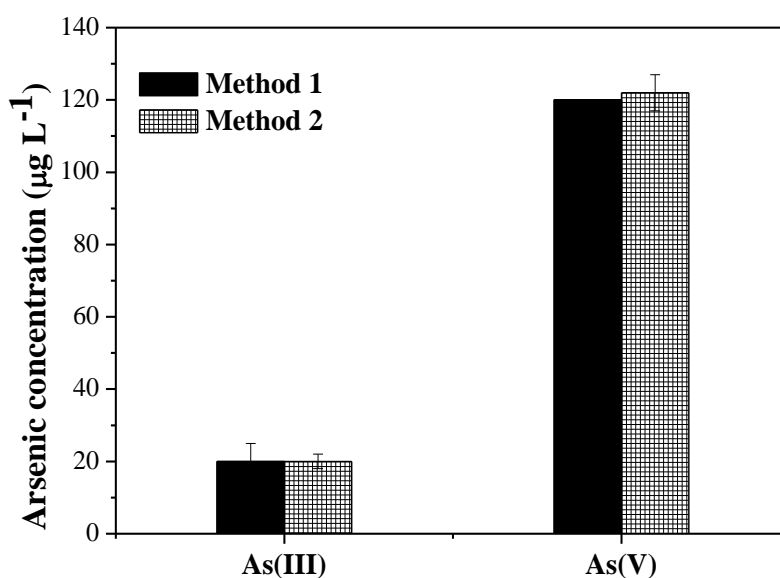**Figure 3.2.** Comparison between reduction method 1 and 2. $C_{As(III)} = 20$ µg L^{-1} and $C_{As(V)} = 100$ µg L^{-1} in ultrapure water at pH = 1 adjusted with nitric acid.

Thus, before proceeding to the analysis of real samples, some trials on solutions containing different amounts of As(III) and As(V) were performed in order to evaluate if the presence of

As(V) could affect the detection of As(III). For this aim, also a mineral water was spiked with different concentrations of both chemical forms and the pH was adjusted to 1 by means of nitric acid as usual. Results are summarized in Table 3.1. As can be noticed, the simultaneous presence of As(V) does not affect the determination of As(III) which reveals a percentage recovery around 100% in all the performed experiments.

Table 3.1. Concentration of As(III)/As(V) in mineral water and ultrapure water

	Added		Found	Recovery (%)
Water Type	As(III)[a]	As(V)[a]	As(III)[a]	As(III)[a]
Ultrapure water	20	100	20 ± 5	100
	100	20	116 ± 18	116
Mineral water	20	100	19.6 ± 0.9	98
	60	60	62 ± 8	103
	100	20	111 ± 1	111

[a] in $\mu g\ L^{-1}$.

As an example, for ultrapure water and mineral waters recoveries of 100% and 98% are respectively registered when 20 $\mu g\ L^{-1}$ of As(III) are added.

3.3 Application to natural waters containing arsenic

The final goal of this study is to apply this novel and low cost methodology to the analysis of arsenic potentially occurring in natural waters for natural or anthropogenic reasons. In the North of Catalonia there are areas in which water shows high concentrations of arsenic, basically as a consequence of rock erosion [245, 246]. In particular, the spring water of Caldes de Malavella (Gironès) and the groundwater of Lles de Cerdanya (Cerdanya) were subject of study. The first one is a place rich in springs, located between the Pyrenees and the Costa Brava in the province of Girona, that possess a great spa tradition. The second one, is a Pyrenean village, province of Girona in Catalonia. The investigation on these waters was carried out by exploiting the developed methodology. In particular, water samples were divided in two beakers (500 mL each one) in order to perform the speciation studies by following the Method 1, previously explained. Thus, the first membrane was analyzed in order to detect As(III) but, as can be noticed in Table 3.2, the EDXRF analysis not revealed the presence of this chemical form. This led to conclude that the potential arsenic present in the samples was only As(V) which, after the reduction and extraction processes, was revealed through the analysis of the second membrane. The interpolation with the calibration curve

allowed to quantify As(V) whose concentration resulted equal to 44 µg L^{-1} and 55 µg L^{-1} for spring and ground waters respectively. In order to test the accuracy of the obtained results, a counter-check was carried out by examining the initial and final solutions by means of ICP-OES. Results are listed in Table 3.2.

Table 3.2. Detection of arsenic in natural water samples by means of both PIM-EDXRF method and ICP-OES

Sample	PIM-EDXRF method		ICP-OES
	As (III)[a]	As (V) [a) b)]	As (Total)[a]
Spring water	n.d.	44 ± 4	49 ± 6
Ground water	n.d.	55 ± 3	68 ± 3

[a] in µg L^{-1}; [b] As(V): As (Total) - As (III)

By taking into account the different approaches followed by the two techniques and the corresponding experimental errors, the results can be considered in agreement.

3.4 Final remarks

The methodology discussed in the Section IV of this thesis is based on PIM containing Cyanex 301 in combination with EDXRF analysis.

- Preliminary extraction tests established that As(V) is not extracted by PIMs containing Cyanex 301 and the best performances in terms of As(III) extraction are achieved by using PIMs made by 50% CTA and 50% Cyanex 301 at pH = 1.

- As(III) preconcentrated in PIMs was analyzed by EDXRF and analytical figures of merit were determined. In particular, a linear correlation between the As(III) concentration and the intensity of the As Kα line was registered, leading to the achievement of a calibration curve, useful for quantification purposes. Moreover, a LOD equal to 0.6 µg L^{-1} was calculated, demonstrating that this combined methodology is able to detect arsenic in drinking waters where the permitted limit is 10 µg L^{-1}.

- Experiments were performed on different water samples spiked with 10 µg L^{-1} of As(III) in order to evaluate the matrix effect on the extraction.

- In order to also detect As(V), a reduction process was tested by employing two reducing agents. The first one only made by thiosulfate and the second one featured by a thiosulfate/iodide mixture. The latter showed the best results and it was selected for performing further analysis.

- Speciation studies were performed on real water samples, naturally containing arsenic, by exploiting the reduction step, followed by the extraction process and, finally, by the EDXRF analysis. The results registered by PIM-EDXRF methodology demonstrated that only As(V) was present in the samples.

Section V

Conclusions

In the Sections II and III of this thesis, the thermodynamic behavior of arsenic in aqueous solution was analyzed by considering arsenic in two different oxidation states, namely +3 and +5. In particular, the attention was focused on the metallic behavior of As(III) (Section II) and on the non-metallic one of As(V) (Section III).

In the Section II, the interaction of As(III) with molecules of biological and environmental interest was investigated. They were divided in:

- Thiols;
- Carboxylic acids;
- Amino acids;
- Nucleotides;
- Phosphonic acids.

Before studing the metal-ligand complexes, the analysis of the acid-base properties of As(III) was performed by potentiometry at T = 298.15 K and in a wide range of ionic strength in NaCl and it was completed by *ab initio* molecular dynamics simulations which confirmed the data obtained experimentally. Potentiometry, considered the most reliable technique for speciation studies in aqueous solution, was the main analytical technique employed for the metal-ligand studies, sometimes supported by spectophotometry, raman spectroscopy and mass spectrometry both able to gain information about the coordination modes and the structures of the determined complex species.

Given the high affinity of As(III) towards the –SH groups, a wide space of the work was reserved to the thiol ligands. In particular:

- It was observed that the stability of the complexes increases by increasing the number of sulfhydryl groups (log K_{111} = 5.58 for *dmsa vs.* 2.09, 3.25, 3.3 and 1.88 for *tla*, *tma*,

cys and *gsh* respectively), but it is also related to the number of carboxylic groups since a greater stability was registered by going from *tla* (one carboxylic group) to *tma* and *dmsa* (two carboxylic groups and one more thiol groups for *dmsa*). The involvement of the –COOH group, together with the –SH one, in the coordination mode of As(III) was also confirmed by computational results.

- The importance of the –COOH moiety in the complexation phenomenon was further examined by studying the interaction of As(III) with pure carboxylic acids having an increasing number of carboxylic groups. Actually, the obtained complex species showed a low stability, being characterized by log K_{111} ranging from 1.31 for *btc* to 2.48 for *mlt*. The higher value obtained for *mlt* could be explained in terms of chelating effect exerted by the six –COOH groups.

- The investigation on the As(III) interaction with biological molecules was continued with the employment of amino acids. With respect to the carboxylic ligands, these ones exibited a shlightly greater stability, probably due to the presence of the amino group, showing log β_{110} = 2.65, 3.3 and 3.73 for *asp*, *lys* and *gly*.

- As regards nucleotides, di-coordinated species differently protonated were determined. By analyzing the ML_2 species, it can be noticed that the stability increases from *AMP* to *ADP* and it decreases in the case of *ATP*. Probably the presence of six phosphate groups (three for each ligand molecules) did not allow an optimal interaction with As(III).

- From the environmental point of view, the chelating properties of phosphonic acids derived from *NTA* towards As(III) were studied. The results obtained showed that the stability of the complexes increases in relation to phosphonic groups, being log β_{110} = 4.14, 4.87 and 5.98 for *NTAP*, *NTA2P* and *NTA3P* respectively. In this case, LD MS/MS measurements confirmed that As(III) coordinates through phosphate groups and, concerning *NTAP* ligand, also the amino group is involved is the coordination mode.

In the Section III, the acid-base properties of arsenate were investigated by means of potentiometry at T = 298.15 K and at different ionic strength values and they were confirmed by molecular dynamics simulations. The interaction with bivalent and trivalent metal cations was also examined by different analytical techniques such as potentiometry and spectrophotometry. As concerns the metal-ligand complexes, the following conclusions can be made by analyzing the achieved results:

- For alkaline-earth metal-arsenate species, the stability of the species increases by following the trend $Mg^{2+} < Ca^{2+} < Sr^{2+}$ showing log $\beta_{110} = 5.21$, 5.41 and 6.31 respectively at $I = 0.1$ mol L^{-1}. The investigations of the dependence of the stability constants on the ionic strength and temperature allowed to predict the speciation in conditions simulating fresh water and sea water. In particular, although the interaction between alkaline-earth metals and arsenate are not particularly strong, high formation percentages are reported in sea water thanks to the high concentrations found in this natural fluid. The opposite trend is registered in fresh water where the protonated species of the ligand prevail over the metal-ligand complexes.

- As concerns trivalent metal cations, Fe^{3+} demonstrated high affinity for arsenate ligand, showing a log $\beta_{110} = 17.77$, while Al^{3+} presented a log β lower and equal to 12.68. In conditions of sea water and, especially, of a typical fresh water, arsenate showed a good sequestering ability towards both metals

Section IV, more applicative than the other ones, is based on the extraction of As(III) from natural waters by means of PIMs, incorporating Cyanex 301, and detection by EDXRF. In particular:

- Several tests were performed in order to verify the best membrane composition designed to extract arsenic. Specifically, As(V) was not extracted by any PIM, regardless of the polymer and the percentage of the employed extractant. On the other hand, the best performance in terms of As(III) extraction was achieved with PIMs made by 50% CTA − 50% Cyanex 301 at pH = 1 which led to obtain a complete extraction after 3h when a PIM with an area of 4 cm^2 was employed.

- As(III) preconcentrated in PIMs was analyzed by EDXRF and figures of merit were defined such as the LOD, resulting equal to 0.6 µg L^{-1}. Moreover, a relationship between the concentration of arsenic in solution and the intensity of the As Kα line was evidenced, exploitable for quantification purpose.

- The combined methodology was applied for determining arsenic in natural waters and for performing speciation analysis in real water matrices affected by high arsenic amount, after carring out a reduction process in order to reduce As(V) to As(III) and be also able to quantify this chemical form. The obtained results pointed out that in the analyzed water samples only As(V) was present and the concentration, first determined by EDXRF, was also confirmed by a counter-check performed by means of ICP-OES.

References

1. S. Shen, X. F. Li, W. R. Cullen, M. Weinfeld, and X. C. Le, *Arsenic binding to proteins.* Chemical Reviews, 2013. **113**(10), 7769-7792.
2. M. Bissen and F. H. Frimmel, *Arsenic - A review. Part I: Occurrence, toxicity, speciation, mobility.* Acta Hydrochimica et Hydrobiologica, 2003. **31**(1), 9-18.
3. M. F. Hughes, *Arsenic toxicity and potential mechanisms of action.* Toxicology Letters, 2002. **133**(1), 1-16.
4. A. Vahidnia, G. B. Van Der Voet, and F. A. De Wolff, *Arsenic neurotoxicity - A review.* Human and Experimental Toxicology, 2007. **26**(10), 823-832.
5. J. Frith, *Arsenic-the "Poison of Kings" and the "Saviour of Syphilis".* Journal of Military and Veterans' Health, 2013. **21**, 11-17.
6. M.A. Gallo, *General Principle of Toxicology*, in *Casarett and Doull's Toxicology:The Basic Science of Poisons*, D. Klaassen, Editor. 2008. 4.
7. J. O. Nriagu, *Arsenic Poisoning Through the Ages*, in *Environmental Chemistry of Arsenic*, J. William T. Frankenberger, Editor. 2001. 1-26.
8. M. F. Hughes, B. D. Beck, Y. Chen, A. S. Lewis, and D. J. Thomas, *Arsenic exposure and toxicology: A historical perspective.* Toxicological Sciences, 2011. **123**(2), 305-332.
9. S. Waxman and K. C. Anderson, *History of the development of arsenic derivatives in cancer therapy.* Oncologist, 2001. **6**(SUPPL. 2), 3-10.
10. INTERNATIONAL AGENCY FOR RESEARCH ON CANCER, *Some Metals and Metallic Compounds*, in *IARC Monographs on the Evaluation of the Carcinogenic Risk of Chemicals to Humans. .* 1980. 39-142.
11. V. D. Martinez, E. A. Vucic, D. D. Becker-Santos, L. Gil, and W. L. Lam, *Arsenic exposure and the induction of human cancers.* Journal of Toxicology, 2011. **2011**.
12. S. J.S. Flora, *Arsenic: Chemistry, Occurrence and Exposure* in *Handbook of Arsenic Toxicology*, F.S. J.S, Editor. 2015, Academic Press. 1-49.
13. N. V. Sidgwick, *Group V B. Arsenic, Antimony, Bismuth*, in *The Chemical Elements and their Compounds*, N.V. Sidgwick, Editor. 1950, Oxford Clarenden Press. 758-803.
14. M. Stoeppler, *Arsenic*, in *Elements and their Compounds in the Environment*, M.A. E. Marian, M. Ihnat and M. Stoeppler, Editor. 2004, Wiley-VCH. 1321-1364.
15. V. K. Sharma and M. Sohn, *Aquatic arsenic: Toxicity, speciation, transformations, and remediation.* Environment International, 2009. **35**(4), 743-759.
16. J. Q. Yang, L. Y. Chai, Q. Z. Li, and Y. D. Shu, *Redox behavior and chemical species of arsenic in acidic aqueous system.* Transactions of Nonferrous Metals Society of China (English Edition), 2017. **27**(9), 2063-2072.
17. B. K. Mandal and K. T. Suzuki, *Arsenic round the world: A review.* Talanta, 2002. **58**(1), 201-235.
18. I. Herath, M. Vithanage, J. Bundschuh, J. P. Maity, and P. Bhattacharya, *Natural Arsenic in Global Groundwaters: Distribution and Geochemical Triggers for Mobilization.* Current Pollution Reports, 2016. **2**(1), 68-89.
19. F. T. Jones, *A broad view of arsenic.* Poultry Science, 2007. **86**(1), 2-14.
20. Y. C. Jang, Y. Somanna, and H. Kim, *Source, Distribution, Toxicity and Remediation of Arsenic in the Environment – A review.* International Journal of Applied Environmental Sciences, 2016. **11**(2), 559-581.
21. M. Borho and P. Wilderer, *Optimized removal of arsenate(III) by adaptation of oxidation and precipitation processes to the filtration step.* Water Science and Technology, 1996. **34**(9 pt 5), 25-31.

22. V. Lenoble, O. Bouras, V. Deluchat, B. Serpaud, and J. C. Bollinger, *Arsenic adsorption onto pillared clays and iron oxides.* Journal of Colloid and Interface Science, 2002. **255**(1), 52-58.

23. M. L. Pierce and C. B. Moore, *Adsorption of arsenite and arsenate on amorphous iron hydroxide.* Water Research, 1982. **16**(7), 1247-1253.

24. A. Jain and R. H. Loeppert, *Effect of competing anions on the adsorption of arsenate and arsenite by ferrihydrite.* Journal of Environmental Quality, 2000. **29**(5), 1422-1430.

25. X. Meng, G. P. Korfiatis, S. Bang, and K. W. Bang, *Combined effects of anions on arsenic removal by iron hydroxides.* Toxicology Letters, 2002. **133**(1), 103-111.

26. T. Tuutijärvi, E. Repo, R. Vahala, M. Sillanpää, and G. Chen, *Effect of competing anions on arsenate adsorption onto maghemite nanoparticles.* Chinese Journal of Chemical Engineering, 2012. **20**(3), 505-514.

27. T. Prohaska and G. Stingeder, *Speciation of Arsenic: Arsenic and Arsenic Species in Environment and Human Nutrition*, in *Handbook of Elemental Speciation II - Species in the Environment, Food, Medicine and Occupational Health*. 2005. 69-85.

28. T. Nakazato, H. Tao, T. Taniguchi, and K. Isshiki, *Determination of arsenite, arsenate, and monomethylarsonic acid in seawater by ion-exclusion chromatography combined with inductively coupled plasma mass spectrometry using reaction cell and hydride generation techniques.* Talanta, 2002. **58**(1), 121-132.

29. P. Bhattacharya, G. Jacks, S.H. Frisbie, E. Smith, R. Naidu, and B. Sarkar, *Arsenic in the environment: a global perspective*, in *Heavy Metals In The Environment*, B. Sarkar, Editor. 2002, Marcel Dekker. Inc.: New York. 147-215.

30. B. A. Fowler, C. H. S. J. Chou, R. L. Jones, D. W. Sullivan, Jr., and C. J. Chen, *Arsenic*, in *Handbook on the Toxicology of Metals: Fourth Edition*. 2014. 581-624.

31. R. Singh, S. Singh, P. Parihar, V. P. Singh, and S. M. Prasad, *Arsenic contamination, consequences and remediation techniques: A review.* Ecotoxicology and Environmental Safety, 2015. **112**, 247-270.

32. J. Y. Chung, S. D. Yu, and Y. S. Hong, *Environmental source of arsenic exposure.* Journal of Preventive Medicine and Public Health, 2014. **47**(5), 253-257.

33. World Health Organization, *Guidelines for Drinking-water Quality: Recommendations.* THIRD EDITION ed. Vol. 1. 2004.

34. M. Raessler, *The Arsenic Contamination of Drinking and Groundwaters in Bangladesh: Featuring Biogeochemical Aspects and Implications on Public Health.* Archives of Environmental Contamination and Toxicology, 2018. **75**(1).

35. D. Chakraborti, S. K. Singh, M. M. Rahman, R. N. Dutta, S. C. Mukherjee, S. Pati, and P. B. Kar, *Groundwater arsenic contamination in the ganga river basin: A future health danger.* International Journal of Environmental Research and Public Health, 2018. **15**(2).

36. M. Calatayud, S. S. Farias, G. S. de Paredes, M. Olivera, N. Á Carreras, M. C. Giménez, V. Devesa, and D. Vélez, *Arsenic exposure of child populations in Northern Argentina.* Science of the Total Environment, 2019. **669**, 1-6.

37. S. Wang and C. N. Mulligan, *Occurrence of arsenic contamination in Canada: Sources, behavior and distribution.* Science of the Total Environment, 2006. **366**(2-3), 701-721.

38. T. Le Luu, *Remarks on the current quality of groundwater in Vietnam.* Environmental Science and Pollution Research, 2019. **26**(2), 1163-1169.

39. R. N. Ratnaike, *Acute and chronic arsenic toxicity.* Postgraduate Medical Journal, 2003. **79**(933), 391-396.

40. Md. I. M. Choudhury, N. Shabnam, T. Ahsan, S. M. Abu Ahsan, Md. S. Kabir, R. Md. Khan, Md. A. Miah, Mohd. K. Uddin, and Md. A. R. Liton, *Cutaneous Malignancy due to Arsenicosis in Bangladesh: 12-Year Study in Tertiary Level Hospital.* BioMed Research International, 2018. **2018**, 1-9.

41. Subcommittee on Arsenic in Drinking Water, Commission on Life Sciences, Division on Earth and Life Studies, and National Research Council, *Disposition of Inorganic Arsenic*, in *Arsenic in Drinking Water*, National Academies Press, Editor. 1999. 150-176.

42. F. Challenger, *Biological methylation.* Chemical Reviews, 1945. **36**(3), 315-361.

43. F. Challenger, *Biological Methylation*, in *Advances in Enzymology and Related Areas of Molecular Biology*, F.F. Nord, Editor. 1951. 429-491.

44. Kirk T. Kitchin, *Arsenic's Interactions with Macromolecules and its Relationship to Carcinogenesis*, in *Biological Chemistry of Arsenic, Antimony and Bismuth* 2010, Wiley.

45. Matthews G. A., *A History of Pesticides*. 2018: CABI, 2018.

46. P. Ravenscroft, H. Brammer, and K. Richards, *Arsenic Pollution: A Global Synthesis.* Arsenic Pollution: A Global Synthesis. 2009. 1-588.

47. A. Emadi and S. D. Gore, *Arsenic trioxide - An old drug rediscovered.* Blood Reviews, 2010. **24**(4-5), 191-199.

48. D. Ho and E. J. Lowenstein, *Fowler's solution and the evolution of the use of arsenic in modern medicine.* SKINmed, 2016. **14**(4), 287-289.

49. F. Bosch and L. Rosich, *The contributions of paul ehrlich to pharmacology: A tribute on the occasion of the centenary of his nobel prize.* Pharmacology, 2008. **82**(3), 171-179.

50. K. Alimoghaddam, A. Shariftabrizi, M. Tavangar, Z. Sanaat, S. Rostami, M. Jahani, and A. Ghavamzadeh, *Anti-leukemic and anti-angiogenesis efficacy of arsenic trioxide in new cases of acute promyelocytic leukemia.* Leukemia and Lymphoma, 2006. **47**(1), 81-88.

51. H. W. Chiu, Y. S. Ho, and Y. J. Wang, *Arsenic trioxide induces autophagy and apoptosis in human glioma cells in vitro and in vivo through downregulation of survivin.* Journal of Molecular Medicine, 2011. **89**(9), 927-941.

52. HW Chiu, JH Lin, YA Chen, SY Ho, and YJ Wang, *Combination treatment with arsenic trioxide and irradiation enhances cell-killing effects in human fibrosarcoma cells in vitro and in vivo through induction of both autophagy and apoptosis.* Autophagy, 2010. **6**(3), 353-365.

53. Y. Zhao, K. Onda, K. Sugiyama, B. Yuan, S. Tanaka, N. Takagi, and T. Hirano, *Antitumor effects of arsenic disulfide on the viability, migratory ability, apoptosis and autophagy of breast cancer cells.* Oncology Reports, 2019. **41**(1), 27-42.

54. S. J. Ralph, *Arsenic-Based Antineoplastic Drugs and Their Mechanism of Action.* Metal-Based Drugs, 2008. **2008**, 1-13.

55. Douglas A. Skoog, F. James Holler, and Stanley R. Crouch, *Principles of Instrumental Analysis*. VI ed. 2007: Thomson Brooks/Cole.

56. Delbert J. Eatough, James J. Christensen, and Reed McNeil Izatt, *Experiments in Thermometric Titrimetry and Titration Calorimetry*. 1974: Brigham Young University Press.

57. L. D. Hansen, G. W. Fellingham, and D. J. Russell, *Simultaneous determination of equilibrium constants and enthalpy changes by titration calorimetry: Methods, instruments, and uncertainties.* Analytical Biochemistry, 2011. **409**(2), 220-229.

58. C. Sgarlata, V. Zito, and G. Arena, *Conditions for calibration of an isothermal titration calorimeter using chemical reactions.* Analytical and Bioanalytical Chemistry, 2013. **405**(2-3), 1085-1094.

59. G. Arena, P. Gans, and C. Sgarlata, *HypCal, a general-purpose computer program for the determination of standard reaction enthalpy and binding constant values by means of calorimetry.* Analytical and Bioanalytical Chemistry, 2016. **408**(23), 6413-6422.

60. R.M. Silverstein, F.X. Webster, D.J. Kiemle, and D.L. Bryce, *Identificazione spettrometrica di composti organici.* 3 ed. 2016: Casa Editrice Ambrosiana.

61. Fangbiao Li, *Imaging Mass Spectrometry for Small Molecules*, in *Using Mass Spectrometry for Drug Metabolism Studies*, W.A. Korfmacher, Editor. 2009, CRC Press.

62. J. Hutter, M. Iannuzzi, F. Schiffmann, and J. Vandevondele, *Cp2k: Atomistic simulations of condensed matter systems.* Wiley Interdisciplinary Reviews: Computational Molecular Science, 2014. **4**(1), 15-25.

63. A. D. Becke, *Density-functional exchange-energy approximation with correct asymptotic behavior.* Physical Review A, 1988. **38**(6), 3098-3100.

64. C. Lee, W. Yang, and R. G. Parr, *Development of the Colle-Salvetti correlation-energy formula into a functional of the electron density.* Physical Review B, 1988. **37**(2), 785-789.

65. S. Grimme, J. Antony, S. Ehrlich, and H. Krieg, *A consistent and accurate ab initio parametrization of density functional dispersion correction (DFT-D) for the 94 elements H-Pu.* Journal of Chemical Physics, 2010. **132**(15).

66. S. Grimme, S. Ehrlich, and L. Goerigk, *Effect of the damping function in dispersion corrected density functional theory.* Journal of Computational Chemistry, 2011. **32**(7), 1456-1465.

67. S. Goedecker and M. Teter, *Separable dual-space Gaussian pseudopotentials.* Physical Review B - Condensed Matter and Materials Physics, 1996. **54**(3), 1703-1710.

68. G. Bussi, D. Donadio, and M. Parrinello, *Canonical sampling through velocity rescaling.* Journal of Chemical Physics, 2007. **126**(1).

69. C. De Stefano, S. Sammartano, P. Mineo, and C. Rigano, *Computer Tools for the Speciation of Natural Fluids*, in *Marine Chemistry - An Environmental Analytical Chemistry Approach*, A. Gianguzza, E. Pelizzetti, and S. Sammartano, Editors. 1997, Kluwer Academic Publishers: Amsterdam. 71-83.

70. A. De Robertis, C. De Stefano, and C. Rigano, *Computer Analysis of Equilibrium Data in Solution. ES5CM Fortran and Basic Programs for Computing Formation Enthalpies from Calorimetric Measurements.* Thermochim. Acta, 1989. **138**, 141-146.

71. P. Gans, A. Sabatini, and A. Vacca, *Determination of equilibrium constants from spectrophometric data obtained from solutions of known pH: The program pHab.* Annali di Chimica, 1999. **89**(1-2), 45-49.

72. L. Alderighi, P. Gans, A. Ienco, D. Peters, A. Sabatini, and A. Vacca, *Hyperquad simulation and speciation (HySS): A utility program for the investigation of equilibria involving soluble and partially soluble species.* Coordination Chemistry Reviews, 1999. **184**(1), 311-318.

73. Peter Gans, Antonio Sabatini, and Alberto Vacca. *HypCal: Determination of stability constants and formation enthalpies from calorimetric data.* 10/09/2019]; Available from: http://www.hyperquad.co.uk/hypdeltah.htm.

74. C. Bretti, F. Crea, O. Giuffrè, and S. Sammartano, *The effect of different aqueous ionic media on the acid-base properties of some open chain polyamines.* J. Solution Chem., 2008. **37**, 183-201.

75. L. Di Palma, E. Petrucci, and B. Pietrangeli, *Environmental effects of using chelating agents in polluted sediment remediation.* Bulletin of Environmental Contamination and Toxicology, 2015. **94**(3), 340-344.

76. P. P. Falciglia, D. Malarbì, R. Maddalena, V. Greco, and F. G. A. Vagliasindi, *Remediation of Hg-contaminated marine sediments by simultaneous application of enhancing agents and microwave heating (MWH).* Chemical Engineering Journal, 2017. **321**, 1-10.

77. M. Niinae, K. Nishigaki, and K. Aoki, *Removal of lead from contaminated soils with chelating agents.* Materials Transactions, 2008. **49**(10), 2377-2382.

78. J. Aaseth, G. Crisponi, and O. Andersen, *Chelation Therapy in the Treatment of Metal Intoxication.* Chelation Therapy in the Treatment of Metal Intoxication. 2016. 1-371.

79. F. Crea, G. Falcone, C. Foti, O. Giuffrè, and S. Materazzi, *Thermodynamic data for Pb^{2+} and Zn^{2+} sequestration by biologically important S-donor ligands, at different temperatures and ionic strengths.* New J. Chem., 2014. **38**, 3973-3983.

80. G. Falcone, C. Foti, A. Gianguzza, O. Giuffrè, A. Napoli, A. Pettignano, and D. Piazzese, *Sequestering ability of some chelating agents towards methylmercury(II).* Anal. Bioanal. Chem., 2013. **405**(2), 881-893.

81. C. De Stefano, A. Gianguzza, D. Milea, A. Pettignano, and S. Sammartano, *Sequestering ability of polyaminopolycarboxylic ligands towards dioxouranium(VI) cation.* J. Alloys Compd., 2006. **424**(1-2), 93-104.

82. C. De Stefano, D. Milea, N. Porcino, and S. Sammartano, *Speciation of phytate ion in aqueous solution. Sequestering ability towards mercury(II) cation in $NaCl_{aq}$ at different ionic strengths.* J. Agric. Food Chem., 2006. **54**(4), 1459-1466.

83. C. De Stefano, D. Milea, N. Porcino, and S. Sammartano, *Speciation of phytate ion in aqueous solution. Cadmium(II) interactions in $NaCl_{aq}$ at different ionic strengths.* Anal. Bioanal. Chem., 2006. **386**(2), 346-356.

84. C. De Stefano, A. Gianguzza, D. Piazzese, N. Porcino, and S. Sammartano, *Sequestration of biogenic amines by alginic and fulvic acids.* Biophys. Chem., 2006. **122**, 221-231.

85. A. Giacalone, A. Gianguzza, A. Pettignano, and S. Sammartano, *Sequestration of organometallic compounds by natural organic matter. Binding of trimethyltin(IV) by fulvic and alginic acids.* Appl. Organomet. Chem., 2006. **20**, 706-717.

86. F. Crea, C. De Stefano, C. Foti, D. Milea, and S. Sammartano, *Chelating agents for the sequestration of mercury(II) and monomethyl mercury(II).* Curr. Med. Chem., 2014. **21**(33), 3819-3836.

87. P. Cardiano, D. Chillè, M. Cordaro, C. Foti, and O. Giuffrè, *Interactions of Inosine 5'-Monophosphate with Ca2+ and Mg2+: A Thermodynamic and Spectroscopic Study in Aqueous Solution.* Journal of Chemical and Engineering Data, 2019. **64**(6), 2859-2866.

88. D. Chillè, C. Foti, and O. Giuffrè, *Thermodynamic parameters for the interaction between etidronic acid and inorganic and organic mercury(II).* Journal of Chemical Thermodynamics, 2018. **121**, 65-71.

89. Eva Margui and Rene Van Grieken, *X-Ray Fluorescence Spectrometry and Related Techniques: An Introduction.* 2013.

90. D. E. Salt, R. C. Prince, and I. J. Pickering, *Chemical speciation of accumulated metals in plants: Evidence from X-ray absorption spectroscopy.* Microchemical Journal, 2002. **71**(2-3), 255-259.

91. M. Filella and P. M. May, *Reflections on the calculation and publication of potentiometrically- determined formation constants.* Talanta, 2005. **65**(5), 1221-1225.

92.   A. Vacca, A. Sabatini, and M. A. Gristina, *Two problems involved in solving complex formation equilibria: the selection of species and the calculation of stability constants.* Coordination Chemistry Reviews, 1972. **8**(1-2), 45-53.

93.   M. Jekel and G. L. Amy, *Chapter 11: Arsenic removal during drinking water treatment*, in *Interface Science and Technology*. 2006. p. 193-206.

94.   Richard C. Ropp, *Group 15 (N, P, As, Sb and Bi) Alkaline Earth Compounds*, in *Encyclopedia of the Alkaline Earth Compounds*. 2013, Newnes.

95.   G. Cassone, D. Chillé, C. Foti, O. Giuffré, R. C. Ponterio, J. Sponer, and F. Saija, *Stability of hydrolytic arsenic species in aqueous solutions: As3+ vs. As5+.* Physical Chemistry Chemical Physics, 2018. **20**(36), 23272-23280.

96.   L. R. Canaval, O. M. D. Lutz, A. K. H. Weiss, C. W. Huck, and T. S. Hofer, *A dissociative quantum mechanical/molecular mechanical molecular dynamics simulation and infrared experiments reveal characteristics of the strongly hydrolytic arsenic(III).* Inorganic Chemistry, 2014. **53**(22), 11861-11870.

97.   O. Coskuner and T. C. Allison, *Dynamic and structural properties of aqueous arsenic solutions.* ChemPhysChem, 2009. **10**(8), 1187-1189.

98.   L. Marini and M. Accornero, *Prediction of the thermodynamic properties of metal-arsenate and metal-arsenite aqueous complexes to high temperatures and pressures and some geological consequences.* Environmental Geology, 2007. **52**(7), 1343-1363.

99.   B. W. Vink, *Stability relations of antimony and arsenic compounds in the light of revised and extended Eh-pH diagrams.* Chemical Geology, 1996. **130**(1-2), 21-30.

100.   M. Styblo, S. V. Serves, W. R. Cullen, and D. J. Thomas, *Comparative inhibition of yeast glutathione reductase by arsenicals and arsenothiols.* Chemical Research in Toxicology, 1997. **10**(1), 27-33.

101.   S. Lin, W. R. Cullen, and D. J. Thomas, *Methylarsenicals and arsinothiols are potent inhibitors of mouse liver thioredoxin reductase.* Chemical Research in Toxicology, 1999. **12**(10), 924-930.

102.   J. A. Vilensky and K. Redman, *British anti-Lewisite (dimercaprol): An amazing history.* Annals of Emergency Medicine, 2003. **41**(3), 378-383.

103.   X. W. Zhang, X. J. Yan, Z. R. Zhou, F. F. Yang, Z. Y. Wu, H. B. Sun, W. X. Liang, A. X. Song, V. Lallemand-Breitenbach, M. Jeanne, Q. Y. Zhang, H. Y. Yang, Q. H. Huang, G. B. Zhou, J. H. Tong, Y. Zhang, J. H. Wu, H. Y. Hu, H. De The, S. J. Chen, and Z. Chen, *Arsenic trioxide controls the fate of the PML-RARα oncoprotein by directly binding PML.* Science, 2010. **328**(5975), 240-243.

104.   M. Prakash, M. S. Shetty, P. Tilak, and N. Anwar, *Total Thiols: Biomedical importance and their alteration in various disorders.* Online Journal of Health and Allied Sciences, 2009. **8**(2).

105.   J. Aaseth, L. Gerhardsson, M. A. Skaug, and J. Alexander, *General Chemistry of Metal Toxicity and Basis for Metal Complexation*, in *Chelation Therapy in the Treatment of Metal Intoxication*. 2016. 1-33.

106.   C. Y. C. Pak, C. Fuller, K. Sakhaee, J. E. Zerwekh, and B. V. Adams, *Management of cystine nephrolithiasis with alpha-mercaptopropionylglycine.* Journal of Urology, 1986. **136**(5), 1003-1008.

107.   G. F. Ferraccioli, F. Salaffi, A. Nervetti, and Manganelli, *Long-term outcome with gold thiosulphate and tiopronin in 200 rheumatoid patients.* Clinical and Experimental Rheumatology, 1989. **7**(6), 577-581.

108.   J. Sany, B. Combe, D. Verdie-Petibon, A. Tagemouati, and J. P. Daures, *Study of the long-term tolerance of thiopronine (Acadione) in the treatment of rheumatoid polyarthritis.* Revue du Rhumatisme et des Maladies Osteo-Articulaires, 1990. **57**(2), 105-111.

109. P. R. Patil and V. Krishnan', *Thiomalates of divalent zinc, cadmium, mercury and lead.* Journal of Inorganic and Nuclear Chemistry, 1978. **40**, 1255--1257.

110. G. Crisponi and V. M. Nurchi, *Chelating Agents as Therapeutic Compounds-Basic Principles*, in *Chelation Therapy in the Treatment of Metal Intoxication*. 2016. 35-61.

111. D. S. Mottram, *Flavour formation in meat and meat products: A review.* Food Chemistry, 1998. **62**(4), 415-424.

112. C. Starkenmann, M. Troccaz, and K. Howell, *The role of cysteine and cysteine-S conjugates as odour precursors in the flavour and fragrance industry.* Flavour and Fragrance Journal, 2008. **23**(6), 369-381.

113. B. C. Dave, J. P. Germanas, and R. S. Czernuszewicz, *The First Direct Evidence for Copper(II)-Cysteine Vibrations in Blue Copper Proteins: Resonance Raman Spectra of 34S-Cys-Labeled Azurins Reveal Correlation of Copper-Sulfur Stretching Frequency with Metal Site Geometry.* Journal of the American Chemical Society, 1993. **115**(25), 12175-12176.

114. N. J. Pace and E. Weerapana, *Zinc-binding cysteines: diverse functions and structural motifs.* Biomolecules, 2014. **4**(2), 419-434.

115. J. M. Wiśniewska, B. Trojanowska, J. Piotrowski, and M. Jakubowski, *Binding of mercury in the rat kidney by metallothionein.* Toxicology and Applied Pharmacology, 1970. **16**(3), 754-763.

116. M. Priori, *Medicina e chirurgia estetica del viso e del collo*, ed. Elsevier. 2007.

117. G. Bellomo, M. Vairetti, L. Stivala, F. Mirabelli, P. Richelmi, and S. Orrenius, *Demonstration of nuclear compartmentalization of glutathione in hepatocytes.* Proceedings of the National Academy of Sciences of the United States of America, 1992. **89**(10), 4412-4416.

118. A. Meister, *Glutathione metabolism and its selective modification.* Journal of Biological Chemistry, 1988. **263**(33), 17205-17208.

119. C. Bretti, C. De Stefano, C. Foti, O. Giuffrè, and S. Sammartano, *Thermodynamic protonation parameters of some sulphur-containing anions in NaClaq and (CH$_3$)$_4$NClaq at t = 25 °C* J. Solution Chem., 2009. **38**(10), 1225-1245.

120. P. Crea, A. De Robertis, C. De Stefano, D. Milea, and S. Sammartano, *Modelling the dependence on medium and ionic strength of glutathione acid-base behavior in LiClaq, NaClaq, KClaq, CaClaq, (CH$_3$)$_4$NClaq and (C$_2$H$_5$)$_4$NIaq.* J. Chem. Eng. Data, 2007(52), 1028-1036.

121. N. A. Rey, O. W. Howarth, and E. C. Pereira-Maia, *Equilibrium characterization of the As(III)-cysteine and the As(III)-glutathione systems in aqueous solution.* Journal of Inorganic Biochemistry, 2004. **98**(6), 1151-1159.

122. A. M. Spuches, H. G. Kruszyna, A. M. Rich, and D. E. Wilcox, *Thermodynamics of the as(III)-thiol interaction: Arsenite and monomethylarsenite complexes with glutathione, dihydrolipoic acid, and other thiol ligands.* Inorganic Chemistry, 2005. **44**(8), 2964-2972.

123. M. Delnomdedieu, M. M. Basti, J. D. Otvos, and D. J. Thomas, *Transfer of Arsenite from Glutathione to Dithiols: A Model of Interaction.* Chemical Research in Toxicology, 1993. **6**(5), 598-602.

124. P. Cardiano, F. Giacobello, O. Giuffrè, and S. Sammartano, *Thermodynamics of Al 3 + -thiocarboxylate interaction in aqueous solution.* Journal of Molecular Liquids, 2016. **222**, 614-621.

125. Giuseppe Cassone, Donatella Chillè, Fausta Giacobello, Ottavia Giuffrè, Viviana Mollica Nardo, Rosina C. Ponterio, Franz Saija, Jiri Sponer, Sebastiano Trusso, and Claudia Foti, *Interaction between As(III) and Simple Thioacids in Water: An*

Experimental and ab Initio Molecular Dynamics Investigation. The Journal of Physical Chemistry B, 2019. **123**, 6090-6098.

126. Y. Feng, A. J. DeGraffenreid, M. D. Phipps, T. L. Rold, N. C. Okoye, F. A. Gallazzi, C. L. Barnes, C. S. Cutler, A. R. Ketring, T. J. Hoffman, and S. S. Jurisson, *A trithiol bifunctional chelate for 72,77 As: A matched pair theranostic complex with high in vivo stability.* Nuclear Medicine and Biology, 2018. **61**, 1-10.

127. N. Scott, K. M. Hatlelid, N. E. MacKenzie, and D. E. Carter, *Reactions of Arsenic (III) and Arsenic (V) Species with Glutathione.* Chemical Research in Toxicology, 1993. **6**(1), 102-106.

128. A.T. Ward, *Raman spectroscopy of sulfur, sulfur-selenium, and sulfur-arsenic mixtures.* Journal of Physical Chemistry, 1968. **72**, 4133-4139

129. S.A. Wood, Tait, C.D., Janecky, D.R. , *A Raman spectroscopic study of arsenite and thioarsenite species in aqueous solution at 25 °C.* Geochemical Transactions, 2002. **3**, 31-39

130. V.K. Sharma, F. Casteran, F.J. Millero, and C. De Stefano, *Dissociation Constants of Protonated Cysteine Species in NaCl Media.* J. Solution Chem., 2002. **31**(10), 783-792.

131. R.M. Cigala, F. Crea, C. De Stefano, G. Lando, D. Milea, and S. Sammartano, *Modeling the acid-base properties of glutathione in different ionic media, with particular reference to natural waters and biological fluids.* Amino Acids, 2012. **43**(2), 629-648.

132. A. Sasson and S. P. Monselise, *Malonic acid, a proposed indicator of orange fruit senescence.* Experientia, 1976. **32**(9), 1116-1117.

133. Francisco López-Muñoz, Ronaldo Ucha-Udabe, and Cecilio Alamo, *The history of barbiturates a century after their clinical introduction.* Neuropsychiatr Disease and Treatment, 2005. **1**(4), 329–343.

134. I. Mir and D. Kumar, *Recent advances in isotropic conductive adhesives for electronics packaging applications.* International Journal of Adhesion and Adhesives, 2008. **28**(7), 362-371.

135. G. Shui and L. P. Leong, *Separation and determination of organic acids and phenolic compounds in fruit juices and drinks by high-performance liquid chromatography.* Journal of Chromatography A, 2002. **977**(1), 89-96.

136. A. B. Pardee and V. R. Potter, *Malonate inhibition of oxidations in the Krebs tricarboxylic acid cycle.* The Journal of biological chemistry, 1949. **178**(1), 241-250.

137. J. B. Russell, *Production of tricarballylic acid by rumen microorganisms and its potential toxicity in ruminant tissue metabolism.* British Journal of Nutrition, 1986. **56**(1), 153-162.

138. V. A. Dehabadi, H. J. Buschmann, and J. S. Gutmann, *Durable press finishing of cotton fabrics: An overview.* Textile Research Journal, 2013. **83**(18), 1974-1995.

139. F. Crea, A. De Robertis, C. De Stefano, and S. Sammartano, *Dioxouranium(VI)-carboxylate complexes. Interaction of UO_2^{2+} with 1,2,3,4,5,6-benzenehexacarboxylate (mellitate) in $0 < NaCl_{aq} < 1.0$ mol L^{-1}.* J. Solution Chem., 2007. **36**(4), 479-496.

140. A. De Robertis, C. De Stefano, and C. Foti, *Medium effects on the protonation of carboxylic acids at different temperatures.* J. Chem. Eng. Data, 1999. **44**, 262-270.

141. A. De Robertis, C. De Stefano, and C. Foti, *Studies on Polyfunctional O-Ligands. Protonation in Different Ionic Media and Alkali and Alkaline Earth Metal Complex Formation of Benzenehexacarboxylate.* Ann. Chim. (Rome), 1996. **86**, 155-166.

142. P. Cardiano, F. Giacobello, O. Giuffrè, and S. Sammartano, *Thermodynamic and spectroscopic study on Al3+-polycarboxylate interaction in aqueous solution.* Journal of Molecular Liquids, 2017. **232**, 45-54.

143. P. de Paz-Lugo, J. A. Lupiáñez, and E. Meléndez-Hevia, *High glycine concentration increases collagen synthesis by articular chondrocytes in vitro: acute glycine deficiency could be an important cause of osteoarthritis.* Amino Acids, 2018. **50**(10), 1357-1365.

144. C. P. S. Badenhorst, E. Erasmus, R. Van Der Sluis, C. Nortje, and A. A. Van Dijk, *A new perspective on the importance of glycine conjugation in the metabolism of aromatic acids.* Drug Metabolism Reviews, 2014. **46**(3), 343-361.

145. P. E. Chen, M. T. Geballe, P. J. Stansfeld, A. R. Johnston, H. Yuan, A. L. Jacob, J. P. Snyder, S. F. Traynelis, and D. J. A. Wyllie, *Structural features of the glutamate binding site in recombinant NR1/NR2A N-methyl-D-aspartate receptors determined by site-directed mutagenesis and molecular modeling.* Molecular Pharmacology, 2005. **67**(5), 1470-1484.

146. M. D. Shoulders and R. T. Raines, *Collagen structure and stability*, in *Annual Review of Biochemistry*. 2009. p. 929-958.

147. M. Yamauchi and M. Sricholpech, *Lysine post-translational modifications of collagen.* Essays in Biochemistry, 2012. **52**(1), 113-133.

148. F. M. Vaz and R. J. A. Wanders, *Carnitine biosynthesis in mammals.* Biochemical Journal, 2002. **361**(3), 417-429.

149. S. R. Pinnell, S. M. Krane, J. E. Kenzora, and M. J. Glimcher, *A Heritable Disorder of Connective Tissue: Hydroxylysine-Deficient Collagen Disease.* New England Journal of Medicine, 1972. **286**(19), 1013-1020.

150. D. H. Rushton, *Nutritional factors and hair loss.* Clinical and Experimental Dermatology, 2002. **27**(5), 400-408.

151. J. Fernandes, G. Van Den Berghe, J. M. Saudubray, and J. H. Walter, *Inborn metabolic diseases: Diagnosis and treatment.* Inborn Metabolic Diseases: Diagnosis and Treatment. 2006. 1-561.

152. C. Bretti, O. Giuffrè, G. Lando, and S. Sammartano, *Modeling solubility and acid–base properties of some amino acids in aqueous NaCl and (CH 3) 4 NCl aqueous solutions at different ionic strengths and temperatures.* SpringerPlus, 2016. **5**(1).

153. C. Bretti, R. M. Cigala, O. Giuffrè, G. Lando, and S. Sammartano, *Modeling solubility and acid-base properties of some polar side chain amino acids in NaCl and (CH3)4NCl aqueous solutions at different ionic strengths and temperatures.* Fluid Phase Equilibria, 2018. **459**, 51-64.

154. C. De Stefano, C. Foti, A. Gianguzza, C. Rigano, and S. Sammartano, *Chemical speciation of amino acids in electrolyte solutions containing major components of natural fluids.* Chemical Speciation and Bioavailability, 1995. **7**(1), 1-8.

155. P. Cardiano, C. Foti, F. Giacobello, O. Giuffrè, and S. Sammartano, *Study of Al 3+ interaction with AMP, ADP and ATP in aqueous solution.* Biophysical Chemistry, 2018. **234**, 42-50.

156. B. Nowack, *Environmental chemistry of phosphonates.* Water Research, 2003. **37**(11), 2533-2546.

157. T. P. Knepper, *Synthetic chelating agents and compounds exhibiting complexing properties in the aquatic environment.* TrAC - Trends in Analytical Chemistry, 2003. **22**(10), 708-724.

158. R. G. G. Russell, *Bisphosphonates: From bench to bedside*, in *Annals of the New York Academy of Sciences*. 2006. p. 367-401.

159. E. Rott, H. Steinmetz, and J. W. Metzger, *Organophosphonates: A review on environmental relevance, biodegradability and removal in wastewater treatment plants.* Science of the Total Environment, 2018. **615**, 1176-1191.

160.   B. Nowack, *Determination of phosphonates in natural waters by ion-pair high-performance liquid chromatography.* Journal of Chromatography A, 1997. **773**(1-2), 139-146.

161.   B. Nowack, *The behavior of phosphonates in wastewater treatment plants of Switzerland.* Water Research, 1998. **32**(4), 1271-1279.

162.   B. Nowack, *Aminopolyphosphonate removal during wastewater treatment.* Water Research, 2002. **36**(18), 4636-4642.

163.   I. Cukrowski, L. Popović, W. Barnard, S. O. Paul, P. H. van Rooyen, and D. C. Liles, *Modeling and spectroscopic studies of bisphosphonate-bone interactions. The Raman, NMR and crystallographic investigations of Ca-HEDP complexes.* Bone, 2007. **41**(4), 668-678.

164.   A. Jung, B. Mermillod, R. Schenk, B. Courvoisier, P. Burkhardt, J. Epiney, and Fleisch, *Use of disodium etidronate (EHPD) in treating 10 cases of symptomatic Paget's disease.* Schweizerische Medizinische Wochenschrift, 1976. **106**(48), 1667-1673.

165.   P. Cardiano, C. De Stefano, C. Foti, F. Giacobello, O. Giuffrè, and S. Sammartano, *Sequestration of HEDPA, NTA and phosphonic NTA derivatives towards Al3+ in aqueous solution.* Journal of Molecular Liquids, 2018. **261**, 96-106.

166.   C. De Stefano, C. Foti, O. Giuffrè, and D. Milea, *Complexation of Hg^{2+}, CH_3Hg^+, Sn^{2+}, and $(CH_3)_2Sn^{2+}$ with phosphonic NTA derivatives.* New J. Chem., 2016. **40**, 1443-1453.

167.   K. L. Nash, L. F. Rao, and G. R. Choppin, *Calorimetric and Laser Induced Fluorescence Investigation of the Complexation Geometry of Selected Europium-gem-Diphosphonate Complexes in Acidic Solutions.* Inorganic Chemistry, 1995. **34**(10), 2753-2758.

168.   C. Bretti, C. De Stefano, G. Lando, and S. Sammartano, *Solubility, acid-base properties and thermodynamics of interaction between three NTA-phosphonate derivatives and the main cationic components (H+, Na+, Mg2+ and Ca2+) of natural fluids.* Journal of Chemical Thermodynamics, 2018. **123**, 117-127.

169.   C. Foti, O. Giuffrè, and S. Sammartano, *Thermodynamics of HEDPA protonation in different media and complex formation with Mg^{2+} and Ca^{2+}.* J. Chem. Thermodynamics, 2013. **66**, 151-160.

170.   H. C. Steinrücken and N. Amrhein, *The herbicide glyphosate is a potent inhibitor of 5-enolpyruvylshikimic acid-3-phosphate synthase.* Biochemical and Biophysical Research Communications, 1980. **94**(4), 1207-1212.

171.   J. P. Slovin and E. M. Tobin, *Glyphosine, a plant growth regulator, affects chloroplast membrane proteins.* BBA - Bioenergetics, 1981. **637**(1), 177-184.

172.   M. Cordaro, C. Foti, F. Giacobello, O. Giuffrè, and S. Sammartano, *Phosphonic Derivatives of Nitrilotriacetic Acid as Sequestering Agents for Ca2+ in Aqueous Solution: A Speciation Study for Application in Natural Waters.* ACS Earth and Space Chemistry, 2019.

173.   L. Di Donna, H. Benabdelkamel, D.Taverna, S. Indelicato, D. Aiello, A. Napoli, G. Sindona, and F. Mazzotti, *Determination of ketosteroid hormones in meat by liquid chromatography tandem mass spectrometry and derivatization chemistry.* Anal Bioanal Chem., 2015. **407**(19), 5835-5842.

174.   F. Mazzotti, L. Di Donna, A. Napoli, D. Aiello, C. Siciliano, C. M. Athanassopoulos, and G. Sindona, *N‐hydroxysuccinimidyl p‐methoxybenzoate as suitable derivative reagent for isotopic dilution assay of biogenic amines in food.* Jornal of Mass Spectrometry, 2014. **49**, 802-810.

175. P. Cardiano, G. Falcone, C. Foti, O. Giuffrè, and A. Napoli, *Binding ability of glutathione towards alkyltin(IV) compounds in aqueous solution.* J. Inorg. Biochem., 2013. **129**, 84-93.

176. P. Cardiano, O. Giuffrè, A. Napoli, and S. Sammartano, *Potentiometric, ^{1}H-NMR, ESI-MS investigation on dimethyltin(IV) cation-mercaptocarboxylate interaction in aqueous solution.* New J. Chem., 2009. **33**, 2286-2295.

177. A. Napoli, D. Aiello, L. Di Donna, A. Sajjad, E. Perri, and G. Sindona, *Profiling of Hydrophilic Proteins from Olea europaea Olive Pollen by MALDI TOF Mass Spectrometry.* Analytical Chemistry, 2006. **78**, 3434-3443.

178. C.E. Reddy, L. Albanito, P. De Marco, D. Aiello, M. Maggiolini, A. Napoli, and A. M. Musti, *Multisite phosphorylation of c-Jun at threonine 91/93/95 triggers the onset of c-Jun pro-apoptotic activity in cerebellar granule neurons.* Cell Death & Disease, 2013. **4**, 852.

179. J. F. J. Dippy, S. R. C. Hughes, and A. Rozanski, *The dissociation constants of some symmetrically disubstituted succinic acids.* Journal of the Chemical Society, 1959, 2492-2498.

180. L. D. Freedman and G. O. Doak, *The Preparation And Properties Of Phosphonic Acids.* Chemical Reviews, 1957. **57**, 479-523.

181. Eleni Barouda, Konstantinos D. Demadis, Sandra R. Freeman, Franca Jones, and Mark I. Ogden, *Barium Sulfate Crystallization in the Presence of Variable Chain Length Aminomethylenetetraphosphonates and Cations (Na+ or Zn2+).* Crystal Growth & Design, 2007. **7**, 321-327.

182. A. Cabeza and M. A. G. Aranda, *Metal Carboxyphosphonates*, in *Metal Phosphonate Chemistry: From Synthesis to Applications*, A. Clearfield and K. Demadis, Editors. 2012, Royal Society of Chemistry.

183. Aurelio Cabeza, Sebastián Bruque, Antonietta Guagliardi, and Miguel A. G. Aranda, *Two New Organo-Inorganic Hybrid Compounds: Nitrilophosphonates of Aluminum and Copper.* Journal of Solid State Chemistry, 2001. **160**(1), 278-286.

184. Abraham Clearfield and Konstantinos Demadis, *Metal Phosphonate Chemistry: From Synthesis to Applications*. 2012: Royal Society of Chemistry.

185. K. D. Demadis and S. D. Katarachia, *Metal-Phosphonate Chemistry: Synthesis, Crystal Structure Of Calcium-Aminotris -(Methylene Phosphonate) And Inhibition Of Caco3 Crystal Growth.* Phosphorus, Sulfur, and Silicon and the Related Elements 2004. **179**, 627-648.

186. Konstantinos D. Demadis, Stella D. Katarachia, Raphael G. Raptis, Hong Zhao, and Peter Baran, *Alkaline Earth Metal Organotriphosphonates: Inorganic−Organic Polymeric Hybrids from Dication−Dianion Association.* Crystal Growth & Design, 2006. **6**, 836-838.

187. F. Crea, C. Foti, D. Milea, and S. Sammartano, *Speciation of Cadmium in the Environment*, in *Cadmium: From Toxicity to Essentiality*, A. Sigel, H. Sigel, and R.K.O. Sigel, Editors. 2013, Springer Science + Business Media B.V.: Dordrecht. 63-83.

188. C. Foti, O. Giuffrè, G. Lando, and S. Sammartano, *Interaction of Inorganic Mercury(II) with Polyamines, Polycarboxylates, and Amino Acids.* J. Chem. Eng. Data, 2009. **54**, 893–903.

189. D. Cucinotta, C. De Stefano, O. Giuffrè, G. Lando, D. Milea, and S. Sammartano, *Formation, stability and empirical relationships for the binding of Sn2+ by O-, N- and S- donor ligands.* J. Mol. Liq., 2014. **200**, 329-339.

190. A. De Robertis, C. De Stefano, D. Milea, and S. Sammartano, *Additivity Factors in the Binding of Diethyltin(IV) Cation by Ligands Containing Amino- and Carboxylic Groups at Different Ionic Strengths.* J. Solution Chem., 2005. **34**(10), 1211-1226.

191. N. Belzile and A. Tessier, *Interactions between arsenic and iron oxyhydroxides in lacustrine sediments.* Geochimica et Cosmochimica Acta, 1990. **54**(1), 103-109.

192. Neupane G., Donahoe R. J., and Arai Y., *Kinetics of competitive adsorption/desorption of arsenate and phosphate at the ferrihydrite–water interface.* Chemical Geology, 2014. **368**, 31-38.

193. J. Gorny, G. Billon, L. Lesven, D. Dumoulin, B. Madé, and C. Noiriel, *Arsenic behavior in river sediments under redox gradient: A review.* Science of the Total Environment, 2015. **505**, 423-434.

194. Antelo J., Arce F., and Fiol S., *Arsenate and phosphate adsorption on ferrihydrite nanoparticles. Synergetic interaction with calcium ions.* Chemical Geology, 2015. **410**, 53-62.

195. T. Stanić, A. Daković, A. Živanović, M. Tomašević-Čanović, V. Dondur, and S. Milićević, *Adsorption of arsenic (V) by iron (III)-modified natural zeolitic tuff.* Environmental Chemistry Letters, 2009. **7**(2), 161-166.

196. R. A. Bideaux, K. W. Bladh, and M. C. Nichols, *Handbook of Mineralogy: Arsenates, Phosphates, Vanadates: 4* 2000: Mineral Data Pub.

197. D. Chillè, C. Foti, and O. Giuffrè, *Thermodynamic parameters for the protonation and the interaction of arsenate with Mg2+, Ca2+ and Sr2+: Application to natural waters.* Chemosphere, 2018. **190**, 72-79.

198. J. C. Raposo, J. Sanz, O. Zuloaga, M. A. Olazabal, and J. M. Madariaga, *The thermodynamic model of inorganic arsenic species in aqueous solutions: Potentiometric study of the hydrolitic equilibrium of arsenic acid.* Talanta, 2002. **57**(5), 849-857.

199. Martell A.E., Smith R.M., and Motekaitis R.J., *Critically Selected Stability Constants of Metal Complexes. National Institute of Standard and Technology.* PC-based Database NIST Gaithersburg, 2004.

200. R. N. Goldberg, N. Kishore, and R. M. Lennen, *Thermodynamic quantities for the ionization reactions of buffers.* Journal of Physical and Chemical Reference Data, 2002. **31**(2), 231-370.

201. P. M. May and K. Murray, *Database of chemical reactions designed to achieve thermodynamic consistency automatically.* Journal of Chemical and Engineering Data, 2001. **46**(5), 1035-1040.

202. Sellers P., Sunner S., and I. Wadso, *Acta Chem.* Scandinavian, 1964. **18**, 202.

203. P. Cardiano, C. De Stefano, O. Giuffrè, and S. Sammartano, *Thermodynamic and spectroscopic study for the interaction of dimethyltin(IV) with L-cysteine in aqueous solution.* Biophys. Chem., 2008. **133**, 19-27.

204. F. Crea, P. Crea, C. De Stefano, O. Giuffrè, A. Pettignano, and S. Sammartano, *Thermodynamic Parameters for the Protonation of Poly(allylamine) in concentrated LiCl(aq) and NaCl(aq).* J. Chem. Eng. Data, 2004. **49**, 658-663.

205. L. Pettit and K.J. Powell, *The IUPAC Stability Constants Database*, A. Software, Editor. 2001.

206. D. K. Nordstrom, J. Majzlan, and E. Königsberger, *Thermodynamic properties for arsenic minerals and aqueous species*, in *Reviews in Mineralogy and Geochemistry*. 2014. p. 217-255.

207. A. M. Manotti Lanfredi and A. Tiripicchio, *Fondamenti di chimica, seconda edizione.* 2006: Casa Editrice Ambrosiana.

208. P. Cabras and A. Martelli, *Chimica degli alimenti.* . 2004: Piccin: Padova.

209. Agency for Toxic Substances and Disease Registry. *PUBLIC HEALTH STATEMENT: Strontium.* 2004 [cited 2019; Available from: https://www.atsdr.cdc.gov/phs/phs.asp?id=654&tid=120.

210. C.F. Baes and R.E. Mesmer, *The Hydrolysis of Cations.* 1976, New York: John Wiley & sons.

211. A. De Robertis, A. Gianguzza, O. Giuffrè, A. Pettignano, and S. Sammartano, *Interaction of methyltin(IV) compounds with carboxylate ligands. Part 1: Formation and stability of methyltin(IV)-carboxylate complexes and their relevance in the speciation of natural waters.* Appl. Organomet. Chem., 2006. **20**, 89-98.

212. C. De Stefano, C. Foti, A. Gianguzza, and S. Sammartano, *The interaction of amino acids with the major constituents of natural waters at different ionic strengths.* Mar. Chem., 2000. **72**, 61-76.

213. C. De Stefano, A. Gianguzza, O. Giuffrè, D. Piazzese, S. Orecchio, and S. Sammartano, *Speciation of organotin compounds in NaCl aqueous solution: Interaction of mono-, di- and triorganotin(IV) cations with nucleotides 5' monophosphates.* Appl. Organomet. Chem., 2004. **18**(12), 653-661.

214. C. Foti, A. Gianguzza, D. Milea, F.J. Millero, and S. Sammartano, *Speciation of trialkyltin(IV) cations in natural fluids.* Mar. Chem., 2004. **85**, 157-167.

215. C. Foti, G. Lando, F.J. Millero, and S. Sammartano, *Experimental study and modeling of inorganic Cd^{2+} speciation in natural waters.* Environ. Chem., 2011. **8**(3), 320-331.

216. A. Gianguzza, O. Giuffrè, D. Piazzese, and S. Sammartano, *Aqueous solution chemistry of alkyltin(IV) compounds for speciation studies in biological fluids and natural waters.* Coord. Chem. Rev., 2012. **256**, 222-239.

217. J. Buffle, *Complexation Reactions in Aquatic Systems - an Analytical Approach.* Ellis Horwood Series in Analytical Chemistry. 1988, Chichester, England.

218. R. J. Bowell, *Sorption of arsenic by iron oxides and oxyhydroxides in soils.* Applied Geochemistry, 1994. **9**(3), 279-286.

219. I. Polowczyk, P. Cyganowski, J. Ulatowska, W. Sawiński, and A. Bastrzyk, *Synthetic Iron Oxides for Adsorptive Removal of Arsenic.* Water, Air, and Soil Pollution, 2018. **229**(6).

220. G. Zhang, F. Liu, H. Liu, J. Qu, and R. Liu, *Respective role of Fe and Mn oxide contents for arsenic sorption in iron and manganese binary oxide: An X-ray absorption spectroscopy investigation.* Environmental Science and Technology, 2014. **48**(17), 10316-10322.

221. J. Yang, L. Chai, M. Yue, and Q. Li, *Complexation of arsenate with ferric ion in aqueous solutions.* RSC Advances, 2015. **5**(126), 103936-103942.

222. S. J. Dixon and B. R. Stockwell, *The role of iron and reactive oxygen species in cell death.* Nature Chemical Biology, 2014. **10**(1), 9-17.

223. S. Maya, T. Prakash, K. D. Madhu, and D. Goli, *Multifaceted effects of aluminium in neurodegenerative diseases: A review.* Biomedicine and Pharmacotherapy, 2016. **83**, 746-754.

224. X. Liu and F. J. Millero, *The solubility of iron hydroxide in sodium chloride solutions.* Geochimica et Cosmochimica Acta, 1999. **63**(19-20), 3487-3497.

225. P. Cardiano, R. M. Cigala, F. Crea, F. Giacobello, O. Giuffrè, A. Irto, G. Lando, and S. Sammartano, *Sequestration of Aluminium(III) by different natural and synthetic organic and inorganic ligands in aqueous solution.* Chemosphere, 2017. **186**, 535-545.

226. P. Cardiano, D. Chillè, C. Foti, and O. Giuffrè, *Effect of the ionic strength and temperature on the arsenic(V) -Fe3+ and -Al3+ interactions in aqueous solution.* Fluid Phase Equilibria, 2018. **458**, 9-15.

227. C. Bretti, R.M. Cigala, F. Crea, C. Foti, and S. Sammartano, *Solubility and activity coefficients of acidic and basic nonelectrolytes in aqueous salt solutions. 3. Solubility and acitivity coefficients of adipic and pimelic acids in NaCl(aq), (CH$_4$)$_4$NCl(aq) and (C$_2$H$_5$)$_4$NI(aq) at different ionci strengths and at t = 25 °C.* Fluid Phase Equilibria, 2008. **263**, 43-54.

228. J. C. Raposo, O. Zuloaga, M. A. Olazabal, and J. M. Madariaga, *Development of a Modified Bromley Methodology for the estimation of ionic media effects on solution equilibria: Part 5. The chemical model of boric acid in aqueous solution at 25°C and comparison with arsenious acid.* Fluid Phase Equilibria, 2003. **207**(1-2), 81-95.

229. N. J. Welham, K. A. Malatt, and S. Vukcevic, *Effect of solution speciation on iron-sulphur-arsenic-chloride systems at 298 K.* Hydrometallurgy, 2000. **57**(3), 209-223.

230. C. Fontàs, E. Margui, M. Hidalgo, and I. Queralt, *Improvement approaches for the determination of Cr(VI), Cd(II), Pd(II) and Pt(IV) contained in aqueous samples by conventional XRF instrumentation.* X-Ray Spectrom, 2009. **38**, 9-17.

231. C. Fontàs, I. Queralt, and M. Hidalgo, *Novel and selective procedure for Cr(VI) determination by X.ray fluorescence analysis after membrane concentration.* Spectrochimica Acta, Part B, 2006. **61**, 407-413.

232. E. Margui, C. Fontàs, K. Van Meel, R. Van Grieken, I. Queralt, and M. Hidalgo, *High-energy polarized-beam energy-dispersive X-ray fluorescence analysis combined with activated thin layers for cadmium determination at trace levels in complex environmental liquid samples.* Analytical Chemistry, 2008. **80**, 2357-2364.

233. G. Elias, E. Marguí, S.Díez, and C. Fontàs, *Polymer inclusion membrane as an effective sorbent to facilitate mercury storage and detection by X-ray fluorescence in natural waters.* Analytical Chemistry, 2018. **90**, 4756-4763.

234. A. St John, S. Kolev, C. Fontàs, *Polymer inclusion membranes for the separation of uraniumand arsenic from diluite aqueous solutions*, in *Membrane technologies for water treatment: removal of toxic trace elements with emphasison arsenic, fluoride and uranium*, J.H. A. Figoli, J. Bundschuh, Editor. 2016, CRC Press/Balkema: London.

235. M. Iñes G.S. Almeida, R.W. Cattral, S.D. Kolev, *Polymer inclusion membranes (PIMs) in chemical analysis - A review.* Analytica Chimica Acta, 2017. **987**, 1-14.

236. G.J. Moody, R.B. Oke, and J.D.R. Thomas, *Calcium-sensitive electrode based on a liquid ion exchanger in a poly(vinyl-chloride) matrix.* Analyst 95, 1970, 910-918.

237. S.D. Kolev, M.I.G.S. Almeida, and R.W. Cattrall, *Polymer inclusion membranes*, in *Handbook of Membrane Separations: Chemical, Pharmaceutical, Food and and Biotechnological Applications*, A.K. Pabby, S.S.H. Rizvi, and A.M. Sastre, Editors. 2015, CRC Press: Boca Raton. 721-737.

238. R. Güell, E. Anticó, S.D. Kolev, J. Benavente, V. Salvadó, and C. Fontàs, *Development and characterization of polymer inclusion membranes for the separation and speciation of inorganic As species.* Journal of Membrane Science, 2011. **383**, 88–95.

239. R. Güell, C. Fontàs, V. Salvadó, E. Anticó, *Modelling of liquid–liquid extraction and liquid membrane separation of arsenic species in environmental matrices.* Separation and Purification Technology, 2010. **72**, 319–325.

240. B. Gupta, Z. Begum I, *Separation and removal of arsenic from metallurgical solutions using bis(2,4,4-trimethylpentyl)dithiophosphinic acid as extractant.* Separation and Purification Technology, 2008. **63** 77–85.

241. D.S. Flett, *Solvent extraction in hydrometallurgy: the role of organophosphorus extractants.* Journal of Organometallic Chemistry, 2005. **690** 2426–2438.

242.   J. Kozlowska, C.A. Kozlowski, J.J. Koziol, *Transport of Zn(II), Cd(II), Pb(II) across CTA plasticized membranes containing organophosphorous acids as an ion carriers.* Separation and Purification Technology, 2007. **57**, 430-434.

243.   P. Liang, L. Peng, P. Yan, *Speciation of As(III) and As(V) in water samples by dispersive liquid-liquid microextraction separation and determination by graphite furnace atomic absorption spectrometry.* Microchimica Acta, 2009. **166**, 47-52.

244.   Q. Zhang, H. Minami, S. Inoue, I. Atsuya, *Differential determination of trace amounts of arsenic(III) and arsenic(V) in seawater by solid sampling atomic absorption spectrometry after preconcentration by coprecipitation with a nickel-pyrrolidine dithiocarbamate complex* Analytica Chimica Acta, 2004. **508**, 99-105.

245.   À. Piqué, F. Grandia, and À. Canals, *Processes releasing arsenic to groundwater in the Caldes de Malavella geothermal area, NE Spain.* Water Research, 2010. **44**(19), 5618-5630.

246.   R. Ventura-Houle, X. Font, and L. Heye, *Groundwater arsenic contamination and their variations on episode of drought: Ter River delta in Catalonia, Spain.* Applied Water Science, 2018. **8**, 128.